AD-A183 911

(12)

AD

SPECIAL PUBLICATION BRL-SP-59

PROCEEDINGS OF THE WORKSHOP ON THE CHEMICAL SUPPRESSION OF ROCKET AFTERBURNING AND OF GUN MUZZLE FLASH

JOSEPH M. HEIMERL

MARCH 1987

DTIC
ELECTE
AUG 1 3 1987
S D
A

APPROVED FOR PUBLIC RELEASE; DISTRIBUTION UNLIMITED.

US ARMY BALLISTIC RESEARCH LABORATORY
ABERDEEN PROVING GROUND, MARYLAND

87 8 13 111

Destroy this report when it is no longer needed.
Do not return it to the originator.

Additional copies of this report may be obtained from the National Technical Information Service, U. S. Department of Commerce, Springfield, Virginia 22161.

The findings in this report are not to be construed as an official Department of the Army position, unless so designated by other authorized documents.

The use of trade names or manufacturers' names in this report does not constitute indorsement of any commercial product.

REPORT DOCUMENTATION PAGE

Form Approved
OMB No 0704-0188
Exp. Date: Jun 30, 1986

1a. REPORT SECURITY CLASSIFICATION Unclassified	1b. RESTRICTIVE MARKINGS
2a. SECURITY CLASSIFICATION AUTHORITY	3. DISTRIBUTION/AVAILABILITY OF REPORT
2b. DECLASSIFICATION/DOWNGRADING SCHEDULE	
4. PERFORMING ORGANIZATION REPORT NUMBER(S) SPECIAL REPORT BRL-SP-59	5. MONITORING ORGANIZATION REPORT NUMBER(S)
6a. NAME OF PERFORMING ORGANIZATION US Army Ballistic Research Laboratory 6b. OFFICE SYMBOL (If applicable) SLCBR-IB	7a. NAME OF MONITORING ORGANIZATION
6c. ADDRESS (City, State, and ZIP Code) Aberdeen Proving Ground, MD 21005-5066	7b. ADDRESS (City, State, and ZIP Code)
8a. NAME OF FUNDING/SPONSORING ORGANIZATION 8b. OFFICE SYMBOL (If applicable)	9. PROCUREMENT INSTRUMENT IDENTIFICATION NUMBER
8c. ADDRESS (City, State, and ZIP Code)	10. SOURCE OF FUNDING NUMBERS PROGRAM ELEMENT NO. 61102A; PROJECT NO. AH43; TASK NO.; WORK UNIT ACCESSION NO.

11. TITLE (Include Security Classification)
Proceedings of the Workshop on the Chemical Suppression of Rocket Afterburning and of Gun Muzzle Flash

12. PERSONAL AUTHOR(S)
Joseph M. Heimerl, Editor

13a. TYPE OF REPORT	13b. TIME COVERED FROM _____ TO _____	14. DATE OF REPORT (Year, Month, Day)	15. PAGE COUNT

16. SUPPLEMENTARY NOTATION

17. COSATI CODES			18. SUBJECT TERMS (Continue on reverse if necessary and identify by block number)
FIELD	GROUP	SUB-GROUP	
19	06		Muzzle Flash; Suppression Mechanisms
21	02		Rocket Afterburning
			Alkali Salts

19. ABSTRACT (Continue on reverse if necessary and identify by block number)

The Workshop formally consisted of 14 presentations. The manuscripts upon which these presentations were based are archived here.

20. DISTRIBUTION/AVAILABILITY OF ABSTRACT ☐ UNCLASSIFIED/UNLIMITED ☒ SAME AS RPT. ☐ DTIC USERS	21. ABSTRACT SECURITY CLASSIFICATION Unclassified
22a. NAME OF RESPONSIBLE INDIVIDUAL DR. JOSEPH M. HEIMERL	22b. TELEPHONE (Include Area Code) 301-278-6168 22c. OFFICE SYMBOL SLCBR-IB-I

DD FORM 1473, 84 MAR 83 APR edition may be used until exhausted
All other editions are obsolete.

PREFACE

This initial Workshop on the Chemical Suppression of Rocket Afterburning and of Gun Muzzle Flash (unclassified) has a twofold purpose. First it addresses the technical questions of:

a. Where are we now in our fundamental understanding of the elementary, controlling processes involved in these phenomena?

b. What are the technical needs?

c. How should (could) one proceed?

Second, this workshop enables fluid dynamicists and kineticists, experimentalists and modelers to meet with each other (in many cases for the first time) and to focus their collective attention to answer these technical questions.

Support for this workshop has been supplied by:

1. The US Army Ballistic Research Laboratory

2. The Army Research Office

3. The Air Force Office of Scientific Research

4. The US Army Research, Development and Standardization Group, London

Special thanks are due to L. Watermeier (BRL), R. Singleton (ARO), Y.S. Park (AFOSR), and F. Oertel (ERO).

JOSEPH M. HEIMERL
Ballistic Research Laboratory
11 June 1986

TABLE OF CONTENTS

		Page
I.	"Gun Muzzle Flash Research at the Fraunhofer-Institute EMI-AFB" by G. Klingenberg	5
II.	"Kinetics Networks and MEFF-Code Predictions: A Progress Report" by J.M. Heimerl and G.E. Keller	45
III.	"Flash Simulation with a Global Reaction Model for Transient Flow from the 84 mm Carl Gustaf Rifle" by M.B. Khalil, E.G. Plett, and D.H. Gladstone	53
IV.	"Detailed High Temperature Oxidation Chemistry of the Alkali Metals In Flames" by M. Steinberg and K. Schofield	93
V.	"Spectroscopic Measurements in the Exhaust Flow of a 7.62 mm Rifle Using Propellants With and Without Chemical Flash Suppressants" by H. Mach	107
VI.	"Chemical Kinetic Studies and Infrared Laser Detection of Potassium and Sodium Species Relevant to Muzzle Flash and Rocket Plume Afterburning Suppression" by C.E. Kolb, M.S. Zahniser, J.A. Silver, and A. Freedman	119
VII.	"Kinetic Studies of Recombination Reactions of Alkali Atoms by Time-Resolved Spectroscopic Methods" by D. Husain	151
VIII.	"Influence of Potassium on OH Decay Rates in Methane-Air Flames" by M. Slack, J. Cox, A. Grillo, R. Ryan, and O. Smith	169
IX.	"The Feasibility of a CARS Technique for the Study of Muzzle Flash" by J.A. Vanderhoff, R.B. Peterson, and A.J. Kotlar	183
X.	"ARDEC Laboratory Flash Studies" by J. Salo and A. Bracuti	219
XI.	"An Overview of the RARDE Facilities for Gun Muzzle Flow and Flash Studies" by P.S. Henning	229
XII.	"Secondary Combustion Suppression in Rocket Exhausts" by G.A. Jones and A.C.H. Mace	239
XIII.	"Suppression Mechanism of Rocket Afterburning" by N. Kubota	261
XIV.	"Suppression in Premixed $H_2/O_2/N_2$ Flames Seeded With HBr" by T. Singh and D.P. Weaver	265
	DISTRIBUTION LIST	283

GUN MUZZLE FLASH RESEARCH AT THE FRAUNHOFER-INSTITUTE EMI-AFB

Guenter Klingenberg

Fraunhofer-Institut fuer Kurzzeitdynamik, Ernst-Mach-Institut,
Abteilung fuer Ballistik (EMI-AFB), Hauptstrasse 18,
D-7858 Weil am Rhein, F.R.G.

ABSTRACT

Gun muzzle flash research in the Fraunhofer-Institut fuer Kurzzeitdynamik (EMI-AFB) began in the late 1960's. Major activities were directed toward the study of two-phase reacting muzzle flows of small-arms weapons. Early work was focused on the gasdynamics involved using visualization methods and measuring quantitatively flow parameters. Then, studies were performed on the generation of gun muzzle flash and on flash inhibition by alkali salts using spectroscopic methods for determining gas phase temperature and gas velocity changes. Most recently, the research emphasis has shifted to the simulation of relatively well-defined, reacting gas flows by means of a gas gun. The gas gun is driven by the combustion of suitably diluted mixtures of hydrogen and oxygen and thus is capable of simulating the gun muzzle flash phenomena with particularly simple chemistry. The present paper summarizes briefly the EMI-AFB activities and presents some results of measurements obtained most recently with the 7.62 mm NATO rifle and the gas gun simulator.

1. INTRODUCTION

Our understanding of the chemical and physical properties that contribute to the phenomenon of gun muzzle flash and of flash inhibition by chemical additives has grown in recent years. At the Fraunhofer-Institut fuer Kurzzeitdynamik (EMI-AFB) research work on transitional ballistics including muzzle blast and flash phenomena commenced in the late 1960's. The EMI-AFB research efforts, partly performed in cooperation with the Franco-German Research Institute (ISL), St. Louis, France, and the U.S. Army Research Laboratory (BRL), APG, MD, USA, have borne a share in the elucidation of gun muzzle flash and flash inhibition phenomena. Relevant EMI-AFB publications in Monographs [1,2], Journals [3-8], Proceedings [9-20], and Laboratory Reports [21-47] are listed in the attached bibliography. The papers listed in references 1 and 2 were also published as EMI-AFB reports [43,44].

One of the results of the above mentioned reviews [2,20,44] has been the extension of a hypothesis [15,17,39,40] on the generation of gun muzzle flash and its inhibition by alkali salt additives. Basically the novel hypothesis states that the ignition source for secondary flash is the temperature of the preceding intermediate flash [17,44]. This temperature may have two sources, namely, (a) shock heating as the propellant muzzle effluents pass through the inner shock disk (Mach disk) which terminates the highly underexpanded jet flow region [3], and (b) exothermic combustion reactions initiated farther downstream from the inner shock disk (Mach disk). The former is well-known while the latter was first assumed in reference 5. More recently, a re-evaluation of experimental data in reference 44 has put new emphasis on the hypothesized combustion reactions in the intermediate flash region and pointed out the importance of the turbulence observed in gun muzzle flows [4,5,6]. The assumption [44] was that oxygen from the air, which is squeezed between the outer blast wave and the muzzle effluent, is already turbulently entrained and carried to the core

region of the intermediate flash during the formation of this flash thus providing the means for initiating combustion in this area. Furthermore, it was proposed that the inhibition of secondary flash by alkali salt additives commences in the intermediate flash region and thus affects the initial combustion reactions so that the temperature in the intermediate flash stays below the ignition level required for the initiation of the secondary flash [17,43,44].

A necessary condition to support the above hypothesis is that the formation of slip lines downstream from the triple points of the inner shock bottle of the expanding muzzle flow must be hindered by, or they must be destroyed by the turbulent flow which prevails in this flow region. If the slip line formation is hindered or destroyed, then mass transport of air to the core flow region of the intermediate flash is possible so that combustion may follow the turbulent mixing of unburnt fuels with the oxygen of the air.

The above condition was most recently investigated in the precursor flow of the 7.62 mm rifle [20]. This precursor flow is free from the complicating effects of the projectile and of chemical reactions because it consists of air that is pushed out of the gun tube ahead of the projectile [1,5,43]. From these first investigations, it was found that the formation of the slip line in the precursor flow of the 7.62 mm rifle is indeed absent at some small distance from the inner shock disk (Mach disk) [20]. In view of the similarities that exist between the first precursor flow and the main propellant gas flow, produced after projectile ejection, it was concluded that slip lines will also be absent in the main flow [20]. The present paper reports on a follow-on study, performed to examine the slip formation in the propellant gas flow of the 7.62 mm rifle. As in reference [20], the propellant gas plume is probed by a laser Doppler velocimeter.

In addition to the above investigation in actual gun firings, simulation experiments are currently under way at EMI-AFB to overcome the limitations encountered in real transitional ballistic cycles [1,8,19,43]. A gas gun that permits the generation of relatively clean, simplified, reacting gas flows with realistic ballistic gas pressures and temperatures has been developed. The gas gun is driven by the combustion of suitably diluted mixtures of hydrogen and oxygen. Therefore, it is capable of simulating the gun muzzle flash phenomena with particularly simple gas phase chemistry [8,19]. Some results of the gas gun studies on the muzzle flash formation and its suppression by alkali salt additives are also presented.

2. BACKGROUND

2.1 Quasi-Steady Flow Approach

Because of the complexity of real muzzle flows from guns, theoretical and experimental analysis of the gas dynamics have often relied on the simplified, quasi-steady flow approach [43,44].

The inner structure of quasi-steady jets such as rocket motor exhausts depends upon the nozzle exit gas properties. The expansion ratio is often described in terms of the nozzle exit gas pressure, p_1, to the ambient pressure, p_o [5,43]. For example, Figure 1 presents the shadowgraph of a free air jet taken for two different pressure ratios [20]. The multiple shock structure at $p_1/p_o = 3.7$ changes to the single shock bottle structure for $p_1/p_o > 7$.

Figure 2 shows schematically the single shock structure of a quasi-steady free jet flow. The highly underexpanded supersonic flow ($M \gg 1$) is terminated laterally by the formation of the barrel shock and axially by the Mach disk. The junction of these two shocks is also intercepted by the reflected shock and the slip line. The highly underexpanded supersonic jet flow region ($M \gg 1$) and the decelerated subsonic flow ($M < 1$), downstream from the Mach disk,

Fig. 1: Steady free air jet flow at p_1/p_o = 3.7 and 7.1 [20]

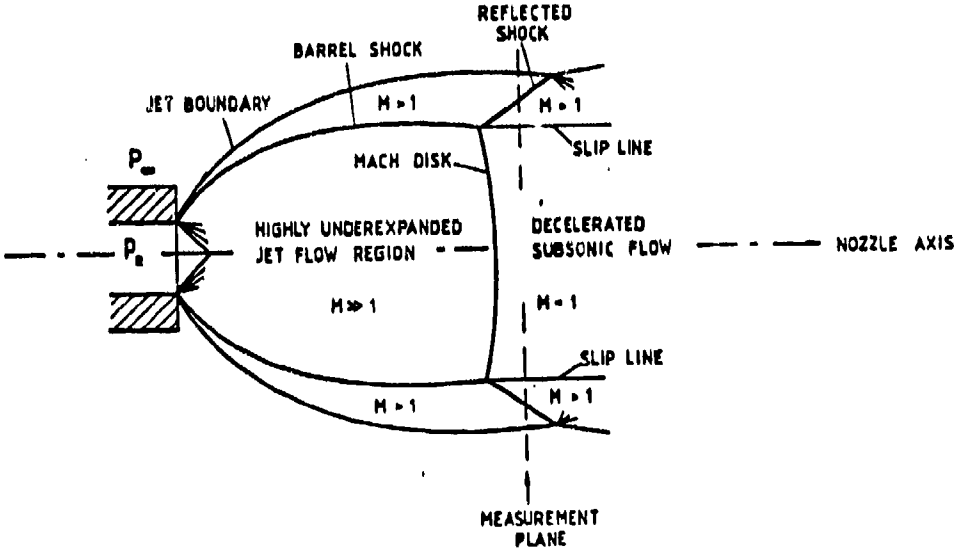

Fig. 2: Schematic of highly underexpanded free jet flow pattern (p_e: muzzle exit pressure, p_∞: ambient pressure)

are both surrounded by a supersonic flow ($M > 1$) which is separated from the core flow region either by the barrel shock or by the slip line. Such slip line formation was experimentally confirmed by velocity measurements [20]. The radial velocity profile at the measurement plane of Figure 2 downstream from the Mach disk would show the discontinuous profile seen in Figure 3. The slip line constitutes a boundary between regions of equal pressure but drastically different flow velocities with the result that mass transport

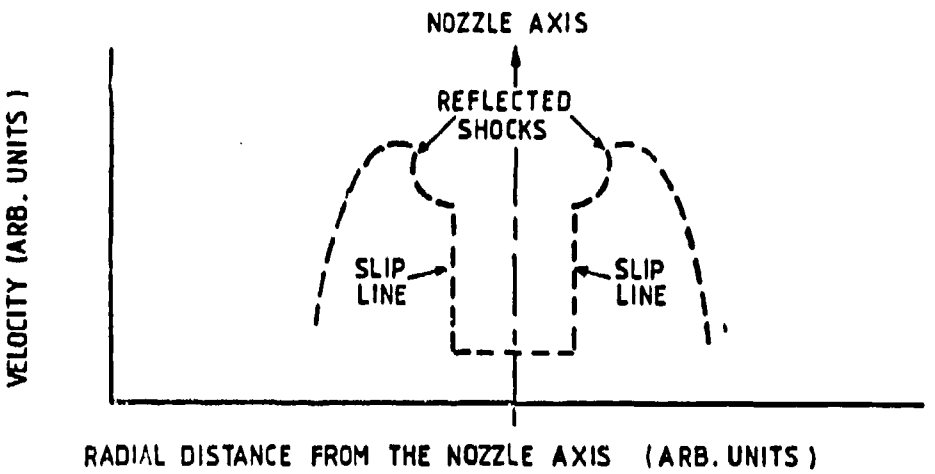

Fig. 3: Schematic of typical velocity profile downstream from the Mach disk of a steady free jet

is prohibited across this boundary. Thus, no influx of air to the core flow region of a quasi-steady rocket exhaust can occur. Therefore, the "intermediate" radiation zone of rocket exhausts that commences downstream from the Mach disk [28,46] is due only to shock heating processes.

2.2 Transient Gun Muzzle Flows

Relative to the case above, highly unsteady gun muzzle exhaust flows are more complex. Their flow patterns are unique in that the formation of the outer strong shock or blast wave which surrounds the muzzle flow field significantly restrains the expanding jet flow. For example, Figure 4 shows the axial trajectories of the visualized 7.62 mm gun muzzle flow discontinuities as obtained from shadowgraphs [5,43]. Figure 4 shows the motion of the inner shock disk (Mach disk) of the two precursors and the main propellant gas flow as well as the motion of the blast waves and the motion of the turbulent gas/air interface as obtained from shadowgraphs [5]. Also, the appropriate $X/D = f(t)$- and $x = f(t)$-laws for the discontinuities of the main propellant gas flow [5] are given in Figure 4.

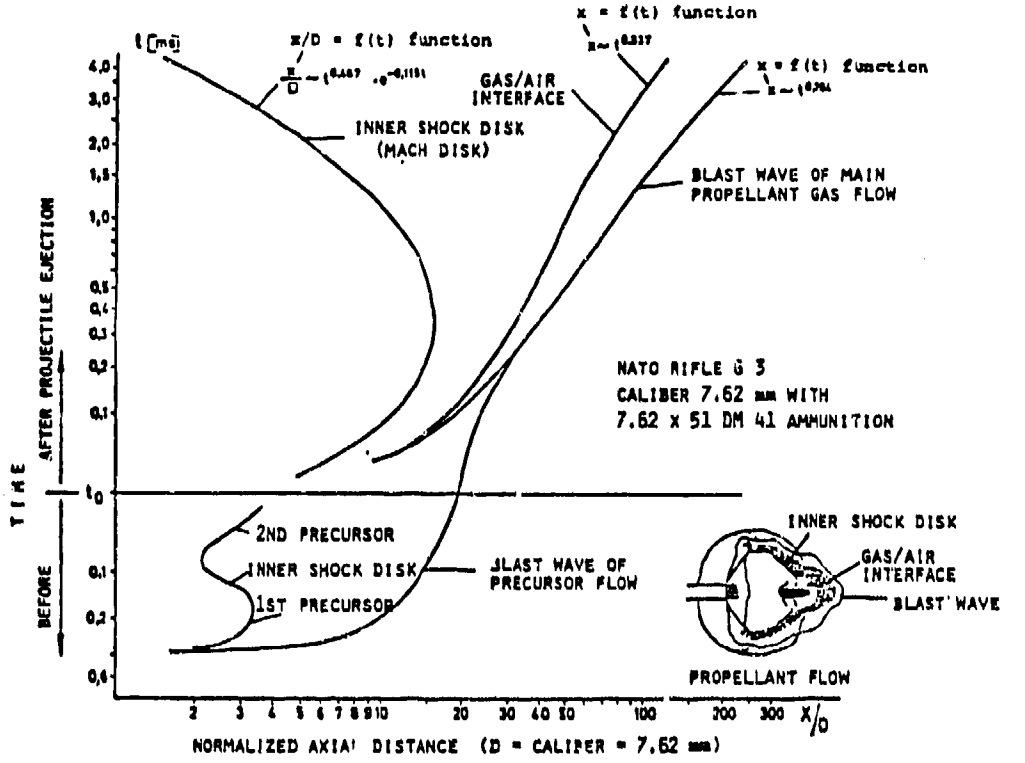

Fig. 4: Axial trajectories of visualized discontinuities of the 7.62 mm gun precursor and main propellant gas flow [5]

As can be seen, for $t < 0.4$ ms, the motion of the inner shock disk (Mach disk) of the main propellant gas flow is closely coupled to the motion of the blast wave. The resulting restraint of the muzzle effluent flow by the blast wave lasts for a relatively long time, and it has important consequences. This restraint affects not only the time-dependent formation of inner shock structures that bound the highly underexpanded supersonic region but also the volume between the outer blast wave and the supersonic region [5].

Figure 5 depicts the flow development of the main propellant gas flow for the situation where the blast wave begins to decouple from the gas plume. For reference, the primary and intermediate flash regions are also marked in this figure. The secondary flash does not appear because it occurs at a still later stage of the development, i.e., at times $t \geq 0.8$ ms [3,5].

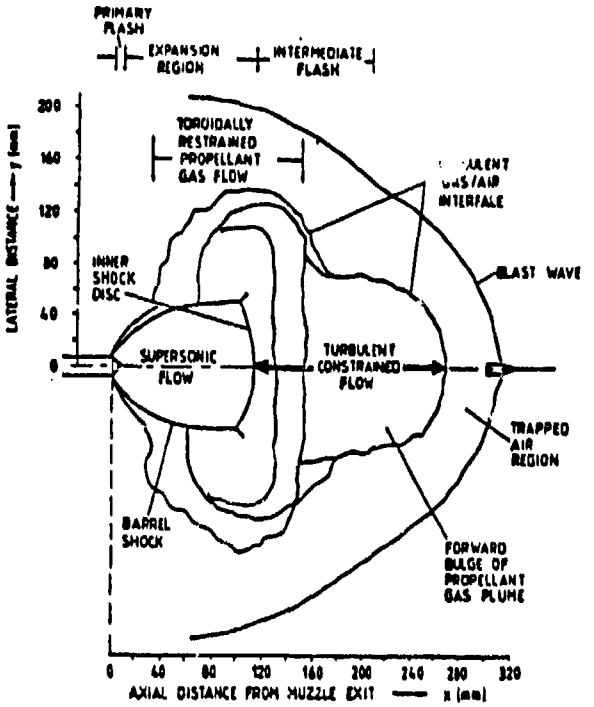

Fig. 5: Schematic of 7.62 mm gun muzzle exhaust flow pattern at t = 0.4 ms after projectile ejection

At t = 0.4 ms (see Figure 5), the triple-point configuration known from steady jet studies has just been formed. At earlier times the shock bottle configuration is different from the steady jet structure and changes significantly with time [5]. The restraint by the outer blast wave has resulted in the formation of the toroidally ring-shaped cloud of gases which surrounds the supersonic flow region. In addition, the flow is turbulently constrained at the forward bulge of the propellant gas plume [5,43]. Between the outer turbulent gas/air interface and the blast wave is a volume of trapped air. This air is turbulently entrained in the gas plume and mixed with the constrained flow.

From previous measurements of flow velocities of the effluent of a 7.62 mm rifle there exist indications that the flow downstream of the Mach disk is turbulent and constrained. One such measurement technique is based on labelling flow elements by luminous tracers

produced by laser-induced gas breakdown [4]. A locally confined plasma blob with a temperature in excess of 10^5 K is generated in a small volume. The blob has a lifetime in excess of 10^{-5} s and is propagated with the surrounding gas. Two open-shutter cameras placed orthogonally determine the direction of flow propagation. (Location within the flow field is obtained from a shadowgraph taken simultaneously with the photographs.) Such measurements show that the flow velocity is greatly diminished in the intermediate flash region for a relatively long time. During this interval the blob does not move at all or only very slowly on twisted trajectories. Sometimes it even moves in an upstream direction. An example of such a velocity measurement is given in Figure 6.

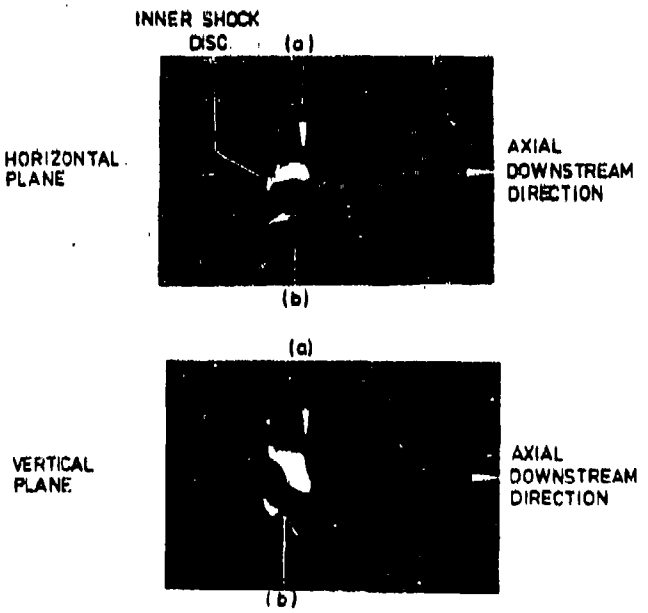

Fig. 6: Open-shutter photographs of the motion of the radiating plasma blob inside the 7.62 mm gun muzzle blast field taken in two orthogonal planes

The laser pulse was focused on axis and the arrows superimposed on the photos show the planar projection of the local gas motion. Such a flow is indicative of turbulence.

Figure 7 shows velocity measurements for a 7.62 mm rifle taken 125 mm from the muzzle. Both the laser tracer [4], just discussed above, and the laser velocimeter measurements show good agreement. The fact that the flow velocity drastically diminishes or even reverses direction was assumed to be due to heat released by combustion in the intermediate flash region [4,5]. We see that the combustion in the intermediate flash is assumed since 1976. This change of flow velocity has a measured duration of about 0.5 ms allowing time for chemical processes to take place [43,44].

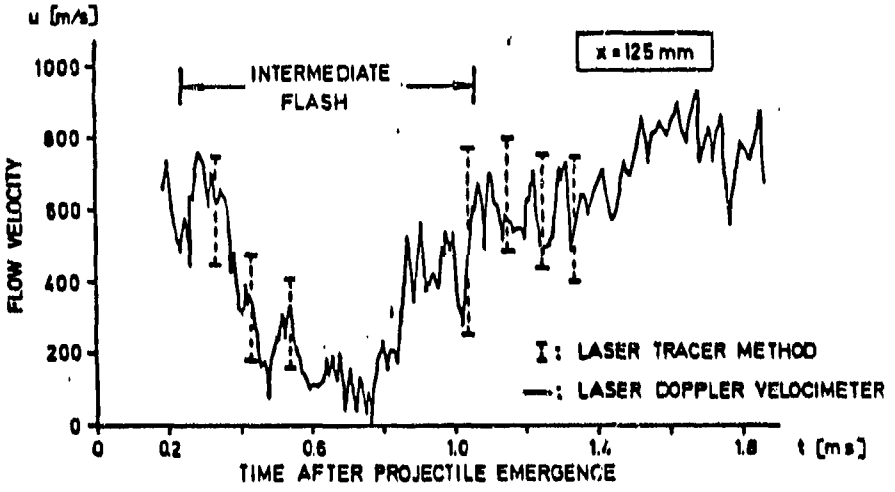

Fig. 7: Axial flow velocity vs. time as measured in the 7.62 mm gun muzzle blast field at a distance of 125 mm from the muzzle by both the laser tracer and the laser Doppler velocimeter methods

A sequence of two schlieren pictures of the propellant gas plume at the muzzle of the 7.62 mm rifle are shown in Figure 8. A recognizable single Mach disk and barrel shock structure can be seen in Figure 8 even 2.985 ms after shot ejection. The picture, taken 4.585 ms after shot ejection, shows the subsequent evolution of the flow into the multiple Mach structure that characterizes steady-state expansions. These two photos, separated by 1.6 ms in time, qualitatively correspond to the photographs of the steady-state, free-jet taken for different exit pressure ratios shown in

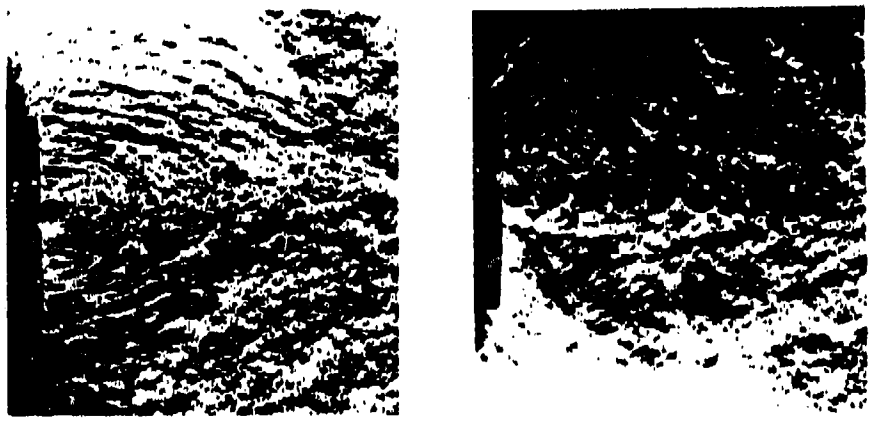

t = 2.985 ms t = 4.585 ms

Fig. 8: Schlieren photographs of muzzle flow from the 7.62 mm rifle at relatively late times

Figure 1. Still evident in the photos of Figure 8 is the great lateral extent of the constrained turbulent propellant gas flow. The entire turbulent gas ball moves only slowly in the axial direction due to the original confinement by the blast wave and the subsequent high degree of turbulence. We also note the obvious asymmetry of the turbulent gas ball which is evident in the picture at t = 4.585 ms after shot ejection in Figure 8. Apparently, flow conditions that approach quasi-steady flows are obtained in gun muzzle flows only at very late times in the flow expansion process.

2.3 Flow and Flash Development

The unsteady, reacting gun muzzle exhaust flow involves many complex processes. They include [1-5]:

- precursor/propellant flow interactions
- the-formation of an outer strong blast wave that encapsulates the subsequent gas plume
- the formation of a highly underexpanded supersonic jet flow at the muzzle exit that is bounded by time-varying inner shock fronts

- the interaction between the restraining outer blast wave and the pushing gases released at the muzzle. This restraint results in the formation of unique flow features with time-varying inner shock contours and turbulent flow structures that prevail in the contrained flow region, i.e., between the outer blast wave and the shock-bounded highly underexpanded supersonic jet flow region
- the entrainment of air across the turbulent gas plume boundary or gas/air interface. The entrained air provides the oxygen required for combustion reactions to take place
- gas/particle interactions, since the muzzle effluents contain high particle concentrations [6,12,43], as well as possible condensation/nucleation reactions during the flow expansion
- possible vaporization and subsequent combustion of flow-borne particles
- the occurrence of muzzle flash
- the generation of overpressures by the secondary flash
- flash inhibition reactions caused by chemical additives which are routinely added to conventional gun propellants

The assessment of the main propellant flow development has led to the definition of three important flow phases [1,15,43]. These three flow developmental phases are the

(1) initial phase
(2) interim phase
(3) unrestrained phase

The initial phase of the flow evolution is determined by the expansion of the exiting propellant gas/particle flow into the rarefied atmosphere of the precursor's underexpanded jet flow region. The subsequent interim phase is governed by the restraint caused by the presence of both the outer blast wave and the depart-

ing projectile. This forces the flow to coalesce successively into lateral inner shocks and into a shock that forms upstream at the base of the projectile. As the blast wave decouples from the propellant gas plume, the unrestrained phase of the flow development starts. In addition, the gas plume radiates at distinct locations in the propellant gas plume forming the phenomenon of gun muzzle flash [43,44]. Figure 9 displays the consecutive development of the radiating 7.62 mm gun muzzle blast field.

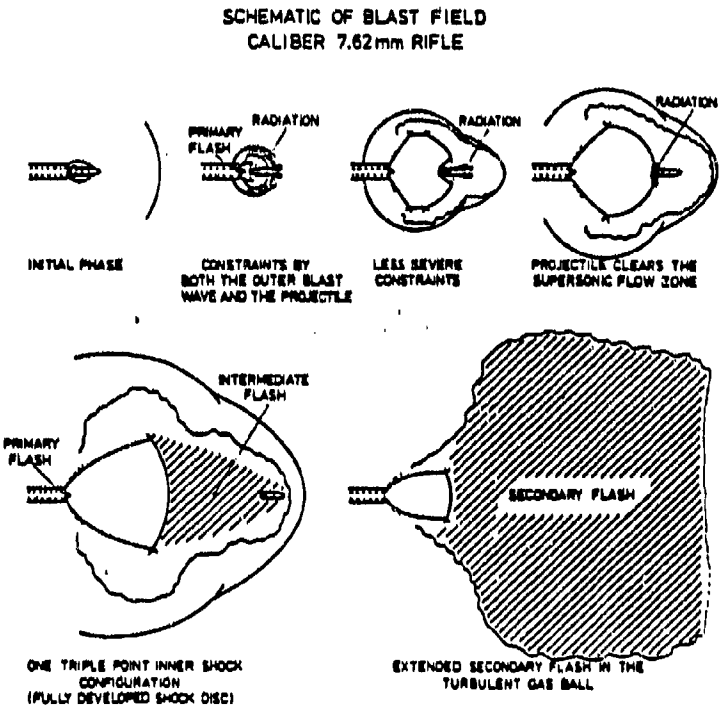

Fig. 9: Consecutive development of the radiating 7.62 mm gun muzzle blast field

In addition to the three main sequential radiating flow areas, usually referred to as

(a) primary flash
(b) intermediate flash
(c) secondary flash

there exists radiation during the initial flow evolution and around

the base of the departing projectile, due to the rapid deceleration of the gas/particle flow [43].

The primary flash, located at the muzzle, is of small spatial extent and low intensity. It is due to the thermal excitation of the gas/particle in-bore flow exiting at the muzzle. This region is separated from the underexpanded supersonic flow portion by an expansion fan [5,43].

The intermediate flash is a more extensive region of greater radiation intensity commencing farther from the muzzle downstream behind the inner shock disk after this shock front has fully developed [3,5,43]. The radiation in this flow region is initially excited by the conversion of convection energy into internal energy of the flow as the gas/particle flow passes the inner shock disk. Then the presumed exothermic chemical reactions are thought to be subsequently induced and disturb the flow expansion in this radiating flow area. The flow disturbance is associated with the reversal of pressure and velocity gradients. During 0.5 to 1 ms the gas/particle flow in this flash region is decelerated to flow velocities of $u < 100$ m/s or even reversed in its direction [4,15,43]. The long residence time enhances the probability of chemical interactions to take place.

The secondary flash is known to commence further downstream from the normal inner shock disk and develops upstream and downstream covering the turbulent gas ball if no chemical flash suppressant is used in the propellant [3,17,43]. It is much more extensive and of much higher intensity than the intermediate flash. It has been confirmed that the secondary flash is caused by the reignition and combustion of fuel-rich gases after they have mixed with the oxygen from the entrained air. Since common gun propellants are stoichiometrically unbalanced, the muzzle effluents provide a mixture of fuel-rich gases and particles. The specific muzzle flow conditions enable the entrainment of air across the turbulent

boundaries of the propellant gas plume. After air is turbulently entrained into the fuel-rich muzzle effluent, the local concentrations may exceed a level at which the mixture is suitable for ignition. Among the sources of ignition are shock heating as, for example, at the radial expansion holes of mechanical muzzle devices, the processes that occur in the intermediate flash yielding temperatures above 1400 K, or even early bright burning of tracers mounted in the base of the projectile. As the local temperature exceeds the ignition temperature fast self-sustaining combustion reactions in the fuel/air mixture can proceed. These combustion reactions consume fuel-rich gases as well as the flow-borne particles and have the tendency to turn over to a regime that exists between deflagration and detonation so that steep pressure gradients are generated. The magnitude of these overpressures may exceed that of the preceding gasdynamically generated blast wave.

Although a significant amount of research has been conducted on muzzle blast and muzzle flash as well as on its suppression by mechanical or chemical means, a detailed understanding is still lacking. In particular, the chemistry of the reacting flow is not yet understood in detail.

2.4 Hypothesis

As mentioned above the experimental evidence has led us to the following hypothesis concerning flash generation and its suppression by alkali salt additives [44].

1. The blast wave produces a restrained propellant/gas flow which promotes turbulence throughout the gas plume volume.

2. The turbulence is such that slip line formation is hindered or that the slip lines are destroyed.

3. In the absence of slip lines, oxygen can be turbulently transported toward the core of the intermediate flash region.

4. The transport of oxygen then permits combustion processes to already take place in the intermediate flash region.

5. The heat released by the combustion adds to the shock heating to raise the temperature in the intermediate flash region so that the ignition temperature for secondary flash is attained.

If this hypothesis be true,then it is easier to understand how such small amounts of alkali salts (less than 2 wt%) can suppress the secondary flash; namely, the addition of alkali salts influences the combustion process in such a way that the temperature in the intermediate flash region is lower than that necessary to ignite the secondary flash.

Crucial to this hypothesis is the entrainment of oxygen from the trapped air region (Fig. 5) toward the center of the flow where the intermediate flash occurs. This requires the absence of slip lines. The following sections present the experimental data concerning muzzle effluent flow and the detection of slip lines. However, we have also to examine whether sufficient air is transported to the intermediate flash region so that the temperature is sensibly changed by combustion reactions. Therefore, at present we measure the temperature in the intermediate flash region for the following three cases:

(a) with ambient air
(b) with ambient nitrogen
(c) with ambient oxygen

If combustion reactions significantly contribute to the temperature in the intermediate flash region, then we anticipate that the observed temperatures will be ranked in the following order:

$$\text{Temperature}_{\text{nitrogen}} < \text{Temperature}_{\text{air}} < \text{Temperature}_{\text{oxygen}}$$

Specially designed intrusive temperature gauges are employed to carry out these measurements. Since these investigations are still

under way, no results can be presented here. These data will be reported later on.

3. FLOW VELOCITY MEASUREMENTS

Figure 10 presents a schematic of the Diehl laser Doppler velocimeter, designed by Smeets (ISL) [6,43].

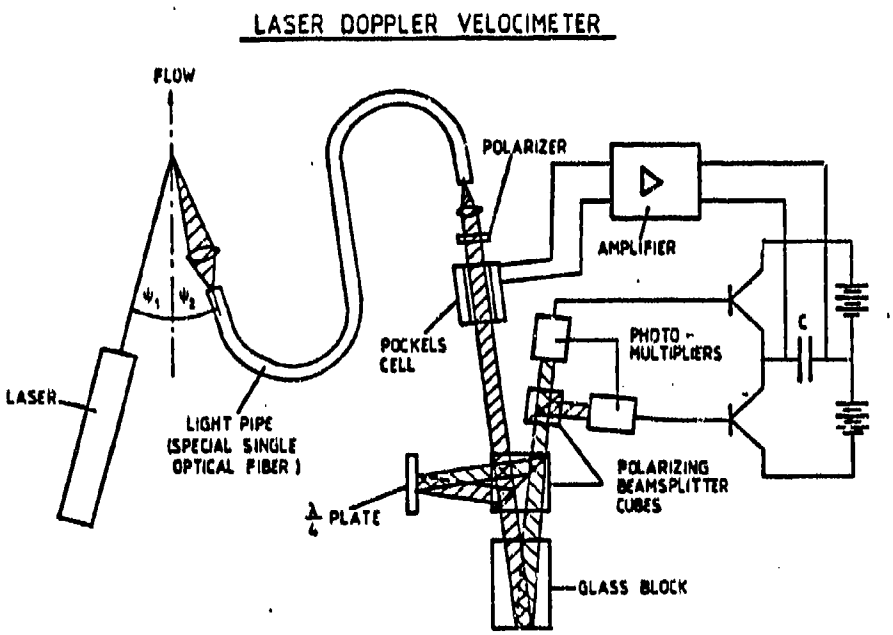

Fig. 10: Schematic of Diehl laser Doppler velocimeter

Scattered and Doppler-shifted monochromatic radiation from the flow is delivered by fiber optic cable to a linear polarizer. This polarized beam then traverses the Pockels cell and is split by the beamsplitter into two linearly polarized beams of equal intensity. These two beams pass through the two legs of the Michelson interferometer, are recombined and pass through a second beam-splitter that is oriented 45° with respect to the first one. Thus, the two beams that arrive at the photomultipliers have complementary interferences. (The glass block in the longer leg improves the light gathering power of the instrument.) The difference of the two photo-

multiplier currents is formed and transmitted to a capacitor. The voltage across this capacitor is amplified and fed to the Pockels cell. The feedback to the Pockels cell nearly instantaneously corrects for the wavelength shift. Then the resulting voltage is proportional to the velocity which, after calibration, can be read directly.

Figure 11 shows the first results of the laser velocimetry measurements taken with a 15 mW HeNe laser in the first precursor of the 7.62 mm rifle.

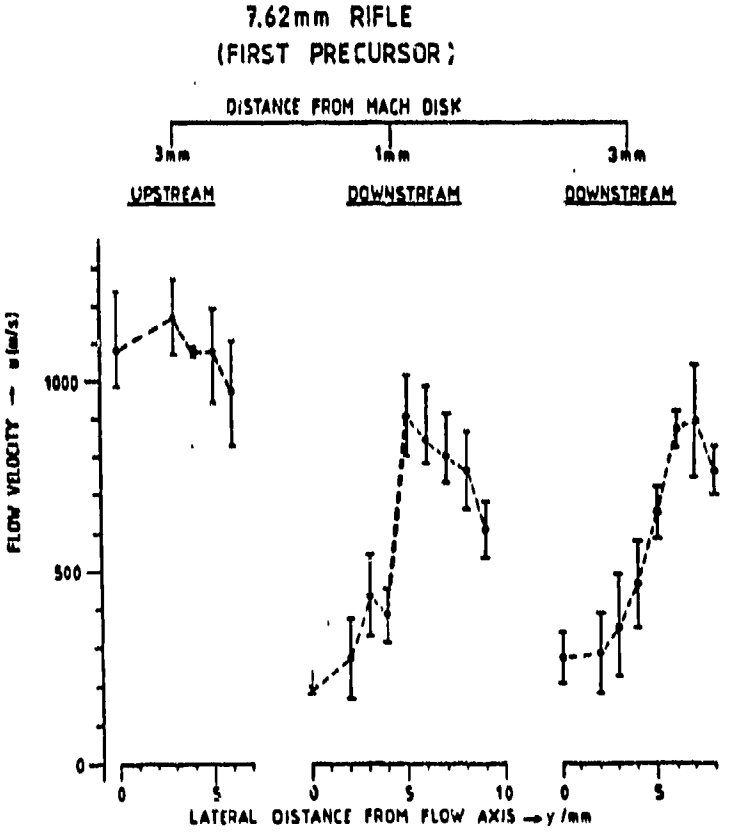

Fig. 11: Lateral velocity profiles in the first precursor flow of the 7.62 mm rifle at selected distances from the inner shock disk [20]

The distances from the inner shock disk (Mach disk) were determined by differencing the distance of the laser focus volume measured from the muzzle of the rifle, and the inner shock disk location,

obtained from shadowgraphs. The distances of the laser focus volume are: 20 mm, 24 mm, and 26 mm corresponding to 3 mm upstream, 1 mm and 3 mm downstream from the inner shock disk, respectively. All velocity measurements shown in Figure 11 were taken at a time 200 μs before shot ejection. Reference to Figure 4 shows that these combinations of time and space place the velocity measurements within the first precursor flow. The lateral distance is measured from the gun axis. The average of at least three measurements are shown. The "error" bars portray the maximum and minimum velocity values observed, i.e., they are not true error bars but rather are a measure of the reproducibility of the data obtained from several firings. The dashed lines connecting the average velocity values are to aid the eye in seeing the trends of the data.

The data taken 3 mm upstream from the inner shock disk provide a check on the overall procedure. We see that the velocities measured are supersonic and gradually fall-off with distance from the axis. Qualitatively, this is just the type of velocity profile one would expect upstream of the inner shock disk and within the highly underexpanded flow terminated by the barrel shock and the inner shock disk (Figure 2).

The most important feature in the velocity profile 1 mm downstream from the inner shock disk is the steep gradient observed between y = 4 mm and y = 5 mm lateral distance. This behavior is qualitatively similar to the steep velocity gradient observed in steady-state measurements when a slip line is encountered (see Figure 3). Thus, we interpret this velocity profile (in Fig. 11) as locating the slip line in the first precursor flow of the 7.62 mm rifle.

The velocity profile 3 mm downstream from the inner shock disk is to be contrasted with the profile 1 mm downstream. Specifically, no steep gradient is observed throughout the region defined by the gun axis and 8 mm perpendicular to this axis. Instead we observe a

rather smooth transition in velocity from the center line outward. We conclude that 3 mm downstream from the inner shock disk slip lines are no longer present.

Though the first precursor and the main propellant gas flow are qualitatively similar in their respective development, there are some important differences. They are:

1. the exit pressure ratio associated with the main flow is about 100 times that associated with the first precursor flow;

2. the projectile is present during the main flow development; and,

3. chemistry is taking place while the main flow develops.

The greater exit pressure ratio of the main flow would tend to increase the shock strengths and therefore the coupling between the blast wave and the main flow; and, lead to an increase in the main flow turbulence. The projectile, in its passage through the main flow, would also tend to increase the turbulence. Finally, although we have assumed that chemistry is involved in the velocity "breakdown" seen in Figure 7, it is not known what the specific effects of the chemistry are upon the development of the main flow. Nevertheless, the effects of chemistry are not likely to lessen the degree of turbulence in the main flow.

We infer then that the neglect of the three properties that distinguish the first precursor flow development from the main flow development would not affect the conclusion that at some small distance downstream from the inner shock disk in the main flow, slip lines are absent.

The statement, inferred above, is proved by the following results of the laser Doppler velocimetry data taken with a powerful Argon laser in the main propellant gas flow of the 7.62 mm rifle. Figure 12 shows the data taken upstream in the highly underexpanded jet flow region versus the lateral distance from the flow axis, y.

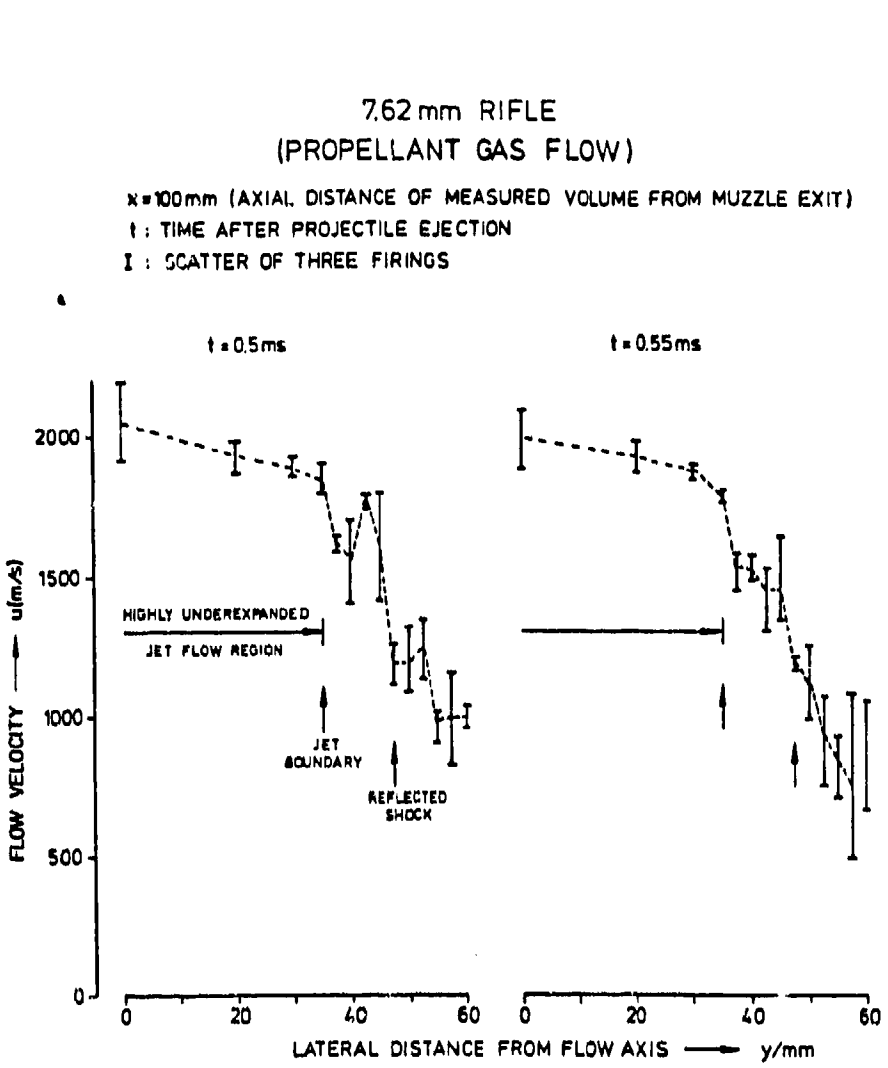

Fig. 12: Lateral velocity profiles in the main propellant gas flow of the 7.62 mm rifle at x = 100 mm from the muzzle and t = 0.5 ms and t = 0.55 ms, respectively

The above velocity profiles again provide a check on the overall procedure. The velocities in the highly underexpanded jet flow region are supersonic and gradually decrease with the lateral distance, y, from the main flow axis. These supersonic data show good agreement when compared to the data taken with the laser tracer method [4], see Figure 7. There is a decrease in velocity (in Figure 12) as both the jet boundary and the reflected shock pass the measurement point.

Figure 13 shows the lateral velocity profiles obtained downstream from the inner shock disk in the main propellant gas flow of the 7.62 mm rifle, i.e., at an axial distance from the muzzle of x = 110 mm.

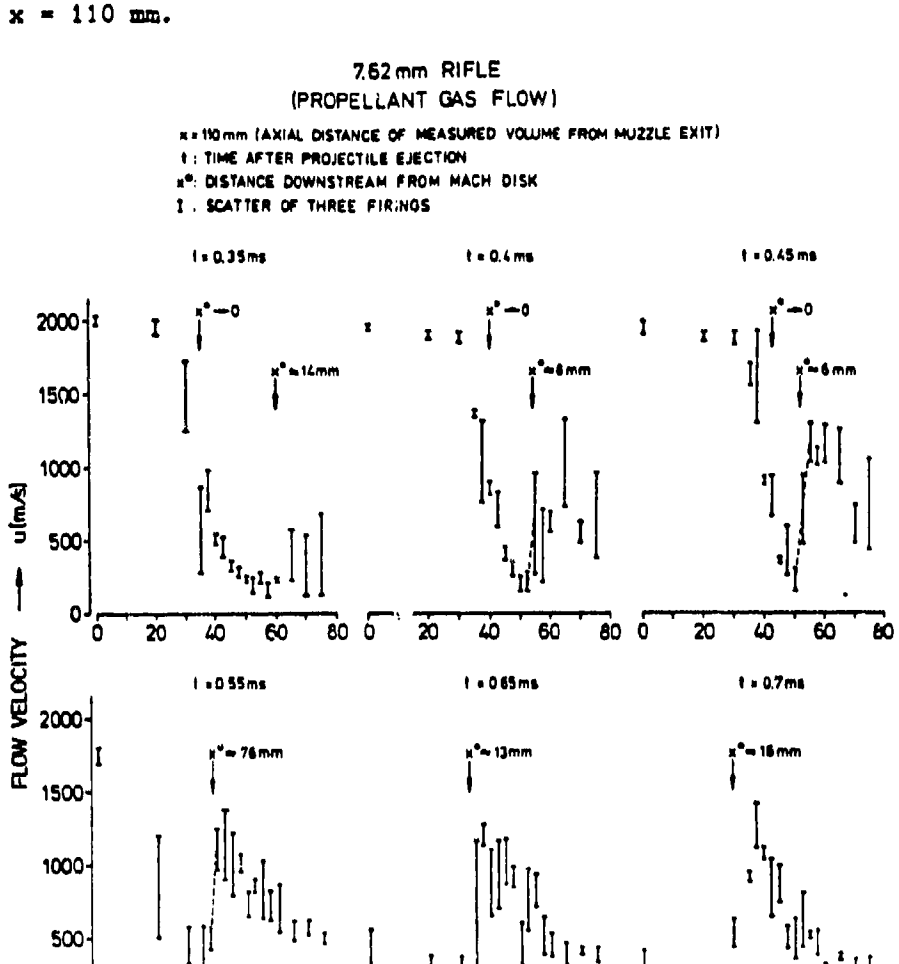

Fig. 13: Lateral velocity profiles in the main propellant gas flow of the 7.62 mm rifle at selected distances x* downstream from the inner shock disk (Mach disk), i.e., at x* = 14 mm, 8 mm, 6 mm, 7.6 mm, 13 mm, and 16 mm, respectively

For distances downstream from the inner shock disk (Mach disk) of the main propellant gas flow, i.e., for $x^* \leq 8$ mm we observe a steep gradient between lateral distances of 30 mm $\leq y <$ 40 mm. This

behavior is similar to the velocity gradient observed in Figure 11, i.e., in the precursor flow. It therefore is attributed to the formation of slip lines. However, for $x^* > 8$ mm, no steep gradient is observed. Instead we find a rather smooth transition in velocity from the centerline outward. We conclude that for $x^* > 8$ mm slip lines are no longer present.

This is confirmed in Figure 14 which shows the data taken in the main propellant gas flow at an axial distance from the muzzle of the 7.62 mm rifle at x = 120 mm.

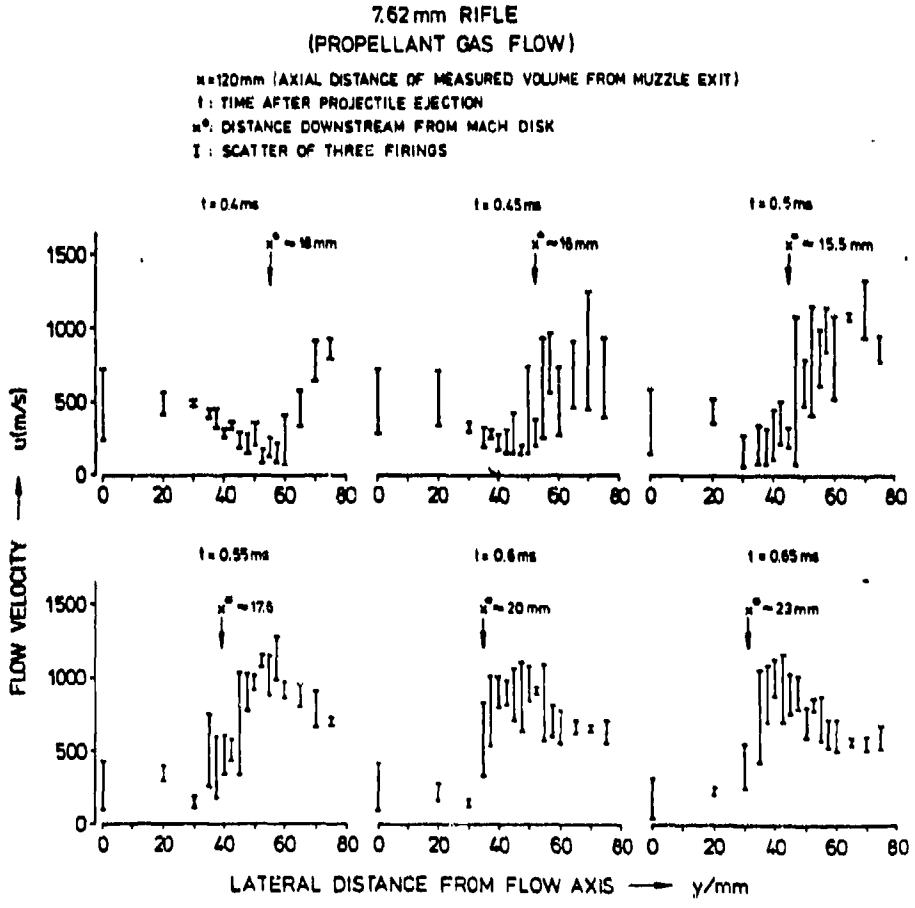

Fig. 14: Lateral velocity profiles in the main propellant gas flow of the 7.62 mm rifle at selected distances x* downstream from the inner shock disk (Mach disk), i.e., at $x^* = 18$ mm, 16 mm, 15.5 mm, 17.6 mm, 20 mm, and 23 mm, respectively

Qualitatively, we find the same behavior as in the first precursor flow of the 7.62 mm rifle. Therefore, we conclude that the formation of slip lines in the reacting main propellant gas flow is indeed hindered by, or rapidly destroyed by the turbulent flow so that they are absent at some distance downstream from the inner shock disk. This conclusion is based on the above velocity profiles, since discontinuous lateral velocity profiles indicate the presence of slip lines (see Fig. 3) while continuous ones show the absence of slip lines [20].

Section 3 described the search for slip lines formed downstream from the inner shock disk of the first precursor and the main propellant gas flow of a 7.62 mm rifle. (The normal DM 41 ammunition is used: 9.45 g projectile and 2.95 g K 503 propellant with 0.8 % KNO_3 and 0.2 % Na_2SO_4 as chemical flash suppressants.) Since there are sufficient similarities in the gasdynamics between the 7.62 mm gun and large caliber weapon firings, it is expected that the above findings can be scaled up to larger calibers. Thus, the proposed influx of oxygen into the core region of the intermediate flash as well as the proposed combustion reaction most likely occur in all conventional weapons.

As mentioned previously, the next step in the experimental program is to measure temperature differences in the intermediate flash region of the 7.62 mm rifle for firings into ambient air, nitrogen, and oxygen. If temperature differences are measured as expected, then the above hypothesis is fully confirmed. In reference 17, it has already been shown that the addition of alkali salts to the propellant charge results in a decrease of temperature in the intermediate flash region. This has already led to the conclusion that the alkali salts affect significantly chemical reactions taking place in the intermediate flash region and so prevent the ignition of the secondary flash. Therefore, the above experiment is to obtain the final approval of the hypothesis.

4. GAS GUN SIMULATION EXPERIMENTS

4.1 Introductory Remarks

In preceding papers [8,19], the importance of adequate simulation experiments has been pointed out in detail. The need to solve problems such as gun tube wear or muzzle flash and blast requires a detailed understanding of the physical and chemical processes that occur during the ballistic cycle of a gun. Such an understanding is often limited by the harsh environments encountered in actual gun firings. On the other hand, these are the very same experimental data that are required to elucidate the basic physical and chemical processes needed in the development of predictive models. The result is that existing present-day models of both the interior and transitional ballistic rely on idealizations of the flow. The solutions obtained from these models and hence their underlying assumptions are often inadequately verified by experimentation, if at all. To overcome these difficulties validation experiments using simulators have been recommended by Klingenberg and Banks [13]. The simulators permit the generation of well-defined, well-controlled, simplified flows beginning with single phase, inert flows and progressing in a step-wise fashion to more complex two-phase, reacting flows. The aim of these efforts is to isolate, identify and understand the important flow phenomena and thereby enhance the chances of successfully modelling the physical and chemical events that occur in actual ballistic flows.

Such simulation experiments are currently under way within the European Community [8]. Table 1 shows a list of such simulation experiments.

These simulators address flow problems with increasing complexity. The compression chamber at Imperial College can consider two-phase flows but is limited to inert gases or particles, and to low pressures and low temperatures. The shock tube facility at the German-French Research Institute (ISL) is used to simulate single

Institute Country	Facility	Maximum Pressure (MPa)	Maximum Temp. (K)	Flow Status	Flow Goal
Imperial* College (UK)	Compression Chamber	1 - 10	---	Inert Two Phase	
I S L (FR/GR)	Shock Tube	15 - 50	3000	Inert One Phase	Reacting Two Phase
I S L (FR/GR)	Light Gas Gun	350 - 400	3000	Inert One Phase	Inert Two Phase
EMI-AFB* (GR)	Gas Gun	350 - 450	3000	Reacting One Phase	Reacting Two Phase

*Supported by the U.S. Army through its European Research Office

Table 1: European simulation experiments

phase, inert flows at temperatures characteristic of ballistic environments, but at pressures that are a factor of six or more lower that those encountered in ballistic flows. The goal is to study two-phase (gas/solid) reacting flows. The light gas gun facility, also at ISL, is being used to simulate single phase, inert flows at pressures and at temperatures that are characteristic of ballistic flows. The goal here is to investigate particle-laden flows. The limitation is that only inert gases and particles can be used. A gas gun facility is used at EMI-AFB to simulate single phase, reacting flows at temperatures and pressures typical of an actual gun. The goal is to address both the interior ballistic and the muzzle flow phenomena for two-phase as well as single phase flow conditions.

While each of these simulators provide the stepwise increase in complexity required for the complete understanding of multi-phase, high temperature, high pressure, reacting flows, only the

gas gun simulator at EMI-AFB permits the simulation of controllable reactive flows with characteristics similar to those of medium caliber gun systems.

4.2 The Gas Gun Simulator in Closed Bomb Mode

The EMI-AFB gas gun simulator has been constructed in two stages. The first stage of construction is the combustion chamber, shown in Figure 15.

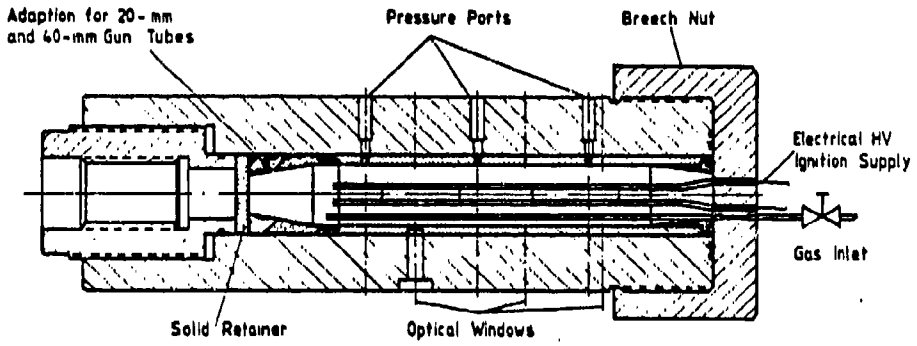

Gas Gun Chamber with Solid Retainer for Closed Chamber Combustion Studies

Fig. 15: Stage 1: Gas gun chamber in closed bomb mode

The gun chamber has a length of 550 mm and a diameter of 70 mm, resulting in a volume of approximately two liters. The inner chamber wall is protected from high pressure hydrogenation by a steel sleeve. The chamber is fitted with pressure ports and optical windows and is pre-pressurized by adding to the chamber first oxygen, then helium, and finally hydrogen in 1 : 8 : 3 mole proportions, respectively. The ignition source consists of releasing 110 J of energy from a 3 kV capacitor bank into four equally spaced exploding wires placed axially in the chamber. The solid retainer allows the chamber to be used in a closed bomb mode.

Typical data obtained in the closed bomb mode are shown in Figure 16. These data are compared to theoretical values, calculated by J.M. Heimerl of the BRL with the BLAKE code using the

virial equation of state for the case of (a) helium, (b) Argon, and (c) nitrogen as a diluent [19].

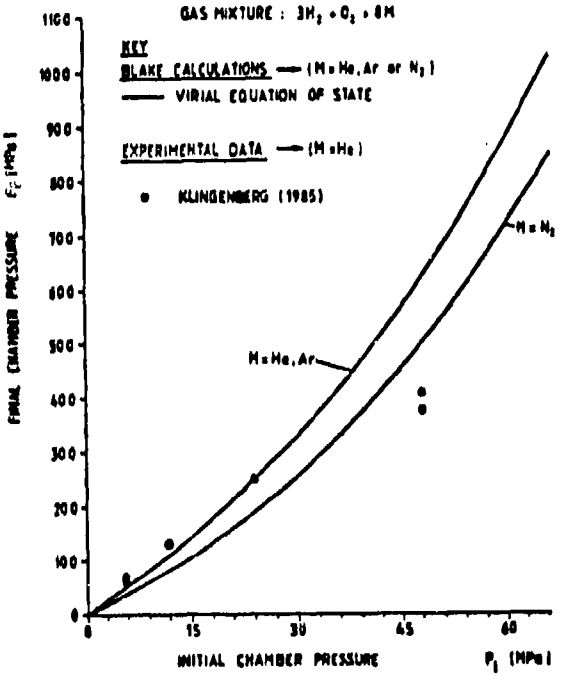

Fig. 16: Final chamber pressure versus initial chamber pressure [19]

The experimental results for the closed bomb mode show that realistic gas pressures of p_{max} = 400 MPa can be obtained in the gas gun chamber, if the gas mixture of $3H_2 + O_2 + 8He$ is pre-pressurized to about 50 MPa. One sees that at the higher pre-pressures there is a noticeable difference in the predicted and measured final chamber pressure data. This difference is attributed to heat transfer to the walls [19].

4.3 Second Stage of Gas Gun

The second stage in the construction of this simulator included a gun tube and a projectile, as shown in Figure 17. The solid retainer of the first stage (see Fig. 6) is replaced by a blow-out disk which can be scored to rupture at a pre-determined pressure. An adaptor permits the mounting of either 20-mm or 40-mm

gun tubes. For the studies reported here we used a 1.8 m long, 20-mm, smooth-bore gun tube fitted with appropriate pressure ports and optical windows.

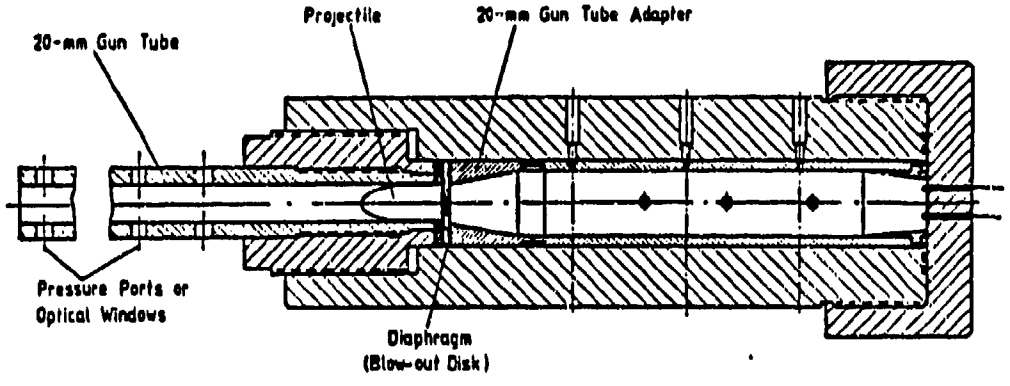

Fig. 17: Stage 2 of gas gun simulator

This configuration permits the study of both interior and transitional ballistics. Since we are dealing with particularly simple chemistry, i.e., suitably diluted hydrogen and oxygen, the gun simulator is expected to be a tool for the reproducible generation of muzzle flash and its suppression by alkali salt additives. We report here the first results of this gun simulator used in the study of muzzle flash.

The test setup used is shown in Figure 18. Pressure ports along the gas gun (M1 to M6), visible and infrared detectors and a drum camera for high-speed photography were the diagnostic tools used in these first experiments.

For the first tests, the exploding wires mentioned above ignited the gas mixture. Later, "soft" ignition by means of a single tungsten wire, placed axially in the chamber, was also tested. The voltage pulse applied across this hot wire is shown in Figure 19. This "soft" ignition yielded the same ballistic performance as the ignition with the exploding wires. The advantage is that the "soft" ignition does not introduce additional particles into the gas gun flow.

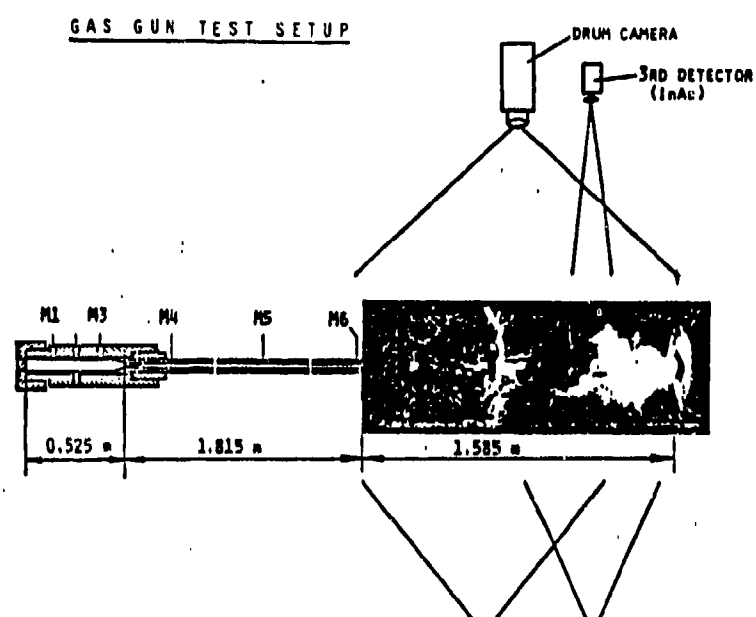

Fig. 18: Test setup for muzzle flash studies with the gas gun

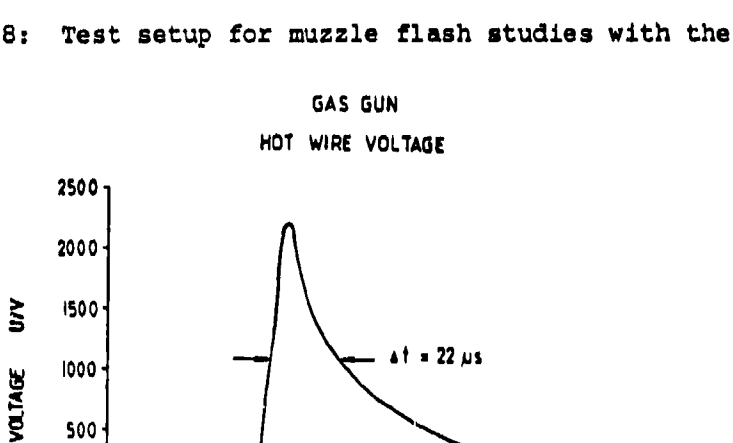

Fig. 19: Hot wire voltage versus time

The filling procedure also is very important. First, the gases were filled into the chamber following the procedure used for the closed bomb mode, i.e., we filled the chamber with oxygen, followed by helium and hydrogen. However, severe pressure oscillations were encountered and in two cases we experienced detonation in the gas

gun chamber [19]. Therefore, in the following experiments, we added a hydrogen/helium premixture to the oxygen. Then no pressure oscillations were found anymore in the pressure versus time recordings.

4.4 Results

Typical pressure histories, recorded at the pressure ports M1, M3, M5, and M6, respectively, are shown in Figure 20. Here, exploding wires and a pre-pressure of 24 MPa was used as well as a premixed He/H_2 gas mixture. Obviously, in these light gas mixtures,

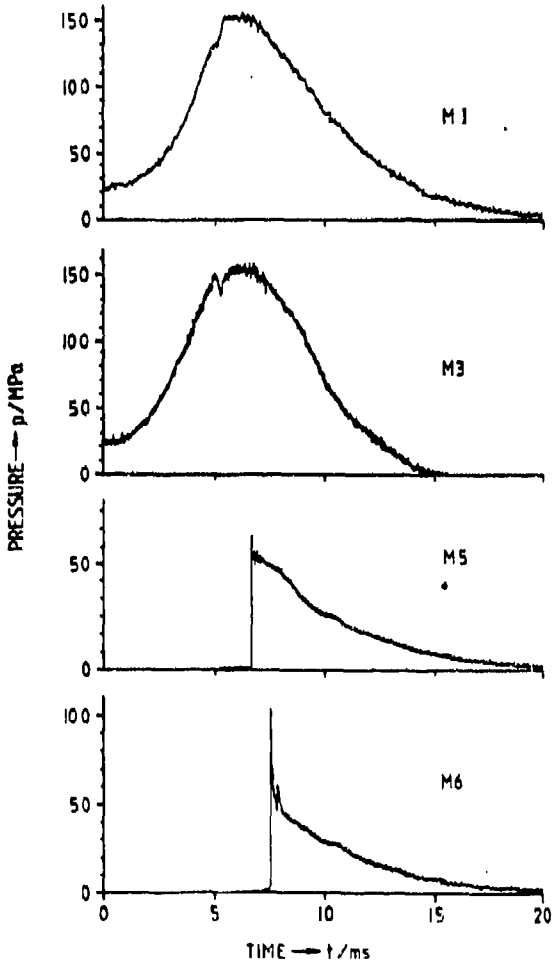

Fig. 20: Typical pressure histories at M1 to M6

a rather steep pressure spike is obtained at M6, i.e., at the muzzle exit of the gas gun.

The pressure histories are changed when we add alkali salts (2 wt% K_2CO_3) to the gas mixture in the gun chamber, Figure 21.

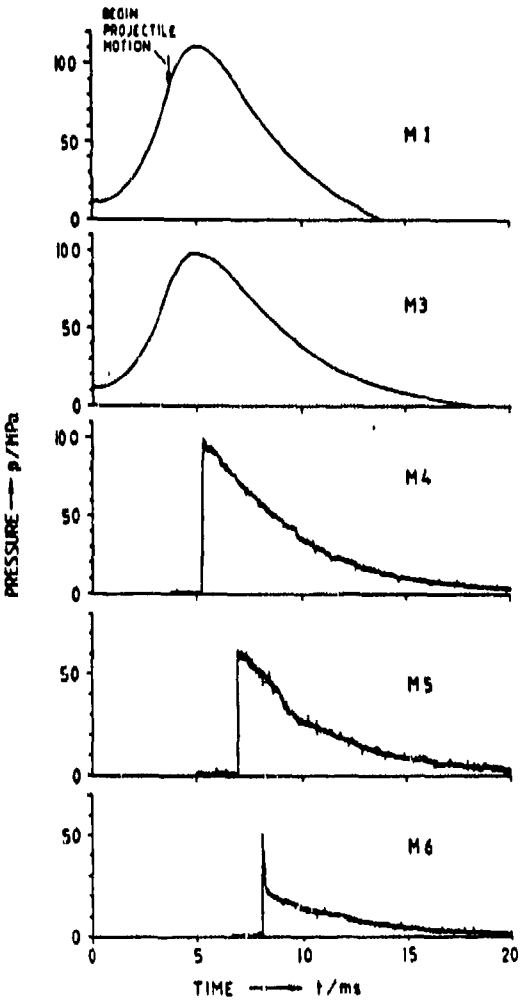

Fig. 21: Pressure histories at 12 MPa pre-pressure and with 2 wt% K_2CO_3 (premixed He/H_2 gases)

With K_2CO_3 we obtain an earlier and slightly steeper pressure rise in the chamber pressure. The comparison shown in Figure 22 emphasizes that gas mixtures with and without alkali salts have different pressure histories. Obviously, as in conventional solid gun propellants, the "vivacity" of the gaseous propellant increases

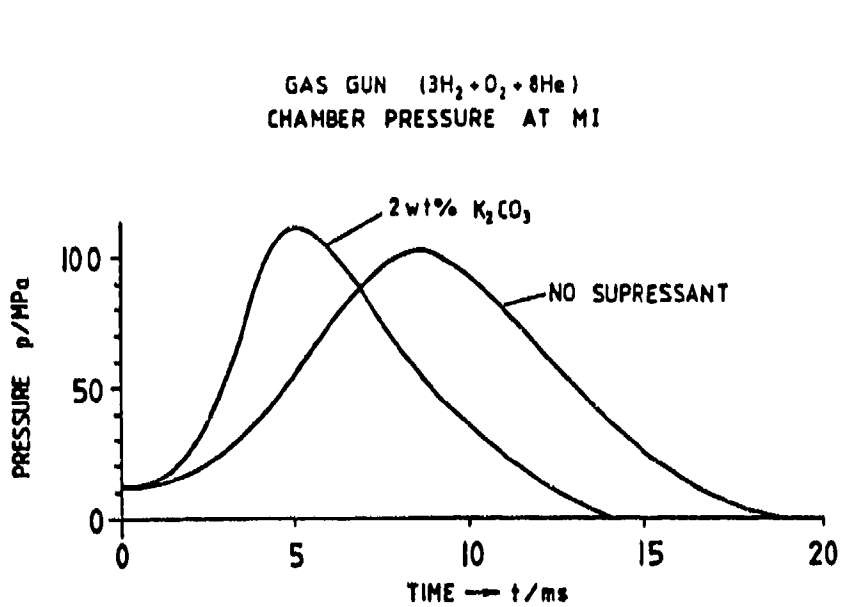

Fig. 22: Comparison of chamber pressure histories (Pre-pressure 24 MPa)

with the addition of alkali salts.

On the other hand, these alkali salts inhibit or suppress completely the secondary flash of the gas gun. For example, Figure 23 shows the time integrated photographs of the muzzle flash from the 20-mm gas cannon precharged with 24 MPa total pressure. The measured muzzle pressure is approximately 100 MPa (see Fig. 20). This is about twice the muzzle pressure of conventional 20-mm guns. An approximate scale is shown at the bottom of the photos in Figure 22. A comparison of the photo taken with no suppressant and that with 1 wt% K_2CO_3 shows that the secondary flash (Fig. 23b, Test No. 3, in the middle photo) is suppressed. The photo with 2 wt% K_2CO_3 also shows suppression. The line of light observed on axis at distances beyond 0.8 m is due to particles, most likely particles of unreacted K_2CO_3. (The suppressant powder was simply placed in the bottom of the chamber before pre-pressurization with the gases.)

A time-resolved, drum camera recording of the unsuppressed case is shown in Figure 24. Qualitatively, this is the typical

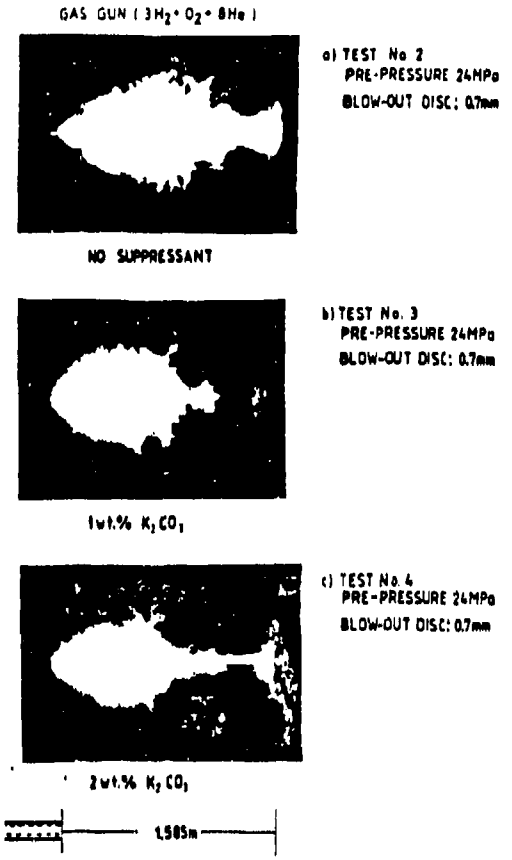

Fig. 23:
Time integrated photographs of the muzzle flash from 20-mm gas gun

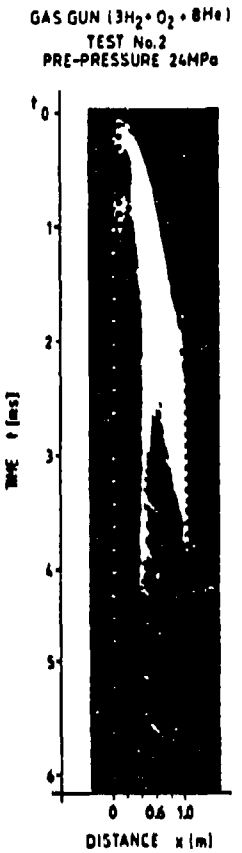

Fig. 24:
Drum camera record of unsuppressed muzzle flash from 20-mm gas gun

picture obtained in gun firings [3,43]. Though it is difficult to tell in the positive, the negative clearly shows that the secondary flash commences about 1.7 ms at a distance of about 0.7 m from the muzzle exit. Unfortunately, the camera angle did not permit the photographing of the entire 1.5 m distance between the muzzle and the projectile "catcher-box"; and so in the time-resolved photo of Figure 24 the region of the secondary flash (from about 0.7 m to 1.5 m) was truncated at 1.0 m. In the time integrated photo of Figure 23, the initiation of the secondary flash has been masked by the intensity of the intermediate flash. However, the detector

recordings, which are not presented here, have confirmed the findings indicated on the photographs. The reason that the intermediate flash is relatively so intense lies in the fact that, for the gas mixture used in the simulator, only about 9 % combustibles remain after combustion in the chamber. In actual gun firings it is known that the amount of combustibles is of the order of 50 % [44].

Thus, we have experimentally determined that mixtures of hydrogen and oxygen (suitably diluted) are sufficient to cause secondary flash. Further it has been demonstrated that amounts of alkali salts similar to those used in actual guns systems are sufficient to suppress the secondary flash. These experimental results support the supposition used by modellers [44] that only the hydrogen (and possibly the CO) chemistry are needed to describe the kinetics pertinent to muzzle flash.

5. SUMMARY AND CONCLUSIONS

The main findings of this investigation can be summarized as follows:

- Quasi-steady state conditions in gun muzzle flows are approached only at very late times in the flow development.
- The formation of the slip line has been shown to be absent in the reacting gun muzzle flow field at some distance from the inner shock disk.
- The proposed influx of oxygen in the intermediate flash region appears to be plausible.
- Specifically, the turbulence may permit oxygen to be entrained and transported even to the axis of the intermediate flash region where combustion processes may take place.

- These processes are assumed to be necessary in the ignition sequence leading to the formation of secondary flash.

- The gas gun simulator pre-charged with suitably diluted mixtures of hydrogen and oxygen permits the generation of relatively clean, reacting gas flows with realistic ballistic gas pressures and temperatures.

- The gas gun is capable of simulating the gun muzzle flash phenomena with particularly simple chemistry.

- The secondary muzzle flash produced by these hydrogen-oxygen mixtures is suppressed by the addition of alkali salts, here K_2CO_3, to the propellant charge.

Acknowledgement

The author would like to acknowledge the help and assistance of Dr. J.M. Heimerl, Mr. O. Wieland and Mrs. E. Messner. Dr. Heimerl was as an Exchange Scientist with EMI-AFB from January 26, 1985 to April 25, 1986. During his stay at EMI-AFB he contributed significantly to the above research work.

Bibliography

A. Monographs

[1] G. Klingenberg, "Experimental Diagnostics in Reacting Muzzle Flows", and

[2] J.M. Heimerl, G.E. Keller, and G. Klingenberg, "Muzzle Flash Kinetics and Modelling"
in Ludwig Stiefel (Ed.), "Gun Propulsion Technology", AIAA Progress Series, American Institute for Aeronautics and Astronautics, New York, in print

B. Journals

[3] G. Klingenberg and H. Mach, "Investigation of Combustion Phenomena Associated with the Flow of Hot Propellant Gases - I: Spectroscopic Temperature Measurements Inside the Muzzle Flash of a Rifle", Combustion and Flame 27, pp. 163-176 (1976)

[4] G. Klingenberg and G.A. Schröder, "- - II: Gas Velocity Measurements by Laser-Induced Gas Breakdown", Combustion and Flame 27, pp. 177-187 (1976)

[5] G. Klingenberg, " - III: Experimental Survey of the Formation and Decay of Muzzle Flow Fields and of Pressure Measurements", Combustion and Flame 29, pp. 289-309 (1977)

[6] G. Klingenberg, H. Mach, and G. Smeets, "Flow Field Measurements of an Unsteady Reacting Muzzle Exhaust Flow", J. of Heat Transfer, Vol. 105, pp. 884-888 (1983)

[7] G. Klingenberg, "Temperature History of the Interior Ballistic Flow of a 20-mm Cannon", J. of Ballistics, Vol. 8, No. 3, pp. 2026-2060 (1985)

[8] G. Klingenberg, E. Schmolinske, H. Mach, and F. Seiler, "Flow Simulation Experiments in Ballistics", J. of Ballistics, Vol. 8, No. 4, pp. 2089-2117 (1985)

C. Proceedings (International Meetings)

[9] G.A. Schröder and G. Klingenberg, "Investigation of Flow Phenomena Associated with the Muzzle Flash of Small Caliber Guns", Proc. 1st International Symposium on Ballistics, Orlando, Florida, November 1974

[10] G. Klingenberg and H. Mach, "Experimental Study of Non-Steady Phenomena Associated with the Combustion of Solid Gun Propellants", Proc. 16th Symposium (International) on Combustion, pp. 1193-1200, 1976

[11] G. Klingenberg, "Analysis of Gun Muzzle Flash", Proc. 4th International Symposium on Ballistics, Monterey, California, October 1978

[12] H. Trinks and G. Klingenberg, "Gun Muzzle Blast Field Research: Multiphase Flow Aspects and Chemistry of Muzzle Flash Including Chemical Flash Suppression", Proc. 6th International Symposium on Ballistics, Orlando, Florida, October 1981

[13] G. Klingenberg and N.E. Banks, "Review on Interior Ballistic Research: State-of-the-Art of Computational and Experimental Efforts", Proc. 6th International Symposium on Ballistics, Orlando, Florida, October 1981

[14] G. Klingenberg, H. Mach, and G. Smeets, "Probing of the Unsteady Reacting Muzzle Exhaust Flow of 20-mm Gun", AIAA/ASME 3rd Joint Thermophysics, Fluids, Plasma and Heat Transfer Conference, St. Louis, Missouri, June 1982

[15] J.M. Heimerl and G. Klingenberg, "Gun Muzzle Flash and its Suppression", Proc. 7th International Symposium on Ballistics, The Hague, The Netherlands, April 1983

[16] G. Klingenberg, "Temperature History of the 20-mm Gun Interior Ballistic Flow From Ignition to Shot Ejection", Proc. 8th International Symposium on Ballistics, Orlando, Florida, October 1984

[17] G. Klingenberg and J.M. Heimerl, "The Effect of Chemical Flash Suppressants on Intermediate Flash", Proc. 8th International Symposium on Ballistics, Orlando, Florida, October 1984

[18] G. Klingenberg, "Measurements of Important Ballistic Flow Properties by Spectroscopic Techniques", Proc. AGARD 66th Specialist Meeting "Interior Ballistics of Guns", Florence, Italy, September 1985

[19] G. Klingenberg, J.M. Heimerl, and E. Schmolinske, "Simulation Experiments - Gas Gun Simulator", Proc. 9th International Symposium on Ballistics, Royal Military College of Science, Shrivenham, England, April 1986

[20] J.M. Heimerl and G. Klingenberg, "New Evidence for the Role of Turbulence in the Ignition of Secondary Flash", Proc. 9th International Symposium on Ballistics, Royal Military College of Science, Shrivenham, England, April 1986

D. EMI-AFB Laboratory Reports

[21] G.A. Schröder, "Strömungsuntersuchungen mit Hilfe des laserinduzierten Gasdurchbruchs", ABF Report No. 12/69, 1969

[22] G.A. Schröder, "Experimentelle Untersuchungen zur Strömungsausbildung in der Pulvergasglocke", AFB Report No. E 4/71, 1971

[23] G. Klingenberg, "Untersuchungen des Mündungsfeuers am Infanteriegewehr G 3", ABF Report No. 1/73, 1973

[24] G. Klingenberg, "Nachverbrennungserscheinungen im Mündungsleuchten eines Infanteriegewehres", ABF Report No. 3/73, 1973

[25] G. Klingenberg, "Spektroskopische Temperaturmessungen im Mündungsleuchten eines Infanteriegewehres", ABF Report No. 2/74, 1974

[26] G. Klingenberg, "Mündungsfeueruntersuchungen bei Verwendung eines Pulvers ohne Feuerdämpfungszusatz", ABF Report No. 3/74, 1974

[27] G. Klingenberg und H. Mach, "Spektroskopische Temperaturmessungen im unmittelbaren Mündungsbereich eines Gewehres", ABF Report No. 4/74, 1974

[28] H. Behrens, G. Klingenberg, H. Mach und F. Rössler, "Vergleich der Treibgasausströmung aus einer Pulverrakete und aus einem Gewehr", ABF Report No. E 9/74, 1974

[29] G. Klingenberg und G.A. Schröder, "Strömungsgeschwindigkeitsmessungen in der Treibgasausströmung eines Infanteriegewehres mittels laserinduziertem Gasdurchbruch", ABF Report No. 1/75, 1975

[30] G. Klingenberg, "Experimentelle Untersuchungen zur Strömungsausbildung vor der Mündung von kleinkalibrigen Waffen", ABF Report No. 5/75, 1975

[31] G. Klingenberg, H. Mach und O. Wieland, "Spektroskopische Temperaturmessungen in der Pulvergasströmung vor der Mündung eines 20-mm-Gasdruckmessers", EMI-AFB Report No. 1/76, 1976

[32] G. Klingenberg, H. Mach, H. Masur, U. Werner und O. Wieland, "Spektroskopische Temperaturmessungen in der Pulvergasströmung im Rohr und an der Mündung einer Maschinenkanone Mk 20", EMI-AFB Report No. 2/76, 1976

[33] G. Klingenberg, "Analysis of Flow and Combustion Phenomena in Transitional Ballistics", EMI-AFB Report No. E 19/77, 1977

[34] G. Klingenberg, "Investigation of Multiphase Flows Encountered in Ballistics Applications", EMI-AFB Report No. E 2/81, 1981

[35] G. Klingenberg, and H. Trinks, "Gun Muzzle Blast Field Research: Multipnase Flow Aspects and Chemistry of Muzzle Flash Including Chemical Flash Suppressants", EMI-AFB Report E 11/81, 1981

[36] G. Klingenberg and N.E. Banks, "Review on Interior and Transitional Ballistic Research: State-of-the-Art of Computational and Experimental Efforts", EMI-AFB Report No. E 12/81, 1981

[37] G. Klingenberg, "Mündungsfeuer und Rauchbildung", EMI-AFB Report No. E 16/81, 1981

[38] G. Klingenberg and J.M. Heimerl, "Investigation of Gun Muzzle Exhaust Flow and Muzzle Flash", EMI-AFB Report No. 1/82, 1982

[39] G. Klingenberg, "Hypothese zur Mündungsfeuerbildung und -dämpfung", EMI-AFB Report No. E 1/83, 1983

[40] J.M. Heimerl and G. Klingenberg, "Gun Muzzle Flash and Its Suppression", EMI-AFB Report No. E 5/83, 1983

[41] G. Klingenberg and E. Schmolinske, "Simulation Experiments on Reacting Two Phase Ballistics Flows - Gas Gun Simulator", EMI-AFB Report No. E 15/83, 1983

[42] G. Klingenberg, "Mündungssignatur von Rohrwaffen", EMI-AFB Report No. E 1/84, 1984

[43] G. Klingenberg, "Experimental Diagnostics in Reacting Muzzle Flows", EMI-AFB Report No. E 12/84, 1984

[44] J.M. Heimerl, G.E. Keller, and G. Klingenberg, "Muzzle Flash Kinetics and Modelling", EMI-AFB Report No. 1/85, 1985

[45] J.M. Heimerl, G. Klingenberg, and F. Seiler, "Note on Muzzle Flash Suppression During the Firing of a Gun" (An English Translation of the Paper by P.M. Demougin entitled: "Note sur l'extinction des lueurs dans le tir", Memorial des Poudres, 1932/33), EMI-AFB Report No. T 1/86, 1986

[46] J.M. Heimerl and G. Klingenberg, "Comparison of the Flow Expansion at the Nozzle of a Solid Fuel Rocket and the Muzzle of a Rifle" (A Translation of the ABF Report E 9/74), EMI-AFB Report No. T 2/86, 1986

[47] J.M. Heimerl, G. Klingenberg, and F. Seiler, "Inhibition of Afterburning of Solid Propellant Rocket", (An English Translation of the Paper by Kubota et al., J. of the Industrial Explosives Society Japan, 1981), EMI-AFB Report No. T 3/86, 1986

KINETICS NETWORKS AND MEFF-CODE PREDICTIONS -- A PROGRESS REPORT

by

J. M. Heimerl and G. E. Keller

Interior Ballistics Division, Ballistic Research Laboratory
Aberdeen Proving Ground, MD 21005-5066

Background

The designers of new weapons systems and sub-systems can test for the presence or absence of secondary muzzle flash by direct empirical testing or by recourse to the recently developed muzzle flash prediction code, MEFF. The development of this model and its more fundamental assumptions has been previously discussed [1,2]. A key feature of the MEFF code is the incorporation of a suppression reaction network composed of elementary kinetic reactions, which permits the continual improvement of the code as more and better kinetic data are obtained.

To construct a reaction network one must know:
a) the identity of the kinetically important chemical species;
b) the reaction network that describes how these species interact; and,
c) the rate coefficients that determine how fast these species interact.

Because no experiments have been made that systematically identify the chemical species and measure their relative abundances, we are forced to estimate the species that are important in the suppression of muzzle flash by potassium salts. It has been known that the effluent from a gun that fires conventional ammunition contains large quantities of hydrogen and carbon monoxide [3-5]. More recently it has been demonstrated that a gas gun pre-charged with hydrogen and oxygen (suitably diluted with helium) can operate at pressures and temperatures characteristic of a fielded gun [6]. Moreover, it was shown that these mixtures of hydrogen and oxygen are sufficient to cause secondary muzzle flash. Thus, the inclusion of the species that correspond to hydrogen and carbon monoxide combustion are appropriate. In References 1 and 2 it is shown that these species are H, O, OH, H_2, O_2, HO_2, H_2O, CO and CO_2. Because air is involved, N_2 is also included, but only as a diluent.

For the selection of the suppressant species we consider K, KO, KO_2, and KOH by analogy with the sodium inhibition studies of Hynes, Steinberg and Schofield [7]. Support for the inclusion of KO_2 comes from the recent tenative identification of this species [8]. Since the muzzle effluent is known to be fuel rich the species KH is also considered.

Thus the 14 reactive species shown in Table 1 and the diluent N_2 form the set of species under current consideration. We wish to stress here that the selection of species shown in Table 1 is speculative. Those chosen to carry the combustion are quite reasonable. However, those selected to carry the suppression mechanism are on much less firm ground. This is important because our formulation of the kinetic

network, as previously discussed [1,2,9], is more or less mechanical once the species have been selected.

TABLE 1. LIST OF ACTIVE SPECIES

		enthalpy (kcal/mole)	entropy (cal/mole/K)	reference
1	H	52.10	27.40	a (p. 106)
2	K	21.30	38.30	b
3	O	59.60	38.50	a (p. 132)
4	H_2	0.00	31.20	b
5	KH	26.30	47.30	c, b
6	KO	17.50	56.90	c, b
7	OH	9.50	43.90	d
8	O_2	0.00	49.00	b
9	HO_2	3.50	54.40	e, b
10	H_2O	-57.80	45.10	b
11	KOH	-54.50	56.90	c, b
12	KO_2	-25.00	62.00	f
13	CO	-26.40	47.20	b
14	CO_2	-94.10	51.10	b

a) J. Phys. & Chem. Ref. Data, Vol. 4, 1975.
b) JANAF Thermochemical Tables, Second Edition, 1971.
c) J. Chem. Thermo., Vol. 14, pp. 1103-1113, 1982.
d) J. Phys. & Chem. Ref. Data, Vol. 3, p. 443, 1974.
e) J. Phys. Chem., Vol. 87, pp. 3479-3482, 1983.
f) Refs. 1 & 2 (see also: BRL Tech. Rep. BRL-TR-2622, Dec. 1984.)

Current Work

Table 2 shows the network of reactions considered in this report. It essentially the same as derived in [1,2] with changes being made only to a few rate coefficients. It is these changes and their effect upon the MEFF-code predictions that constitute the subject matter for the remainder of this report.

The rate coefficient for reaction (27) has been changed from the derived value of 0.25E-30/T [7] to the more recent value of 0.128E-25/T**(1.28) $cm^6/molecule^2/sec$ [10].

In addition the rate coefficient for reaction (28) has been measured using two different experimental techniques. Silver, et al. [11] have used a flow reactor to measure the rate coefficient over the temperature range 300-700K. Husain and Plane [12] have employed time resolved atomic resonance spectroscopy to measure this rate coefficient at 753 and 873K. Figure 1 shows the values of these rate coefficients for nitrogen as the chaperon plotted against temperature. Since reaction (28) is thought to be a crucial one in this suppression network, the difference in the values at high temperatures might prove important. E.g. at 2000K the difference is approximately a factor of two.

TABLE 2. NETWORK OF REACTIONS

	reaction	A	B		C
1	$OH + H_2 = H_2O + H$	0.17E-15	-1.6		-3298.8
2	$H + O_2 = OH + O$	0.20E-06	0.9		-16573.2
3	$O + H_2 = OH + H$	0.25E-16	-2.0		-7551.4
4	$H + O_2 + M = HO_2 + M$	0.55E-29	0.8		0.0
5	$H + HO_2 = OH + OH$	0.25E-09	0.0		-1003.5
6	$H + HO_2 = H_2 + O_2$	0.42E-10	0.0		-693.5
7	$OH + HO_2 = H_2O + O_2$	0.33E-10	0.0		0.0
8	$O + HO_2 = OH + O_2$	0.33E-10	0.0		0.0
9	$H + H + M = H_2 + M$	0.50E-29	1.0		0.0
10	$H + H + H_2 = H_2 + H_2$	0.27E-30	0.6		0.0
11	$OH + OH = O + H_2O$	0.25E-14	-1.1		0.0
12	$H + KO_2 = KO + OH$	0.12E-09	0.0		0.0
13	$KO + H_2O = OH + KOH$	0.17E-09	0.0		0.0
14	$H + KOH = K + H_2O$	0.17E-10	0.0	***	0.0
15	$H + KO = K + OH$	0.33E-10	0.0		0.0
16	$H + KO_2 = O + KOH$	0.33E-11	0.0		0.0
17	$H + KO_2 = K + HO_2$	0.33E-10	0.0		0.0
18	$K + HO_2 = O + KOH$	0.66E-13	0.0		0.0
19	$K + HO_2 = KO + OH$	0.33E-11	0.0		0.0
20	$O + KO = K + O_2$	0.33E-11	0.0		0.0
21	$O + KO_2 = KO + O_2$	0.17E-11	0.0		0.0
22	$H_2 + KO = H + KOH$	0.83E-09	0.0		0.0
23	$KO + OH = O + KOH$	0.10E-09	0.0		0.0
24	$KO + HO_2 = OH + KO_2$	0.33E-11	0.0		0.0
25	$KO + HO_2 = O_2 + KOH$	0.17E-09	0.0		0.0
26	$OH + KO_2 = O_2 + KOH$	0.50E-12	0.0		0.0
27	$K + OH + M = KOH + M$	0.13E-25	1.3	***	0.0
28	$K + O_2 + M = KO_2 + M$	see text for values used			
29	$KO + KO = K + KO_2$	0.17E-09	0.0		0.0
30	$H + KO + M = KOH + M$	0.83E-30	1.0		0.0
31	$O + KO + M = KO_2 + M$	0.83E-30	1.0		0.0
32	$K + O + M = KO + M$	0.83E-30	1.0		0.0
33	$H + KH = K + H_2$	0.17E-09	0.0		0.0
34	$O + KH = H + KO$	0.83E-10	0.0		0.0
35	$O + KH = K + OH$	0.83E-10	0.0		0.0
36	$KH + KO = K + KOH$	0.17E-09	0.0		0.0
37	$KH + OH = H + KOH$	0.17E-10	0.0		0.0
38	$KH + OH = K + H_2O$	0.17E-09	0.0		0.0
39	$KH + O_2 = K + HO_2$	0.17E-09	0.0		0.0
40	$H + KO_2 = KH + O_2$	0.17E-09	0.0		0.0
41	$H + K + M = KH + M$	0.83E-30	1.0		0.0
42	$CO + OH = H + CO_2$	0.73E-17	-1.5		741.0
43	$CO + O_2 = O + CO_2$	0.42E-11	0.0		-47800.0
44	$CO + HO_2 = OH + CO_2$	0.25E-09	0.0		-23590.0
45	$CO_2 + O = CO + O_2$	0.28E-10	0.0		-52580.0
46	$CO_2 + H = CO + OH$	0.27E-09	0.0		-26300.0
47	$O + CO + M = CO_2 + M$	0.15E-33	0.0		4540.0
48	$KO + CO = K + CO_2$	0.17E-09	0.0		0.0

The rate coefficient = A x T**(-B) x exp(C/RT)
where A in units of cm-particle-sec
C in units of calorie/mole

Table 3 shows the MEFF predictions using the above changes in the rate coefficients for three mortar and several artillery cases. The propellant and its additive (if any) are shown in the first column. The second and third columns, labelled "Husain" and "Silver", respectively, show the maximum temperature computed by the MEFF code. Our interpretation is associated with each of these computed temperatures. "F" means that flash is predicted and "N" means that suppression of the flash (i.e., no flash) is predicted. Column five shows the field observations where available.

One other series of computations was made using only the two-step suppression mechanism recommended by Jensen, Jones and Mace [13]. For these computations the reaction network given in Table 2 was dramatically reduced. Only reactions (14) and (27) were retained as the suppression mechanism (See *** in Table 2) and all other reactions involving potassium species were deleted from the network. This left 19 reactions. The rate coefficients for reactions (14) and (27) were taken from [13], i.e. for reaction (14): $k=1.8E-11*\exp(-1987/RT)$ $cm^3/molecule/sec$ and for reaction (27): $k=1.5E-27/T$ $cm^6/molecule^2/sec$. The results of these MEFF code computations can be seen in column four, labelled "Jensen", of Table 3.

TABLE 3. MODEL PREDICTIONS

	MAXIMUM TEMPERATURE			
	HUSAIN	SILVER	JENSEN	Observation
81-mm MORTAR PROPELLANT				
Nominal M10 from which the suppressant has been removed.	---2100=F---		2048=F	Flash
Nominal M10 which contains about 1% K_2SO_4 suppressant.	1157=N	1159=N	2312=F	No Flash
Nominal M10 but with 2% K_2SO_4 suppressant.	1149=N	1149=N	2189=F	No Flash
155-mm HOWITZER PROPELLANT				
Nominal M30A1 from which the suppressant has been removed.	---2084=F---		2084=F	Flash
Nominal M30A1 which contains 1% K_2SO_4 suppressant.	1081=N	1082=N	2175=F	Flash
Nominal M30A1 but with 2% K_2SO_4 suppressant.	1064=N	1064=N	1061=N	
Nominal M30A2 which includes 2.7% KNO_3 suppressant.	1095=N	1095=N	2113=F	Occasional
HMX with L-35 polyether binder.	859=N	846=N	859=N	

Discussion

As can be seen in Table 3, the results of the MEFF computations with the reaction network as shown in Table 2 are not sensitive to differences in the values of the rate coefficient for reaction (28) (See Figure 1). In fact all of the cases in which there is suppressant added to the propellant are computed not to flash (See Table 3). This leads to the suspicion that there is something amiss with the suppression network itself. One possibility is the following.

For values of those reaction rate coefficients which have not been measured we had adopted gas kinetic rate coefficients that are independent of the temperature. More realistic coefficients might be able to be established by analogy with reactions for which the rate coefficient has been measured. E.g. the hydrogen analogue of reaction (19) is reaction (6); and so the value of the rate coefficient for reaction (6) could be adopted as the value for reaction (19). These type of changes have yet to be made.

The wholesale substitution of the two-step suppression mechanism proposed by Jensen and coworkers [13] leads to improved predictions for the 155-mm howitzer cases, but this mechanism also leads to incorrect predictions in the 81-mm mortar cases. Since all properties of the MEFF code except the kinetic suppression mechanism have been held fixed, one can make the plausable assumption that the differences between the computed and observed results are due to the change in the kinetic mechanism. We suggest that the mechanism proposed [13] is in fact a global one. If this is the case then it becomes extremely difficult to see how one could improve it. On the other hand, the general methodology of network development employed [1,2] allows for the evolution and improvement of the network shown in Table 2.

As stated above, the identity of the alkali-containing species is crucial in the establishing of the reaction network. We need to know what species are present during the suppression of muzzle flash. Because the transient nature of gun muzzle flash makes a species survey quite difficult, a likely technique would be a mass-spectrometric determination of the species present during the inhibition of a suitable flat flame.

References

[1] J.M. Heimerl, G.E. Keller and G. Klingenberg, "Muzzle Flash Kinetics and Modelling," Fraunhofer-Institut fuer Kurzzeitdynamic, EMI-AFB Report 1/85, May 1985.

[2] J.M. Heimerl, G.E. Keller and G. Klingenberg, "Muzzle Flash Kinetics and Modelling," to appear in AIAA Progress Series On Gun Propulsion Technology, L. Stiefel, Ed.

[3] "Lehrbuch Der Ballistik" by C. Cranz, Springer Verlag, Berlin, 1926, See Vol. 2 "Innere Ballistik," p. 185.

[4] S.P. Carfagno, Handbook on Gun Flash, The Franklin Institute, Nov. 1961.

[5] G. Klingenberg and J.M. Heimerl, "Investigation of Gun Muzzle Exhaust Flow and Muzzle Flash," Fraunhofer-Institut fuer Kurzzeitdynamic, EMI-AFB Report 1/82, 1982.

[6] G. Klingenberg, J.M. Heimerl and E. Schmolinske, "Simulation Experiments - Gas Gun Simulator," The Proceedings of the 9th International Symposium on Ballistics, 29 April - 1 May, 1986, at the Royal Military College of Science, Schrivenham, England, pp 1-57 through 1-63.

[7] A.J. Hynes, M. Steinberg and K. Schofield, "The Chemical Kinetics and Thermodynamics of Sodium Species in Oxygen-Rich Hydrogen Flames," J. Chem. Phys., Vol. 80, pp 2585-2597, 1984.

[8] J.W. Hastie, K.F. Zmbov and D.W. Bonnell, "Transpiration Mass Spectrometric Analysis of Liquid KCl and KOH Vaporization," High Temperature Science, Vol. 17, 1984, pp 333-364.

[9] D. Indritz, M. Maday and R. Sheinson, "Construction of Large Reaction Mechanisms," NRL Report 8498, October 1981.

[10] D. Husain, J.M.C. Plane and C.C. Xiang, "A Direct Kinetic Study of the Reaction K+OH+He-->KOH+He by Time-resolved Molecular Resonance-fluorescence Spectroscopy, OH(A-X), Coupled with Steady Atomic Fluorescence Spectroscopy, K(5P-4S)," J. Chem. Soc., Faraday Trans. 2, Vol. 80, 1984, pp 1465-1483.

[11] J.A. Silver, M.S. Zahniser, A.C. Stanton and C.E. Kolb, "Temperature Dependent Termolecular Reaction Rate Constants For Potassium and Sodium Superoxide Formation," Twentieth Symposium (International) on Combustion, The Combustion Institute, 1984, pp 605-612.

[12] D. Husain and J.M.C. Plane, "Kinetic Investigation of the Third-order Rate Processes between $K+O_2+M$ by Time-resolved Atomic Resonance Absorption Spectrocopy," J. Chem. Soc., Faraday Trans. 2, Vol. 78, 1982, pp 1175-1194.

[13] D.E. Jensen, G.A. Jones and A.C.H. Mace, "Flame Inhibition by Potassium," J. Chem. Soc., Faraday Trans. 1, Vol. 75, 1979, pp 2377-2385.

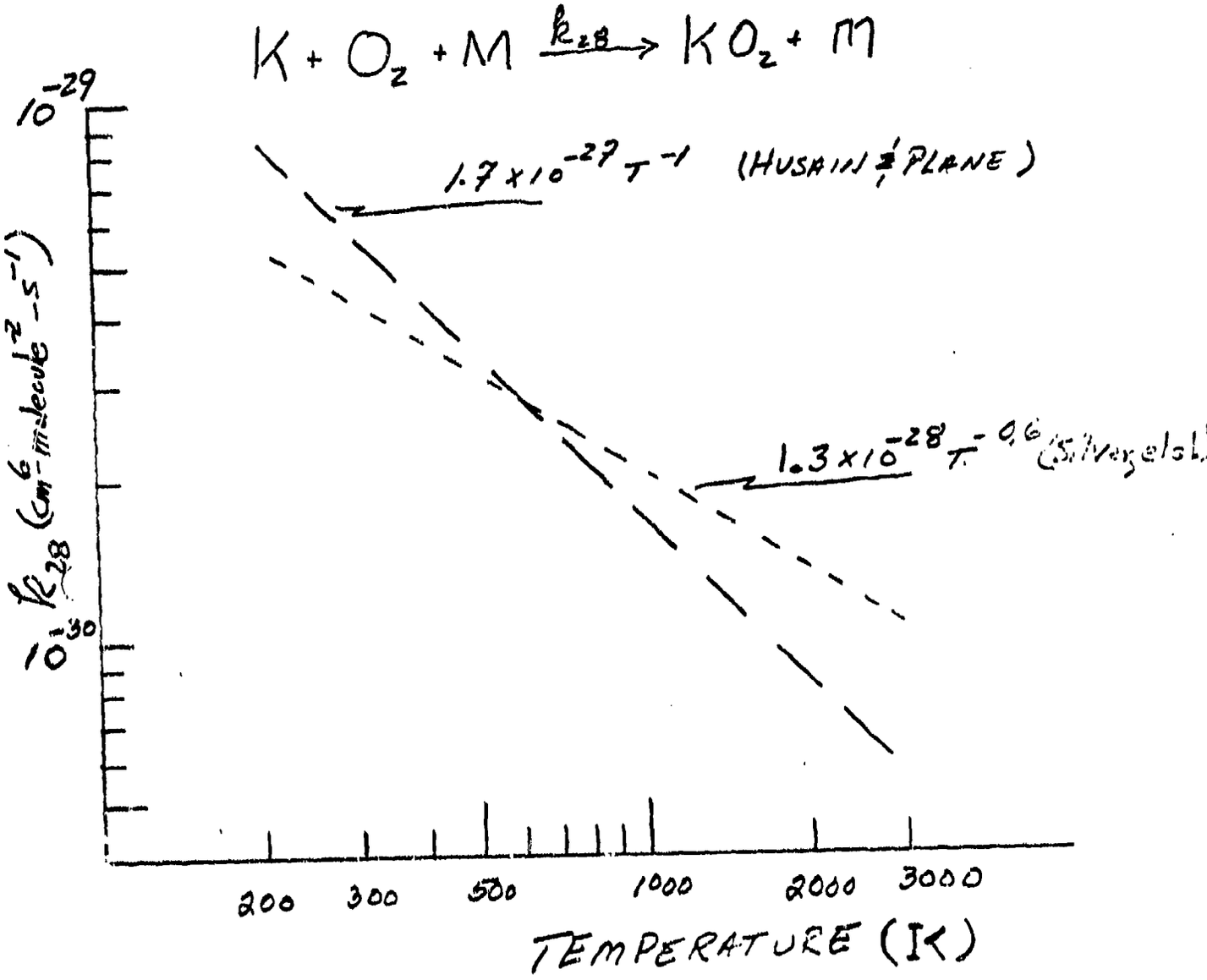

Fig. 1 Rate Coefficient for Reaction (28) vs. Temperature

Flash Simulation with a Global Reaction Model for Transient Flow from the 84 mm Carl Gustaf Rifle+

By

M.B. Khalil,* E.G. Plett,* and D.H. Gladstone**

Abstract

The paper begins with a brief review of the state-of-the-art of previous work on gun flash. Then a description is given of the approach taken to implement reaction kinetics in the computations of the flow from the 84 mm Carl Gustaf recoilless rifle to determine the effect of secondary flash on the blast noise signature. The conservation equations are modified to include conservation of several species which are allowed to exist in each of the cells of the computational grid. An Arrhenius model is used to describe the reaction rate between the species that can burn, with combustibles considered as one species. This is utilizing a one-step global reaction.

Results of computations implementing this approach in a finite difference code which computes the transient flow for the breech nozzle of the Carl Gustaf rifle are presented. Results of the numerical computations show that even such a simple approach illustrates the important factors regarding the effect of secondary flash on blast noise. It was found that the blast noise (peak over-pressure) increases noticeably as the amount of combustibles in the breech effluent increases if ignition of a combustible mixture is permitted according to the Arrhenius rate equation.

The approach, however, may need to be expanded to include a wider list of species and a more comprehensive list of chemical reactions. This can be done as an extension of the present approach. Flux-corrected transport and turbulence effects should also be incorporated in the code in order to improve the accuracy of the simulation of the real phenomena.

---

* Asecor Ltd., P.O. Box 929, Manotick, Ontario K0A 2N0 Canada

**Defence Research Establishment Valcartier, Quebec, P.Q. Canada

+ Based on work supported by DND, Defence Research Establishment, Valcartier under contract 8SD85-00063

Review of Gun Flash

As the projectile moves in the barrel toward the muzzle, some of the fuel-rich propellant gas may leak through the clearance between the projectile base and the inner surface of the barrel.[1] These propellant gases will mix with the air in the barrel ahead of the projectile or in front of the muzzle and form a combustible mixture that gets ignited at the muzzle producing 'preflash'. Preflash can also arise from forcing out of the air in the barrel (or the gases from a previous firing) in front of the projectile. This air or gases are at high temperature and therefore would glow at the muzzle. The same phenomenon can be found in the Carl Gustaf recoilless rifle after the pressure in the combustion chamber reaches shot-start pressure and the diaphragm closing the recoil nozzle breaks. The release of the projectile from the muzzle allows a sudden burst of high temperature, high pressure gases to leave the barrel and mix with the ambient air and therefore burn in what is termed 'primary flash'. The gases effluent from the muzzle in this case form an underexpanded jet which is then allowed to expand to atmospheric pressure while attaining a very high velocity (in the supersonic range in the order of 2000 m/s).[2] Although the projectile situation is absent in the breech side of the Carl Gustaf rifle, which prevents primary flash from taking place, the underexpanded jet still forms in this case with the subsequent increase in velocity upon expansion in the ambient air. This high velocity stream on either side of the gun makes way for the formation of a normal shock wave (Mach disc) which keeps on moving downstream away from the gun. As the gases pass through the Mach disc, their temperature will rise and thereby glow with radiation in the visible range producing 'intermediate flash'.[3] Following the Mach disc, the gases will continue to expand and mix with the atmospheric air. Due to the fact that a large portion of the gas flowing from the muzzle is made of CO and H_2 (up to 70%),[1] especially from the breech of the Carl Gustaf[2] where unburnt propellant particals may also exist, it can form a combustible mixture as it mixes with the ambient air. If the temperature of the mixture is near the self ignition temperature, or some burnt particles are present to initiate combustion, the mixture will ignite and produce 'secondary flash'. The strength of the blast resulting from the reactions causing the previously described flashes is much less than that associated with the secondary flash.[1,5,6] Also, the light accompanying the secondary flash surpasses in its brightness the summation of that from the other flashes. Photographs from firings of the Carl Gustaf show clearly that the glow from the breech side is much brighter and of a larger extent than that from the muzzle. These photos support, until now, the hypothesis that a large portion of the propellant escapes unburned with the breech gases and gets ignited outside the

gun producing this huge glow and strong blast. Figure 1 shows several schematic drawings of the various flashes encountered from the muzzle.

There are three main factors affecting secondary flash. The first relates to chemical factors such as propellant composition,[7,8,9] the presence of flash suppressants[10,11,12,13] and flame temperature of the propellant. Physical factors include the thermodynamic condition of the propellant gases at the muzzle or breech ends (temperature, pressure and velocity) and the location, extent and strength of the Mach disc in the flow passage. The third group of factors are those of mechanical nature such as flash hiders, muzzle extensions, muzzle brakes, baffles and liners (on the breech side).

The intense brightness of gun flash reveals the presence of the gun and leads to identifying its location by the enemy troops. Also, the bright glow of gun flash at night causes momentary blindness for the gun crew. The blast noise resulting from gun flash adds to the original blast signature, and the blast from gun flash exceeds all other blasts in its over-pressure strength, which has a serious consequential effect on the hearing ability of the gun crew.[1,15,20]

Approaches for Preventing Gun Flash

Over the years of development and applications of guns, several approaches have been introduced to overcome or eliminate gun flash. These approaches are summarized by classifying them as follows:

Mechanical Devices[14,16]

These are simply attachments of conical or slotted shape fitted at the muzzle end. At the breech end, liners of various shapes and geometry can be utilized. These devices are used to enhance cooling of the propellant gases as they gradually mix with the ambient air to bring the temperature of the mixture below that of self ignition. This delays the formation of a combustible mixture allowing for the cooling effect by the diffusion of the ambient air to bring the temperature down. Some mechanical devices would allow the gases to expand in a controlled passage for some distance to prevent the formation of the Mach disc entirely, and thereby prevent the secondary flash onset which results from the temperature rise as the gases pass through the Mach disc.

Aqueous Foams[17,18]

This is similar in its approach to the mechanical devices. It is carried out by installing a box or a bag at the muzzle and/or breech ends of the gun after filling the box or the bag with aqueous foam (similar to shaving cream). This

was found to eliminate gun flash (including preflash, primary and intermediate) and reduced the blast noise by ~10 db when applied to the muzzle end. No such application has been attempted with recoilless rifles such as the Carl Gustaf, to date.

Chemical Additives[10,11,12,13,19,33]

This is the most widely used approach for flash suppression. These additives are, in general, small proportions (1-6%) of alkali salts (sodium or potassium) mixed with the propellant charge. The additives that are used on a large scale are K_2SO_4, KNO_3 and $K_2C_2O_4$. The complete list of the additives in use as flash suppressants and their evaluation can be found in a report by Heimerl et al.[33] from BRL and EMI-AFB. Several research programs were carried out to investigate the mechanism of flash suppression by alkali salts.[10-13,33] Some of these tests were performed on actual firings of guns using propellant charge with different additives at various proportions. Other tests were performed using a shock tube approach by blending gases from commercial gas bottles to simulate the mixture from the muzzle and performing some tests to determine the effectiveness of the various additives in suppressing gun flash. There is a general agreement among researchers that gaseous KOH is the inhibiting species in potassium salts. Recent studies[20,31] suggest that alkali salts act as flame supressents by altering the chemical composition of the fuel-rich muzzle effluent and thereby increasing the ignition delay time or ignition limit. This delay is enough to allow further cooling of the mixture as it mixes with the ambient air and hence no flash occurs. This delay may, on the other hand, provide a chemical pathway that effectively competes with the chain-branching reaction and thus depletes the pool of radicals. It is believed that in a fuel-rich H-C-N-O combustion process, the reaction which promotes secondary flash is the chain branching reaction:[20]

$$H + O_2 \text{ ---> } OH + O + 71 \text{ kJ/mole} \quad (1)$$

Several researchers suggested that flame inhibition occurs via the reaction:

$$KOH + H \text{ ---> } H_2O + K - 138 \text{ kJ/mole} \quad (2)$$

or

$$KOH + OH \text{ ---> } H_2O + KO + 22 \text{ kJ/mole} \quad (3)$$

Reactions (2) and (3) were studied carefully by Heimerl and Klingenberg,[20] and they concluded that these two reactions are oversimplified explanations of suppression mechanisms by KOH. They suggested a further detailed study to be carried out to identify the real intermediate reactions which take place during flash inhibition by KOH.

A comparison was done by Heimerl et al.[33] of the flash supressing compounds in terms of their effectiveness as reported by researchers from various establishments. They found that the effectiveness results are at variance from one report to another. A unification of conditions and test equipment, however, is needed for a fair basis of comparison.

Firing of guns, the propellant charge of which contains alkali salts as flash suppressant results in increase in smoke production.[21,22,32] This is considered a serious drawback of suppressing flash by means of chemical additives, because smoke will reveal the gun location if the gun is fired during the day.

Encapsulated Oxanide Coolant[22]

Brodman et al. introduced, in a U.S. patent, another approach to suppress secondary flash without adding alkali salts to the propellant charge and thereby eliminate smoke production. Their approach uses a 'novel' propellant with more energetic nitramine composition and a microencapsulated oxanide coolant additive to cool the gases effluent from the weapon. The oxanide is encapsulated with gelatin and the resulting microcapsules are coated with a plastic resin. The coating is made to survive the ignition conditions in the combustion chamber of the gun and decomposes during travel along the barrel to cool exiting gases and hence eliminate flash. Test firing of the 7.62 mm M14 rifle with 2.4% coolant resulted in complete elimination of secondary flash and smoke. The idea, however, seems to suit the muzzle side more than the breech side, unless recoil compensation is accomplished with a counter projectile.

Techniques for Prediction of Secondary Flash

Several techniques have been developed to predict the onset of gun flash through knowledge of propellant composition, including suppressant additives, to aid charge designers and reduce the expensive cost of experimental testing. Some models rely completely on chemical reaction rates (chemical kinetics of the reaction network involved) in their prediction, others need the results of actual experimental firings of the same propellant charge (and suppressant). Given below is a brief overview of the various models developed for this purpose.

Analytic Models

Muzzle Exhaust Flow Field Model (MEFF)

This model was developed by Yousefian,[23,24] to describe muzzle exhaust flow field. The model, Figure 2, assumes 1-D flow of the gas exiting from the muzzle downstream to the position of the Mach disc. Then the gas expands as it mixes with the entrained air. Yousefian uses the LAPP[34] code, a $2\frac{\varepsilon}{A}$ model which describes the mixing and chemical reaction processes downstream of the Mach disc, to compute the properties of the mixture after the temperature rise it encountered as it passed the Mach disc. Empirical correlations were used in MEFF to locate the position of the Mach disc and to estimate its diameter. The initial reactions network used by Yousefian in MEFF employed 13 reactions and 13 atomic and molecular species.[25] However, later on,[15] the same number of species was linked by an 'extended kinetics' reaction network of 25 reactions. Presently[33] the reaction network includes a set of 55 reactions, but some of them are deleted from the network due to their small contribution in comparison with other reactions. Heimerl et al.[33] describe the final network of reactions as single-bond-breaking reactions and gives the constants for 48 of them as pertaining to gun flash. Ignition which leads to flash in the Yousefian model is indicated by a sharp rise in the temperature of the mixture as the temperature of the mixture is calculated versus the axial distance measured from the muzzle end. Figure 3 shows a sample of temperature plots versus distance for various proportions of chemical suppressants.[15] A more recent listing of the code MEFF together with a User's Manual was prepared by Keller[26] of BRL. This latest version describes in more detail the other programs which MEFF uses to compute the various boundary conditions in the field in addition to interior ballistics in the gun.

Standard Plume Flow Model (SPF)

This model was used at BRL,[29] after being developed by the Aerochem Research Laboratories for AFRPL. Therefore, it is originally a rocket flow code and not intended to perform gun flash computations. The version used at BRL starts with the conditions at the exit plane of the rocket nozzle and calculates the size and locations of the Mach disc and barrel shock. The code BOAT within SPF performs detailed time stepping calculations, using detailed chemistry, of the pressure, temperature, density, etc. downstream of the Mach disc. SPF predicts the onset of flash in a similar fashion to MEFF, i.e. by a sharp rise in the temperature of the mixture. The code originally has 9 species and 10 equations for their reaction kinetics which are many less than MEFF. The code also does not include suppressant chemistry.

The code requires supersonic flow at the nozzle exit plane and cannot handle the starting of subsonic or sonic flows. This implies that more development is needed in this code if it is to be used as a gun flash prediction tool.

Algebraic Models

Carfagno's Model[27]

This model has evolved after extensive experimental investigation, using shock tubes, regarding the occurrence of gun flash under different conditions. Through these experiments,[8,9] Carfagno developed a set of ignition temperature limits of air and propellant gas at atmospheric pressure. Five propellants are simulated by allowing the shock tube to contain 40-70% combustibles of CO and H_2. The muzzle gas combustibles were simulated from commercial gas bottles and then mixed with air and water vapour. The mixture was placed in a shock tube and subjected to the incident and reflected waves in order to achieve the required pressure (atmospheric) and temperature.

Figure 4 shows the ignition temperature results obtained from these tests.[27] Using these ignition temperature limits, Carfagno[27] developed a 1-D model to characterize the flow process that led to ignition. Figure 5 shows the model developed by Carfagno in which he assumes that the propellant gas expands isentropically to atmospheric pressure, mixes with ambient air, passes through the Mach disc where its temperature is raised, re-expands to atmospheric pressure and finally ignites if the mixture temperature exceeds the specified limits of Figure 4.

Carfagno, May and Einstein Model (CME)

May and Einstein[28] found out that their experimental measurements do not agree with the flow model suggested by Carfagno, Figure 5. They suggested that only the propellant gas (instead of propellant gas mixture) passes through the Mach disc in the exhaust plume. They developed a model, shown in Figure 6, in which the propellant gas expands to atmospheric pressure, passes through the Mach disc and re-expands to atmospheric pressure where mixing with air takes place followed by possible ignition. The muzzle exit conditions used by May and Einstein were more correct compared to those used by Carfagno due to the use of an improved interior ballistics model.

Schmidt's Model[1,6,29]

Figure 7 shows a schematic drawing of the model developed and used by Schmidt.[1,6] He used the same interior ballistic model that May/Einstein used to compute the gas condi-

tions at the muzzle exit. He allowed for the expansion to continue to sonic if the initial exit velocity is subsonic. Schmidt utilized the assumption of the MEFF model of Yousefian to make the Carfagno/May/Einstein model (CME) more realistic. The jet plume is approximated as a steady plume with shock structure and mixing of the propellant gas streams processed through the lateral shocks and the Mach disc as in MEFF. Mixing of the propellant gas and air is assumed to be instantaneous, 1-D as in the CME model. Schmidt also used the ignition temperature criterion developed by Carfagno[27] to determine the flash onset of the mixture. Schmidt suggested that in order to account for the transient development of the flow, the decay of the muzzle properties should be computed in an approximate manner and then coupled with the descriptions of growth and decay of the propellant gas plume and associated air blast. The model also includes allowance for the presence of muzzle brakes.

Algebraic Criterion by Yousefian[15]

Due to the complexity of the MEFF model,[23,24] Yousefian developed a simpler model using an algebraic criterion. It predicts the onset of flash based on conditions which lead to continuous (monotonic) growth of the concentration of the minor species (H, OH, O and HO_2). This was done by analyzing the conservation equations[2] of the minor species along any streamline (to justify neglecting the effects of turbulent mixing). From the chemical reaction rates of the minor and major species (H_2O, CO, H_2, CO_2, O_2 and KOH), neglecting turbulent and diffusion effects, Yousefian arrived at a set of linear differential equations. Several simplifications were made by Yousefian based on analysis of the order of magnitude, to solve the set of linear differential equations. From the solution of these linear differential equations, he gives the algebraic criterion in the form of non-equality relating the oxygen concentration in the mixture to the concentration of the suppressant in the propellant and the absolute temperature of the mixture as follows:

$$Y < Y^0 = \frac{1.0}{1.0 + 0.214 X_{09}\ \mathrm{Exp}(7250/T)}$$

where Y = concentration of oxygen (or KOH) in mixture

X_{09} = concentration of suppressant in propellant

T = absolute temperature of mixture

Flash onset is predicted if the value of Y becomes equal to or greater than that of Y^0. Figure 8 (taken from Ref. 15) shows a plot of Y vs Y^0 for three different suppressant concentrations.

Yousefian conducted several experiments as well as numerical predictions with both MEFF and the algebraic criterion models. He found that results from the algebraic criterion were consistent with predictions of MEFF and with experimental observations.

Implementing Secondary Flash Predictions Into the Computations of JET

JET is a FORTRAN computer code which computes the transient compressible flow in 2-D cylindrical coordinates. Detailed description of the numerical technique used in JET together with several important features can be found in a paper by Plett et al.[35] which describes the usage of JET to compute the flow resulting from the open end of a shock tube. The driving conditions for JET, therefore, can be those from a shock tube code or quasi-steady conditions at the exit section of a pipe or a nozzle. The original purpose of developing JET, however, was to be used with an interior ballistics code REGUN developed at DREV[36] to provide the driving conditions to compute the breech flow or the muzzle flow of a recoilless rifle.[37] Application of JET to compute the overpressure at some selected positions in the flow passage from the open ended shock tube showed, in general, satisfactory agreement with experimental measurements.[35] On the other hand, the application of JET to perform similar computations for the flow resulting from the breech of the 84 mm Carl Gustaf rifle did not agree with experimental measurements.[38] The reason was attributed to the absence of chemical kinetics in the computations of JET, especially on the breech side where some propellant particles might escape without burning inside the combustion chamber of the gun, but ignite on contact with the ambient air. This hypothesis was supported by visual observation of actual firings of the gun which produces a huge ball of bright light on the breech side behind the gun.

Reviewing the various modelling approaches developed thus far for secondary flash prediction, as given earlier, provided basis for our approach to be utilized in the computations of JET. The absence of any detailed available experimental data on the secondary flash of the Carl Gustaf rifle implied that such models requiring experimental results cannot be used here. These models include Carfagno's, Carfagno/May/Einstein's and Schmidt's as well as the algebraic model developed by Yousefian. Due to the fact that their models, in addition to requiring experimental testing to be done in most cases, have the computations end upon predicting whether

the propellant gases will flash or not. This implies that they cannot be used in the computations of JET to predict the effect of secondary flash on the flow characteristics.

At this point we turned our attention to the models which predict secondary flash numerically such as MEFF or SPF models. The MEFF code was made available to us. After code was installed on our Network of Apollo Computers, several statements and commands had to be changed or replaced to get the code operational. Following the success of getting MEFF operational, it was realized that it requires a very long time on our mini-computers to perform a complete cycle of computations. This implies that utilizing MEFF in JET on a transient basis is very impractical and it will tax our computers for uneconomically long periods of time. Added to this is the fact that MEFF starts its computations from the position of the Mach disc, whereas the JET code requires consideration of the entire computational grid extending from the nozzle.

The Approach Followed in the Code JET to Account for Chemical Kinetics

The approach followed to account for chemical kinetics in the computations of JET stems from the very basis of deriving the finite difference equations used in JET. This was carried out by allowing for several species to exist in the computational field. As a first approximation to determine the validity of the approach, it was decided to consider three species only to coexist in the flow field. These species were assumed to be oxygen, inerts (including nitrogen and completely burnt propellant gases) and combustibles in the propellant gas. It was realized shortly after developing the required code that nitrogen should have been considered as a separate species, however, this is very easy to implement and the source term for nitrogen is zero. A separate conservation equation is used for each of the species considered with a source term. The momentum equations are similar to those in the previous version of JET, but the energy equation contains a source term due to the energy released upon combustion of the fuel in the flow field. The finite difference equations are derived for both steps, as described in Ref. 35, by applying the conservation principles to a suitable control volume. The source term, for the present development, was only considered in the second step, but implementing it in both steps is straightforward, if considered necessary. The finite difference equations for the first and second steps are given below in the matrix form:

$$U^{n+1/2}_{i,j+1/2} = \frac{1}{2}\{U^{n}_{i,j} + U^{n}_{i,j+1}\} + \frac{1}{2}\frac{\Delta t}{\Delta z}\{F^{n}_{i,j} - F^{n}_{i,j+1}\}$$

$$+ \frac{1}{2}\frac{\Delta t}{\Delta r}\{a\, G^n_{i-1/2,j+1/2} - b\, G^n_{i+1/2,j+1/2}\}$$

$$U^{n+1/2}_{i+1/2,j} = \frac{1}{2}\{U^n_{i,j} + U^n_{i+1,j}\} + \frac{1}{2}\frac{\Delta t}{\Delta z}\{F^n_{i+1/2,j-1/2}$$

$$- F^n_{i+1/2,j+1/2}\} + \frac{1}{2}\frac{\Delta t}{\Delta r}\{c\, G^n_{i,j} - d\, G^n_{i+1,j}\}$$

where $U = \begin{bmatrix} \rho_O \\ \rho_I \\ \rho_F \\ \rho v_z \\ \rho v_r \\ \rho e \end{bmatrix}$ $F = \begin{bmatrix} \rho_O v_z \\ \rho_I v_z \\ \rho_F v_z \\ \rho v_z^2 + p \\ \rho v_z v_r + \tau_{zr} \\ (\rho e + p) v_z \end{bmatrix}$

$G = \begin{bmatrix} \rho_O v_r \\ \rho_I v_r \\ \rho_F v_r \\ \rho v_z v_r + \tau_{zr} \\ \rho v_r^2 + p \\ (\rho e + p) v_r \end{bmatrix}$

$$a = 1 - \frac{\Delta r}{2r} \quad , \quad b = 1 + \frac{\Delta r}{2r} \quad , \quad c = \frac{1}{1 + \frac{\Delta r}{2r}} \quad , \quad d = \frac{1 + \frac{\Delta r}{r}}{1 + \frac{\Delta r}{2r}}$$

$$\rho = \rho_O + \rho_I + \rho_F$$

The subscripts O, I, F stand for oxygen, inerts and fuel (combustibles) repectively.

$$U_{i,j}^{n+1} = U_{i,j}^{n} + \frac{\Delta t}{\Delta z}\{F_{i,j-1/2}^{n+1/2} - F_{i,j+1/2}^{n+1/2}\}$$

$$+ \frac{\Delta t}{\Delta r}\{a\, G_{i-1/2,j}^{n+1/2} - b\, G_{i+1/2,j}^{n+1/2}\} + S$$

where $S = \begin{bmatrix} S_O \\ S_F \\ S_F \\ 0.0 \\ 0.0 \\ S_h \end{bmatrix}$ = source term array

It should be noted here that subscripts i,j (or full subscripts) refer to quantities at the node of the cell whereas i,j $\pm$1/2 (or half subscripts) refer to quantities at the boundaries of the cell.

The source terms were calculated using an Arrhenius model for the rate of reaction between the fuel (combustibles in the propellant gas) and oxidant (oxygen in the atmospheric air) assuming one step reaction as follows:

Fuel (Combustibles) + Oxidant ---> Inert Products

The combustibles in the propellant gas consist[1] mainly of CO and H_2. The lack of information regarding reaction kinetics of mixtures of CO and H_2 together with the desire to simplify our first attempt in handling the problem suggested the use of the kinetics of some known fuel in our calculations as a first approximation. We chose CH_4 due to its simplicity and wide application by several combustion researchers at the Imperial College of London University, London, England and at several American Universities. The rate of comsumption of the fuel (CH_4) given in Arrhenius form by Khalil et al.[39] is as follows:

$$R_{fu} = -m_{fu}\, \rho^2\, m_{ox}\, A \exp(-E/RT)$$

where R_{fu} = rate of reaction of fuel

m_{fu} = mixture fraction of fuel

m_{ox} = mixture fraction of oxidant

A = Arrhenius constant = 10^{10} m^3/kg s (ref. 39)

E = activation energy

R = universal gas constant, $E/R = 1.84 \times 10^4$ K (ref. 39)

T = absolute temperature K

The source term in the combustibles conservation equation is derived on the basis of the above equation. The source term for the oxidant conservation equation can be derived from the fuel source term and the stoichiometric ratio of oxidant/fuel (knowing the chemical composition of the fuel). The source term for the inert products is found from the combination of the above source terms. The source term for the energy equation is calculated from the heat of combustion of the fuel and the fuel source term. The heat of combustion of CH_4 as used by Peck[40] is 5×10^7 J/kg.

It can be noted that the effect of turbulence was neglected for the time being and ideal gas laws were assumed to apply for all the species and any mixtures thereof. The thermodynamic constants required were obtained from thermody-

namic texts and their values were also assumed to be constant, independent of temperature to simplify, as much as possible, the approach used in this model.

The effect of using a suppressant in the propellant charge is added in the form of a constant multiplier to the Arrhenius reaction rate, as follows:

$$R_{fu} = -(1 - f_s)\ m_{fu}\ \rho^2\ m_{ox}\ A \exp(-E/RT)$$

where f_s = constant depends on the effect of suppressant on the reaction rate

The suppressant constant might be introduced inside the exponential term to reflect the effect of suppressents on the active temperature of the mixture as had been followed in the Carfagno model. However, due to lack of any experimental results on suppressants to the Carl Gustaf propellant charges, it was decided to postpone use of this constant for future developments.

The occurrence of flash can be detected in the code JET if temperature history is kept for some positions, along the axis for example, and a sudden rise in temperature is encountered in any of these plots.

Results and Discussion

Four computational runs have been carried out using the JET_FLASH code for the computations of the breech flow field. The runs differred only in that one parameter changed from one run to another. This parameter is the proportion of combustibles in the breech effluent and whether reaction is allowed or not (which in some ways is equivalent to having no combustibles). The first two runs used 5% and 20% combustibles but the gases were not allowed to react, which was accomplished by switching off the reaction kinetics in the code. The other two runs contained 20 and 50% of the breech effluent as combustilbles and reaction kinetics were switched on to permit a combustible mixture in any cell in the computational field, if formed and if the temperature of the mixture is sufficient for ignition, to burn. All runs used a 60 x 90 grid of 2 cm x 2 cm cells and were allowed to perform computations over 5 ms real time following reaching shot-start pressure in the combustion chamber.

Figures 9-11 show the numerical results of over-pressure versus time for three positions in the computational field of the breech of the Carl Gustaf recoilless rifle. Figure 12 provides a schematic drawing to indicate the three positions

with respect to the Carl Gustaf rifle. In each figure three plots are given, one for 20% combustibles with reaction kinetics switched off, and the other two plots are for 20 and 50% combustibles respectively with reaction kinetics switched on. The figures show clearly the effect of implementing reaction kinetics in the numerical computations of the breech nozzle effluent. At the three positions, the negative pressure becomes less and less as more combustibles are allowed to burn in the computational field and the peak over-pressure increases as well. It should be mentioned here that the results of 5% and 20% combustibles that were not allowed to ignite by switching off the reaction kinetics, were almost identical.

Figure 13 shows the contours of pressure in the computational field for the three cases mentioned above, for the previous figures. It can be seen that the main features of the pressure contours did not change appreciably upon allowing the combustible mixture to ignite or increase in amount. However, the details of the contours vary from one plot of one run to another and the maximum pressure experienced with the 50% combustibles which were able to ignite was 3207.3 kPa wheras the corresponding value for the 20% case was 2978.7 kPa, a difference of about 10%. This is expected due to the release of the chemical energy which is added to the sensible energy of the mixture in the cell and thereby increases the value of pressure as it is computed from the energy utilizing the ideal gas equation of state but allowing for a co-volume coefficient.

Figure 14 shows a sequence of contour plots of the oxidant density at several times following shot-start pressure for the 50% combustibles case where ignition was permitted. The figure shows the development of the jet as well as the diffusion of oxygen from the ambient air into it. The contours up to 1.0 ms indicate also the location of the Mach disc; but, due to the numerical diffusion implemented in the code for stability reasons, the position of the Mach disc is smeared over a broader region in the computational field. The oxidant contours become monotonically uniform after ~2.0 ms which indicates that the underexpanded jet has begun to decay. This was confirmed by the fact that the same shape of contours was obtained for the 20% case with combustion permitted as with the 5% case where no combustion was permitted in the computational domain.

Figures 15 and 16 show similar contour plots for the same test case for inerts and combustibles, respectively. Again, the plots show the development of the jet as the inerts and combustibles are added to and depleted respectively. Most of the changes in the shape and magnitude of the contours occurs in the first 2.0 ms. The location and extent of

the Mach disc can be identified in these contour plots up to 2.0 ms then diffusion of the species dominates the entire computational field.

Examining the Figures 14-16 and comparing the shape of the contours obtained with three of the 5% and 20% combustibles with no reaction kinetics and the 20% combustibles where reaction kinetics was switched on, revealed the fact that the shape of the contours does not change appreciably among them. Figure 17 shows the contours of the density of oxidant, inerts and combustible at 1 ms for the three run 5% combustibles with no reaction kinetics, 20% and 50% combustibles with reaction kinetics, as a sample of the various cases. It can be seen from the figure that only very specific details that change from one set of contours to another whereas the main shape remains unchanged. The difference in the quantitative value for each contour is understood due to the variation in the proportion of the combustibles in the breech effluent.

Figure 18 shows the contours of the density of combustibles at 5.0 ms for the three test cases indicated in Figure 17. Figure 18 indicates that the diffusion of combustibles in the flow where reaction kinetics were permitted is much smoother than the case where reaction kinetics was switched off. This is concluded from the stepping shape of the contours for the case where combustion was not permitted and the extent of the zero contour in the computational field.

Figure 19 shows the contours of the mass fraction of oxidant, inerts and combustibles after 1 ms, for the test case of 5% combustibles with no reaction kinetics. The figure indicates the smoothness of these fractions contours; however, they do not reflect any important features of themselves or about the flow.

Summary and Conclusions

The paper outlines a simple approach to include reaction kinetics in the computations of the transient flow from the 84 mm Carl Gustaf recoilless rifle. The approach includes implementing a global reaction rate model of the Arrhenius type to describe the rate of consumption of combustibles in the computational field. Those species were assumed to exist simultaneously in the cells of the computational grid. Separate mass conservation equations were derived for each of the species with a source term in each of the equations. The momentum equations do not have a source term, but the energy equation contains a source term due to the energy released upon ignition of the combustibles. The approach is two-dimensional axisymmetric in nature, except for the reaction rate model, and computations are performed for each cell of the computational field.

Results of test runs using the code which implemented the above mentioned approach, showed that reaction kinetics has a considerable effect on the blast noise level in the computations of underexpanded jets, such as the one from firing of the Carl Gustaf rifle.

It should be noted that several refinements, which can be easily added were not included in producing the results given in this paper. These include isolating nitrogen from inerts as a separate species which equation has no source term and applying flux-corrected transport technique in the code to produce sharper shock fronts (where shock waves are encountered) in the computational grid.

The results obtained thus far show that the approach works for what it was desired to do, and possible expansion should be straightforward. Preciseness of the code can be improved by increasing the number of species to as many as 13 and to use the 13 reactions initially used by Yousefian in MEFF. This would be done while keeping the simple form of the species conservation equation and by neglecting turbulence at the present time. If this is combined with using flux-corrected transport in the code, the results are expected to be greatly improved; and the versatility of JET will be truly enhanced.

References

1. Schmidt, E.M., "Muzzle Flash and Blast" Proc., 16th Int. Symp. on Ballistics, October 1981.

2. Klingenberg, G. and Schroder, G.A., "Investigation of Combustion Phenomena Associated with the Flow of Hot Propellant Gases II: Gas Velocity Measurements by Laser-Induced Gas Breakdown." Combustion and Flame, Vol. 27, pp 177-187, 1976.

3. Klingenberg, G. and Mach, H., "Investigation of Combustion Phenomena Associated with the Flow of Hot Propellant Gases - I: Spectroscopic Temperature Measurements Inside the Muzzle Flash of a Rifle," Combustion and Flame, Vol. 27, pp 163-176.

4. Schroder, G.A. and Klingenberg, G., "Investigation of Flow Phenomena Associated with the Muzzle Flash of Small Caliber Guns", presented at: First Int. Symp. on Ballistics, November 1974.

5. Keller, G.E., "Secondary Muzzle Flash and Blast of the British 81-mm L16A2 Mortar", U.S. Army Ballistic Research Laboratory AD-A104-324, July 1981.

6. Schmidt, E.M., "Secondary Combustion in Gun Exhaust Flows", U.S. Army Ballistic Research Laboratory, AD-A107-312, October 1981.

7. Keller, G.E., "The Effect of Propellant Composition on Secondary Muzzle Blast Overpressure." U.S. Army Ballistic Research Laboratory, AD-A127-277, April 1983.

8. Carfagno, S.P. and Rudyj, O.N., "Relationship Between Propellant Composition and Flash and Smoke Produced by Combustion Products." The Franklin Institute, Laboratories for Research and Development, March 1959.

9. Carfagno, S.P., Franklin, R.G., Rudyj, O.N. and Taylor, F.R., "Relationship Between Propellant Composition and Flash and Smoke Produced by Combustion Products", The Franklin Institute, September 1959.

10. Heimerl, J.M., "An Advanced Flash Suppression Network Involving Alkali Salts", U.S. Army Ballistic Research Laboratory, BRL-TR-2622, December 1984.

11. Cohen, A. and Decker, L., "Chemical Mechanism for Secondary Flash Suppression", 18th Symp. (Int.) on Combustion, The Combustion Institute, 1981, pp 225-231. Also in 16th JANNAF Combustion meeting, Monterey CA, Sept. 1979.

12. McHale, E.T., "Flame Inhibition by Potassium Compounds", Combustion and Flame, Vol. 24, pp 277-279 (1975).

13. Birchall, J.D., "On the Mechanism of Flame Inhibition by Alkali Metal Salts", Combustion and Flame, Vol. 14, pp 85-95, 1970.

14. Backofen, J.E. Jr., "The Development of a Muzzle Device to Suppress the Secondary Muzzle Flash on the GAU8IA Gun." Battelle-Columbus laboratories, March 1977.

15. Yousefian, V., "Muzzle Flash Onset: An Algebraic Criterion and Further Validation of the Muzzle Exhaust Flow Field Model", U.S. Army Armament Research and Development Command, U.S. Army Ballistic Research Laboratory. ARBRL-CR-00506, March 1983.

16. Walting, W.H., "Accoustical and Visual Attenuation Through Dynamic Regulation of Muzzle Gas Flow", Springfield Armory, July 1966.

17. Pater, L.L. and Shea, J.W., "Use of Foam to Reduce Gun Blast Noise Levels", Naval Surface Weapon Center, TR-81-94, March 1981.

18. Shea, J.W. and Pater, L.L., "Foam Filled Muzzle Blast Reducing Device", U.S. Department of the Navy, Patent, serial no. 352.448, Filing Date 25, February, 1982.

19. Bracuti, A.J., Bottei, L.A. and Davis, R., "Potential Multipurpose Additives - Flash Erosion Suppressant", U.S. Army Armament Research and Development, TR.83028, June 1983.

20. Heimerl, J.M. and Klingenberg, G., "Gun Muzzle Flash and its Suppression", Proceedings, Seventh Int. Symp. on Ballistics, April 1983.

21. Nardi, A.V., "Smoke Problem in 20mm VAD System: The Effect of Flash Suppressant and Antifoulent Propellant Additives", Frankford Arsenal, Philadelphia, PA., March 1973.

22. Brodman, B.W. et al, "Propellant Charge with Reduced Muzzle Smoke and Flash Characteristics", U.S. Patent, serial no. 133,946, filing date 9 April, 1980.

23. Yousefian, V., "Muzzle Flash Onset", Aerodyne Research Inc., 45 Manning Rd., Billerica, MA., ARI-RR-236, Nov. 1980.

24. Yousefian, V., May, I.W., and Heimerl, J.M., "Modelling the Occurrence of Muzzle Flash in Guns", 17th JANNAF Combustion Meeting, CPIA Publication 329, November 1980.

25. Yousefian, V. and May, I.W., "Prediction of Muzzle Flash Onset", 16th JANNAF Combustion Meeting, 1979.

26. Keller, G.E., "A MEFF (Muzzle Exhaust Flow Field) User's Guide", U.S. Army Armament Research and Development Center, ARBRL-MR-03362, July 1984.

27. Carfagno, S.P., "Handbook on Gun Flash", The Franklin Institute, Contract No. DA-36-034-501-ORD-78RD, November 1961.

28. May, I.W. and Einstein, S.I., "Prediction of Muzzle Flash", U.S. Army Armament Research and Development Command, ARBRL-TR-02229, March 1980.

29. Keller, G.E., "An Evaluation of Muzzle Flash Prediction Models", U.S. Army Ballistic Research Laboratory ARBRL-MR-03318, November 1983.

30. Klingenberg, G., "Investigation of Combustion Phenomena Associated with the Flow of Hot Propellant Gases. III: Experimental Survey of the Formation and Decay of Muzzle Flow Fields and of Pressure Measurements", Combustion and Flame, Vol. 29, pp 289-309 (1977).

31. Heimerl, J.M., "Muzzle Flash and Alkali Salt Inhibition from an Elementary Kinetic Point of View", U.S. Army Armament Research and Development Command, ARBRL-TR-02479, March 1983.

32. Brode, H.L. and Enstrom, J.E., "Interior Ballistics and Gun Flash and Smoke", United States Air Force Project RAND, RM-6127-PR, October 1969.

33. Heimerl, J.M, G.E. Keller and G. Klingenberg, "Muzzle Flash Kinetics and Modelling", EMI Report E 1/85, May 1985.

34. Dash, S.M. and H.S. Pergament, "The JANNAF Standard Plume Flowfield Model (SPF)", MICOM Technical Report RD-CR-82-9, April 1981 and Program User's Manual for interim version (SPF-1) MICOM Special Report RD-81-4, July 1981.

35. Plett, E.G., M.B. Khalil and D.H. Gladstone, "Open Ended Shock Tube Flow as a Tool to Aid Development of a Two-Dimensional Compressible Nonsteady Computer Code", AIAA-86-0120, 24th Aerospace Sciences Meeting, Jan. 6-9, 1986.

36. Gladstone, D., "A Computer Code for Analyzing the Interior Ballistics of Recoilless Rifles", DREV Report No. 4223/82, Feb. 82.

37. Gladstone, D.H., M.B. Khalil and E.G. Plett, "The JET Code: A Useful Tool for Intermediate Ballistic Analysis", Presented at the 9th International Symposium on Ballistics, England, April 1986.

38. Unpublished experimental data obtained at DREV, Sept. 1984.

39. Khalil, E.E., D.B. Spalding and J.H. Whitelaw, "The Calculation of Local Flow Properties in Two-Dimensional Furnaces", Int. J. of Heat and Mass Transfer, vol. 18, pp 775-791, 1975.

40. Peck, R.E., "Eddy Viscosity Modelling in the Prediction of Combustion-Chamber Flows", Ph.D. thesis, University of California, Irvine, 1976.

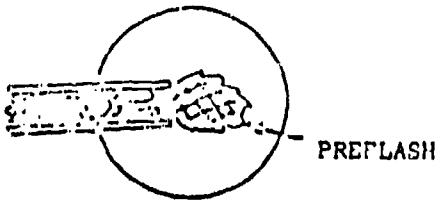

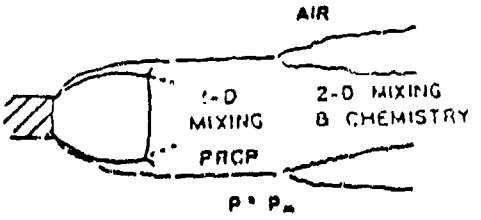

Figure 2. Yousefian flow model.

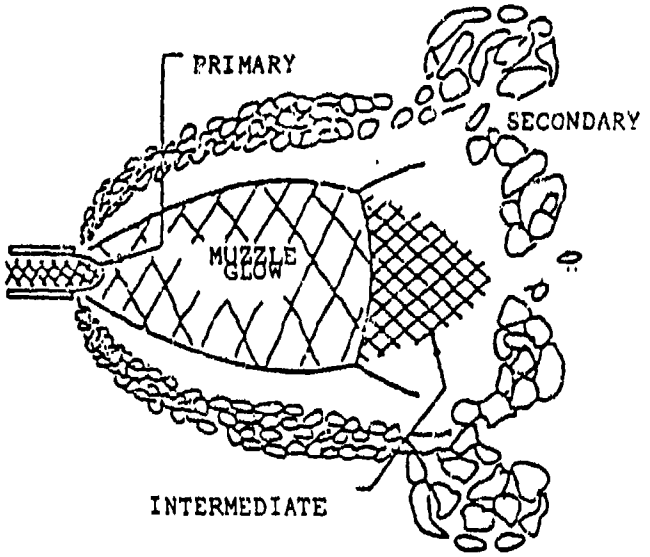

Figure 1. Schematic of muzzle flashes.

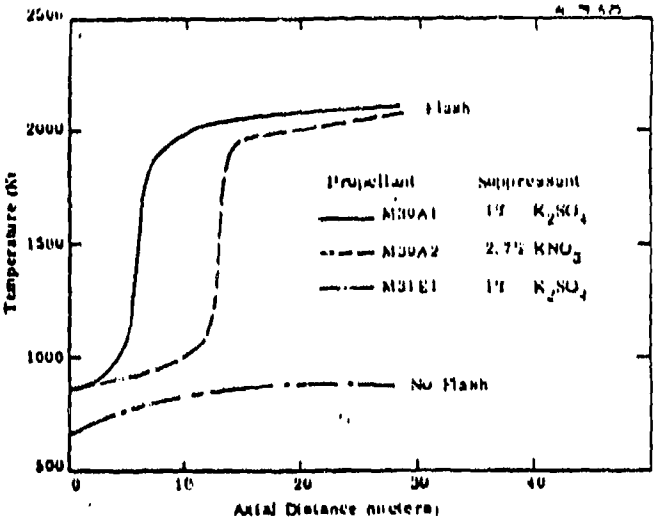

Figure 3. Predicted Maximum Axial Plane Temperature of Plume versus Propellant Type (Distance Measured From Normal Shock).

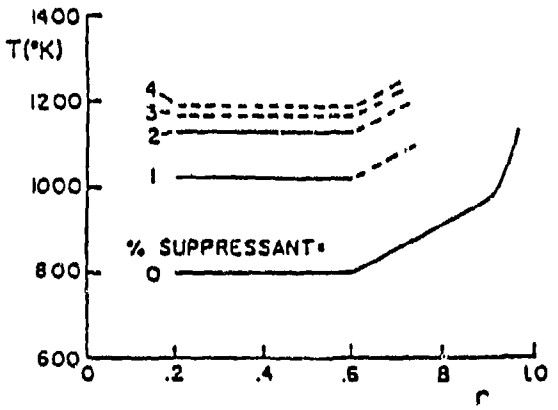

Figure 4. Carfagno ignition limits: r = 0, all propellant gas, and r = 1.0, all air (note: limits include 100 K safety factor)

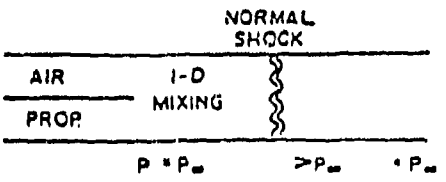

Figure 5. Carfagno flow model.

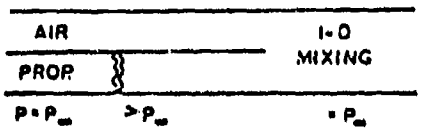

Figure 6. May and Einstein flow model.

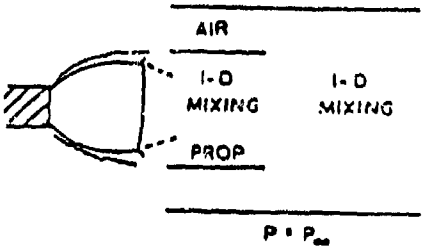

Figure 7. Schmidt Flow Model

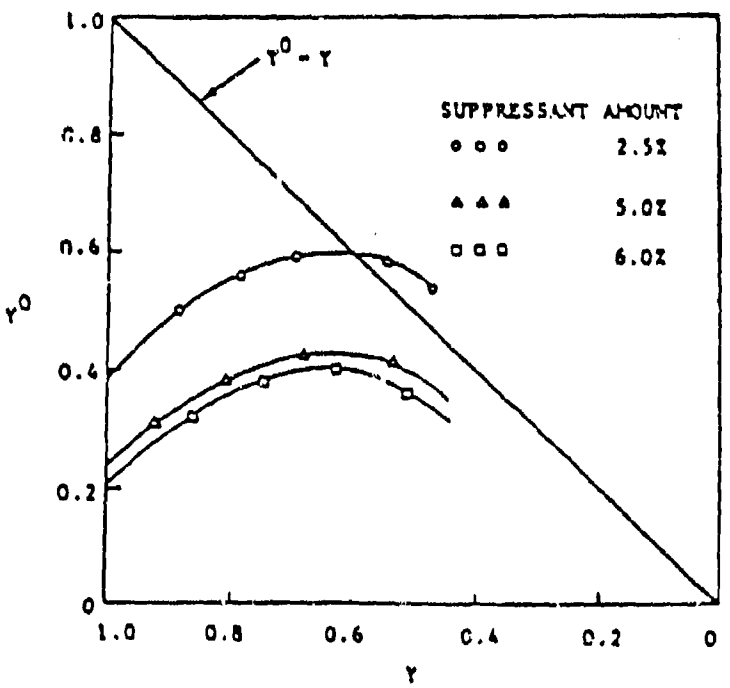

Figure 8. Variation of Y^0 vs. Y for Three Different Values of X_{09}, the Amount of Suppressant.

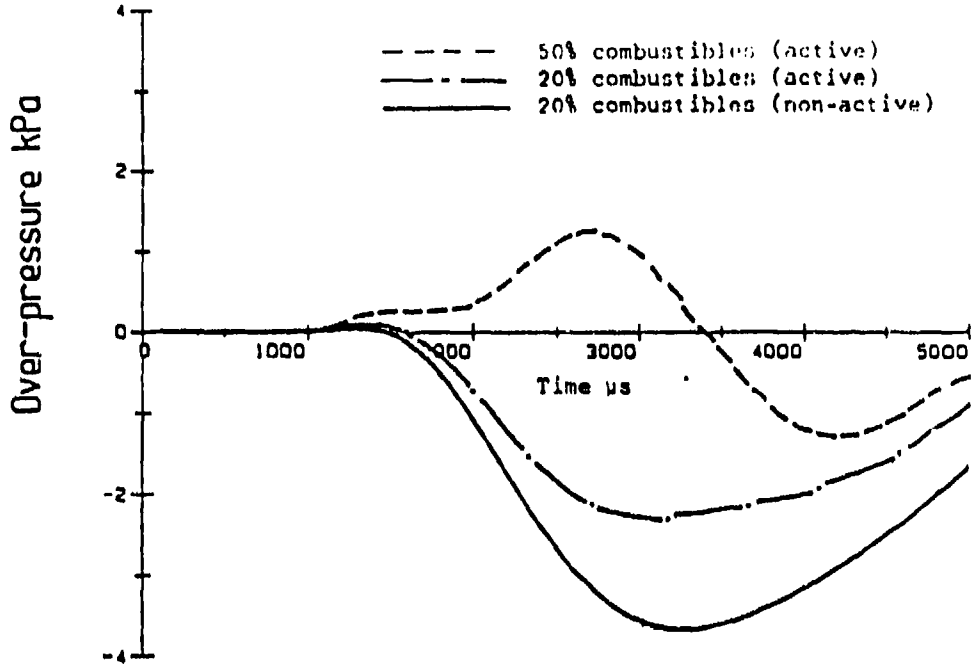

Figure 9 Over-pressure vs time at position #3 (see Figure 12 for location w.r.t. Carl Gustaf rifle)

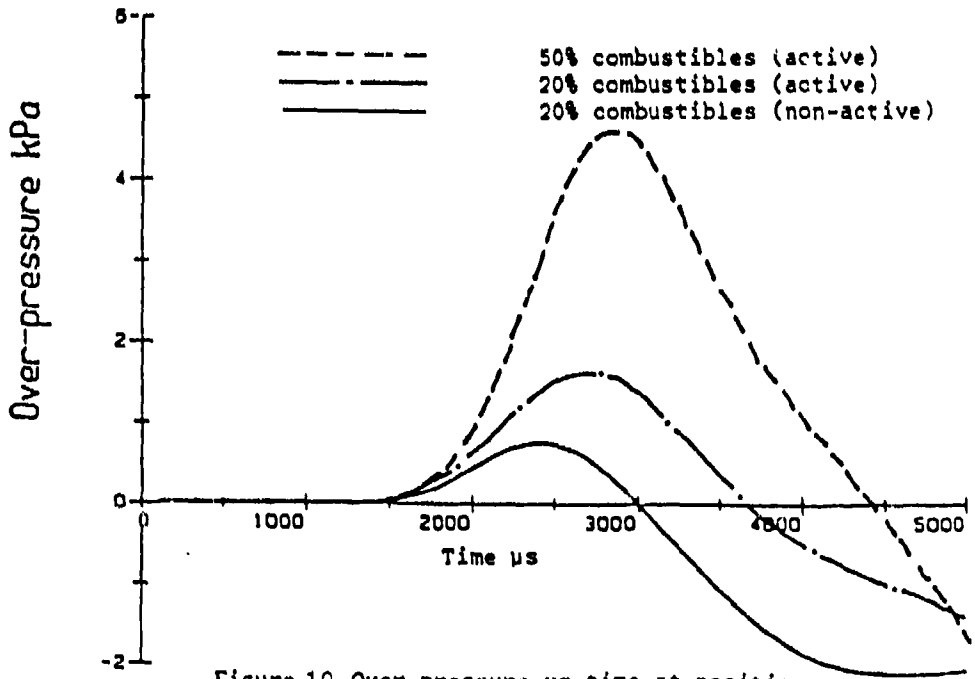

Figure 10 Over-pressure vs time at position #4 (see Fig. 12 for location w.r.t. Carl Gustaf rifle)

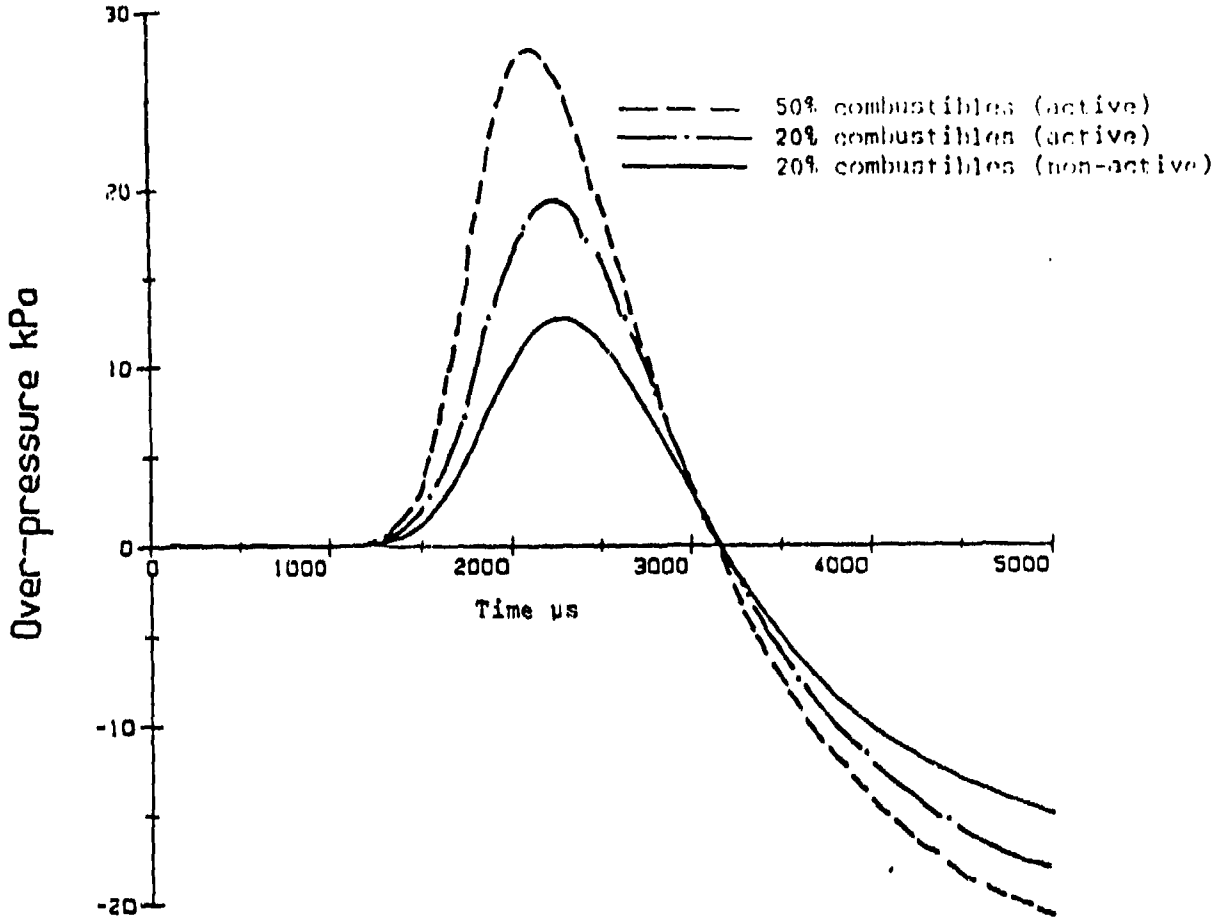

Figure 11 Over-pressure vs time at position #5 (see Figure12 for location w.r.t. Carl Gustaf rifle)

Figure 12

MEASUREMENT POSITIONS NEAR THE 84 mm CARL GUSTAF

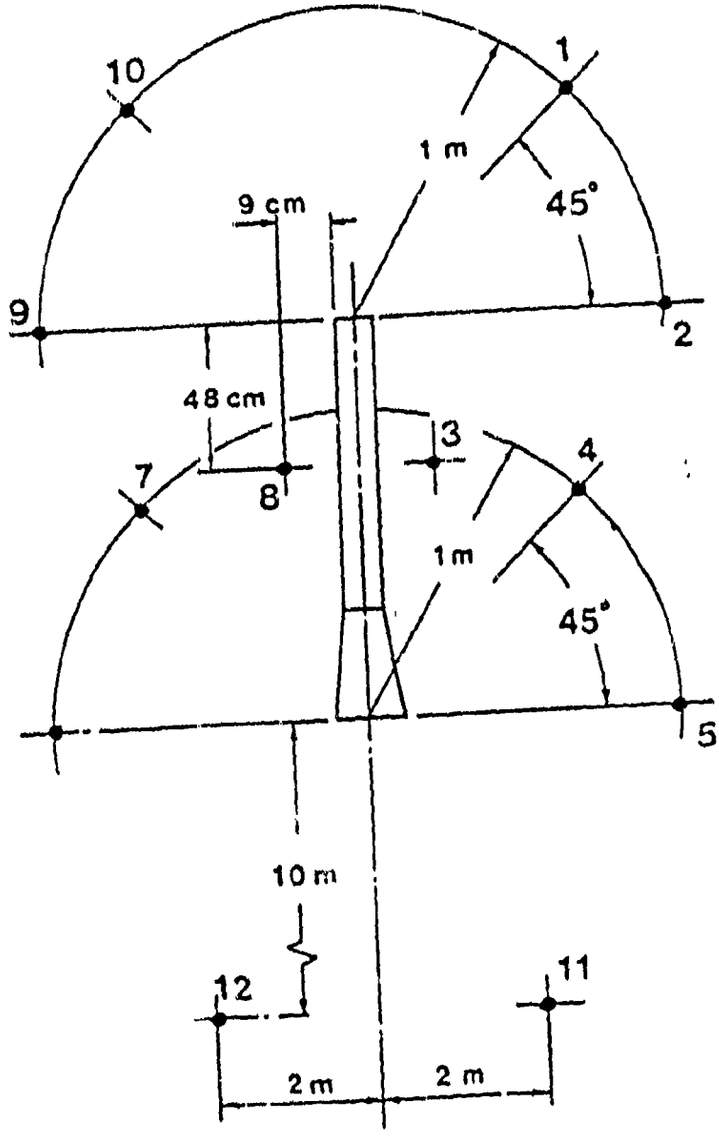

P_{min} = 0.0

P_{max} = 2978.7 kPa

ΔP = 100 kPa

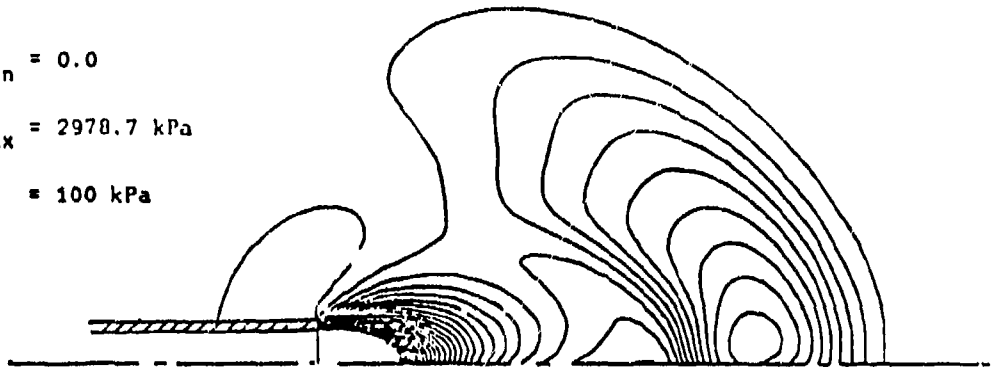

Figure 13a Pressure contours after 1 ms for the test run of 20% combustibles (non-active)

P_{min} = 0.0

P_{max} = 2978.7 kPa

ΔP = 100.0 kPa

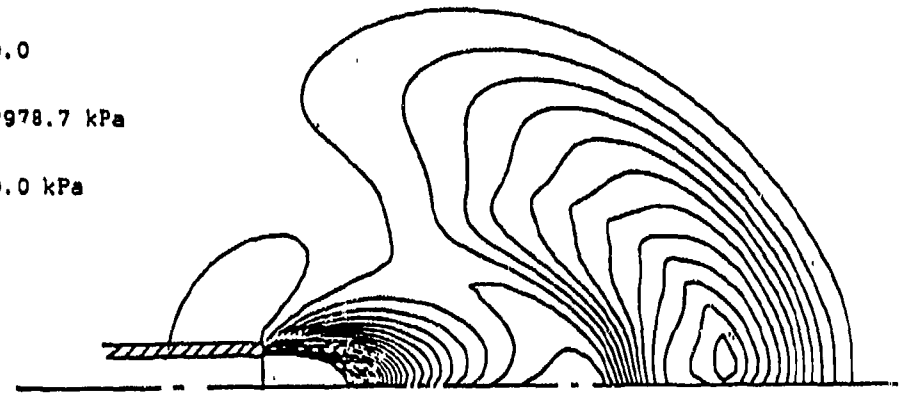

Figure 13b Pressure contours after 1 ms for the test run of 20% combustibles (active)

P_{min} = 0.0

P_{max} = 3207.3 kPa

ΔP = 100 kPa

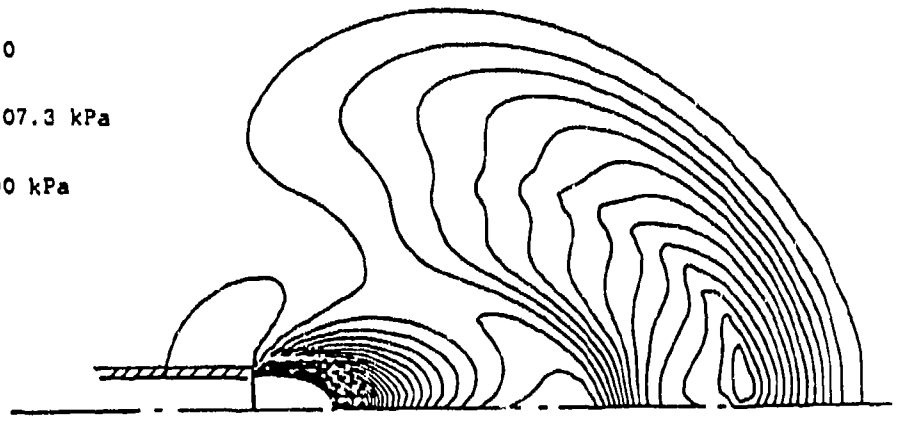

Figure 13c Pressure contours after 1 ms for the run of 50% combustibles (active)

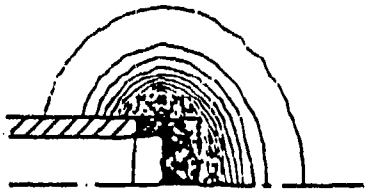

a. Time = 0.2 ms

$\rho_{O,min}$ = 0.0, $\rho_{O,max}$ = 0.24, $\Delta\rho_O$ = 0.002 kg/m^3

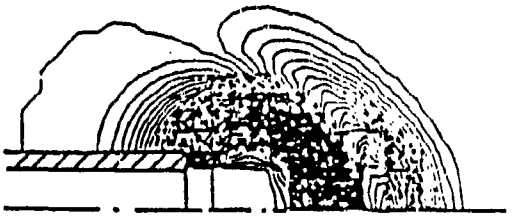

b. Time = 0.3 ms

$\rho_{O,min}$ = 0.0, $\rho_{O,min}$ = 0.37, $\Delta\rho_O$ = 0.002 kg/m^3

$\rho_{O,min}$ = 0.0

$\rho_{O,max}$ = 0.4 kg/m^3

$\Delta\rho_O$ = 0.002 kg/m^3

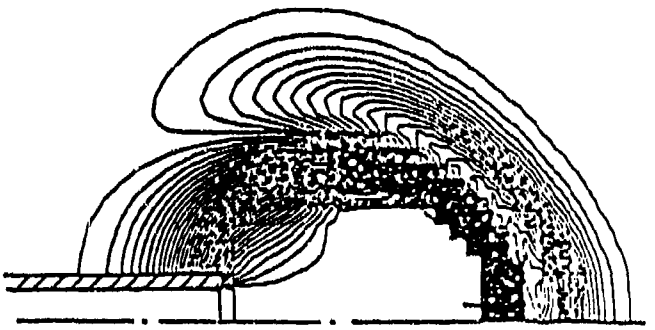

c. Time = 0.5 ms

$\rho_{O,min}$ = 0.0

$\rho_{O,max}$ = 0.42 kg/m^3

$\Delta\rho_O$ = 0.002 kg/m^3

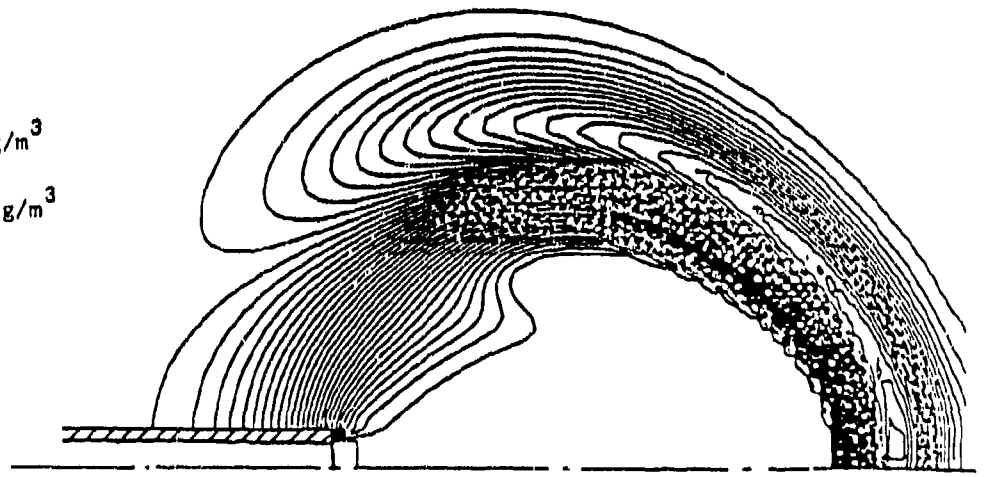

d. Time = 1.0 ms

Figure 14 Contours of oxidant density at various times

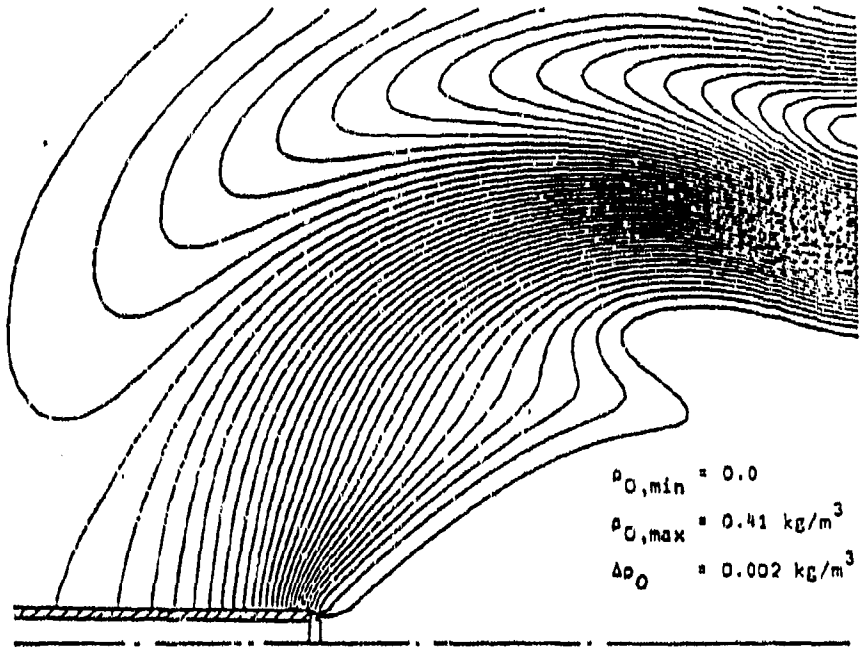

e. Time = 2.0 ms

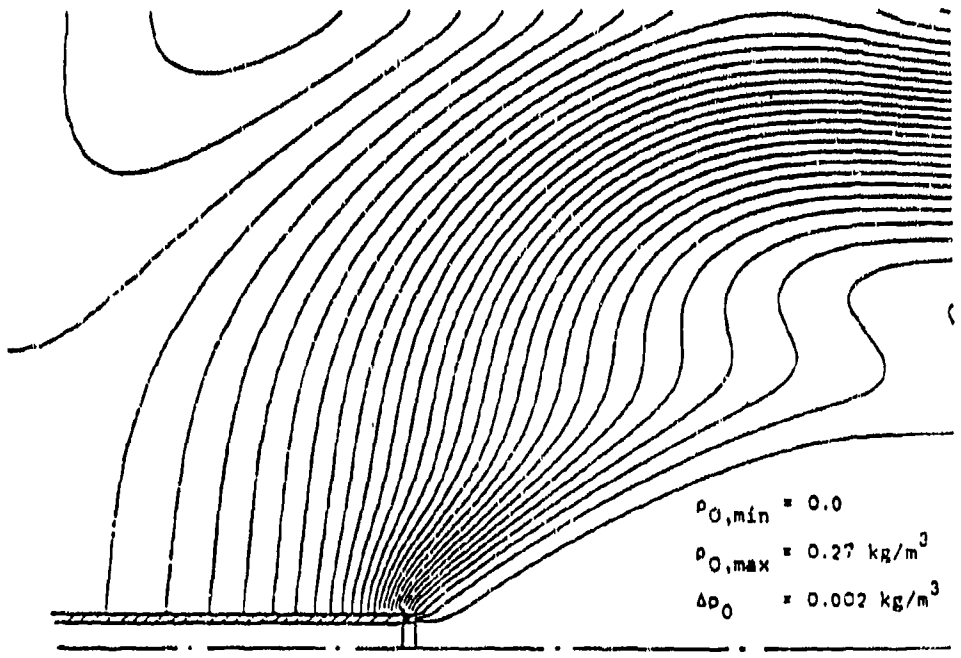

f. Time = 3.0 ms

Figure 14cont. Contours of oxidant density at various times

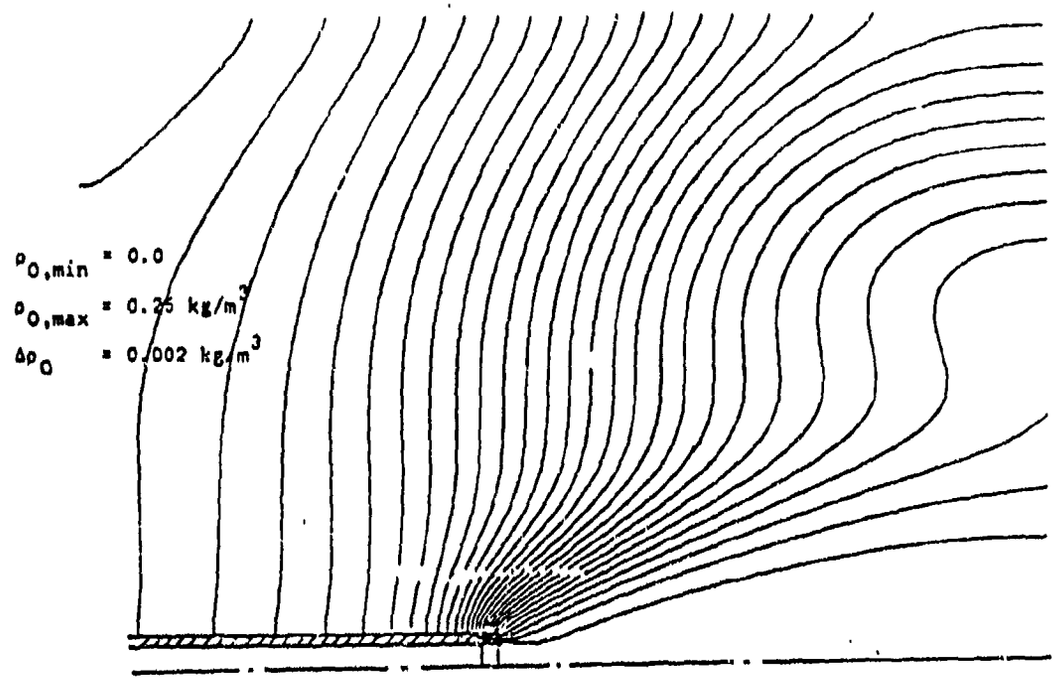

g. Time = 4.0 ms

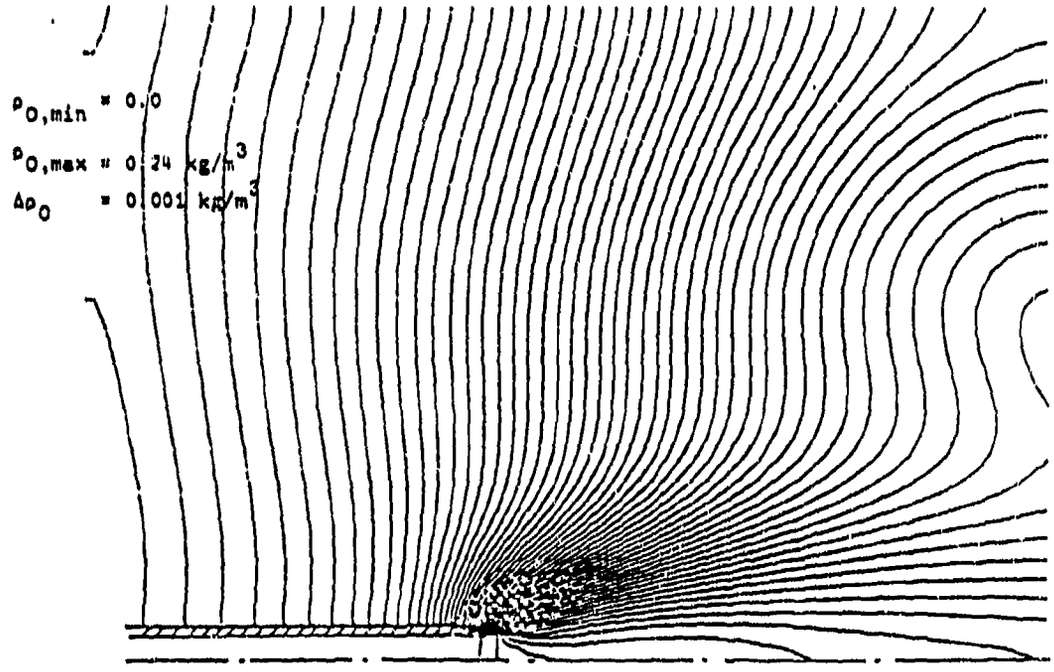

h. Time = 5.0 ms

Figure 14cont. Contours of oxidant density at various times

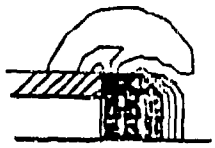

a. Time = 0.2 ms

$\rho_{I,min}$ = 0.0, $\rho_{I,max}$ = 1.86 kg/m^3, $\Delta\rho_I$ = 0.01 kg/m^3

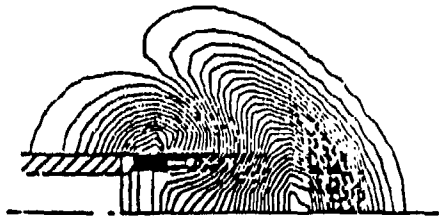

b. Time = 0.3 ms

$\rho_{I,min}$ = 0.0, $\rho_{I,max}$ = 1.52 kg/m^3, $\Delta\rho_I$ = 0.01 kg/m^3

$\rho_{I,min}$ = 0.0

$\rho_{I,max}$ = 1.46 kg/m^3

$\Delta\rho_I$ = 0.01 kg/m^3

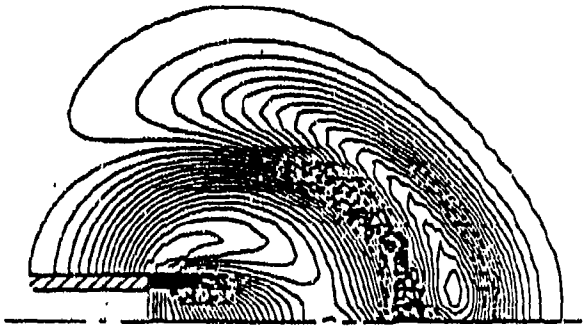

c. Time = 0.5 ms

$\rho_{I,min}$ = 0.0

$\rho_{I,max}$ = 3.0 kg/m^3

$\Delta\rho_I$ = 0.01 kg/m^3

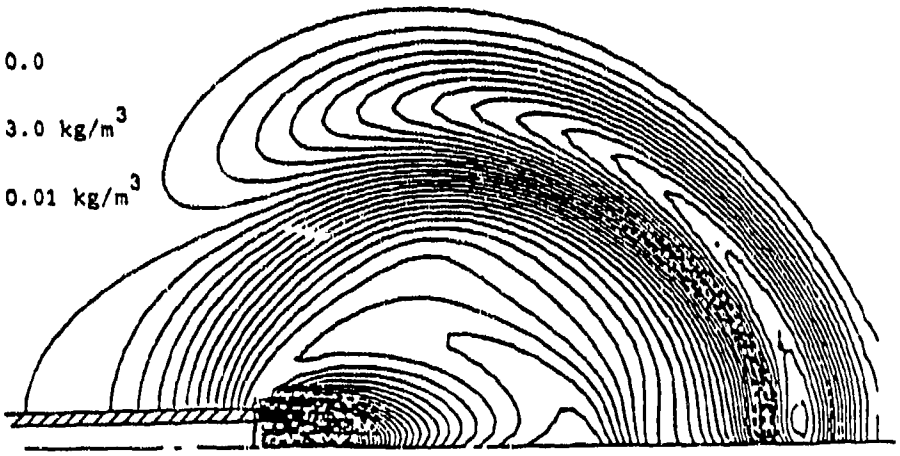

d. Time = 1.0 ms

Figure 15 Contours of inerts density at various times

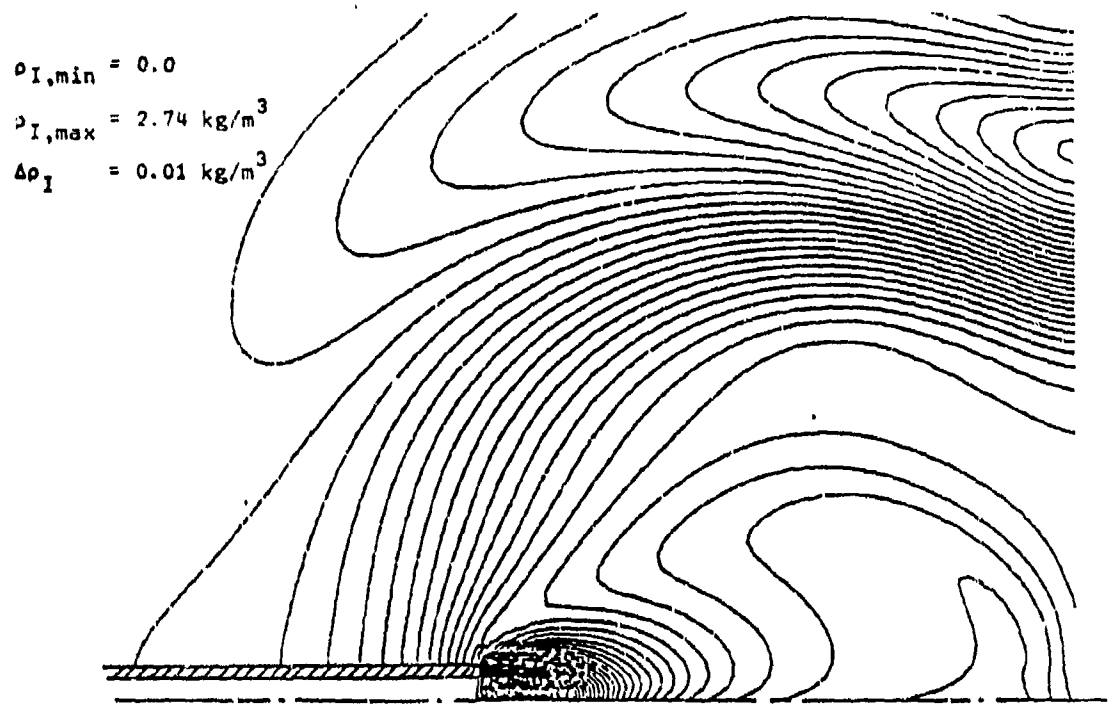

e. Time = 2.0 ms

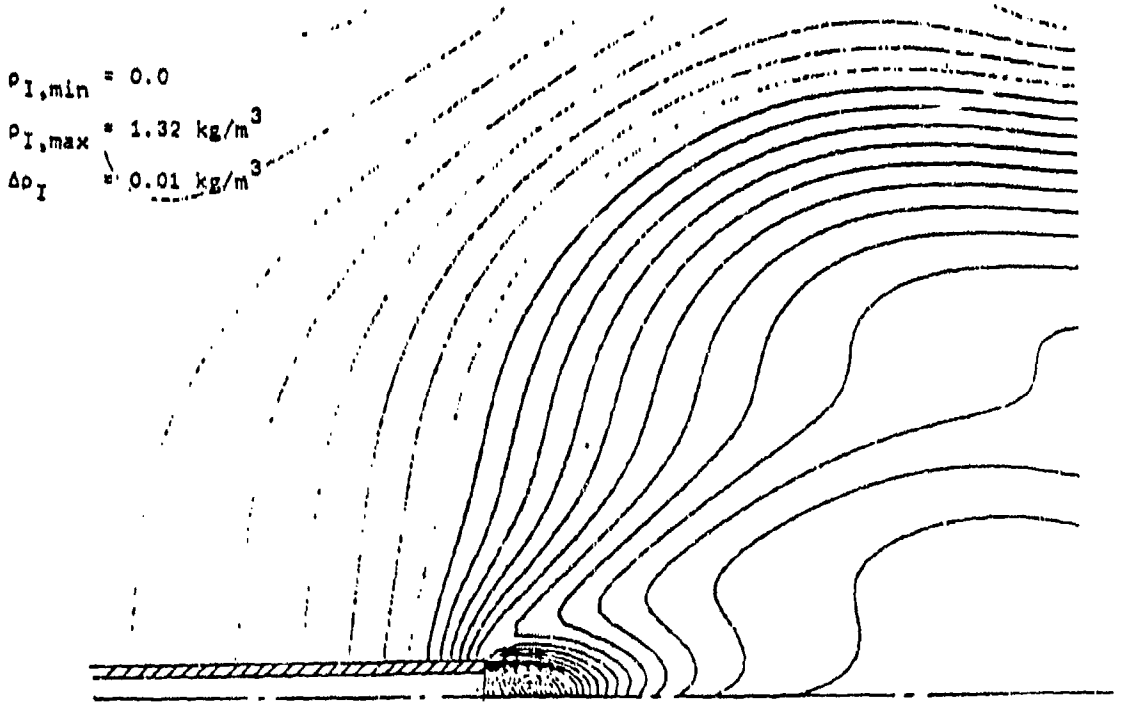

f. Time = 3.0 ms

Figure 15cont. Contours of inerts density at various times

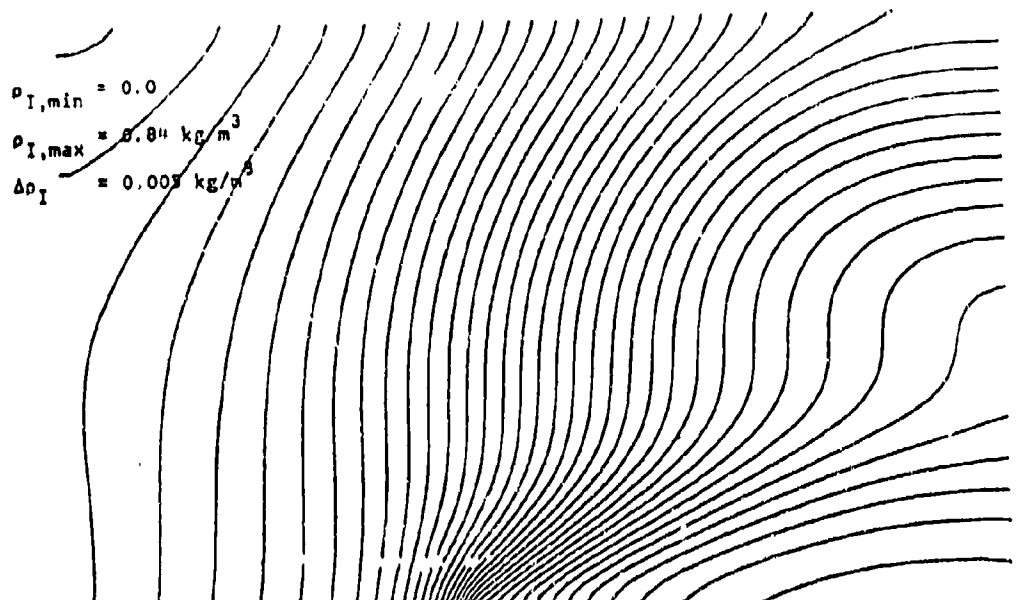

g. Time = 4.0 ms

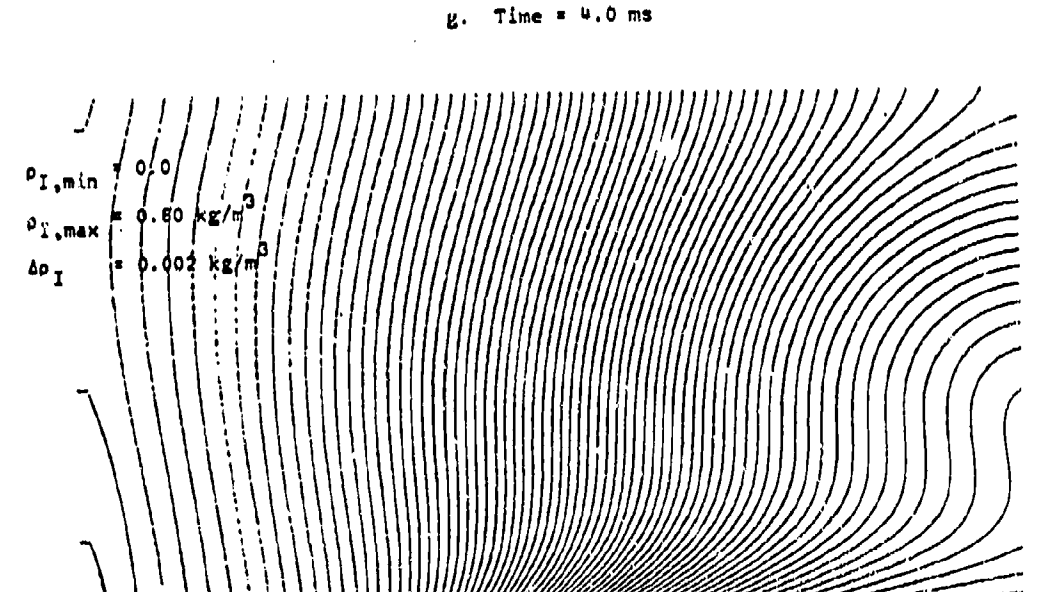

h. Time = 5.0 ms

Figure 15cont. Contours of inert density at various times

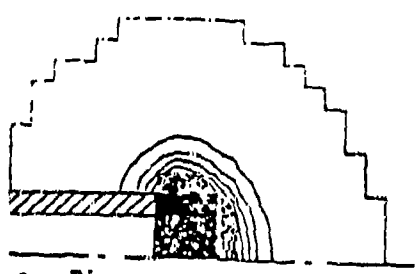

a. Time = 0.2 ms

$\rho_{C,min}$ = 0.0, $\rho_{C,min}$ = 1.86 kg/m^3, $\Delta\rho_C$ = 0.01 kg/m^3

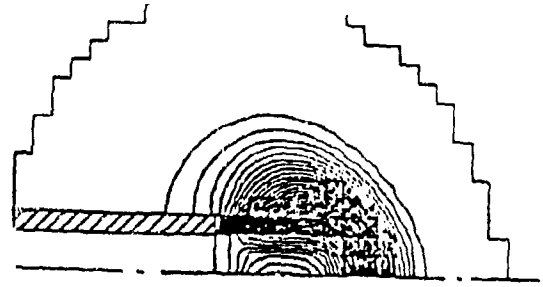

b. Time = 0.3 ms

$\rho_{C,min}$ = 0.0, $\rho_{C,max}$ = 1.04, $\Delta\rho_C$ = 0.01 kg/m^3

$\rho_{C,min}$ = 0.0

$\rho_{C,max}$ = 1.42 kg/m^3

$\Delta\rho_C$ = 0.01 kg/m^3

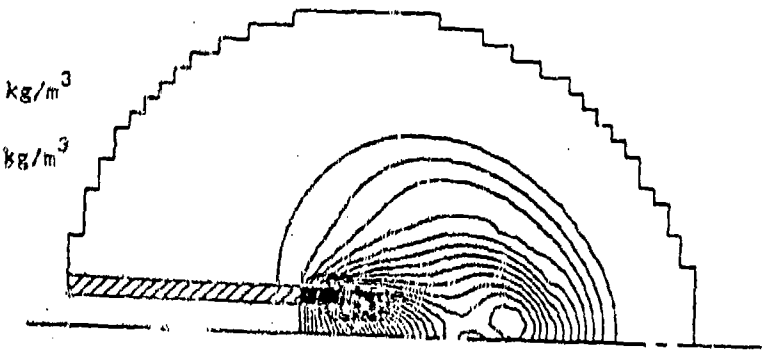

c. Time = 0.5 ms

$\rho_{C,min}$ = 0.0

$\rho_{C,max}$ = 3.0 kg/m^3

$\Delta\rho_C$ = 0.01 kg/m^3

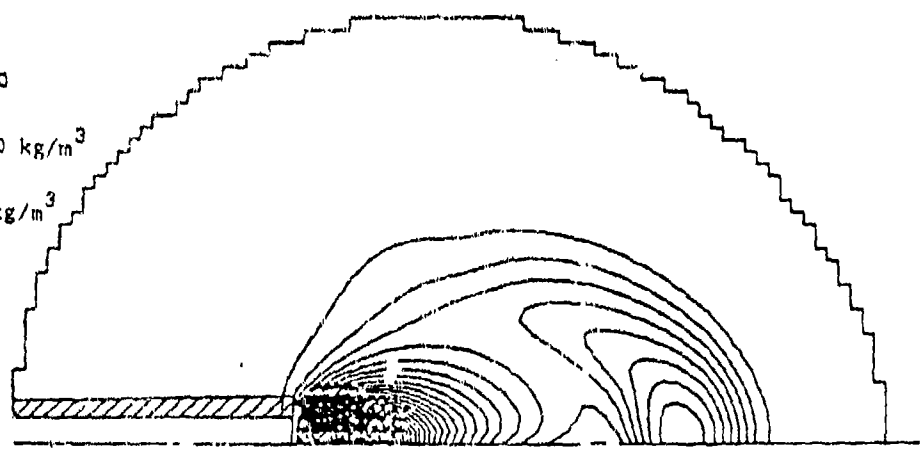

d. Time = 1.0 ms

Figure 16 Contours of combustibles density at various times

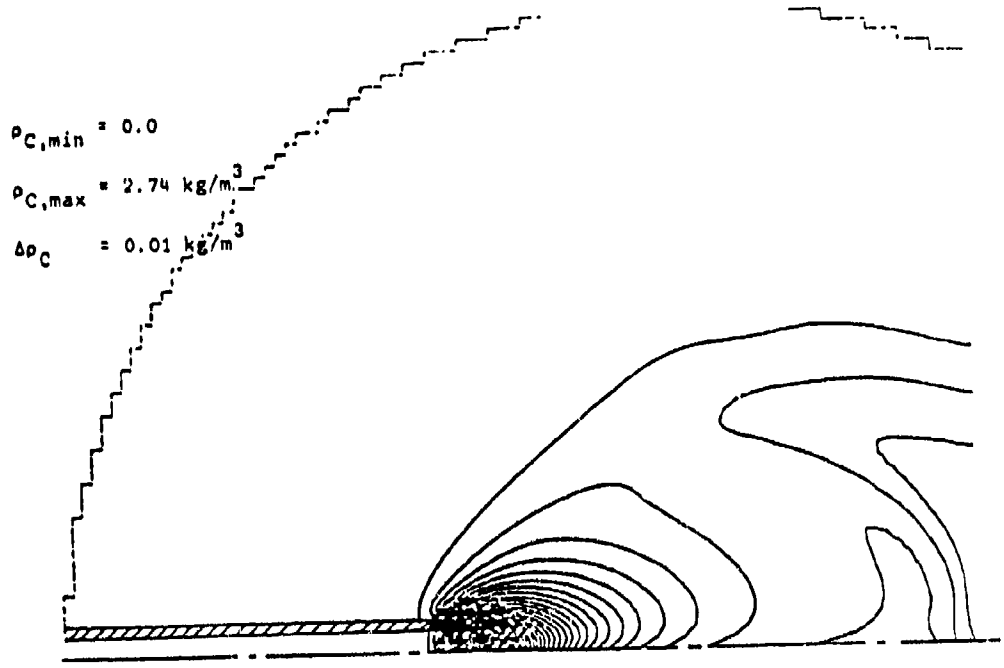

e. Time = 2.0 ms

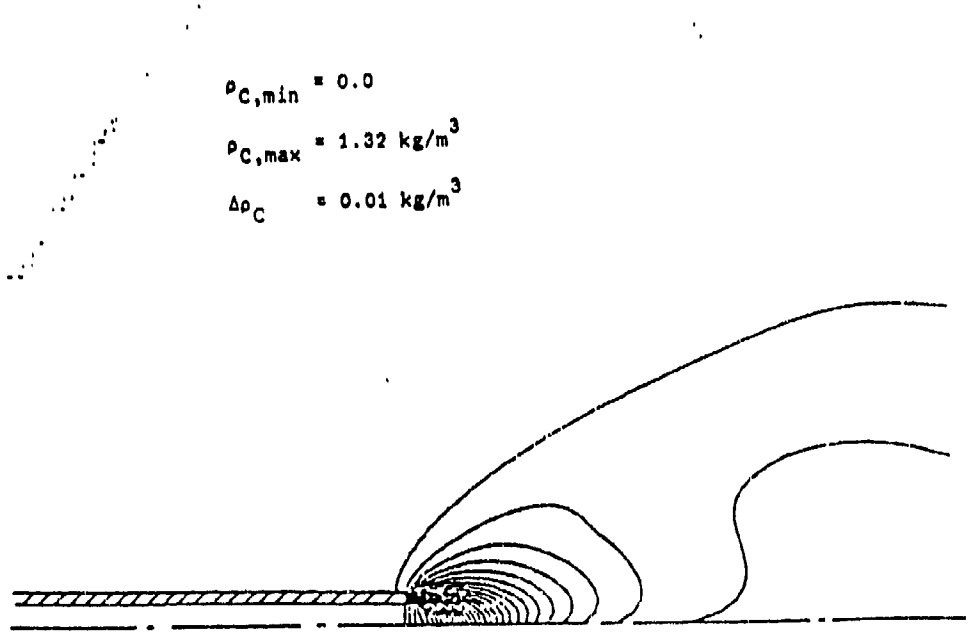

f. Time = 3.0 ms

Figure16 cont. Contours of combustibles density at various times

$\rho_{C,min}$ = 0.0

$\rho_{C,max}$ = 0.52 kg/m^3

$\Delta\rho_C$ = 0.005 kg/m^3

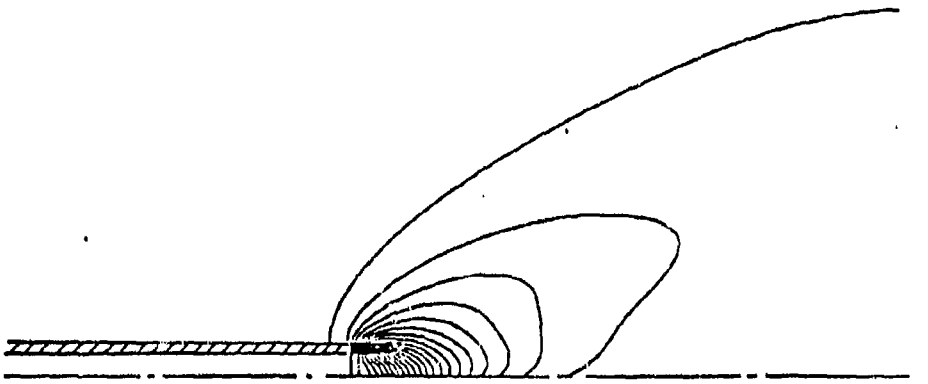

g. Time = 4.0 ms

$\rho_{C,min}$ = 0.0

$\rho_{C,max}$ = 0.23 kg/m^3

$\Delta\rho_C$ = 0.001 kg/m^3

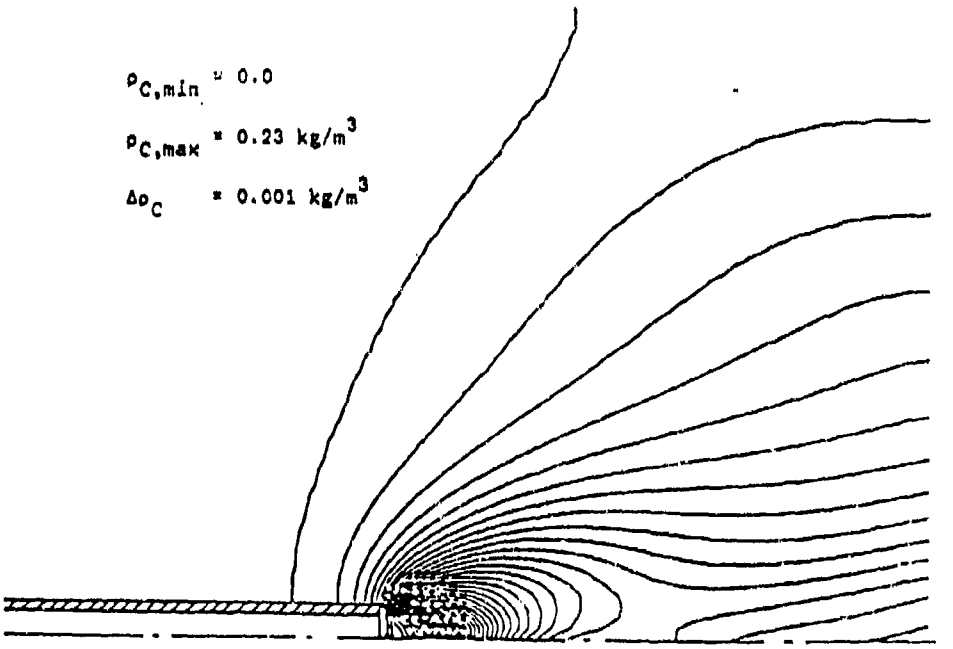

h. Time = 5.0 ms

Figure 16 cont. Contours of combustibles density at various times

$\rho_{O,min}$ = 0.0

$\rho_{O,max}$ = 0.44 kg/m^3

$\Delta\rho_O$ = 0.003 kg/m^3

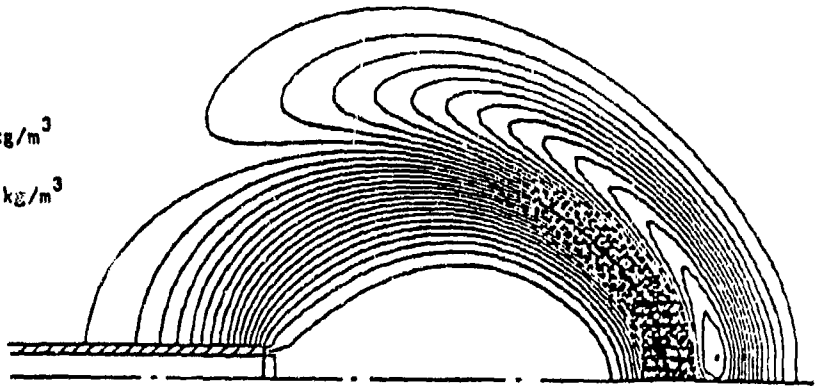

a. 5% combustibles (non-active)

$\rho_{O,min}$ = 0.0

$\rho_{O,max}$ = 0.44 kg/m^3

$\Delta\rho_O$ = 0.002 kg/m^3

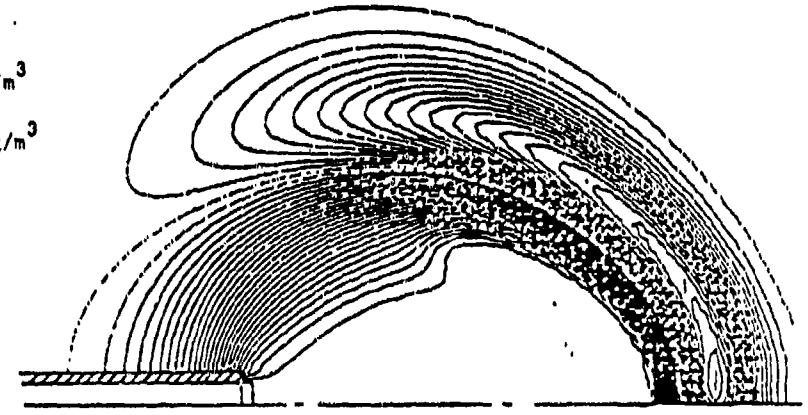

b. 20% combustibles (active)

$\rho_{O,min}$ = 0.0

$\rho_{O,max}$ = 0.44 kg/m^3

$\Delta\rho_O$ = 0.003 kg/m^3

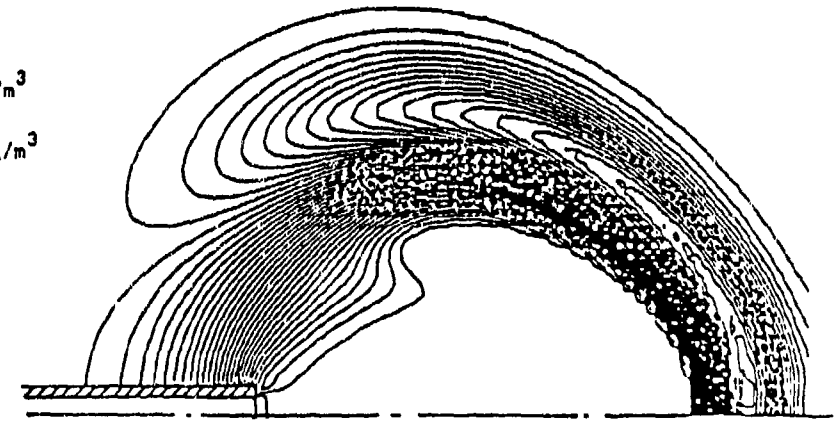

c. 50% combustibles (active)

Figure 17a Contours of oxident density at 1.0 ms for various proportions of combustibles from the breech nozzle

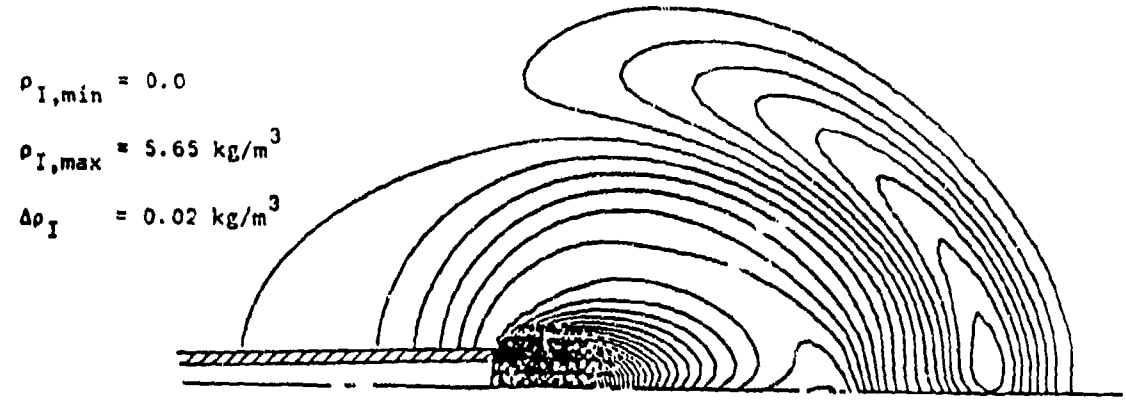

a. 5% combustibles (non-active)

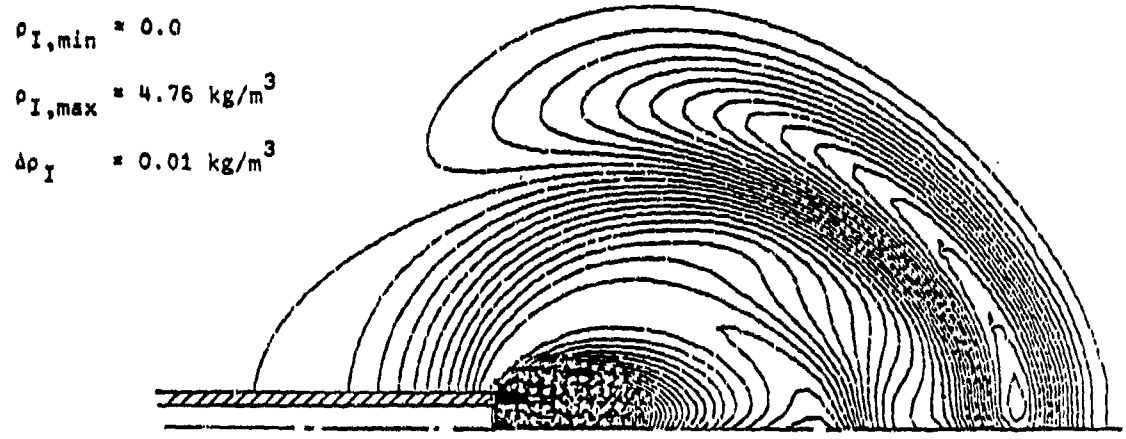

b. 20% combustibles (active)

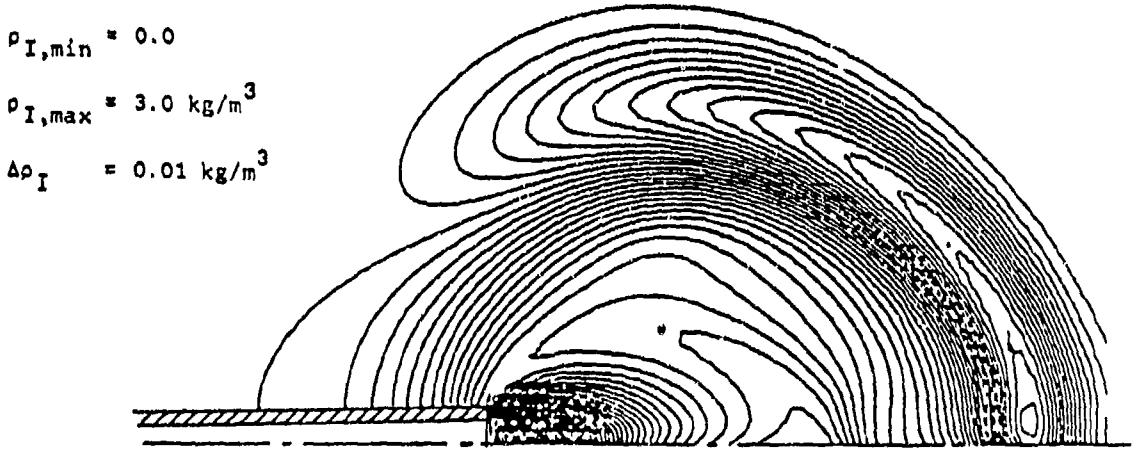

c. 50% combustibles (active)

Figure 17b Contours of inerts density at 1.0 ms for various proportion of combustibles from the breech nozzle

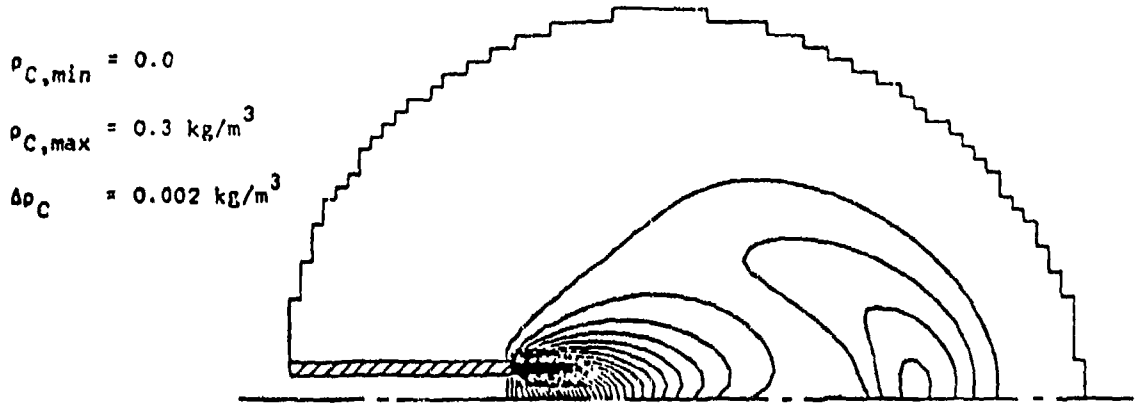

a. 5% combustibles (non-active)

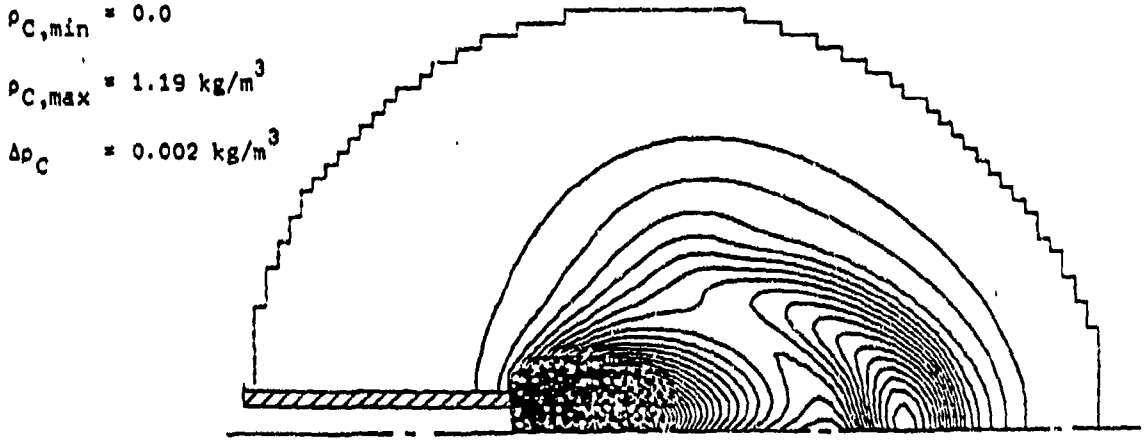

b. 20% combustibles (active)

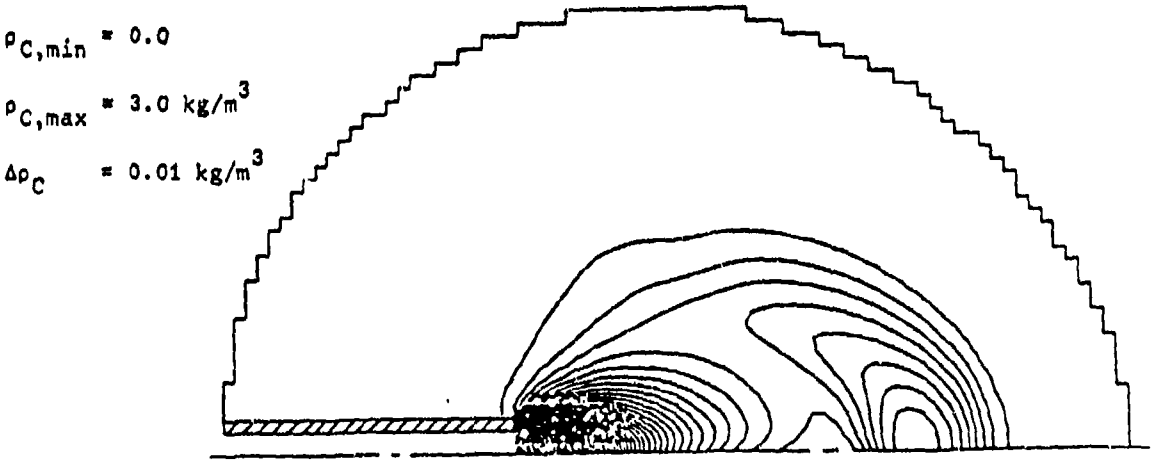

c. 50% combustibles (active)

Figure 17c Contours of combustibles density at 1.0 ms for various proportions of combustibles from the breech nozzle .

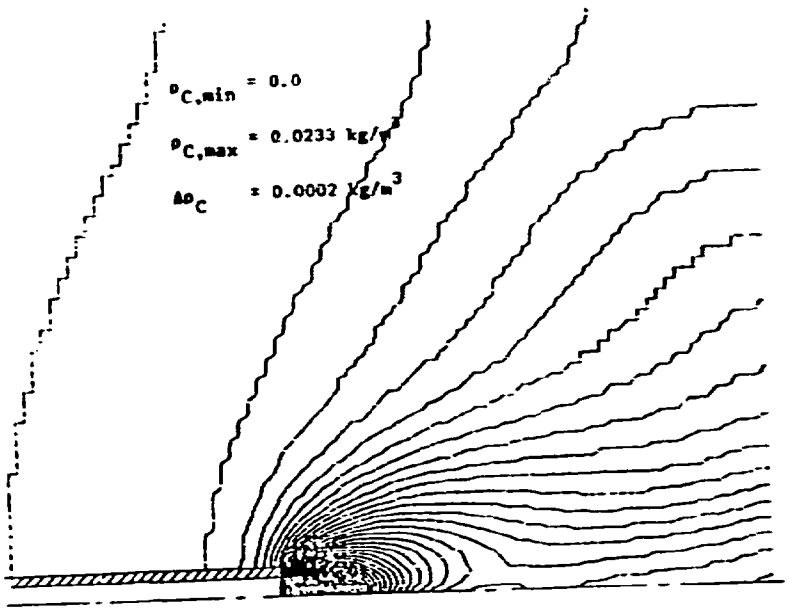

a. 5% combustibles (non-active)

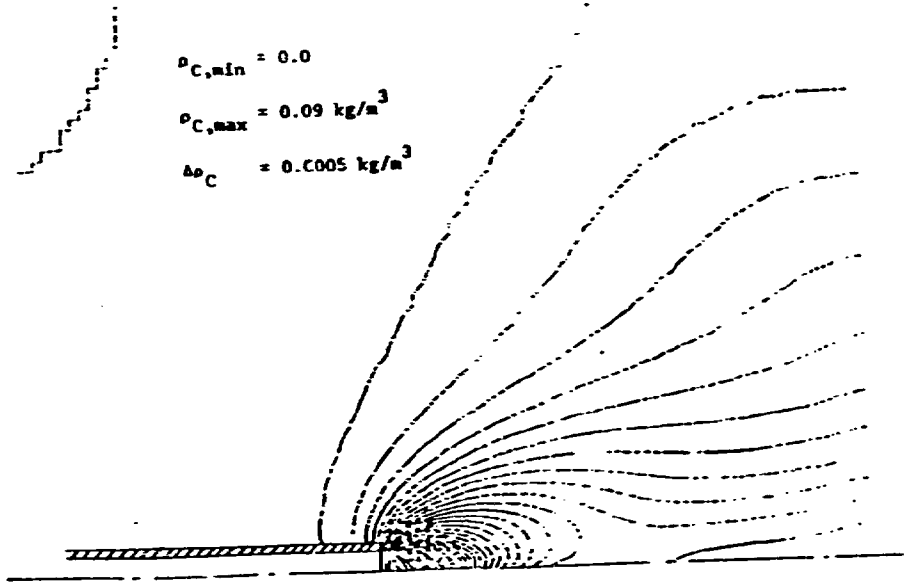

b. 20% combustibles (active)

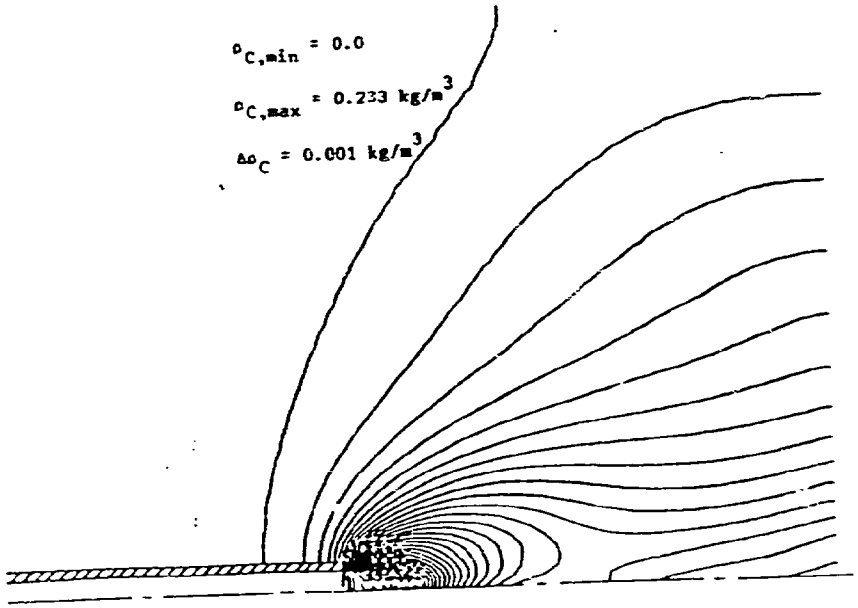

c. 50% combustibles (active)

Figure 18 Contours of combustibles density at 5.0 ms for various proportions of combustibles from the breech nozzle

$m_{O,min}$ = 0.0

$m_{O,max}$ = 0.233

Δm_O = 0.005

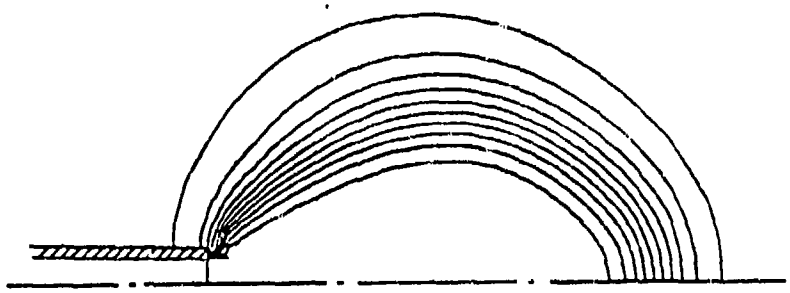

a. oxident

$m_{I,min}$ = 0.0

$m_{I,max}$ = 0.95

Δm_I = 0.01

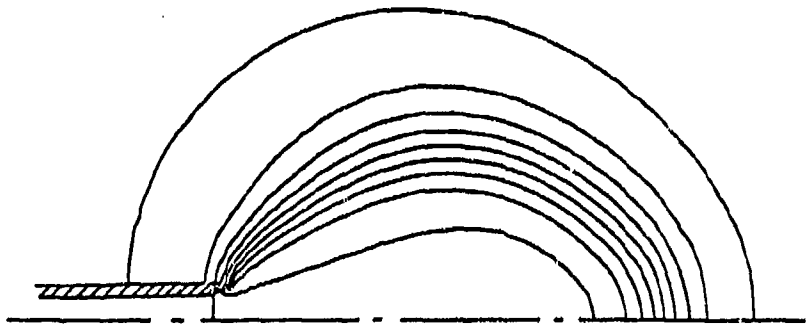

b. inerts

$m_{C,min}$ = 0.0

$m_{C,max}$ = 0.05

Δm_C = 0.0005

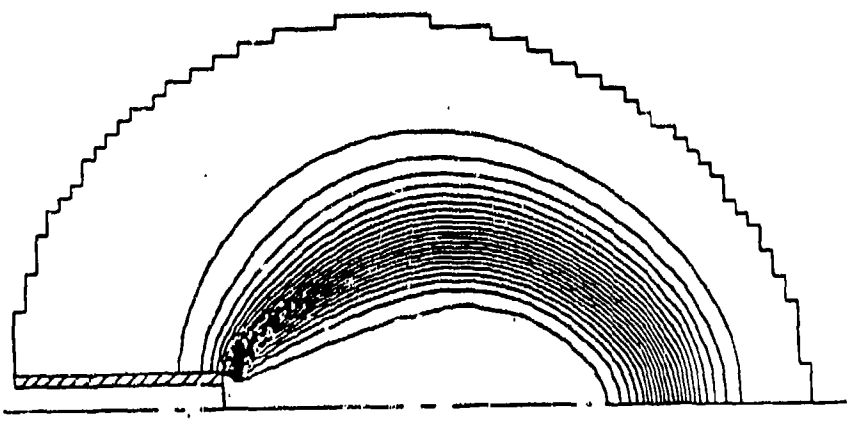

c. combustibles

Figure 19 Contours of mass fraction for various species at 1 ms for the case of 5% combustibles (non-active)

DETAILED HIGH TEMPERATURE OXIDATION CHEMISTRY OF THE ALKALI METALS IN FLAMES

M. Steinberg and K. Schofield

Quantum Institute, UC Santa Barbara

Table I. Experimental flame matrix and characteristics.

$H_2/O_2/N_2$	Temperature K	H_2O	O_2 molecule cm^{-3}	OH
0.6 1 1	1906 - 1929	1.0 (18)	1.2 (18)	3.8 → 0.7 (16)*
1 1 2	2066 - 2100	9.9 (17)	4.8 (17)	3.8 → 1.1 (16)
1 1 3	1667 - 1730	9.5 (17)	4.7 (17)	3.7 → 0.3 (16)
1.4 1 3	2125 - 2197	9.8 (17)	2.0 (17)	3.5 → 1.4 (16)
1.4 1 4	1810 - 1847	9.8 (17)	2.1 (17)	3.6 → 0.5 (16)
1.4 1 5	1654 - 1669	9.3 (17)	2.0 (17)	3.6 → 0.3 (16)
1.8 1 3	2280 - 2405	1.1 (18)	5.9 (16)	4.0 → 1.9 (16)
1.8 1 4	2060 - 2228	9.8 (17)	5.1 (16)	3.6 → 1.4 (16)
1.8 1 5	1825 - 1916	1.0 (18)	5.3 (16)	3.2 → 0.7 (16)
1.8 1 6	1695 - 1726	9.7 (17)	5.2 (16)	3.1 → 0.4 (16)

*Concentrations, read as 3.8×10^{16} (0.25 ms) decaying to 0.7×10^{16} (4.0 ms).

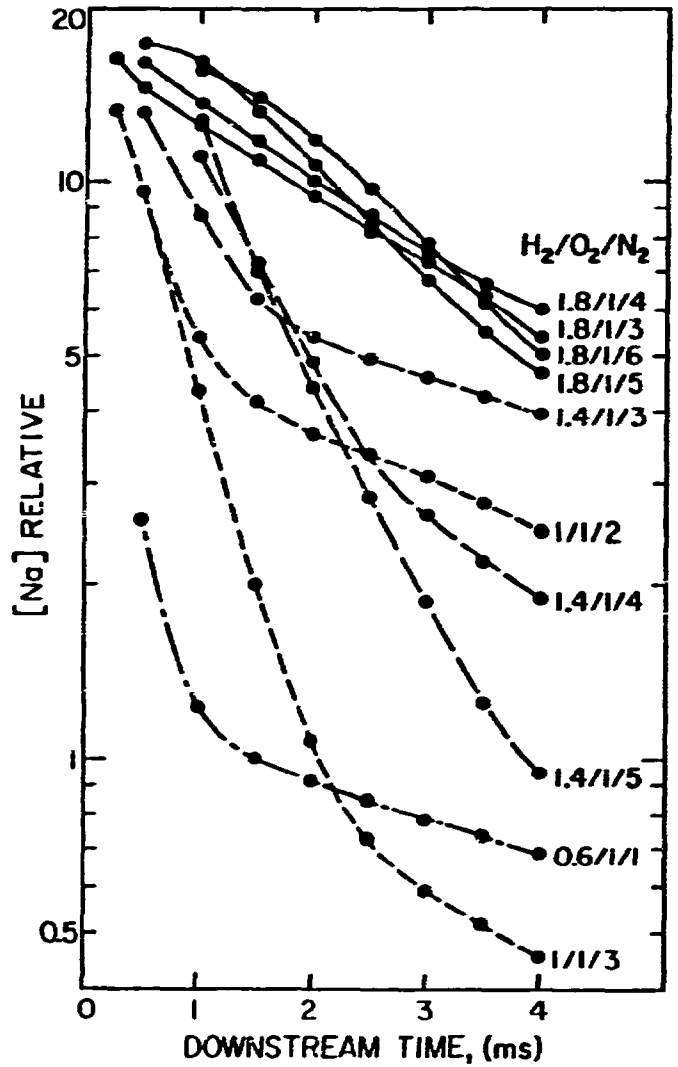
20
10
5
1
0.5
[Na] RELATIVE
0
1
2
3
4
DOWNSTREAM TIME, (ms)
$H_2/O_2/N_2$
1.8/1/4
1.8/1/3
1.8/1/6
1.8/1/5
1.4/1/3
1/1/2
1.4/1/4
1.4/1/5
0.6/1/1
1/1/3

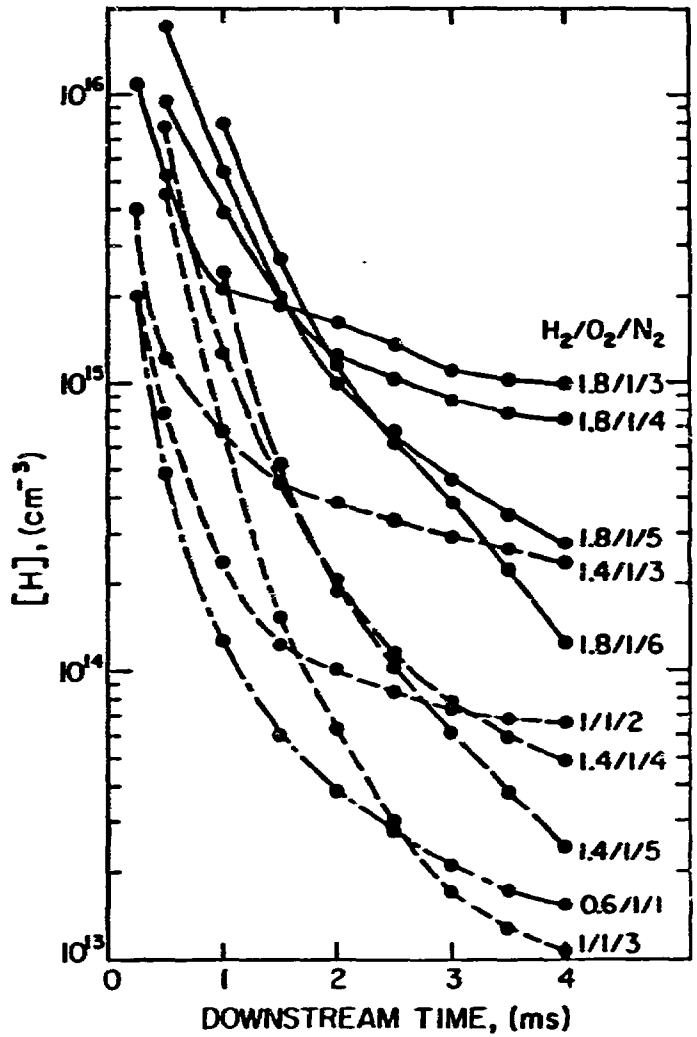
10^{16}
10^{15}
10^{14}
10^{13}
[H], (cm^{-3})
0
1
2
3
4
DOWNSTREAM TIME, (ms)
$H_2/O_2/N_2$
1.8/1/3
1.8/1/4
1.8/1/5
1.4/1/3
1.8/1/6
1/1/2
1.4/1/4
1.4/1/5
0.6/1/1
1/1/3

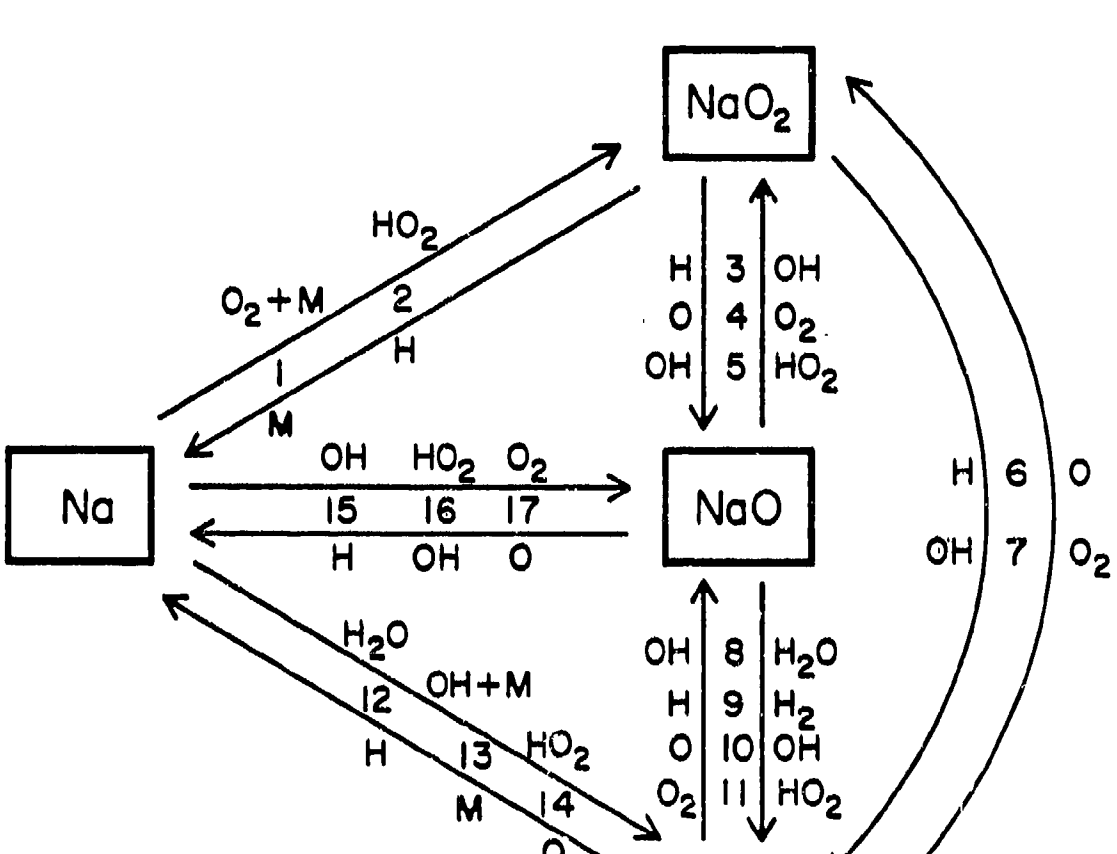
NaO2
HO2
O2+M
2
H
1
M
H 3 OH
O 4 O2
OH 5 HO2
Na
OH HO2 O2
15 16 17
H OH O
NaO
H 6 O
OH 7 O2
H2O
OH+M
12
H
13
HO2
M
14
O
OH 8 H2O
H 9 H2
O 10 OH
O2 11 HO2
NaOH

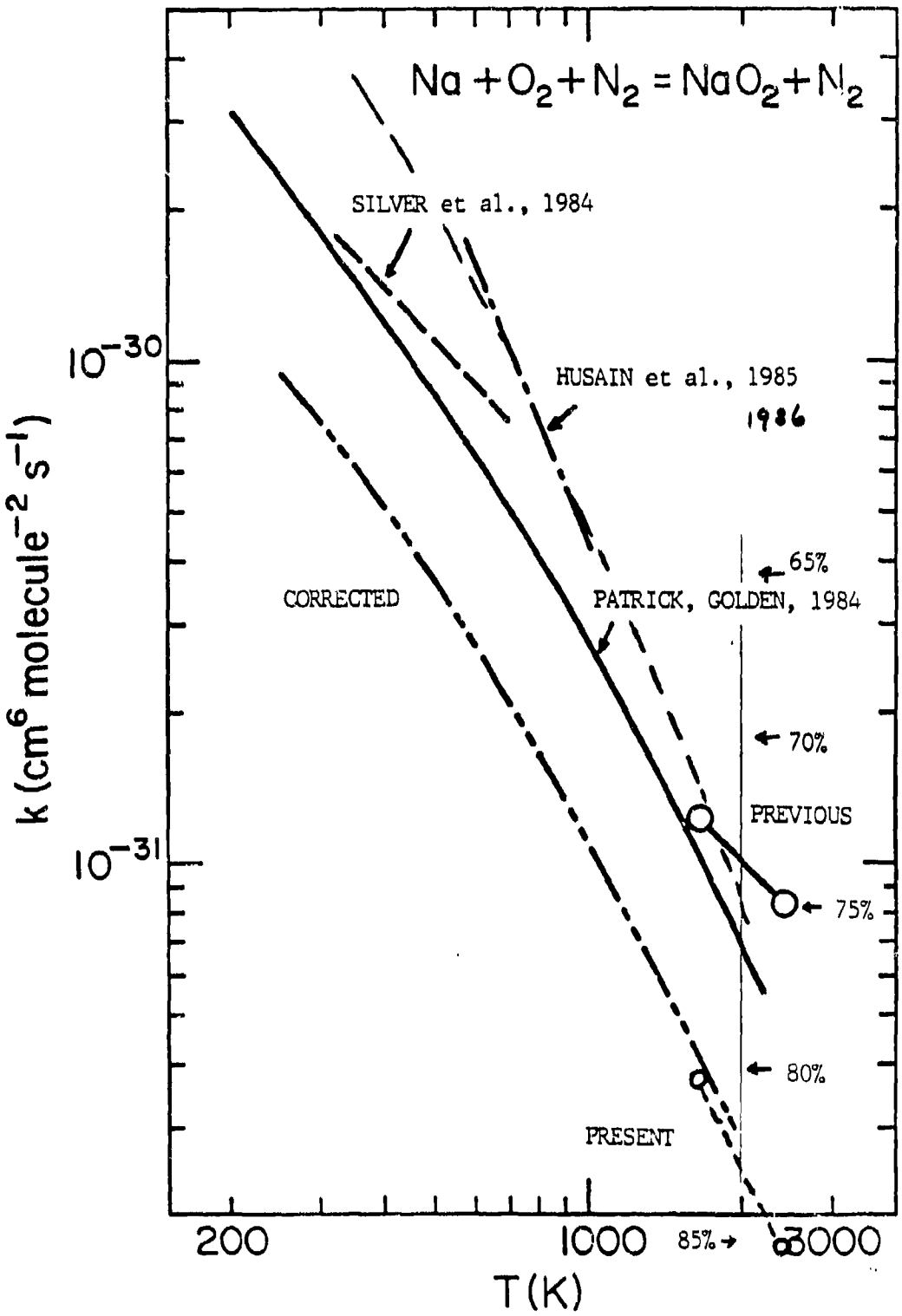
Na + O2 + N2 = NaO2 + N2
SILVER et al., 1984
HUSAIN et al., 1985
1986
CORRECTED
PATRICK, GOLDEN, 1984
65%
70%
PREVIOUS
75%
80%
PRESENT
85%
10^-30
10^-31
k (cm^6 molecule^-2 s^-1)
200
1000
3000
T(K)

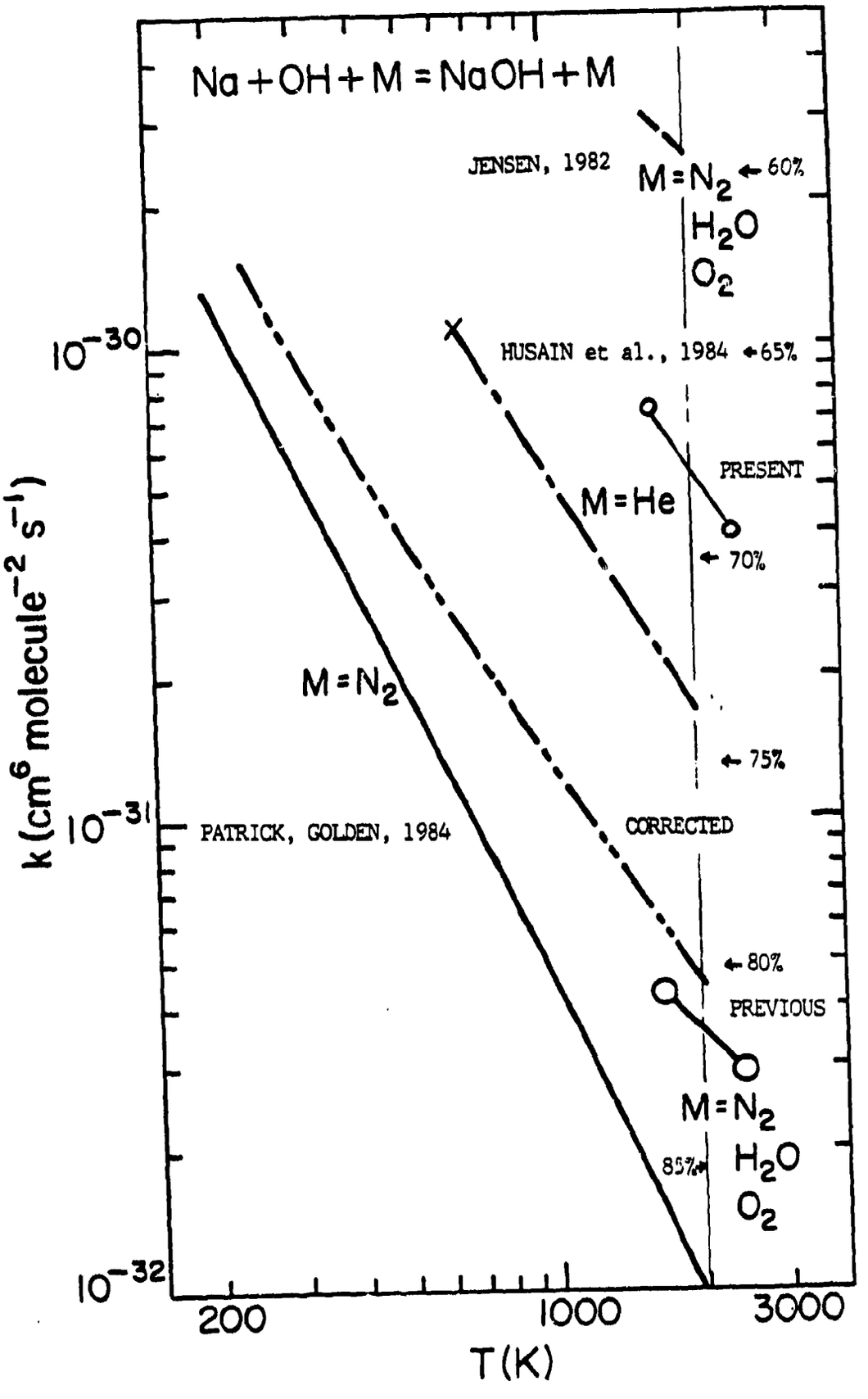
Na + OH + M = NaOH + M
JENSEN, 1982
M = N2
H2O
O2
60%
HUSAIN et al., 1984
65%
PRESENT
M = He
70%
M = N2
75%
CORRECTED
PATRICK, GOLDEN, 1984
80%
PREVIOUS
M = N2
H2O
O2
85%
k (cm6 molecule-2 s-1)
10-30
10-31
10-32
200
1000
3000
T(K)

CONCLUSIONS FOR SODIUM

1. ONLY A FEW (5-6) OF THE 17 POSSIBLE REACTIONS CONTROL THE DISTRIBUTION BETWEEN Na, NaO_2, NaO, NaOH.

2. AT LOWER TEMPERATURES (<2000K) AND IN MORE O_2 RICH FLAMES, SODIUM IS MORE EXTENSIVELY IN ITS MOLECULAR FORMS THAN EXPECTED FROM Na + H_2O ALONE.

3. NaO_2 PLAYS A DOMINANT ROLE AS AN ALTERNATE KINETIC ROUTE TO NaOH.

4. ALTHOUGH MORE STABLE THAN WE REPORTED PREVIOUSLY (NOW D(Na-O_2) 55 kcal mol^{-1}) ITS CONCENTRATION IS LOW (DUE TO ITS REACTIVITY) EXCEPT IN O_2 RICH, LOWER TEMPERATURE FLAMES.

5. NaO IS COUPLED IN EQUILIBRIUM TO NaOH AND IS UNIMPORTANT IN H-CONTAINING FLAMES.

6. RATE CONSTANTS ARE ALL CONSISTENT AND OF A REASONABLE MAGNITUDE. THE LIMITED DATA FOR Li + O_2 + M AND Li + OH + M ALSO APPEAR CONSISTENT WITH EXPECTED DISSOCATION RATES.

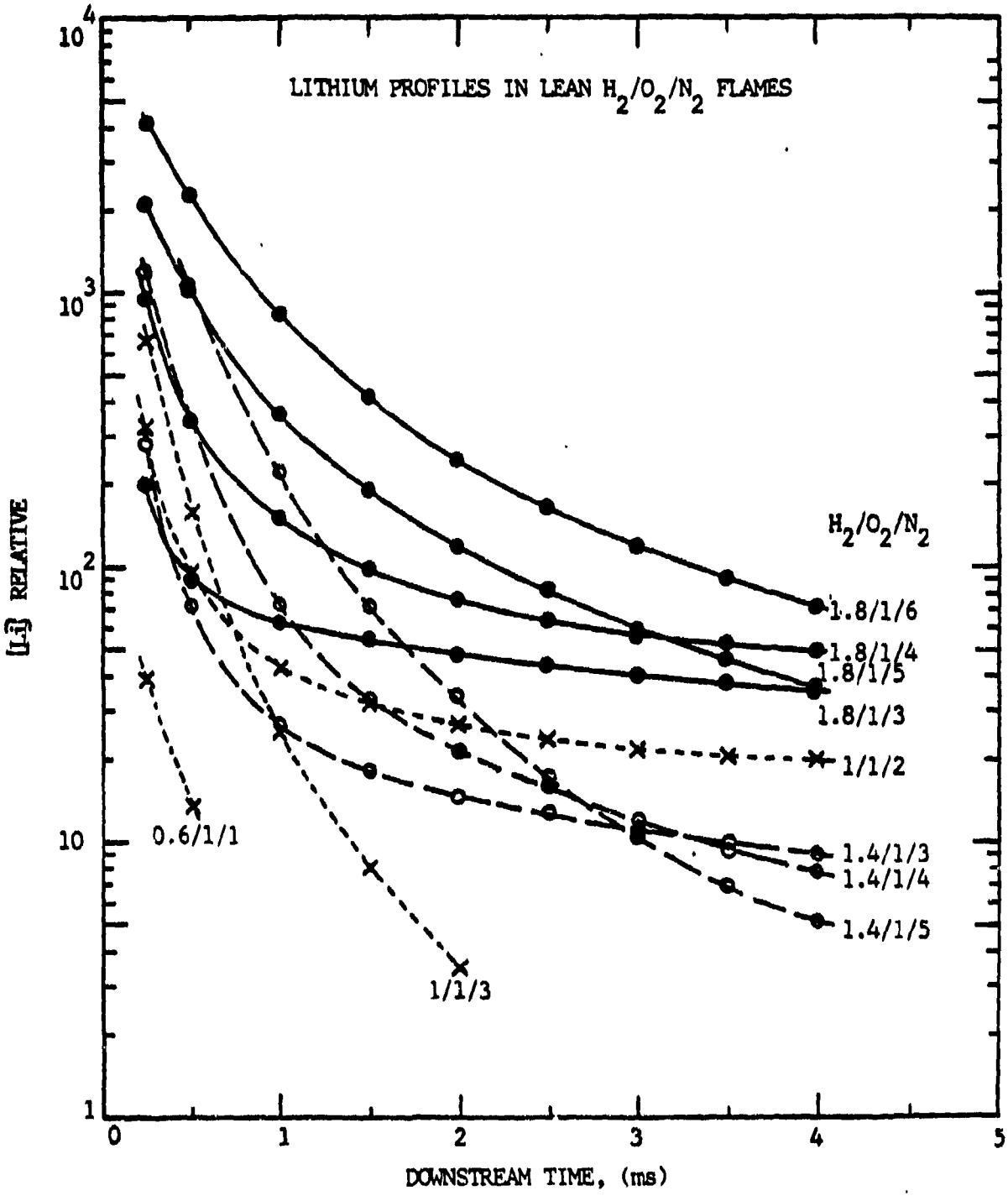
LITHIUM PROFILES IN LEAN $H_2/O_2/N_2$ FLAMES
[Li] RELATIVE
DOWNSTREAM TIME, (ms)
$H_2/O_2/N_2$
1.8/1/6
1.8/1/4
1.8/1/5
1.8/1/3
1/1/2
0.6/1/1
1.4/1/3
1.4/1/4
1.4/1/5
1/1/3

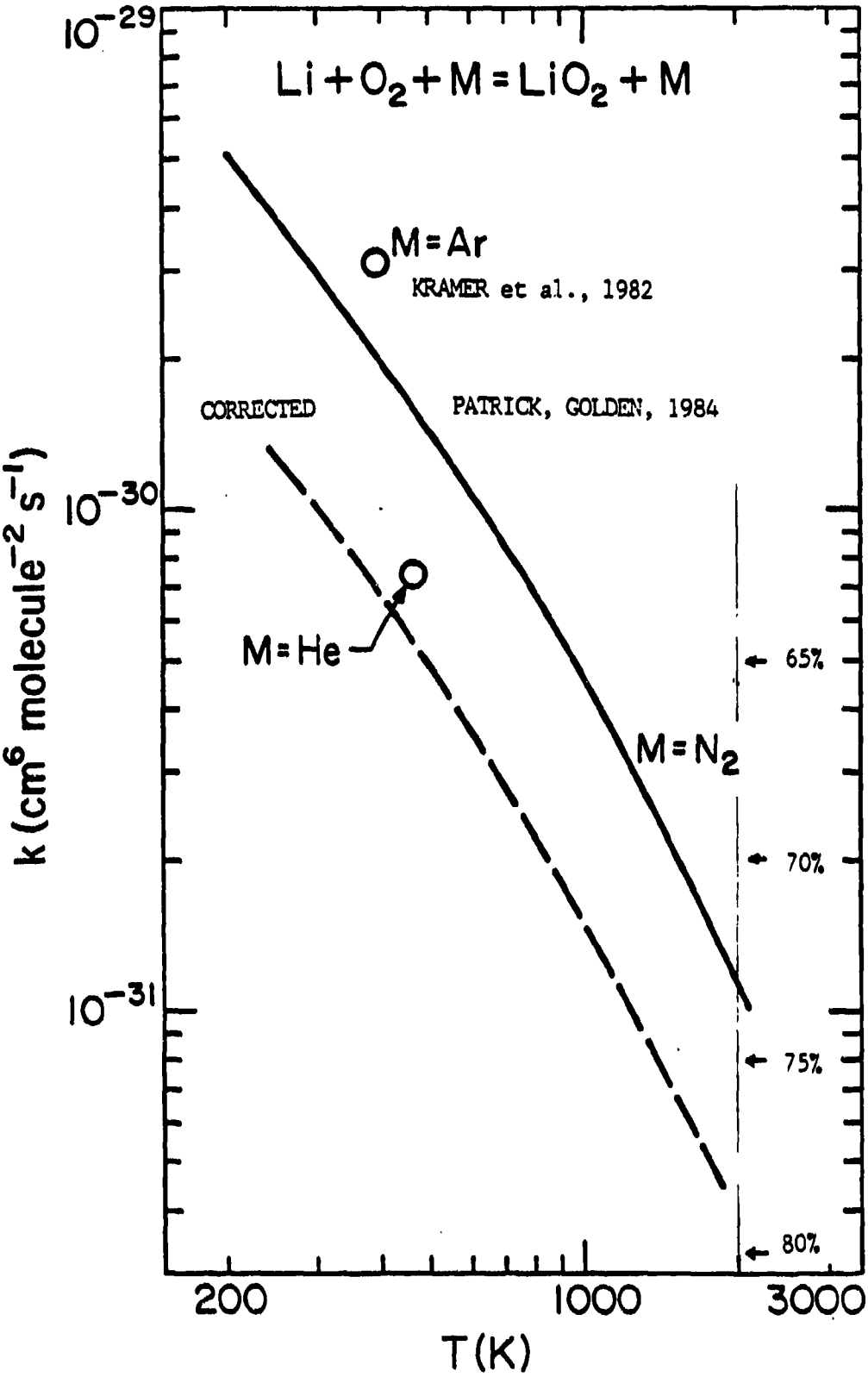
Li + O2 + M = LiO2 + M
M = Ar
KRAMER et al., 1982
CORRECTED
PATRICK, GOLDEN, 1984
M = He
M = N2
65%
70%
75%
80%
10^-29
10^-30
10^-31
k (cm^6 molecule^-2 s^-1)
200
1000
3000
T(K)

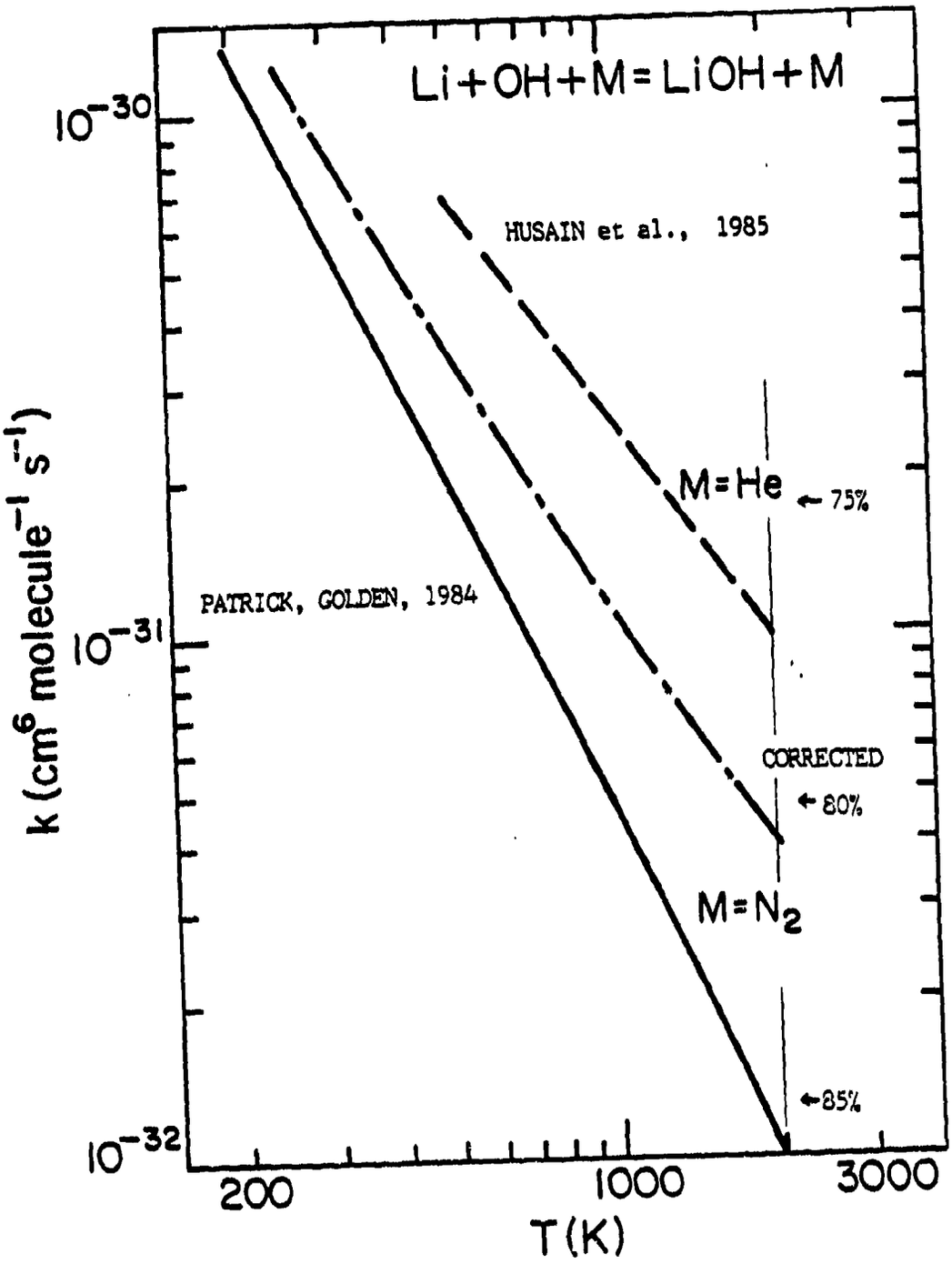
Li+OH+M=LiOH+M
HUSAIN et al., 1985
M=He
75%
PATRICK, GOLDEN, 1984
CORRECTED
80%
M=N2
85%
k (cm6 molecule-1 s-1)
10-30
10-31
10-32
200
1000
3000
T(K)

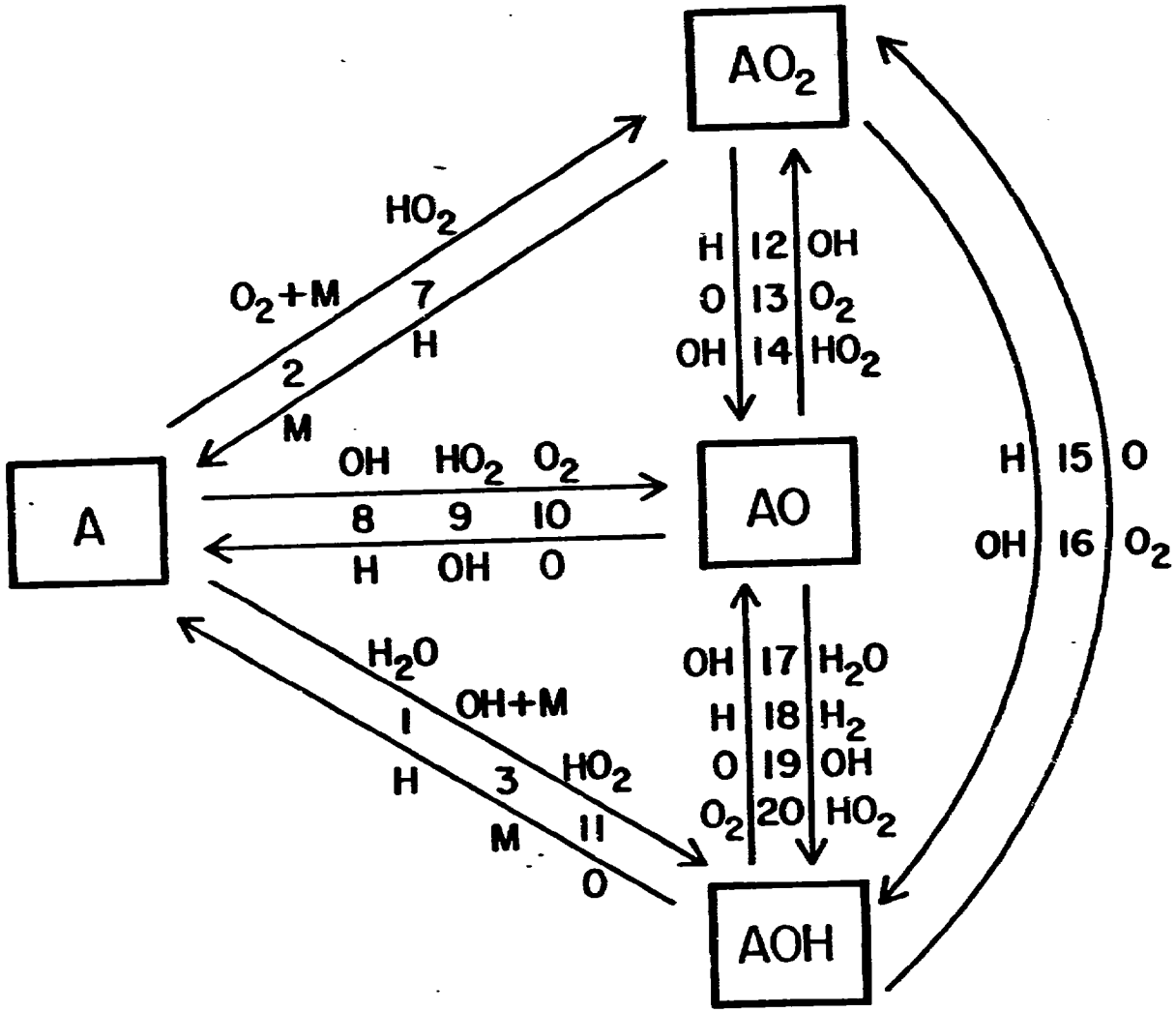
AO2
A
AO
AOH
HO2
O2+M
7
H
2
M
H 12 OH
O 13 O2
OH 14 HO2
OH HO2 O2
8 9 10
H OH O
H 15 O
OH 16 O2
H2O
OH+M
1
H
3
HO2
M
11
O
OH 17 H2O
H 18 H2
O 19 OH
O2 20 HO2

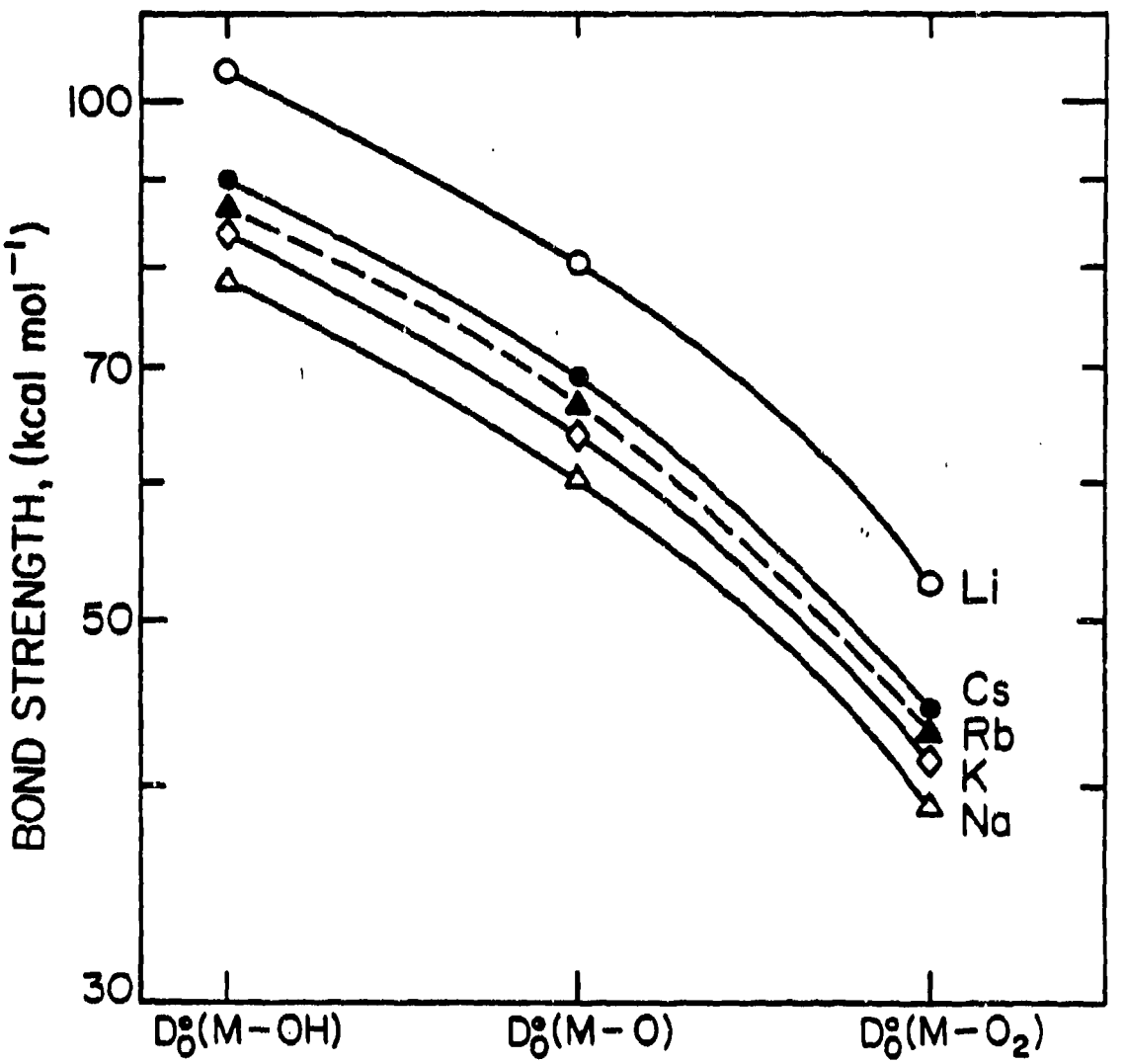
BOND STRENGTH, (kcal mol⁻¹)
100
70
50
30
Li
Cs
Rb
K
Na
D°₀(M–OH)
D°₀(M–O)
D°₀(M–O₂)

NEAR FUTURE PLANS

1. PUBLISH REFINED MODELING OF SODIUM OXIDATION CHEMISTRY -- MOST SENSITIVE TO $D(Na-O_2)$

2. COMPLETE THE ANALYSIS OF LITHIUM, ESTABLISH $D(Li-O_2)$ AND ITS KINETIC ROLE

3. MEASURE THE CONCENTRATION PROFILES OF K IN THE 10 FLAMES USING SATURATED LIF

Spectroscopic measurements in the exhaust flow of a 7.62 mm rifle using propellants with and without chemical flash suppressants

Hans Mach

Franco-German Research Institute St-Louis (ISL)
68301 Saint-Louis, France

Abstract

This paper describes measurements of gas velocities, gas temperatures and infrared absorption coefficients of some combustion products (CO_2, CO, H_2O, particles) along the centerline ($1 < x/d < 100$) of the muzzle exhaust flow of a 7.72 mm rifle. Ammunition with and without chemical muzzle flash suppressant have been used.

Introduction

The processes responsible for the muzzle flash and for its suppression can only be determined if sufficient measuring results exist. This paper relates to experiments which aimed at investigating the behaviour of the particle phase occurring in the exhaust flow and its interaction with the essential elements of the combustion gases CO_2, CO and H_2O. In particular, flow velocities, spectral radiances, spectral absorption coefficients and the temperatures in the exhaust flow field were to be measured. For this purpose we shall limit our investigation to the centerline zone $0 < x/d < 100$ during the first 0.5 - 6.0 ms when the projectile has left the muzzle. Some of the results obtained have been published previously [1, 2].

2. Experimental

The ammunition without suppressant was German A/S 300 propellant and with suppressant we chose French 6 BSp 85 of about the same composition but with an alkali additive of 0.5 K_2SO_4 and 0.07% Na_2SO_4. Muzzle velocity was about 800 m/s. Maximum pressure and temperature at the muzzle were 60 MPa and 1600 K, respectively. In order to measure the flow velocity we used the interference laser-Doppler velocimeter type ISL described previously [3]. This set-up has been successfully tested in earlier measurements probing the muzzle exhaust flow of the 7.62 mm rifle [4] and a 20 mm gun [5, 6]. In particular the measurements using the 20 mm gun yielded both the axial and lateral velocity components simultaneously, so that velocity vector projections could be obtained.

The experimental set-up is shown in Fig. 1a. The slightly focussed beam of an Ar-ion laser (λ = 514.5 mm) is transmitted particularly through the flow and measures the light scattered by particles. The light scattered under 45° is then collected by a lens and transmitted to the velocimeter using fiber optics. The velocimeter is basically a phase-stabilized Michelson interferometer of high sensitivity and luminosity. The Doppler shifted scattered light is transformed into a real-time signal being linearly proportional to the particle velocity. The time resolution is less than 10 µs, the spatial resolution in the x-direction 0.4 mm.

In order to measure both the gas and solid phase spectral emission and absorption, the experimental apparatus shown in Fig. 1b was used. It consists of the source, a calibrated globar and the detection unit. The radiant beam from the globar is focussed, chopped for identification with 22 kHz and collimated into the flow. Then it is focussed on the entrance of two InSb detectors by means of a beamsplitter. The wavelength selection was performed by interference filters. The spectral radiance L_λ and the optical transmittance τ_λ for several wavelengths λ were measured at selected wavelengths that correspond to strong bands of relevant molecules (CO_2, CO, H_2O). Between the bands the continuum background is due to incandescent particles. Therefore, measurements at the band free spectral region located on $\lambda = 3.8$ µm gives information on particulates. All measurements were made at several locations between 0.5 and 75 cm along the centerline of the flow.

From the transmittance τ measured along the right line the optical thickness $D = \ell n\ 1/\tau$ is obtained. Therefore, for exact determination of absorption coefficients $k = D/\ell$ a test section of an accurately known length ℓ is needed. Such a measured distance of 10 cm in length has been realized by guiding the measuring radiation into thin tubes of 13 mm outer diameter outside the test section. These tubes were closed by CaF_2 windows in the direction towards the measuring path.

3. Results

3.1 Solid phase

The wavelength dependence of the absorption coefficient can be written by the formula

$$k_\lambda = k_0 \left(\frac{\lambda_0}{\lambda}\right)^\nu \quad , \qquad (1)$$

ν being the dispersion exponent.

Measurements have shown [2] that ν lies in the near infrared region between 0.7 and 0.8. The absorption coefficient k_0 measured for a certain wavelength λ_0 can thus be calculated for other wavelengths λ as well. Small deviations from this behaviour can be explained by the fact that the particles do not only absorb the incident radiation but they can also scatter it. Measuring results show that a measured light extinction is for 80% due to real absorption and 20% of it are caused by light scattering.

3.1.1 Velocity

Fig. 2 shows an equivalent sequence of velocity recordings $v_x(t)$. Here, the steep variations across the shock disc are more apparent. The first velocity rise corresponds to the forward motion of the shock disc while the velocity drop describes the backward motion of the shock. It is interesting to note that the velocity increases again downstream behind the disc and decreases below zero because of the interactions occurring in the intermediate flash region [2, 5, 6].

The velocity measurements allow two further statements.

1) If the back-running shock disc of the exhaust flow field passes the measuring point the shock disc profile can be scanned. This yields the velocity ratio at both sides of the shock disc. If the pressure ratio is also measured, it is possible to determine the adiabatic coefficient k = 1.20, the temperature ratio (max. 2) and the Mach number of the shock disc (max. 3), under the condition that the Rankine-Hugoniot relations are valid.

   Taking into account that the measured velocities are related to particles having a certain inertia, the shock front profile must have a certain width which is a measure for the particle's relaxation time. This relaxation time, and resulting from it, the particle diameter can thus be obtained by scanning the velocity profile. It is remarkable to note that the relaxation times measured during 2 ms decreased from about 4.5 µs to 20 µs corresponding to a decrease of particle size from 1.3 µm to 0.5 µm [2]. This effect was independent of alkali salt additives in the propellant charge.

2) Another result can be obtained from an integration of the measured velocity values. This yields projectile trajectories in a x-t-diagram. Fig. 3 shows the result when ammunition containing alkali salt additives is used. Several particle trajectories a - h are indicated; the hatched zone representing the intermediate flash.

3.2 Measurements of emission and absorption

3.2.1 Emission

Taking into account emission/absorption recordings of rounds made with propellants with and without suppressant (Fig. 4) we see that for x = 7.5 cm and λ = 4.3 µm (CO_2) the second emission peak of the propellant with suppressant is only slighlty lower than that of the propellant without suppressant. The emission of the flow species is shown in the lower curve whereas the transmittance is given by the distance of the two curves at any time divided by the distance at t = 0. Without suppressant, it seems, however, that a strong emission takes place at about 1.3 ms which is totally lacking in the propellant with suppressant. Here, the emission decreases slowly and after 3.0 ms nothing can be seen anymore.

At the point x = 15 cm the phenomena are comparable to those described above. For λ = 4.3 µm the emission is again much stronger than for 3.8 µm, it even increases considerably between 2.0 and 3.0 ms, whereas for 3.8 µm the maximum is already reached at 1.6 ms.

Fig. 5 shows a series of emission/absorption recordings the length of the measuring path being exactly 10 cm. Measuring wavelength was 4.3 µm (CO_2 vibrational band). Qualitatively, the recordings are identical with that on fig. 4. With the rounds without suppressant the emission begins in about the same way as in the rounds with suppressant. At a certain moment both reach a maximum which, in the experiments without suppressant, increases in height proportional to the distance x. Without suppressant, however, the emission increases strongly at a given moment, when the emission with suppressant already decreases. Only after some ms it decreases again. Due to strong turbulence the emissions of course show strong fluctuations.

After calibrating the measured emission signals can be transformed into values of radiance. If the emission curves of a number of wavelengths (1 in this case) are combined, emission spectra for well-defined times and locations can be determined. Fig. 6 shows two such IR-spectra. They are relating to gas packages moving along two trajectories a and g (from fig. 3) on the flow axis, with x as parameter. The wavelengths showing the strongest emission are at 2.7 µm (CO_2, H_2O) and 4.3 µm (CO_2). At 3.8 µm there is a minimum which cannot be attributed to any molecule band, but corresponds to a continuum created by particles.

3.2.2 Temperature measurements

The recorded emission and absorption signals can be used to determine the temperature. It must, however, be taken into account that the considered flow field is not homogeneous. Three different methods were used:
The first method is based on averaging over the whole diameter of the flow. The radiance or the black body temperature S_λ integrated over the diameter, as well as the transmittance τ along the diameter, are measured. Then, temperature can be calculated from the well known formula

$$\frac{1}{T} = \frac{1}{S_\lambda} + \frac{\lambda}{c_2} \ln (1 - \tau) \qquad c_2 \text{ is a constant.} \qquad (2)$$

It is represented in Fig. 7 for two measuring points (x = 7.5 cm and x = 15 cm) using several wavelengths λ versus time. As can be easily seen the measuring results are identical for several wavelengths except for λ= 589 nm. The wavelength λ = 589 nm (resonance line of Na) leads to temperatures that are not only considerably higher than the values obtained with the other wavelengths, but they also do not follow their time curve. This behaviour has also been found by other authors. It can be assumed that it is based on non-equilibrium excitation of Na-atoms [7].

Measuring Na- or K-reversal temperatures in reacting gases as they occur in the muzzle flash therefore yields inexact results. Better results can be obtained for temperatures measured with the other wavelengths. For ammunition containing alkali additive a temperature maximum of about 1600 K takes place at x = 15 cm and t = 0.6 ms, as can be viewied on fig. 7.

The second method was only used in few cases. It is based on measurements of the lateral distribution of radiance and optical thickness and achieves a radial temperature distribution by numerical integral transformation, described in [2] and [7].

The third method is again an integral method like the first one, however, it does not use the whole diameter of the flow, but only a section of 10 cm. The results for rounds with and without suppressant (dashed curves) were obtained at the wavelengths λ = 4.3 µm, λ = 4.6 µm and λ = 2.5 µm and are drawn for different measuring points in fig. 8. Due to the high turbulence of the flow the measured values showed great dispersion, especially when no suppressant was used.

Thus, it was not possible to find different behaviour with and without suppressant at the temperature maximum and at the locations x = 15 cm and x = 20 cm. But at all locations it was evident that without suppressant temperature is much longer on a high level than with suppressant. Especially at the locations $x \geq 30$ cm temperature maxima without suppressant are significantly higher, at x = 50 cm they reach their highest value at a

temperature of 2700 K. The difference at x = 60 cm is equally clearly visible. With suppressant more than 2000 K and without only 500 K are reached.

3.2.3 Measurement of the spectral absorption coefficients

From the transmittance measurements absorption coefficients k_λ for the wavelengths 3.8 µm, 4.3 µm, 4.6 µm and 6.3 µm have been determined which can be attributed to the particulate phase and to CO_2, CO and H_2O-molecular bands, respectively. However, the absorption coefficients corresponding to the molecular bands only result from subtraction of the background continuum when the formula (1) is applied. They are indicated on the figure 9 versus time for three measuring distances x and for ammunition with and without suppressant. As can be seen the values show great dispersion. This is not astonishing taking into account the strong turbulence of the flow. The absorption coefficients of CO_2 and CO show quite similar behaviour. For short distances (x = 20 cm) we found higher absorption-coefficients with suppressants than without. For greater distances just the contrary is true. In any case the differences are only here clearly visible.

The relation between absorption-coefficients and gas or particle density has already been set up earlier. According to this we have about

$$p_{CO_2}/p_{CO} = 0.2\,\frac{k_{4.3}}{k_{4.6}} \quad . \qquad (3)$$

For the absorption-coefficients obtained from the particle phase (Fig. 9a) at the shortest distance x = 15 cm (and also present at x = 20 cm) just at the beginning a strong maximum is observed which is followed by a minimum. The minimum coincides with the temperature maximum (t = 0.6 ms). This indicates that particle concentration and gas density are proportional.

At later moments and greater distances we find curves similar to 4.3 µm and 4.6 µm. That means, without suppressant higher absorption-coefficients, and thereby higher particle concentrations n are found. According to earlier measurements the relation $n = 6.9 \cdot 10^4 \cdot k_{3.8}$ [cm^{-3}] is valid [2].

We thus have a maximum number density of $n_{max} = 2 \cdot 10^7 \cdot cm^{-3}$.

Fig. 10 shows a x-t-diagram of the centerline region where are drawn the movement of the shock disc and the lines for the beginning of notable absorption, as well as the lines for the beginning and ending of the emission. We differ between the end of emission with and without suppressant. In addition, the beginning of the second emission is shown for ammunition without suppressant. If no suppressant is used it looks as if the secondary flash is due to propellant gases having left the muzzle after 0.8 - 1.8 ms.

In an early study [2] absorption measurements were also made for OH-rotation lines and K-lines in the spectral region at 310 nm in order to determine OH and K concentrations, respectively . But only at the distance x = 35 cm notable quantities in the order of magnitude of 100 - 200 ppm OH could be found, the concentration for rounds without suppressant being a little higher.

Conclusions

1. During the passage of the combustion gases through the shock disc and the intermediate flash zone the particle concentration decreases relative to the CO and H_2O concentration, but the decrease is especially strong relative to CO_2. This leads to the conclusion that a particle pyrolysis with formation of CO_2 takes place.

2. The temperatures measured at different distances from the muzzle traverse a maximum which, of course, occurs later if the distance is greater. When using ammunition without suppressant the maximum temperature (T = 1500 K) firstly decreases with longer distances, then it reaches its lowest value at about 20 - 25 cm (T = 1300). Afterwards at x = 50 cm it mounts up to nearly 2700 K. Then it decreases slowly. In contrast to this the ammunition with suppressant shows at the beginning the same temperature history, but then decreases much more rapidly after having reached the maximum. At x = 40 cm the maximum becomes lowest (1200 K) but at x = 50 it again rises, but only up to nearly 2000 K. Afterwards, (x > 50 cm) a rapid decrease follows. If the temperature change is drawn in a x-t diagram (as isothermal distributions Fig. 11 and Fig. 12)) it can be observed that without suppressant the temperature decrease after passing through the maximum continues until a distance of about 24 cm (t = 0.9 ms), but then a new increase up to x = 50 cm (t = 2.4 ms) with temperatures of up to 2700 K occurs due to afterburning. Then we find a slow decrease. If ammunition with suppressant is used the minimum only occurs after a distance of x = 40 cm (t = 1.8 ms). Afterwards, these is only a relatively short temporal temperature increase until about 2000 K, followed by a very rapid decrease.

3. The absorption coefficients and the partial densities of the propellant gases incl. particles do not vary much when travelling along the centerline. The values measured for different distances generally pass through a maximum with not very different heigth for rounds without and with suppressant. The difference being that with suppressant the density decrease after the maximum occurs much more rapidly.

   For the interpretation of the results we best look again at an x-t diagram(Fig. 13). For all rounds it has been observed that gas and particle ejection at the muzzle takes not place in regular intervals, but that in the region between 1.5 ms and 2.0 ms the gas leaves the muzzle with a maximum absorption coefficient, i.e. maximum density. Later on this density normally diminishes more and more. For CO_2, however, we find in rounds without suppressant at the distances x > 40 cm a new increase of the concentration its maximum being at x = 60 cm (t = 4.5 ms). Without suppressant this maximum is not observed.

   In the particle phase the difference when using suppressant consists in the acceleration of concentration decrease. Just the same happens with the CO_2.

Summarizing we have to conclude that the observed intensity differences in rounds with and without alkali suppressants can only be attributed to changes in temperature. Significant changes of the concentration of the particle phase as well as of the species CO_2, CO and H_2O as being caused by rounds with and without alkali suppressants could not be detected during the secondary flash event.

References

[1] H. MACH
Measurements of two-phase exhaust flow parameters of a small caliber gun associated with muzzle flash phenomena, Seventh Internat. Sympos. on Ballistics. The Hague, the Netherlands, 19-21 April 1983, published also under ISL report CO 212/83

[2] H. MACH, U. WERNER, H. MASUR
Measurements on the two-phase exhaust flow of a 7.62 mm rifle
Report ISL (in German) R 110/84

[3] G. SMEETS, A. GEORGE
Michelson spectrometer for instantaneous Doppler velocity measurements
J. Phys. E: Sci. Instrum. 14, 1981, 838

[4] H. MACH, H.J. SCHÄFER, G. KLINGENBERG
Laser anemometry applied to unsteady two-phase reacting propellant flow
Report ISL CO 217/82, 1982

[5] H. MACH, U. WERNER, H. MASUR
Measurement of the unsteady velocity field in the muzzle exhaust flow of a 20 mm rifled gun using a laser Doppler interferometer
Report ISL R 128/81, 1981

[6] G. KLINGENBERG, H. MACH, G. SMEETS
Probing of the unsteady reacting muzzle exhaust flow of 20 mm gun
AIAA/ASME. Third Joint Thermophysics, Fluids, Plasma and Heat Transfer Conference, St-Louis,Missouri (USA), June 7-11, 1982

[7] G. KLINGENBERG, H. MACH
Spectroscopic temperature measurements in interior ballistic environments.
Proc. 10th ICIAST 20.-23.9.83, ISL, St-Louis, France

[8] I.S. ZASLONKO et al.
Excitation of sodium in certain reactions behind shock waves.
Combustion, Explosions, Shock Waves, 8, 1972, 175

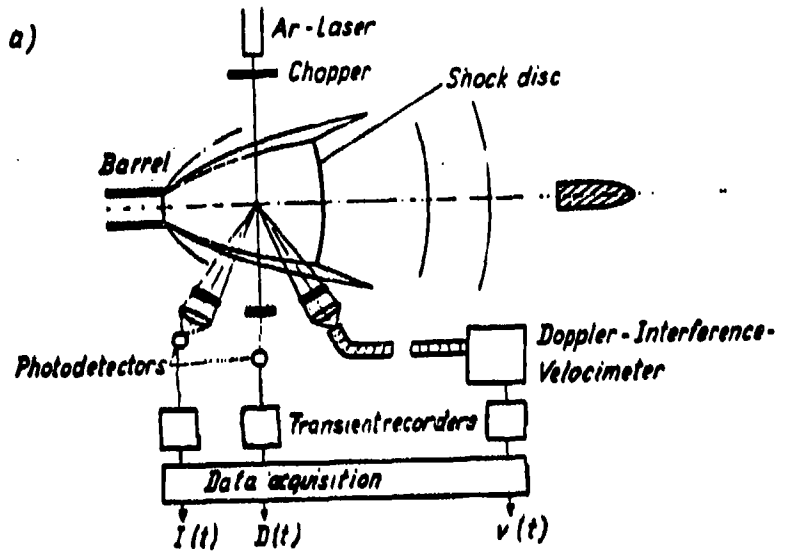

Fig. 1 Scheme of experimental set-up

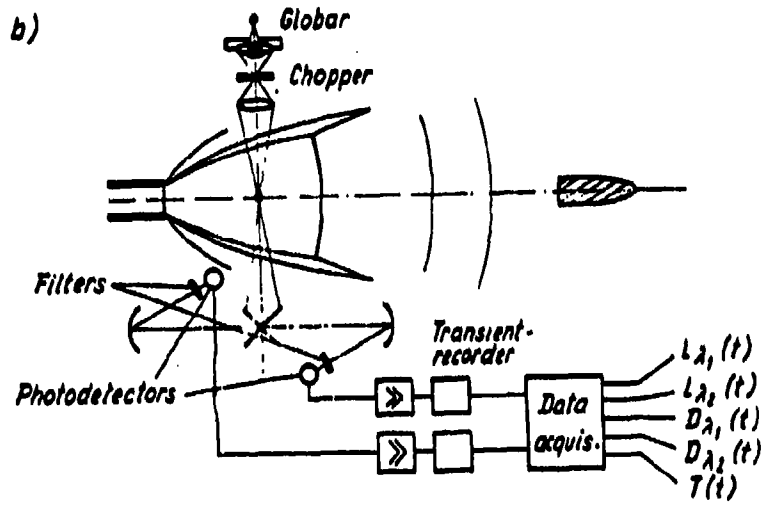

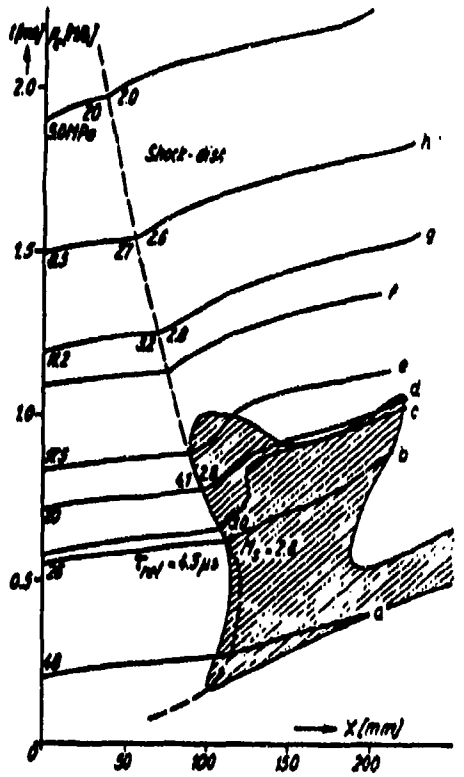

Fig. 3 Selected particle trajectories

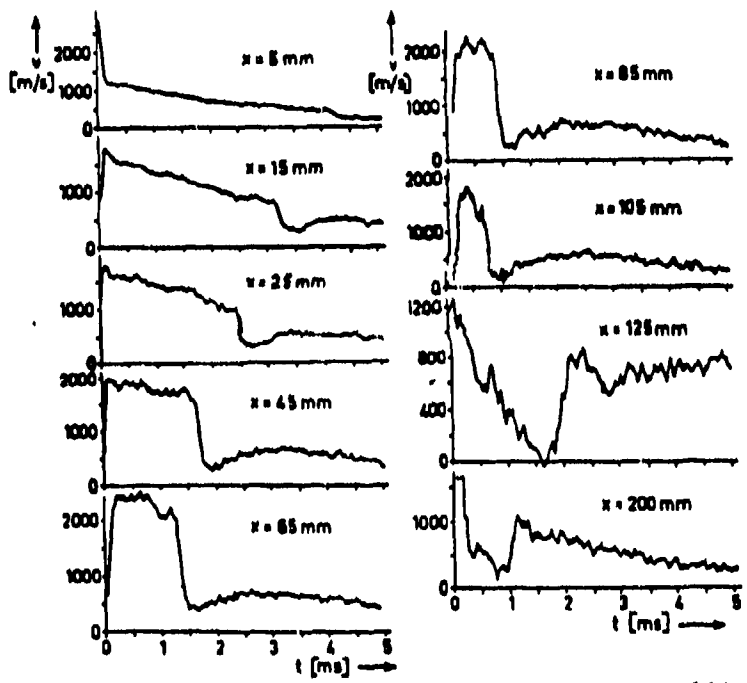

Fig. 2 Velocity histories at selected positions x

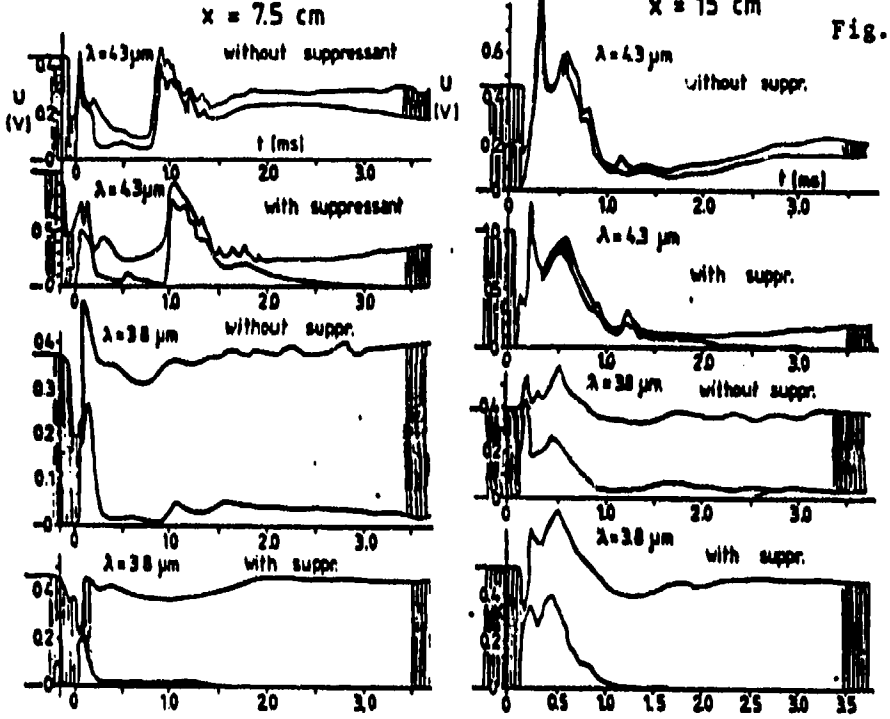

Fig. 4 Infrared-emission and absorption at x = 7.5 cm and x = 15 cm (λ_1 = 4.3 μm (CO_2), λ_2 = 3.8 μm (particles))

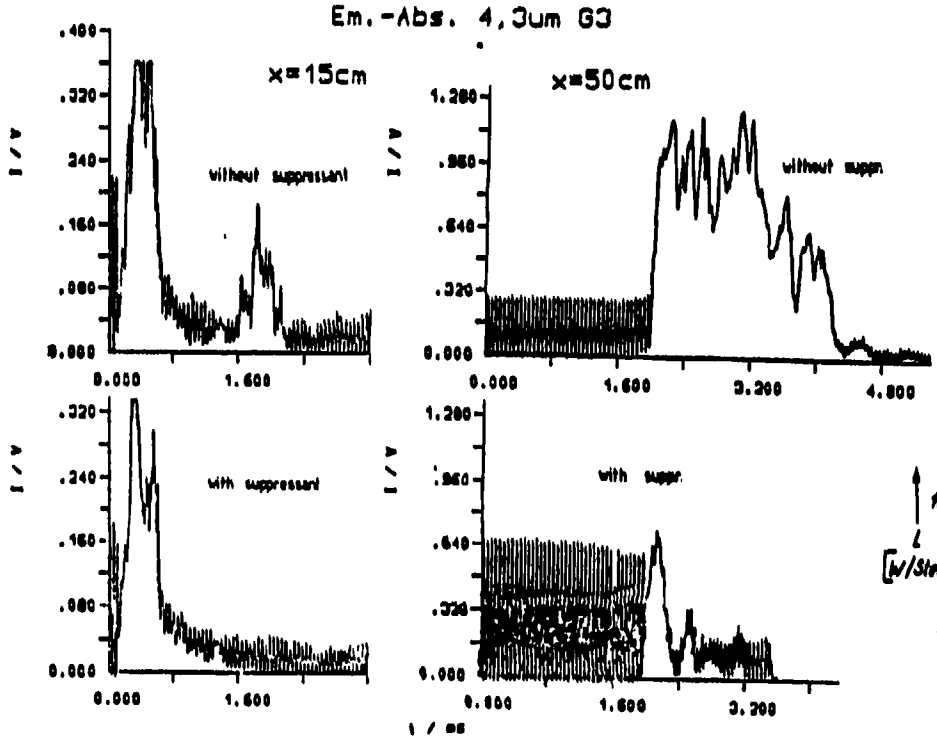

Fig. 5 IR-emission and absorption at x = 15 cm and x = 50 cm

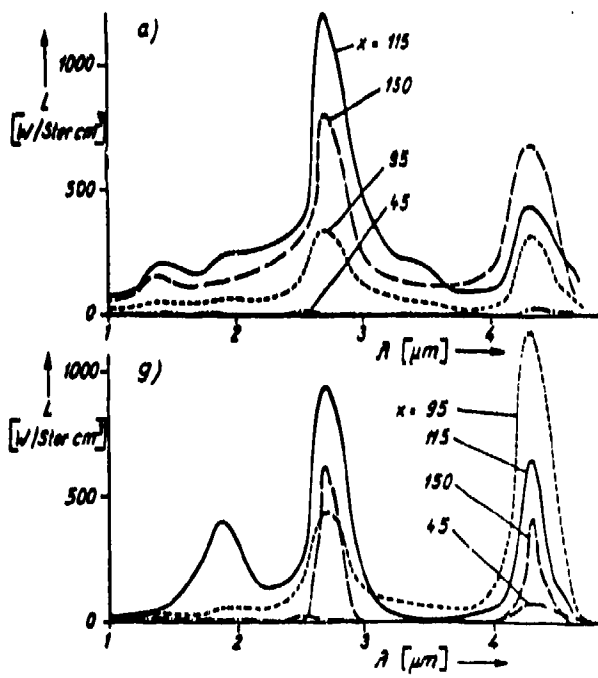

Fig. 6 IR-emission-spectra for the trajectories a and g of Fig. 3

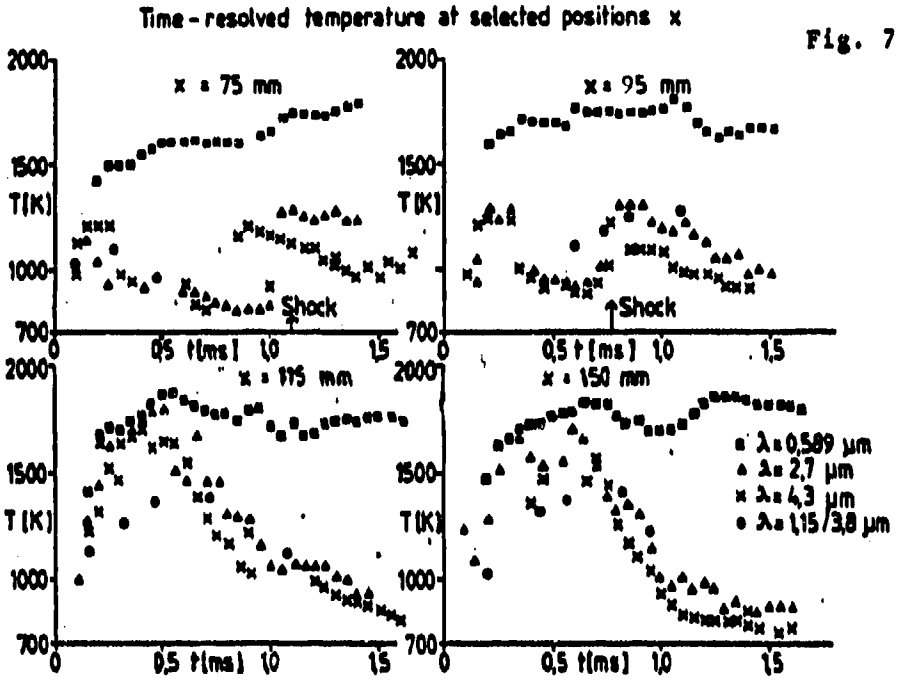

Fig. 7 Time-resolved temperature at selected positions x

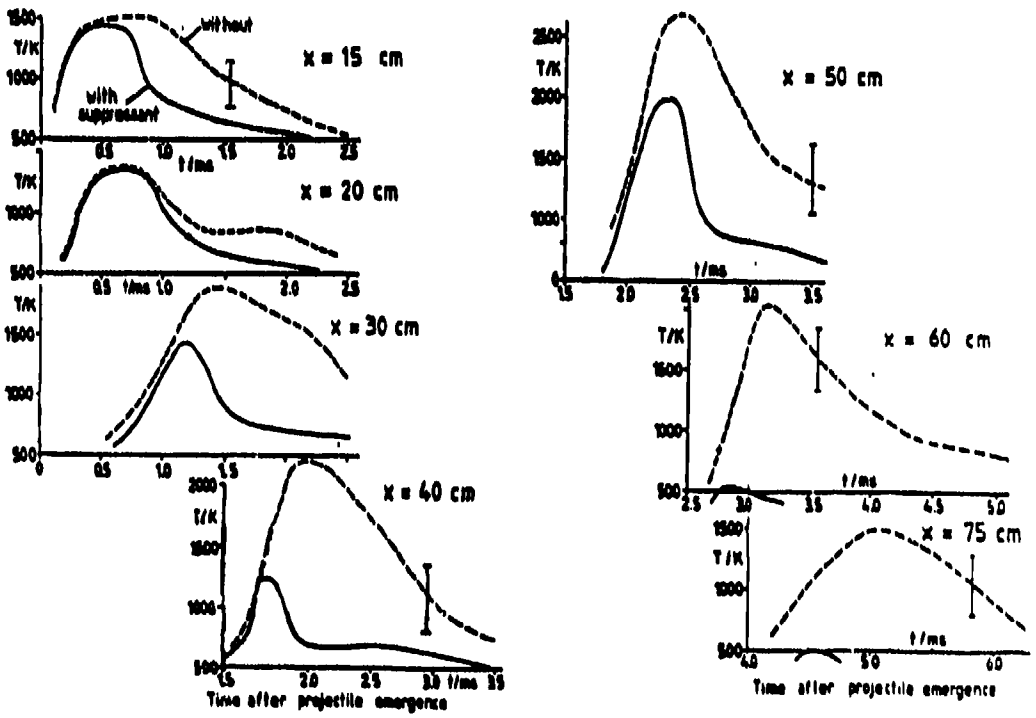

Fig. 8 Averaged temperature histories at selected positions x using ammunition with and without alkali suppressant

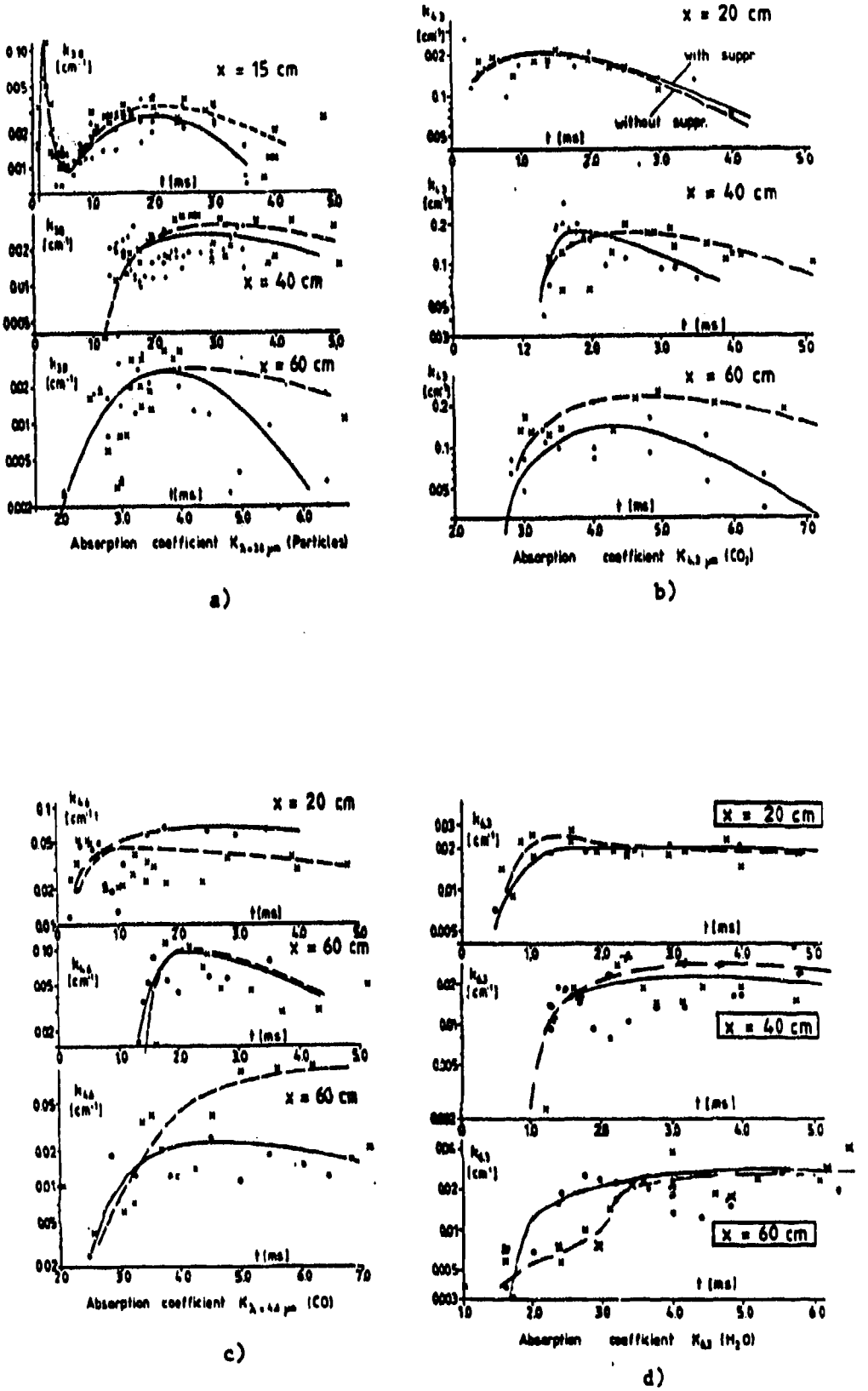

Fig. 9 Spectral absorption coefficient of the particulate phase at $\lambda = 3.8\ \mu m$ (a) and of the gaseous species CO_2 (b), CO (c) and H_2O (d)

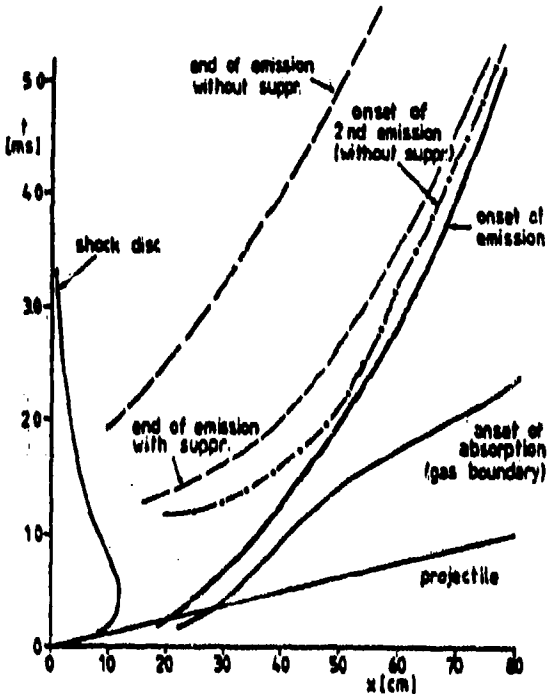

Fig. 10 Emission and absorption-lines (on set and end of emission and absorption)

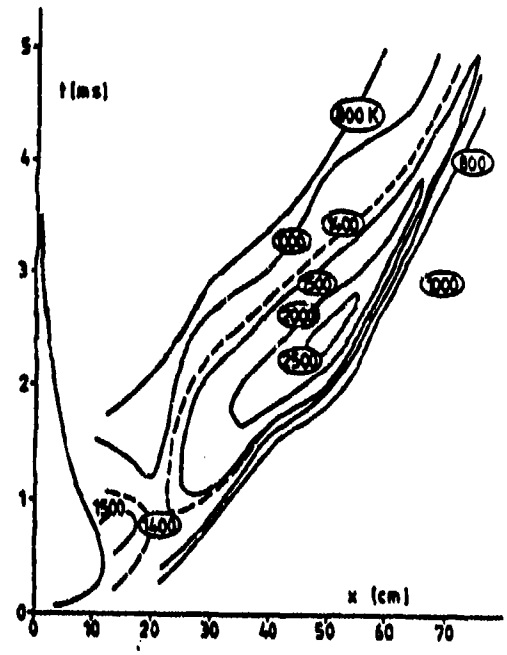

Fig. 11 Temperature distribution using ammunition without alkaline suppressant

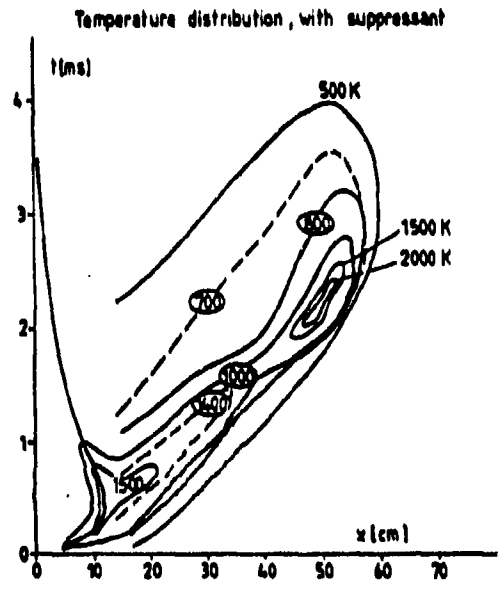

Fig. 12 Temperature distribution using ammunition with alkaline suppressant

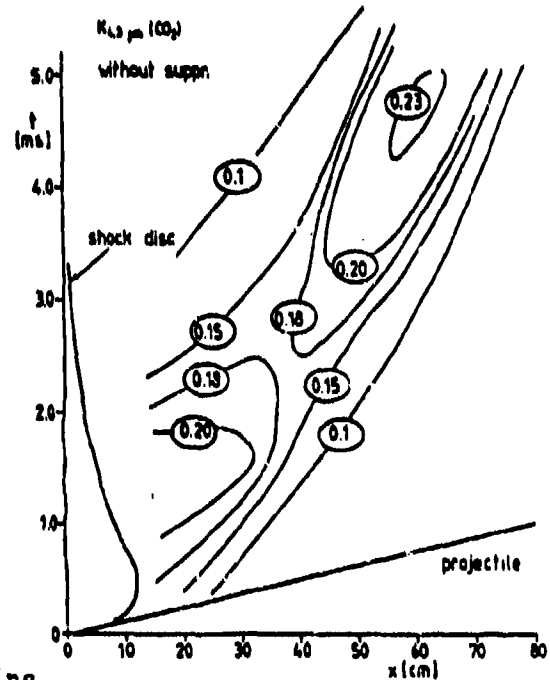

Fig. 13 Distribution of the absorption coefficient $K_{4.3}/cm^{-1}$ using ammunition without alkaline suppressant

CHEMICAL KINETIC STUDIES AND INFRARED LASER DETECTION OF POTASSIUM AND SODIUM SPECIES RELEVANT TO MUZZLE FLASH AND ROCKET PLUME AFTERBURNING SUPPRESSION

Prepared by

C.E. Kolb, M.S. Zahniser,
J.A. Silver and A. Freedman
Center for Chemical and Environmental Physics
Aerodyne Research, Inc.
45 Manning Road
Billerica, MA 01821

Prepared for

Workshop on the Chemical Suppression of
Afterburning and of Gun Muzzle Flash
Ballistic Research Laboratory
Aberdeen Proving Ground, MD 21005

June 1986

TABLE OF CONTENTS

Section		Page
	ABSTRACT	
1	INTRODUCTION	1-1
2	ALKALI SPECIES SOURCES AND DETECTION METHODS	2-1
	2.1 Development of Sources for Alkali Oxide and Hydroxide Species	2-1
	2.2 Detection Methods for Gas Phase Alkali Species	2-3
	2.3 Kinetic Studies of Alkali Species	2-4
3	TUNABLE DIODE LASER DETECTION OF GASEOUS ALKALI SALTS IN LABORATORY AND COMBUSTION FLOWS	3-1
	3.1 Background	3-1
	3.2 Experimental Studies	3-2
	3.2.1 Tunable Diode Laser Apparatus and Methodology	3-2
	3.2.2 Production of Gas Phase Alkali Compounds	3-4
	3.2.3 Results	3-6
	3.3 Estimated Detection Sensitivities for Combustion Applications	3-8
	3.4 Preliminary Assessment of Spectral Interferences	3-14
	3.5 Conclusions	3-15
4	ACKNOWLEDGEMENTS	4-1
5	REFERENCES	5-1

ABSTRACT

Rate constants have been determined for gas phase reactions of alkali species which are relevant to flame suppression chemistry by sodium and potassium compounds. Sources and detection methods for gas phase molecular alkali species KO, KO_2, Na, NaO_2 and NaOH have been developed and applied to kinetic studies of these species using a high temperature fast flow reactor.

Rate constants for the recombination reactions of alkali atoms with molecular oxygen, $K + O_2 + M \rightarrow KO_2 + M$ and $Na + O_2 + M \rightarrow NaO_2 + M$, have been measured as a function of temperature from 300 to 700 K. Laser induced fluorescence is used to monitor the disappearance of Na or K as a function of O_2 and M. The reactions are studied in their low pressure third order limit from 1 to 8 torr total pressure with N_2, He, and Ar as third bodies.

The reactions of NaOH, NaO_2 and NaO with HCl at 300 K are found to proceed at their gas kinetic limits to form NaCl. Other reactions studies include: $NaOH + H \rightarrow Na + H_2O$, $NaCl + H \rightarrow Na + HCl$ and both Na and K with H_2O_2. Product analysis for the latter two shows that for Na 0.6 of the reactions form NaOH + OH with the remainder forming $NaO + H_2O$ with less than 2×10^{-3} going to KOH + OH. An upper limit of 3×10^{-15} cm^3 s^{-1} is established for the reaction $K + H_2O \rightarrow KOH + H$ at 1273 K.

Accurate studies of KOH and NaOH with H and other radicals require a direct detection method for these species. We propose the utilization of tunable diode laser infrared absorption. This method has wide applicability for direct detection of a number of molecular alkali species for laboratory kinetic studies and for in situ combustion flame diagnostics, possibly including muzzle flash simulations. Theoretical sensitivity estimates are calculated for KOH, KO_2, KO, NaOH, NaO_2, NaO and NaCl for both high temperature, atmospheric pressure and low pressure flow tube conditions. A direct measurement of KF in our laboratory shows the basic applicability of the method.

1. INTRODUCTION

The secondary combustion of CO and H_2 rich propellant exhaust gases from large caliber guns (muzzle flash) and tactical rockets (afterburning) is a basic combustion phenomenon with seriously detrimental characteristics. Propellant formulators have long known that these secondary combustion processes can be suppressed by the addition of sodium and/or potassium salts to the propellant mix.

Modeling of secondary combustion in both rocket and muzzle exhaust flows strongly indicates that this suppression takes place via the scavenging of combustion radical chain carriers (H, OH, HO_2, O) through interactions with gas phase alkali species.[1-5] Key reactions in this scavenging process include:

$$KOH\ (NaOH) + H \rightarrow K\ (Na) + H_2O \qquad (1)$$

$$K(Na) + O_2 + M \rightarrow KO_2\ (NaO_2) + M \qquad (2)$$

$$KO_2\ (NaO_2) + H \rightarrow K(Na) + HO_2 \qquad (3)$$

Model calculations indicate that reaction (1) is the major chain radical scavenging reaction operating under rocket exhaust plume or muzzle flow field conditions.[1-5] Model kinetic sensitivity studies also show that reactions (2) and (3) are capable of regenerating flame radical species, thus countervailing reaction (1).[5]

Solid propellants which contain halogen components such as ammonium perchlorate also produce gaseous HCℓ as a major exhaust species. Gaseous HCℓ can intervene in the desired suppression chemistry by promoting formation of gaseous alkali chloride:

$$KOH\ (NaOH) + HC\ell \rightarrow KC\ell\ (NaC\ell) + H_2O \qquad (4)$$

$$KO_2\ (NaO_2) + HC\ell \rightarrow KC\ell\ (NaC\ell) + HO_2 \qquad (5)$$

A thorough knowledge of the kinetic rate parameters of reactions 1-5 is required for accurate computer modeling of the effects of alkali afterburning

suppression as a function of propellant formulation and gun or rocket operating parameters. Without such models, propellant formulators have a difficult time determining the proper trade-off between the desirable secondary combustion suppression and the undesirable reduced primary combustion and enhanced corrosion effects imparted by alkali salt propellant additives.

The work presented in this report represents advanced experimental efforts to develop the capability to directly measure the required gas phase reaction rate parameters for refractory molecular species such as KOH, NaOH, KO_2 and NaO_2. Prior to this work, direct, gas phase, kinetic measurements involving these species were largely non-existent.

In order to perform these direct kinetic measurements, two preliminary problems had to be solved: first, reliable gas phase sources for the relevant alkali species K, Na, KOH, NaOH, KO_2 and NaO_2 had to be developed; second, reliable and sensitive ways to detect these species also had to be perfected. Only after the successful development of both generation and detection techniques for these refractory species could specific reaction rate parameters be determined. Direct detection methods for KOH, NaOH, KO_2 and NaO_2 remain unproven, but KF has been directly monitored using tunable diode laser infrared spectroscopy and extension of this technique to the oxide and hydroxide compounds appears to be straightforward.

The following sections of this report will present the development of both the gaseous alkali sources and detection techniques as well as the results of specific reaction rate parameter measurements.

2. ALKALI SPECIES SOURCES AND DETECTION METHODS

2.1 Development of Sources for Alkali Oxide and Hydroxide Species

Since the determination of reaction rate constants in the laboratory depends on the ability to create clean and well defined sources of the reactants, considerable effort was expended in the development of sources for K, Na, KO_2, NaO_2, KOH and NaOH which are suitable for flow reactor kinetic studies. Although the alkali species K and Na are relatively straight-forward to produce from vaporization of the solid, the oxide and hydroxide species are not readily produced by direct vaporization. The low vapor pressures of the solid alkali hydroxides combined with their chemical corrosiveness and tendency to form dimers makes direct vaporization unsuitable as a reactant source. We therefore explored gas phase chemical reactions whereby the easily vaporized Na or K could be converted quantitively and cleanly into the corresponding oxide or hydroxide.

NaO_2 and KO_2 may be formed by the direct recombination of the alkali atom with molecular oxygen

$$K\ (Na) + O_2 + M \rightarrow KO_2\ (NaO_2) + M\ . \qquad (2)$$

These reactions are relatively rapid compared to other three body processes and proceed with rate constants greater than 10^{-30} $cm^6 s^{-1}$ at 300 K as determined in one of our publications from this work.[6] They can be used as a clean source of superoxide in flow reactors by prereacting the alkali atom with O_2 in a separate region with higher O_2 concentration to drive the reaction to completion before the products enter the main flow tube.

An alternative method for NaO_2 formation is the combination of bimolecular reactions of Na with ozone

$$Na + O_3 \rightarrow NaO + O_2 \qquad (6)$$

$$NaO + O_3 \rightarrow NaO_2 + O_2 \qquad (7a)$$

$$\rightarrow Na + 2O_2 \qquad (7b)$$

These reactions have been studied recently at Aerodyne[7] and are found to be rapid with $k_6 = 3.2 \times 10^{-10}$ cm^3s^{-1}, $k_7 \sim 10^{-10}$ cm^3s^{-1} and $k_{7a}/k_{7b} \sim 3$. Although some Na is initially reformed in Reaction 7b, the larger branching ratio for NaO_2 formation in 7a eventually dominates so that all Na will be converted to NaO_2. This bimolecular source of NaO_2 may be superior to the O_2 recombination source in experiments where the presence of minimal amounts of O_2 are desirable.

NaOH may be formed cleanly and quantitatively by reaction of Na with hydrogen peroxide

$$Na + H_2O_2 \rightarrow NaOH + OH \qquad (8a)$$

$$\rightarrow NaO + H_2O \qquad (8b)$$

Our measurements[8] of this reaction rate constant and branching ratio give values $k_{8a} = 4.2 \times 10^{-11}$ cm^3s^{-1} and $k_{8b} = 2.7 \times 10^{-11}$ cm^3s^{-1}. Although Reaction 8 gives a mixture of NaOH and NaO, a pure source of NaOH may be produced by adding CO. This converts NaO back to Na via the reaction

$$NaO + CO \rightarrow Na + CO_2 \qquad (9)$$

After several cycles through Reactions 8 and 9 all the initial Na is converted to NaOH. This source and its application to the reaction of NaOH with HCl is described in detail in Reference 8.

The analogous reaction for K with H_2O_2 was also studied under this program. In this case, however, the channel forming KOH is considerably less than the KO channel,

$$K + H_2O_2 \rightarrow KOH + OH \qquad (10a)$$

$$\rightarrow KO + H_2O \; . \qquad (10b)$$

Attempts to observe KOH directly by observation with tunable diode laser absorption and indirectly by conversion back to K with atomic hydrogen, as was done successfully in the NaOH studies, indicated no detectable reaction for 10a. Attempts to detect the OH product using laser induced fluorescence also indicated no reaction although the analogous experiment in the Na case under the same experimental conditions did produce quantitative amounts of OH from reaction 8a. From the ratio of our OH detection limit and a quantitative measure of the initial K-atom concentration we obtain an upper limit to the branching ratio $k_{10a}/k_{10b} < 2 \times 10^{-3}$. The overall reaction rate for k_{10} was determined from the disappearance of K in excess H_2O_2 to be $k_{10} = 1 \times 10^{-11}$ cm^3s^{-1} which is somewhat slower than the analogous Na reaction.

2.2 Detection Methods For Gas Phase Alkali Species

Although atomic K and Na are readily detectable in the gas phase using laser induced fluorescence (LIF), the alkali oxides and hydroxides are much more difficult to detect sensitively and specifically. Since detection of these species is an important component for laboratory kinetic studies and eventually for in situ detection in combustion and atmospheric environments, we have made the development of detection methods a major emphasis of this program. These methods may be divided into two categories: (1) chemical conversion of the alkali oxide or hydroxide into the readily detectable Na or K atomic species and (2) direct spectroscopic methods using high resolution infrared absorption. The chemical conversion method has been used for NaOH, NaO_2 and NaO in our published studies from this program.[8,9] The direct spectroscopic detection of KOH using infrared tunable diode laser absorption has also been accomplished under this program as described below. High resolution infrared absorption shows particular promise for the detection of other alkali species and is presently under further development at Aerodyne with Department of Energy sponsorship. More details on this method and sensitivity estimates for both sodium and potassium compounds are given in Section 3.

Detection of NaOH and NaO by chemical conversion to Na is accomplished by addition of excess atomic hydrogen in the detection region just upstream of the LIF probe:

$$NaOH + H \rightarrow Na + H_2O \qquad (11)$$

$$NaO + H \rightarrow Na + OH \qquad (12)$$

The rate constant for reaction 11 has been determined in this study[8] to be $k_{11} > 4 \times 10^{-12}$ $cm^3 s^{-1}$. Although H-atom addition and subsequent Na detection by LIF would not distinguish between NaOH and NaO, the latter may be detected independently by adding CO to the detection region which converts NaO to Na via reaction 9. No reaction was observed between NaOH and CO so that alternate additions of H and CO could be used to specifically detect either alkali species.

The main advantage of the chemical conversion of molecular alkali species to the corresponding atomic species is the extreme sensitivity of LIF detection for Na and K. Detection limits of less than 10^5 atoms cm^{-3} are achievable due to the high oscillator strengths of the D-line transitions.

2.3 Kinetic Studies of Alkali Species

The sources and detection methods described above have been employed in the study of a number of reactions during the course of this program. Reaction rate constants and product branching ratios have been determined using a high temperature fast flow reactor which can operate over the range 300 to 1300 K. The apparatus and methods used have been described in previous publications.[10,11] The specific applications to alkali chemistry are described in detail in the publications resulting from this work.[6-9] The reactions studied and the measured rate constants are summarized in Table 1.

The recombination reactions of Na and K with O_2

$$K\ (Na) + O_2 + M \rightarrow KO_2\ (NaO_2) + M \qquad (2)$$

Table 1. Summary of Measured Reaction Rate Constants for Alkali Species

Reaction	T(K)	Rate Constant	
$K + O_2 + N_2 \rightarrow KO_2 + N_2$	302-720	$(5.4 \pm 0.2) \times 10^{-30}(T/300)^{-0.56 \pm 0.20}$	$cm^6 s^{-1}$
$K + O_2 + He \rightarrow KO_2 + He$	296-520	$(2.0 \pm 0.5) \times 10^{-30}(T/300)^{-0.9 \pm 0.5}$	$cm^6 s^{-1}$
$K + O_2 + Ar \rightarrow KO_2 + Ar$	300	$(3.5 \pm 1) \times 10^{-30}$	$cm^6 s^{-1}$
$Na + O_2 + N_2 \rightarrow NaO_2 + N_2$	320-700	$(1.9 \pm 0.4) \times 10^{-30}(T/300)^{-1.1 \pm 0.5}$	$cm^6 s^{-1}$
$Na + O_2 + He \rightarrow NaO_2 + He$	310-470	$(1.4 \pm 0.3) \times 10^{-30}(T/300)^{-0.9 \pm 0.5}$	$cm^6 s^{-1}$
$Na + O_2 + Ar \rightarrow NaO_2 + Ar$	324	$(1.2 \pm 0.3) \times 10^{-30}$	$cm^6 s^{-1}$
$Na + H_2O_2 \rightarrow NaOH + OH$	308	$(4.1 \pm 1.8) \times 10^{-11}$	$cm^3 s^{-1}$
$Na + H_2O_2 \rightarrow NaO + H_2O$	308	$(2.8 \pm 1.2) \times 10^{-11}$	$cm^3 s^{-1}$
$K + H_2O_2 \rightarrow KOH + OH$	300	$< 2 \times 10^{-14}$	$cm^3 s^{-1}$
$K + H_2O_2 \rightarrow KO + H_2O$	300	$(1.0 \pm 0.5) \times 10^{-11}$	$cm^3 s^{-1}$
$K + H_2O \rightarrow KOH + H$	1273	$< 3 \times 10^{-15}$	$cm^3 s^{-1}$
$NaOH + H \rightarrow Na + H_2O$	300	$> 4 \times 10^{-12}$	$cm^3 s^{-1}$
$NaOH + HCl \rightarrow NaCl + H_2O$	300	$(2.8 \pm 0.9) \times 10^{-10}$	$cm^3 s^{-1}$
$NaO + HCl \rightarrow NaCl + OH$	300	2.8×10^{-10}	$cm^3 s^{-1}$
$NaCl + H \rightarrow Na + HCl$	300	5×10^{-14}	$cm^3 s^{-1}$
$NaO_2 + HCl \rightarrow NaCl + HO_2$	300	$(2.3 \pm 0.4) \times 10^{-10}$	$cm^3 s^{-1}$

have been studied over the temperature range 300 to 700 K and with M = N_2, He and Ar. The resulting rate constants (Table 1) are greater than those deduced from earlier flame studies of Carabetta and Kaskan[12] which were the only ones available for flame suppression modeling at the beginning of this program. Several other studies[13-15] have since confirmed this faster rate and it is now well established that these reactions are sufficiently rapid to be important in combustion and alkali flame suppression chemistry.

Measurements of the reaction of sodium hydroxide with atomic hydrogen

$$NaOH + H \rightarrow Na + H_2O \qquad (1)$$

indicate that this reaction is rapid with a rate constant greater than 4×10^{-12} $cm^3 s^{-1}$ at 300 K. This is an important result for flame suppression modeling since this reaction is believed to be the main radical scavenging mechanism in alkali-seeded flames. Our result for this rate constant is considerably greater than that extrapolated from the flame data by Jensen and Jones[16] who obtain a value of 1.8×10^{-11} $e^{-990/T}$ or 6.6×10^{-13} $cm^3 s^{-1}$ at 300 K.

The rate constant for the analogous reaction of potassium hydroxide with atomic hydrogen

$$KOH + H \underset{(-1)}{\overset{(1)}{\rightleftarrows}} K + H_2O$$

has not yet been determined. Direct detection methods for both KOH, using infrared diode laser absorption, and for H-atoms, using resonance fluorescence at 121.6 nm, can be implemented on our flow tube. The rate measurement, however, has been hindered by the lack of a suitable source of gas phase KOH. The reaction of K with hydrogen peroxide

$$K + H_2O_2 \rightarrow KOH + OH \qquad (10a)$$

$$\rightarrow KO + H_2O \qquad (10b)$$

was found to yield mostly KO rather than KOH with $k_{10a}/k_{10b} < 2 \times 10^{-3}$. The analogous Na reaction yielded nearly 60% NaOH. The other source of KOH which was tried, high temperature sublimation of solid KOH, also proved unsuitable as a flow tube source due to its highly corrosive nature and its tendency to form KOH dimers. A more suitable source of gas phase KOH needs to be developed before this reaction rate can be directly determined.

An attempt to determine the rate of KOH + H through measurement of the rate constant for the reverse reactions

$$K + H_2O \rightarrow KOH + H \qquad (11)$$

also proved unsuccessful. In this experiment the resonance fluorescence signal for atomic potassium was monitored as water vapor was added to the flow reactor. Experiments at temperatures of 973, 1173 and 1273 K showed no detectable reaction which establishes an upper limit for this rate constant of $k_{-1} < 3.6 \times 10^{-15}$ cm^3s^{-1}. In theory an upper limit for k_1 may be established by combining k_{-1} with the thermodynamic equilibrium constant

$$K_{eq} = k_1/k_{-1}.$$

In this case, combining our upper limit for k_{-1} with K_{eq} implies only that $k_1 < 2 \times 10^{-10}$ cm^3s^{-1}. A lower measurable limit for k_{-1} or a higher experimental temperature is required to set a more meaningful upper limit for k_1. Attempts to extend the experimental temperature range to 1500 K, however, were thwarted by the large K background fluorescence from the hot flow tube walls which prevented meaningful measurements of the decay rate of K with H_2O at these temperatures.

The reaction of gas phase NaOH with HCl[8]

$$NaOH + HCl \rightarrow NaCl + H_2O \qquad (4)$$

was found to procede essentially at its gas kinetic limit with a rate constant of 2.8×10^{-10} cm^3s^{-1} at 308 K. This reaction could be an important process in flame suppression chemistry of fuels such as perchlorates with a high halogen content. The reaction may also be important in upper atmospheric chemistry of meteor-ablated sodium and was measured in conjunction with other programs to study the effects of alkali chemistry on stratospheric ozone. Other reactions studied during this program[8,9] include

$$NaO + HCl \rightarrow NaC + OH \quad (13)$$

$$NaO_2 + HCl \rightarrow NaC + HO_2 \quad (14)$$

and

$$NaCl + H \rightarrow Na + HCl$$

which could also participate in perchlorate fuel flame suppression chemistry. Both the NaO + HCl and NaO_2 + HCl reactions were found to procede at their gas kinetic limits with $k_{13} = 2.8 \times 10^{-10}$ cm^3s^{-1} and $k_{14} = 2.3 \times 10^{-10}$ cm^3s^{-1} at 300 K.[19] Since these bimolecular reactions are already in their gas kinetic limits and since they procede via an electron jump mechanism, no large temperature dependence is expected and these rate constants should also be applicable to combustion temperatures. The NaCl + H reaction is much slower with $k_{15} \sim 5 \times 10^{-14}$ cm^3s^{-1}. The successful measurements of these reaction rate constants vividly demonstrates the versatility of the fast flow reactor technique for further kinetic studies of alkali oxide and hydroxide species.

3. TUNABLE DIODE LASER DETECTION OF GASEOUS ALKALI SALTS IN LABORATORY AND COMBUSTION FLOWS

3.1 Background

Detection of gaseous alkali compounds in either a laboratory flow apparatus or a hot combustion stream is a difficult proposition. The criteria for such a device include:

- Non-intrusive but in situ
- Specificity
- Sensitivity, and
- Real-time detection.

The first criterion insures that the probe does not interfere with the operation of the combustor or perturb the flow so as to bias the results. The device must be specific as to the exact identity of the detected species since the downstream effects are dependent on the molecular structure or the deposited salt. Validation of combustion models also requires specificity. Sensitivities of parts per million are desirable.

In fact, there are very few ways in which alkali molecules can be detected under in situ combustion conditions. Mass spectrometry is intrusive, expensive, and is extremely difficult to calibrate. Grab sample techniques severely perturb the composition and no true measure of gas phase concentrations can be made. Visible or UV laser induced fluorescence will not work because there are no bound electronic states in alkali halides or hydroxides, and CARS (Coherent Anti-Stokes Raman Spectroscopy) is too difficult to set up and not nearly sensitive enough. Photofragment emission is non-specific and is extremely difficult to quantify.

We believe infrared absorption is favored because alkali molecules are predicted to have large absorption linestrengths, thus good for detection with a tunable diode laser. Although the vibrational band positions for most alkali molecules are generally known, the exact positions of the rotational

lines in these bands are not known at all (except for LiF), and there have been no direct measurements of the absorption linestrengths for any alkali molecule published to date. These linestrength positions are crucial toward the development of an alkali monitor which is capable of rejecting interferences from unwanted species and for providing absolute concentrations.

The primary objective of our work to date was to demonstrate the efficacy of high resolution infrared tunable diode laser absorption techniques in detecting an alkali halide or alkali hydroxide molecule. The specific technical questions to be studied included:

- The line positions of the rovibrational transitions in the ν_1 band of an alkali halide or hydroxide
- Determination of the linestrengths of the located transitions
- An assessment of this detection technique applied to combustion conditions.

3.2 Experimental Studies

3.2.1 Tunable Diode Laser Apparatus and Methodology

The instrumentation for a tunable diode laser diagnostic is shown in Figure 1. The diode laser itself is housed in a temperature-controlled closed cycle refrigerator. This system is a commercial system from Spectra-Physics (Laser Analytics Division). An off-axis paraboloidal reflector is used to collect and collimate the multimode laser emission. This emission is mechanically chopped and refocused at the entrance slit of a 0.25 meter monochromator, equipped with a 30 groove/mm grating blazed for 25 μm. The single laser mode selected by the monochromator is then transmitted by additional reflective optics through the multi-pass analysis region and ultimately to a cryogenically cooled infrared detector. A fraction of the

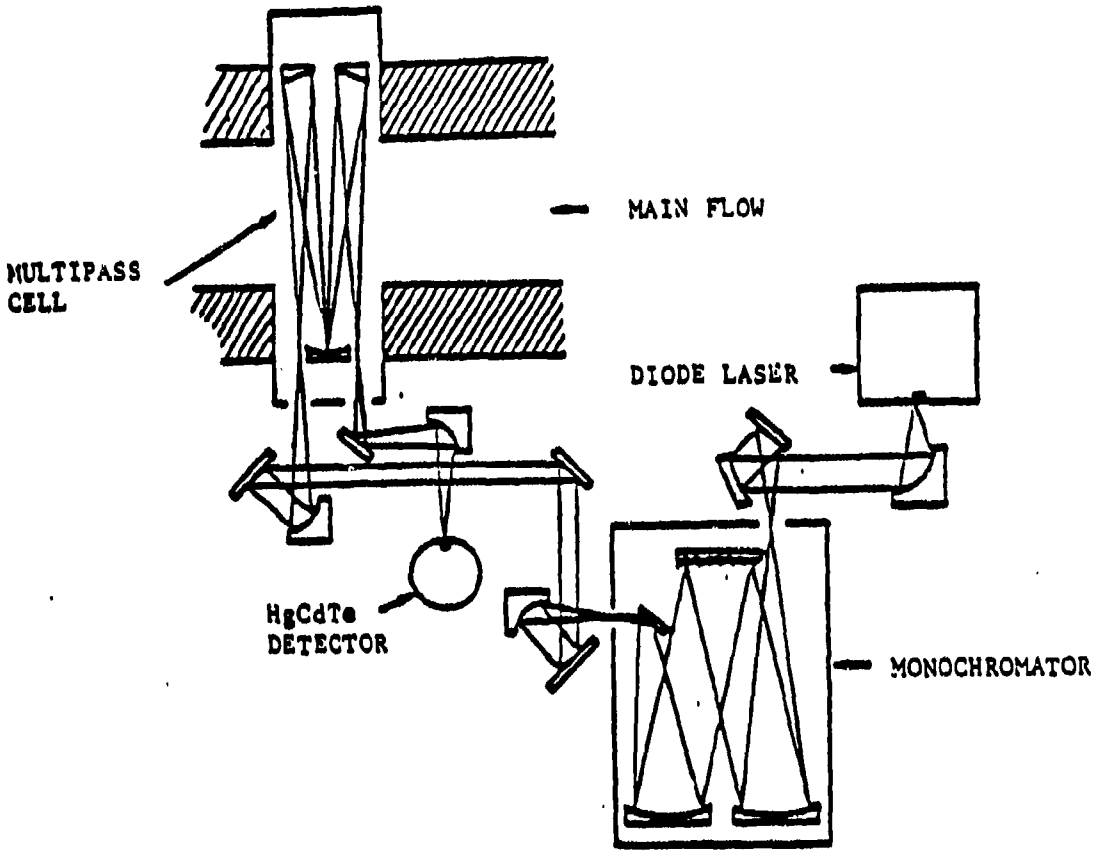

Figure 1. Typical Setup for IR Diode Absorption Experiments

laser beam intensity is split off prior to entering the analysis region and is focused on a second detector. This dual beam (analysis beam and reference beam) arrangement permits the direct measurement of fractional absorption in the analysis region as the laser is tuned across a molecular absorption feature. The amplified signals from the detectors are fed to lock-in amplifiers for synchronous measurement. The lock-in amplifier outputs are digitized with a simultaneous sample and hold A/D system and the data are transferred to a microcomputer (IBM Personal Computer XT, DMA interface) for ratioing, analysis, and graphical display.

The multipass cell is a White cell[17] of Aerodyne's manufacture. This type of cell, which has been used in a number of previous experiments at Aerodyne, easily allows as many as 100 or more optical passes through the analysis region. A practical limit to the useful number of passes is set by mirror reflectivity losses which ultimately reduce signal-to-noise. Our

previous experience suggests that 40 passes is optimum. For the approximately 10 cm flow width of the flowtube exhaust stream, the total multiple pass path length (40 passes) is approximately 4 meters.

High resolution tuning (laser linewidth $\approx 10^{-4}$ cm^{-1}) of the laser wavelength is accomplished by variation of the laser current. A typical laser mode of the recently introduced stripe geometry diode lasers has a current tuning range of ~2 cm^{-1}. Atmospheric pressure absorption lines have linewidths (full width at half maximum) of approximately 0.1 cm^{-1}. Thus the laser will easily tune across the full width of these broad absorption lines with complete resolution of the absorption profile. Wavelength calibration of the lasers is accomplished by measurement of the low pressure absorption spectrum of a well-characterized calibration gas. For measurements in the 350 to 450 cm^{-1} region, where many of the molecular alkali species have absorption bands, the CS_2 ν_2 band provides a rich source of calibration lines.[18]

3.2.2 Production of Gas Phase Alkali Compounds

Gas phase alkali species were produced at room temperature in a low pressure flow tube (P = 2 torr) by heating a crucible filled with the alkali metals (100-200°C), entraining the gas phase alkali in a flow of helium, and reacting the metal with various reagents near the detection zone. Various alkali compounds were produced in the following sequences:

KF

$$K + F_2 \rightarrow KF + F \qquad (1)$$

NaOH

$$Na + H_2O_2 \rightarrow NaOH + OH \qquad (2)$$

KOH

$$K + N_2O \rightarrow KO + N_2 \qquad (3a)$$

$$KO + CH_4 \rightarrow KOH + CH_3 \qquad (3b)$$

The rate constant and products for Reaction 2 has been measured in our laboratory[8] as producing a 60% yield. The equivalent reaction for potassium has also been shown in the same study not to produce KOH, a result that is not fully understood. The sequence in Eqs. (3a) and (3b) is expected to be reasonably efficient; the sodium analog of Eq. (3a) is reasonably fast (8×10^{-13} cm^{-3} s^{-1} $molecule^{-1}$). Methane is expected to react with KO to produce KOH with a high yield. Ager and Howard[19] report that hydrogen reacts with NaO:

$$Na + H_2 \rightarrow NaOH + H \quad k = 2.6 \times 10^{-11} \text{ cm}^3 \text{ mole}^{-1} \text{ s}^{-1} \qquad (4a)$$

$$\rightarrow Na + H_2O \quad k = 1 \times 10^{-11} \text{ cm}^3 \text{ mole}^{-1} \text{ s}^{-1} \qquad (4b)$$

to produce NaOH with high yield. We tried using hydrogen to make KOH but discovered that most of the KO was being converted back into K, probably due to

$$KOH + H + M \rightarrow K + H_2O + H \quad , \qquad (5)$$

a reaction that becomes efficient at the high concentrations used in this experiment. The choice of methane was based on the unlikelihood of free methyl radicals attacking KOH to produce methanol.

The presence of vapor phase alkali metal was monitored using laser induced fluorescence at the 5890 Å transition in sodium and 4044 Å transition in potassium. Reagents were added (fluorine, hydrogen peroxide, and nitrous oxide) until the fluorescence was extinquished indicating that all the alkali metal had reacted. In the case of KOH, a large excess of methane was added ($\sim 3 \times 10^{14}$ cm^{-3}). If the chemistry presented in Eqs. (1) - (4) was correct, the expected yield of alkali compound was $\sim 10^{13}$ cm^{-3}. Unfortunately, it was clear that the simple mechanisms that applied to low concentrations in

previous flow tube experiments were too limited to explain the chemistry in our experiment. Large quantities of chemiluminescence could be usually seen, indicating that important secondary chemistry was taking place. The significance of this fact will be discussed in the next section.

3.2.3 Results

KF

KF was chosen as the first species to be detected since its vibrational overtone spectrum had been detected using a tunable diode laser in the 408-435 cm^{-1} region.[20] Using second derivative techniques, regions of the spectrum were scanned using a liquid nitrogen cooled HgCdTe detector. Each scan covered a range at least twice that of the rotational constant to assure observation of a rotational line. A typical spectrum is shown in Figure 2. The upper curve shows the absorption spectrum of carbon disulfide which provides a calibration for the laser diode. The inset is a second derivative spectrum in the presence of KF. The rovibrational line at 408.073 cm^{-1} produced approximately a 1.5% absorption, much less than expected. Using a calculated absorption strength as described in Subsection 3.4, we calculate that the concentration of KF in our detection path was no more than 5×10^{10} cm^{-13}, three orders of magnitude less than we had initially anticipated. The spectrum shown in Figure 2 represents the first unambiguous detection of a vapor phase alkali halide or hydroxide using a fundamental vibrational transition.

NaOH, KOH

The detection of these molecules was hampered by two factors. The first was the lower than expected production rates as evidenced by the KF observations. The second was the uncertainty in the line positions of the ν_1 vibrational bands, experimental observations of which are tainted by the presence of dimers. In the case of NaOH, Spinar and Margrave heated powdered NaOH in an absorption cell and using a broad band light source, observed a feature at 437 ±10 cm^{-1},[21] Acquista and Abramowitz[22] performed similar

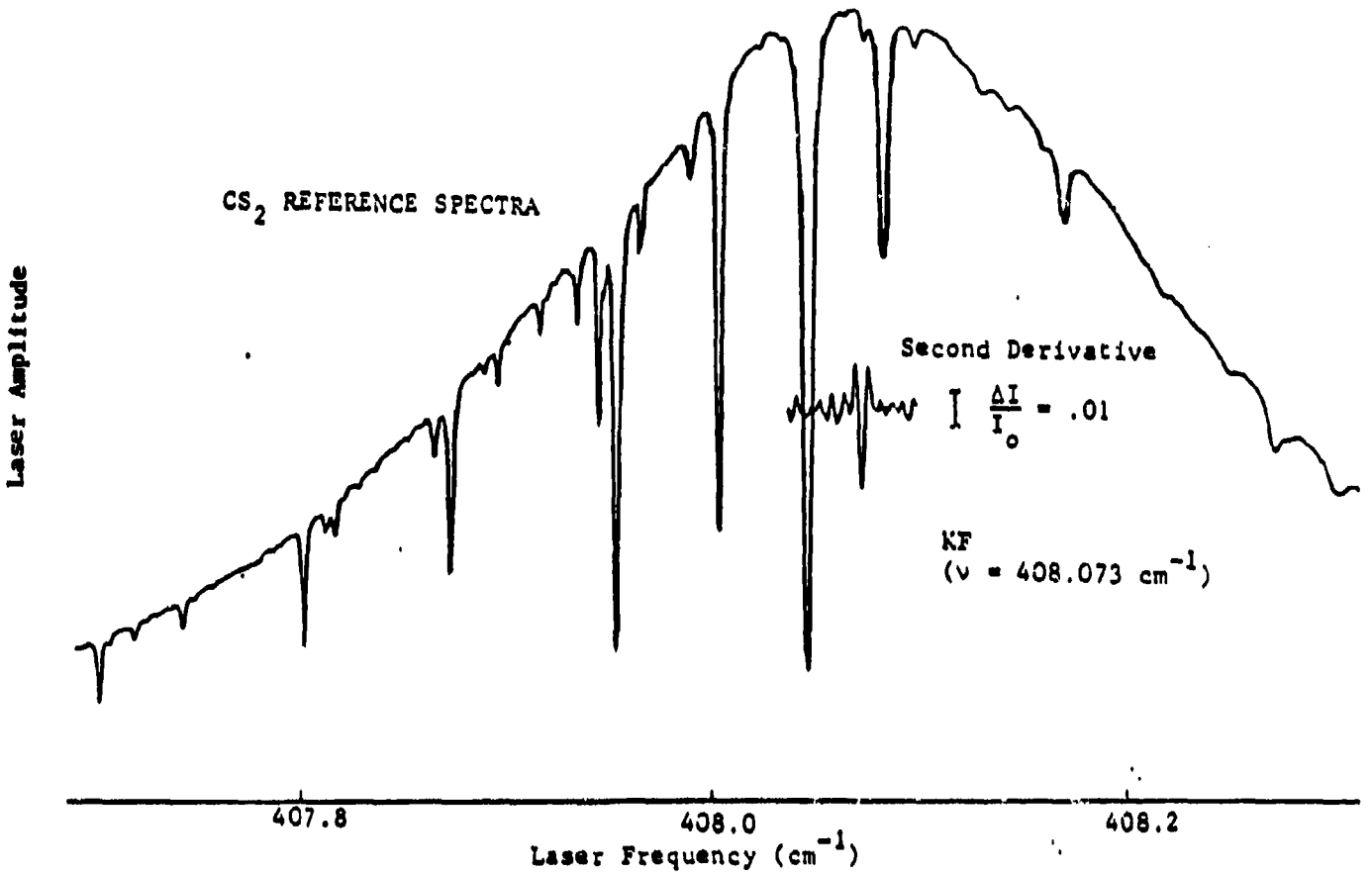

Figure 2. Diode Laser Scan of KF Fundamental P-Branch Line

measurements in argon matrices. They assigned strong absorption bands at 431 cm^{-1} to the NaOH ν_1 band. On the other hand, one expects the NaOH ν_1 band to be quite similar to those found for the isoelectronic and isobaric NaF whose gas phase band center is at 529.2 cm^{-1}. Absorption spectra were taken at 376, 378, 407.5 424, 448, 477, and 497 cm^{-1}, the entire range of the diode. No feature assignable to NaOH could be detected.

Similar problems are presented for KOH as well. Spinar and Margrave quote a value of 408 cm^{-1} for KOH,[21] while a matrix isolation study of Belyaeva, et al[23] quotes the same value, a surprising result given an expected matrix shift of 20 to 50 cm^{-1}. Laser scans at 396 and 424 cm^{-1} in the present experiment produced no observable features at a sensitivity of 0.5% absorption.

The lack of observable NaOH and KOH spectra is explained by newly published and extremely accurate calculations by Bauschlicher, et al.[24] These ab initio configuration interaction calculations give bond distances and bond strengths for the alkali and alkaline earth hydroxides and fluorides which agree very closely with experimental evidence and can thus be deemed very accurate. They fix the fundamental frequencies of NaOH and KOH at 579 and 467 cm^{-1} respectively, much higher than the previously reported values which we had used to base our search. They conclude that the NaOH band experimental observations must be ascribed to dimers or polymers and predict that the accuracy of their calculations is no worse than 30 cm^{-1}. Unfortunately, the funds for this project were expended before new studies could begin to corroborate these exciting new results.

3.3 Estimated Detection Sensitivities for Combustion Applications

The sensitivity for detection of a given species by tunable diode laser absorption depends essentially on two factors: the minimum fractional absorption measurable by the instrumentation, and molecular parameters which determine the absorption strength corresponding to a given species concentration. We briefly examine these issues in this subsection and provide estimates for the detection sensitivities for several molecular alkali species.

Tunable diode laser systems are capable of very high sensitivity for measurement of small fractional absorptions. This high sensitivity derives from the brightness of the laser (typically 0.01-0.1 mW single mode source power), high detectivity of the cryogenically cooled detectors ($D^* > 10^{10}$ cm $Hz^{0.5}$ W^{-1}), and exceptionally low amplitude noise of the lasers (often detector-limited). In our experience, fractional absorptions as low as 0.01% can be detected routinely with these lasers for low pressure absorption lines, and detection of 0.001% absorption has been reported (e.g., Ref. 20) even for lines at atmospheric pressure. Detection of these broad lines (0.1 cm^{-1}) is nonetheless more difficult than measurement of low pressure lines, because substantial variation of the laser baseline intensity normally occurs over the

absorption linewidth and accurate measurement of this slow variation is difficult even with a dual-beam system. In addition, turbulence in the combustion stream imposes an additional noise source on the probe beam and may result in degraded sensitivity. In consideration of these factors, we adopt 0.1% fractional absorption as a conservative estimate of the detection sensitivity of the instrumentation for measurement of pressure-broadened lines in the combustor exhaust stream. We emphasize, however, that an improvement by 1 to 2 orders of magnitude in this sensitivity may be possible.

The absorption strength for molecular absorption lines may be calculated if the vibrational band strength (the integrated absorption strength of the band) is known. In general, this parameter is not known for the alkali species, however estimates are possible based on simple models of the bonding in these molecules. The parameter of interest is the dipole moment derivative along the bond axis, evaluated at the equilibrium atomic separation. The vibrational band strength, in units of cm^{-2} (STP atm)$^{-1}$ is then[25]

$$S_{band} = \frac{188}{M_r} \left|\frac{d\mu}{dR}\right|^2_{R_e} , \qquad (6)$$

where M_r is the reduced mass in a.m.u. and $(d\mu/dR)_{R_e}$ is the dipole moment derivative in debye A^{-1}.

The simple model which we adopt to describe bonding in the alkali halides, hydroxides, and monoxides is the "Rittner Model."[26] In this model, the molecule is pictured as being constituted of a positive and negative ion, each of which is polarized by the electrostatic field of the other. Expressions for the dipole moment and dipole moment derivative may then be derived on the basis of classical theory, depending only on the ion polarizabilities. For the dipole moment derivative, the resulting expression is[23]

$$\left.\frac{d\mu}{dR}\right|_{R_e} = 3e - \frac{2\mu}{R_e} \quad , \tag{7}$$

where e (4.8 debye A^{-1}) is the electronic charge. Eqs. (6) and (7) may then be used as a basis for estimating the band strengths.

The estimated band strengths for several molecular alkali species are given in Table 2. For the alkali halides, accurate experimental values are available for R_e and the dipole moment, μ. These values are used in Eq. (7) whenever possible. To our knowledge only one direct comparison to an experimental value for the dipole moment derivative is available for the species in our table, i.e., for LiF. For LiF, the measured derivative (and therefore the band strength) are actually larger than the values predicted by the simple theory. Interestingly, a much more rigorous quantum mechanical calculation of the dipole moment derivative for LiF[27] produces much poorer agreement with the experimental value than does the simple Rittner model.

The band strengths for these species as estimated in Table 2 are quite strong, although not out of line with the vibrational band strengths for more familiar species. For example, the measured values of S_{band} for CO and CO_2 (asymmetric stretch) are 250 cm^{-2} (STP atm)$^{-1}$ [28] and 2680 cm^{-2} (STP atm)$^{-1}$,[29] respectively. Experimental evidence that these alkali species can be measured by infrared absorption in the gas phase comes from the recent diode laser measurements of Maki and Lovas.[20] Maki and Lovas had little difficulty in measuring the first overtone spectrum of gas phase KF with a tunable diode laser[20] over a 36 cm path length. The KF fundamental band indicated in Table 2 should be substantially stronger than the overtone bands which Maki and Lovas measured. Measurements of this fundamental transition were performed, for the first time, in our laboratory.

Table 2 - Estimated Dipole Moment Derivatives (Rittner Model) and Infrared Vibrational Band Strengths for Selected Alkali Halide, Hydroxide, and Monoxide Species[a]

Species	ν_o (cm^{-1})	R_e (A)	μ_e(debye)	$\left(\frac{d\mu}{dR}\right)_{Re}$ (debye/A)	S_{Band} (cm^{-2} STP atm^{-1})
^7LiF	894.0	1.5639	6.2839	6.4 7.94[b]	1500 2600[b]
NaF	528.4	1.9259	8.1234	6.0	650
$Na^{35}Cl$	361.1	2.3609	8.9721	6.8	630
NaOH[c]	579[24]	1.95[34]	6.9[d]	7.9	1200
NaO	526[35]	2.05[35]	9.8[e]	4.8	460
KF	421.393[20]	2.1715	8.5583	6.5	620
$K^{35}Cl$	277.5	2.6668	10.2384	6.7	460
KOH[c]	467[24]	2.2115[36]	7.7 [d]	7.4	870
KO	384[35]	2.22[35]	10.7[e]	4.8	380

[a] Unless otherwise indicated, experimental values for $\nu_o = \omega_e - 2\omega_e x_e$, R_e, and μ_e are abstracted from the summary of data given in Brumer and Karplus.[30]

[b] Obtained from experimental measurement of the v = 1 radiative lifetime for ^6LiF using an electric-resonance molecular beam technique.[31]

[c] M-OH bonds

[d] Calculated dipole moments obtained from the Rittner model.[32] For most alkali halides, the Rittner model underpredicts the dipole moment (as compared with experimental values) by 5% to 15%.[30]

[e] Estimated as the point charge dipole moment, $\mu_{pc} = eR_e$. The tendency of this model is to overpredict the dipole moment for the alkali halides by 20% to 30%.[30]

From the estimated band strengths, the absorption cross section at line center of individual lines can be obtained, and estimates of the detection sensitivity follow directly. The line strength (cm^2 $molecule^{-1}$ cm^{-1}) for these simple diatomic and linear triatomic molecules, at temperature T is

$$S_J = \frac{S_{band}}{N_o} \frac{\nu_J}{\nu_o} (1 - e^{-\nu_o h c/kT}) \frac{hcB}{kT} (2J+1) e^{-BJ(J+1)hc/kT} , \qquad (3)$$

where J is the rotational quantum number of the lower level in the transition, B is the rotational constant, N_o is Loschmidt's number (2.69×10^{19} molecules cm^{-3}), and ν_J is the frequency of the particular P or R branch line originating from J. The line center absorption cross section for an atmospheric pressure-broadened line can be estimated as

$$\sigma_o \approx \frac{S_J}{0.1} \text{ cm}^2 \text{ molecule}^{-1} , \qquad (4)$$

where 0.1 cm^{-1} is the approximate linewidth at atmospheric pressure. Finally, the minimum detectable concentration n_{min} (cm^{-3}) may be estimated from

$$\left(\frac{\Delta I}{I_o}\right)_{min} = n_{min} \sigma_o \ell = 0.001 \qquad (5)$$

or

$$n_{min} = \frac{0.001}{400 \sigma_o} , \qquad (6)$$

where we assume an absorption path length ℓ of 400 cm and a minimum detectable fractional absorption of 0.1%. At elevated temperatures, excited vibrational levels ($v > 0$) become significantly populated in many cases, which means that n_{min} should be replaced in Eqs. (5) and (6) with $(n_{lower} - n_{upper})_{min}$.

These population differences can be calculated from thermal Boltzmann distributions and related to the total number density of the species. The overall effect of this is to degrade the minimum detectable concentration.

The estimated line center absorption cross sections and minimum detectable concentrations (including vibrational partitioning) for several molecular alkali species at T = 1200 K are given in Table 3, based on Eqs. (3) through (6) and the band strength estimates of Table 2. In addition, we include estimates for KO_2 and NaO_2 detection in the 400 cm^{-1} region, assuming similar band strengths as the corresponding monoxide species. Potassium chloride is not included in the table because the vibrational frequency for KCl (~278 cm^{-1}) is outside the wavelength range of commercial diode lasers.

The strongest IR-active bands of the alkali sulfate species, measured in argon or nitrogen matrices, are in the 1100 cm^{-1} region.[33] Measurement of these latter two species may be more difficult, however, because virtually nothing is known about the spectroscopy and also the vibrational bands are likely to be weak compared with the bands of smaller molecules.

Table 3 - Estimated Line Center Absorption Cross Sections and Minimum Detectable Concentrations at T = 1200 K, p = 1 atm, for Tunable Diode Laser Measurement of Molecular Alkali Species (Multiple Pass Path Length = 400 cm, $(\Delta I/I)_{min}$ = 0.1%)

Species	σ_o (cm^2 $molecule^{-1}$)	Detectable Concentration, cm^{-3}
NaOH	3.5×10^{-16}	2.4×10^{13} (3.9 ppm)
NaCl	1.1×10^{-16}	1.0×10^{13} (1.6 ppm)
NaO	1.5×10^{-16}	6.8×10^{12} (1.1 ppm)
NaO_2	(1.5×10^{-16})	5.7×10^{13} (9.3 ppm)
KOH	2.0×10^{-16}	4.4×10^{13} (7.2 ppm)
KO	8.2×10^{-19}	1.3×10^{13} (2.1 ppm)
KO_2	(8.2×10^{-19})	1.0×10^{14} (16 ppm)
Na_2SO_4	?	Probably > 10 ppm
K_2SO_4	?	Probably > 10 ppm

The sensitivity estimates shown in the table indicate that concentrations of a few ppm of the various chloride, hydroxide, and oxide species should be readily measurable by diode laser absorption for combustor test conditions. We reemphasize that evan greater sensitivity (detection of less than 0.1%absorption) should be possible with appropriate attention to the instrumentation. Also, the technique is attractive in that only one or two diode lasers would be required to cover the wavelength tuning range needed for measurement of these species (~350 - 550 cm^{-1}), permitting measurement of all of them within a period of a few minutes experimental run time. By conducting suitable calibration experiments in the diagnostic development stage the measurements can be made quantitative, and potential spectroscopic interferences can be understood and avoided.

3.4 Preliminary Assessment of Spectral Interferences

Any assessment of spectral interferences in a combustion flowstream starts with the major constituents that are active in the infrared, water and carbon dioxide. Fortunately, neither species will provide much interference. Water absorption lines appear at irregular spacings 0.2 to 3.0 cm^{-1} apart, greater than the line broadened resolution of 0.1 cm^{-1}. Diode laser absorption should easily be able to resolve alkali and water lines under these circumstances. Carbon dioxide lines exist, but are so weak so as to be unmeasurable ($\sigma(\lambda) \approx 10^{-25}$ cm^2 or over 1 million times weaker than the expected alkali line strengths). As far as other species go, only the region above 450 cm^{-1} contain possible interferences. Both SO_2 and N_2O have fairly dense spectra with intensities sufficient to cause interferences. Although these spectra are not as sparse as that presented for water, there are gaps of 0.3 - 1.0 cm^{-1} which present adequate opportunity for observing NaOH and KOH. Any final selection of spectral region for a real device will have to assess this problem.

3.5 Conclusions

The result obtained in the experimental efforts represents the first high resolution infrared absorption measurements of an alkali halide or hydroxide species at the fundamental vibrational frequency. Potassium fluoride rovibrational lines between 408-430 cm^{-1} were detected at very low KF concentrations (~1-5 x 10^{10} cm^{-3}) at low pressure. The results agree with the overtone measurements of Maki[20] at the National Bureau of Standards. Thus, the detection of such molecules under controlled conditions has been demonstrated. In addition, theoretical calculations and a sensitivity analysis indicate that diode laser absorption measurements can detect 1-10 parts per million of such molecules under typical combustion conditions if a purged multiple pass mirror configuration can be installed in the combustor. Detection of 10^{10} to 10^{11} cm^{-3} is possible in low pressure laboratory kinetic studies.

The vibrational band locations of NaOH and KOH could not be established due to what we presume was the incorrect assignment of these transitions in the literature. Fortunately, new and accurate ab initio calculations provide sufficient accuracy to guide future studies.[24]

4. ACKNOWLEDGEMENTS

The work presented in this paper was performed under Army Research Office contract DAAG29-81-C-0024, Air Force Geophysics Laboratory Contract Number F19628-83-C-0010 and Department of Energy Contract DE-AC01-85-ER-80303.

The interest and input of D. Squires and R. Shaw at ARO as well as E. Murad, W. Swider, and C. Gallagher at AFGL is gratefully acknowledged.

5. REFERENCES

1. D.E. Jensen, and B.C. Webb, AIAA J. 14, 947 (1976).

2. M.E. Gersh, J.S. Draper, J.C. Wormhoudt, J.B. Elgin, C.E. Kolb, D.C. Robertson and L.B. Bernstein, Aerodyne Research, Inc. and J.E. Reardon, REMTECH, Inc., "JANNAF Handbook: Rocket Exhaust Plume Technology - Chapter 3, Rocket Exhaust Plume Radiation,"CPIA Publications 263, Chemical Propulsion Information Agency, Laurel, MD (1980).

3. J. Wormhoudt and C.E. Kolb, Work performed for and reported to the JANNAF Tactical Rocket Exhaust Plume Signature Panel, Aerodyne Research, Inc. (1979).

4. V. Yousefian and I.W. May, "Prediction of Muzzle Flash Onset," 16th JANNAF Combustion Meeting, CPIA Publication 308 (December 1979).

5. V. Yousefian, I.W. May and J.M. Heimerl, "Modeling the Occurrance of Muzzle Flash in Guns," 17th JANNAF Combustion Meeting, CPIA Publication xxx (September 1980) - (ARI-RR-223).

6. J.A. Silver, M.S. Zahniser, A.C. Stanton and C.E. Kolb, "Temperature Dependent Termolecular Reaction Rate Constants for Potassium and Sodium Superoxide Formation," Twentieth Symp. (International) on Combustion, The Combustion Institute, 1984, pp 605-612.

7. J.A. Silver and C.E. Kolb, "Determination of the Absolute Rate Constants for Reactions of Atomic Sodium With Ozone and Nitrous Oxide," J. Phys. Chem., in press, due June 1986.

8. J.A. Silver, A.C. Stanton, M.S. Zahniser and C.E. Kolb, "Gas-Phase Reaction Rate of Sodium Hydroxide With Hydrochloric Acid," J. Phys. Chem. 88, 3123 (1984).

9. J.A. Silver and C.E. Kolb, "Gas Phase Reaction Rate of Sodium Superoxide With Hydrochloric Acid," in press, J. Phys. Chem., due June 1986.

10. M.E. Gersh, J.A. Silver, M.S. Zahniser, C.E. Kolb, R.G. Brown, C.M. Gozewski, S. Kallelis and J.C. Wormhoudt, Rev. Sci. Instrum. 52, 1213 (1981).

11. M.S. Zahniser and A.C. Stanton, J. Chem. Phys. 80, 4951 (1984).

12. R. Carabetta and W.E. Kaskan, J. Phys. Chem. 72, 2483 (1968).

13. A.J. Hynes, M. Steinberg and K. Schofield, J. Chem. Phys. 80, 2585 (1984).

14. D. Husain and J.M.C. Plane, J. Chem. Soc. Faraday Trans. II 78, 1175 (1982).

15. D. Husain and J.M.C. Plane, J. Chem. Soc. Faraday Trans. II 78, 2843 (1982).

16. D.E. Jensen and G.A. Jones, J. Chem. Soc. Faraday Trans. I 78, 2843 (1982).

17. J.U. White, J. Opt. Soc. Am. 32, 285 (1942).

18. K. Jolma and J. Kauppinan, J. Mol. Spectrosc. 82, 214 (1980).

19. J. Ager and C. Howard, Aeronomy Laboratory, NOAA Environmental Research Labs, private communication (1985).

20. A.G. Maki and F.J. Lovas, J. Mol. Spectrosc. 95, 80 (1982).

21. L.H. Spinar and J.L. Margrave, Spectrochimica Acta 12, 244 (1958).

22. N. Acquista and S. Abramowitz, J. Chem. Phys. 51, 2911 (1969).

23. A.A. Belyaeva, M.I. Dvorkin, and L.D. Sheherba, Opt. Spectrosc, 31, 210 (1971).

24. C.W. Bauschlicher Jr., S.R. Langhoff, and H. Partridge, J. Chem. Phys. 84, 901 (1986).

25. M.S. Zahniser and M.E. Gersh, J. Chem. Phys. 75, 52 (1981).

26. E.S. Rittner, J. Chem. Phys. 19, 1030 (1951).

27. S.W. Harrison and C.R. Fischer, Phys. Rev. A 13, 910 (1976).

28. H.S. Lowry and C.J, Fisher, J. Quant. Spectrosc. Radiat. Transfer 27, 585 (1982).

29. L.S. Bernstein, D.C. Robertson, and J.A. Conant, J. Quant. Spectrosc. Radiat. Transfer 23, 169 (1980).

30. P. Brumer and M. Karplus, J. Chem. Phys. 58, 3903 (1973).

31. D.R. Bedding and T.I. Moran, Phys. Rev. A 9, 2324 (1974).

32. V.G. Solomonik and T.P. Pogrebnaya, "Dipole Moments and Spectroscopic Constants of Alkali Metal Hydroxide Molecules," Technical Report SPSTL 857 KHP-D80, available from Chemical Abstracts Service, Columbus, OH (1980).

33. R.M. Atkins and K.A. Gingerich, Chem. Phys. Lett. 53, 347 (1978).

34. P. Kuijpers, T. Toriing, and A. Dymanus, Chem. Phys, 15, 457 (1976).

35. K.P. Huber and G. Herzberg, Molecular Spectra and Molecular Structure IV. Constants of Diatomic Molecules (Van Nostrand Reinhold, New York, 1979).

36. E.F. Pearson and M.B. Trueblood, J. Chem. Phys. 58, 826 (1973).

"Kinetic studies of recombination reactions of alkali atoms by time-resolved spectroscopic methods"

by David Husain,
The Department of Physical Chemistry,
The University of Cambridge,
Lensfield Road,
CAMBRIDGE CB2 1EP,
ENGLAND

Paper delivered at the "Workshop on the Chemical Suppression of Rocket Afterburning and of Gun Muzzle Flash", at the Ballistics Research Laboratory,
Interior Ballistics Division,
Aberdeen Proving Ground,
Maryland 21005 - 5066,
U.S.A.

11th. and 12th. June , 1986.

"Kinetic studies of recombination reactions of alkali atoms by time-resolved spectroscopic methods"

by David Husain,
The Department of Physical Chemistry,
The University of Cambridge,
Lensfield Road,
CAMBRIDGE CB2 1EP,
ENGLAND.

Characterisation of kinetic parameters governing recombination reactions of alkali atoms are fundamental to an understanding of the properties of flames seeded with alkali metals[1-4] and in elucidating the roles of species such as Na and K and their hydroxides, for example, in flame inhibition.[5-7] Thus, the pair of processes

$$K + OH + M \longrightarrow KOH + M \qquad (1)$$

$$H + KOH \longrightarrow H_2O + K \qquad (2)$$

catalyse the overall recombination reactions

$$H + H + M \longrightarrow H_2 + M \qquad (3)$$

$$H + OH + M \longrightarrow H_2O + M \qquad (4)$$

The detailed quantification of the extent of such catalysis is dependent on the individual rate parameters employed for the fundamental processes.[6,8] Reactions of the type

$$Na, K + O_2 + M \longrightarrow Na,KO_2 + M \qquad (5)$$

are also of special interest in this context in flames and have been the object of flame modelling and rate measurements in those environments.[3,4,9-11]. Recent years have seen the development of experimental techniques permitting direct characterisation of absolute rate constants for a number of these fundamental processes by time-resolved spectroscopic methods, isolated from the complexities of flame environments and related systems where sets of kinetic data and thermodynamic data are intimately linked. This paper describes absolute rate measurements on three classes of reactions:

(I) $X + O_2 + M \longrightarrow XO_2 + M$ (X = Na, K) (6)

(II) $X + OH + M \longrightarrow XOH + M$ (X = Na, K, Rb, Cs) (7)

(III) $X + I + M \longrightarrow XI + M$ (X = K, Rb, Cs) (8)

(where M is the third body) obtained in our laboratory by their isolation in real time with direct spectroscopic monitoring, and direct characterisation of k_6, k_7 and k_8. Where possible, rate data are compared with those derived from diffusion flames, laser-induced fluorescence measurements on flow systems and from flame modelling.

(I) $X + O_2 + M \longrightarrow XO_2 + M$

The recombination reactions (5) for Na and K in particular, whilst formally describing atom-radical recombination processes involving $O_2(X^3\Sigma_g^-)$, are inherently accessible by direct experiment as the oxygen molecule is a stable species. The reactions between Na + O_2 + M and K + O_2 + M (M = He, N_2, CO_2) were investigated by Husain and Plane[12,13] by time-resolved atomic resonance absorption spectroscopy on Na and K at λ = 589 nm ($Na(3^2P_J) \longleftarrow Na(3^2S_{1/2})$) and λ = 768 nm ($K(4^2P_J) \longleftarrow K(4^2S_{1/2})$) following the generation of these transient atoms by the pulsed irradiation of NaI and KI vapours at elevated temperatures. These early investigations[12,13] were motivated by the low values of k_5 that had been reported hitherto[9,11] resulting Na and K in flames, and the recognised limitations in employing estimates of rate parameters for Na and K using analogues for H atoms.[14] The initial experimental system for those measurements shown in Figure 1 was restricted to limited temperature ranges (724 and 844 K for Na, 753 and 873 K for K). Nevertheless, absolute rate data for k_5 (for Na and K) were accessible. Briefly, the decay of $Na(3^2S_{1/2})$ and $K(4^2S_{1/2})$ generated in the pulsed mode can be described by the rate equations (presented for $Na(3^2S_{1/2})$):

$$-d(Na)/dt = (k_{diff} + k_5(Na)(O_2)(M))(Na) \quad (i)$$

or

$$-d(\ln(Na))/dt = k_{diff} + k_5(O_2)(M) = k' \quad (ii)$$

where k' is the overall first-order decay coefficient for the loss of the alkali atom and k_{diff} represents the removal of Na and K by diffusion in the absence of O_2 and permits charecterisation of the diffusion coefficients for these alkali atoms.[12,13] Alternatively, k_{diff} can be taken as an empirical correction for the removal of Na and K in M alone (M = He, N_2, CO_2). Equations (i) and (ii) coupled with the Beer-Lambert law for the time-resolved resonance absorption:

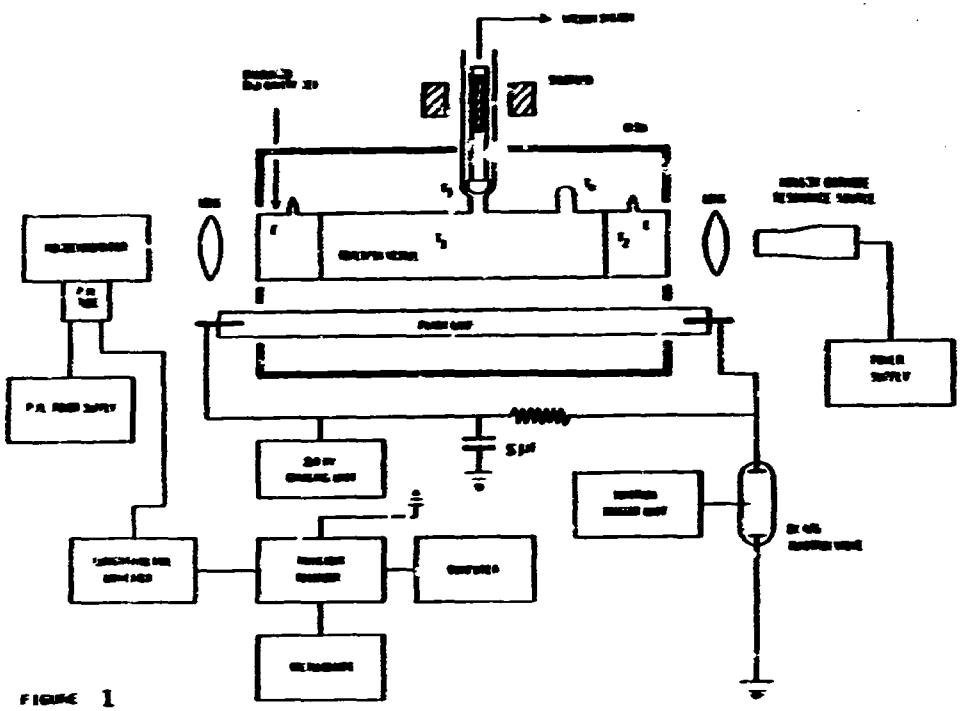

FIGURE 1

Block diagram of the apparatus for the kinetic study of Na(3²S) at elevated temperatures by time-resolved attenuation of atomic resonance radiation in the "single shot" mode.

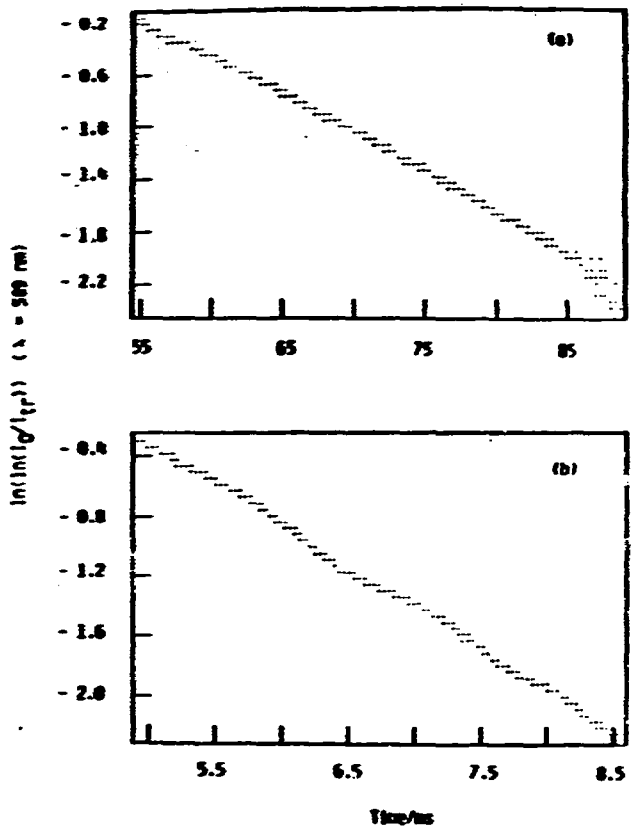

Figure 2

Typical pseudo first-order plots for the decay of ground state sodium atoms, generated from the pulsed irradiation of NaI, obtained by monitoring atomic resonance absorption at $\lambda = 589$ nm ($Na(3^2P_J \leftarrow 3^2S)$).

E = 125 J; T = 724 K; first-order plots constructed from the smoothed digitised data of the "A" time base of the transient recorder.

(a) p_{N_2} = 200.1 torr, p_{O_2} = 0 torr;

(b) p_{N_2} = 199.5 torr, p_{O_2} = 20.2 mtorr.

$$I_{tr} = I_0 \exp(-\varepsilon c l) \qquad \text{(iii)}$$

(c = (Na) and (K)), and the first-order decay for the alkali atom

$$c = c_0 \exp(-k't) \qquad \text{(iv)}$$

yields k'. Examples of the first-order decay profiles for Na in the absence and the presence of O_2 are shown in Figure 2. A resumé of the third-order rate data derived from these earlier measurements is summarised in Table 1.

Table 1

Comparison of third-order rate constants (k_R/cm^6 molecule^{-2} s^{-1}) for Na , K + O_2 + M (refs. (12), 13))

M	K($4^2S_{1/2}$) (753 - 873 K)	Na($3^2S_{1/2}$) (724 - 844 K)
He	$(9.8 \pm 1.5) \times 10^{-28}\ T^{-1}$ (a) (1.3×10^{-30} calc. T = 784 K)	$(6 \pm 1) \times 10^{-31}$ (a)
N_2	$(1.7 \pm 0.6) \times 10^{-27}\ T^{-1}$ (a) (2.2×10^{-30} calc. T = 784 K)	$(1 \pm 0.2) \times 10^{-30}$ (a)
CO_2	$4 \times 10^{-27}\ T^{-1}$ (a) (5.0×10^{-30} calc. T = 784 K)	2×10^{-30} (a)
Flame Composition ($H_2 + N_2 + H_2O$, T = 1420 - 1600 K)	1.0×10^{-33} (b)	8.2×10^{-34} (b)

((a), time-resolved atomic resonance absorption, (b) flame measurements)

Subsequently, the early apparatus[12,13] was modified with an improved high temperature reactor assembly capable of measurement across the temperature range ca. 415 - 1016 K and with computer interfacing.[15,16] First-order decay profiles for Na($3^2S_{1/2}$) were analysed by the form:

$$I_{tr} = I_0 \exp(-A\exp(-k't)) \qquad \text{(v)}$$

Examples of such profiles are shown in Figure 3. Figure 4 shows the variation of k' for Na with (O_2) and (N_2) for T = 571 and 1016 K, yielding the recombination rate constants ($k_5 = k_R$) at these temperatures. Figure 5 summarises the data

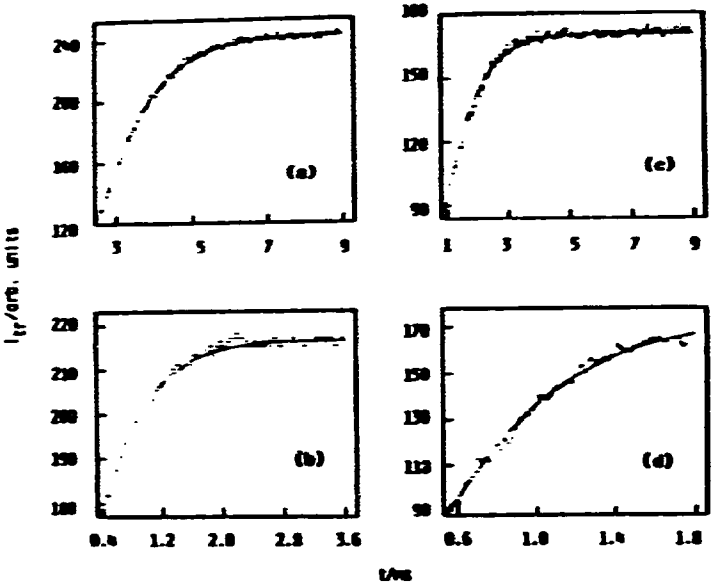

Figure 3

Digitised time-variation of the transmitted light intensity (I_{tr}) at λ = 589 nm ($Na(3^2P_J - 3^2S_{1/2})$) indicating the decay of resonance absorption by ground state sodium atoms in the presence of O_2 and H_2 following the pulsed irradiation of NaI.
E = 350 J ; T = 726 K ; :: digitised data points ; smoothed curve = computerised fitting to the form $I_{tr} = I_0 \exp(-A\exp(-k't))$.

	$[H_2]/10^{17}$ molecules cm^{-3}	$[O_2]/10^{16}$ molecules cm^{-3}
(a)	4.84	10.3
(b)	4.84	25.2
(c)	7.28	11.6
(d)	17.2	11.6

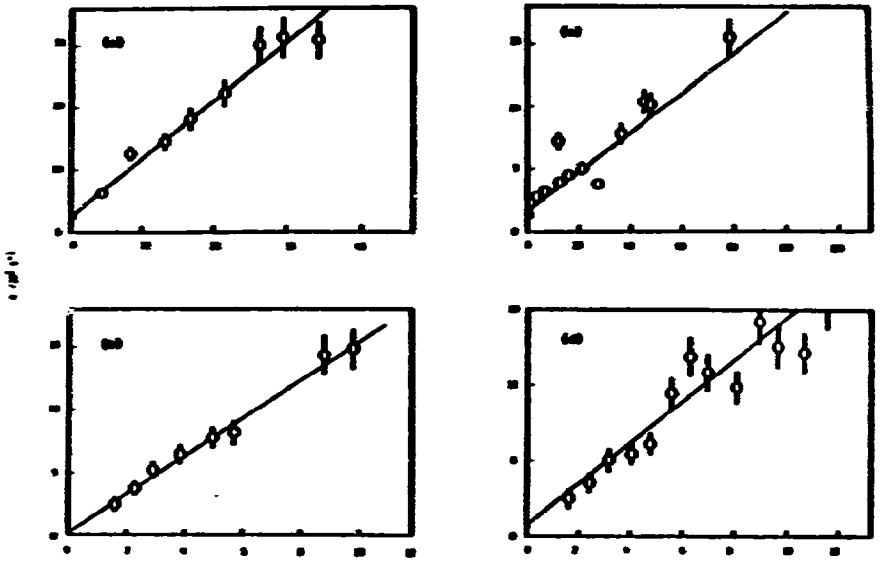

Figure 4

derived from time-resolved atomic resonance absorption measurements for $Na + O_2 + N_2$ with those reported from laser-induced atomic fluorescence measurements on a flow system,[17] flame modelling[4] and standard extrapolation using unimolecular reaction rate theory of Troe".[18,19] It may be stressed that an empirical extrapolation of the type $\ln(k_R)$ vs. $\ln(T/K)$ (Figure 6) across a temperature range of the type employed here yields results close to that obtained using the Troe" theory and, of course, independent of it. The Troe" extrapolation in Figure 5 for the data for $Na + O_2 + N_2$ can be expressed in the form:

$$\ln(k_R/cm^6\ molecule^{-2}\ s^{-1}) = -0.3225(\ln T)^2 + 2.133\ln(T) - 69.21 \qquad (vi)$$

Finally, we may note the development of atomic resonance ionisation spectroscopy by Kramer et al.[20,21] for the study of $Li + O_2 + M$ and $Cs + O_2 + M$.

(II) $X + OH + M \longrightarrow XOH + M$

A significant development in recent years for the direct determination of absolute rate data for the recombination of alkali atoms with free radicals has been the construction of a system, initially designed for the measurement of k_7 for the reaction:[22]

$$K + OH + He \longrightarrow KOH + He \qquad (7)$$

and subsequently modified in each case for the analogous measurements for X = Na,[23] Rb[24] and Cs.[25] The system is necessarily complex involving measurement of the decay of the free radical OH, generated by pulsed irradiation in a high temperature reactor, using time-resolved molecular resonance fluorescence on $OH(A^2\Sigma^+ - X^2\Pi, (0,0), \lambda = 307\ nm)$, with repetitive pulsing, pre-trigger photomultiplier gating and signal averaging. For the specific case of K, the decay of OH is monitored in the presence of excess potassium atoms derived from a heat pipe oven and themselves monitored in the steady mode by atomic resonance fluorescence at $\lambda = 404\ nm$ $(K(5^2P_J) - K(4^2S_{1/2}))$ using phase sensitive detection, and in the presence of excess helium buffer gas. Analogous measurements are carried out on other alkali atoms. The decay of OH by diffusion and reaction (7) is given by

$$-d(OH)/dt = (k_{diff} + k_7(K)(He))(OH) = k'(OH) \qquad (vii)$$

and the intensity of the time-resolved OH(A - X) resonance fluorescence signals are given by the standard form:

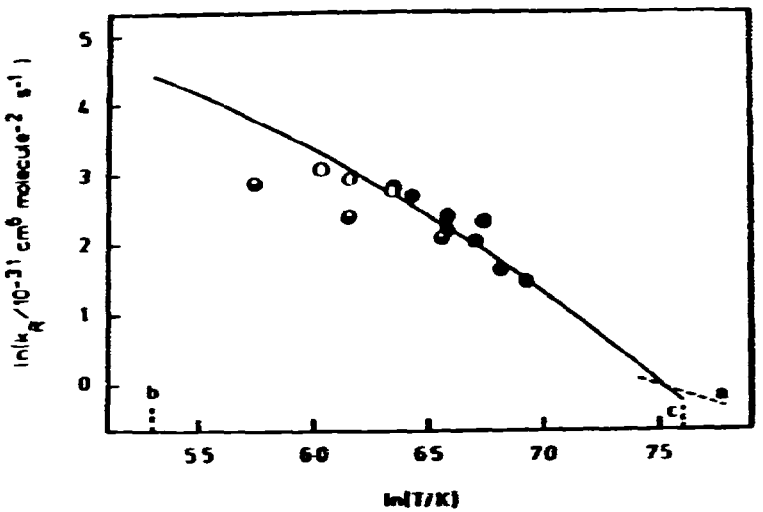

Figure 5

Data for the absolute third-order rate constant, k_R, for the reaction $Ru + O_2 + N_2 \rightarrow RuO_2 + N_2$ (b = 220 K; c = 2000 K)

O,● resonance absorption spectroscopy

● resonance absorption spectroscopy

◒ flow reactor ---a flame modelling

— Troe extrapolation

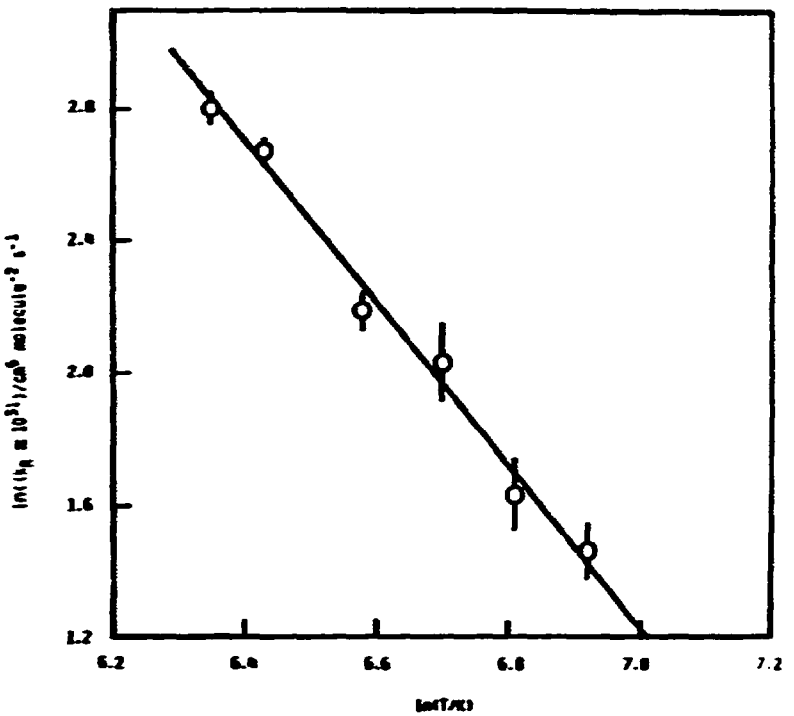

Figure 6

Variation of the absolute third-order rate constant (k_R) for the recombination reaction $Ru + O_2 + N_2 \rightarrow RuO_2 + N_2$ as a function of temperature over the range 570 to 1016 K. ($\ln(k_R \equiv 10^{31}$ l/cm^6 molecule^{-2} s^{-1}) against ln(T/K))

$$I_F(t) = \frac{\Phi(OH(X^2\Pi))_{t=0}\exp(-k't)}{1 + \Sigma\, k_Q(Q)/A_{nm}} \qquad \text{(viii)}$$

Figure 7 shows a block diagram of the apparatus for K + OH + He and Figure 8, examples of the decay of OH in the presence of K and He. These profiles are, in fact, analysed to the form:

$$I_F = \Theta_1 + \Theta_2\exp(-k't) \qquad \text{(ix)}$$

to allow for the effect via Θ_1 of steady scattered light. Figure 9 shows examples of the resulting values of k' derived from equations (viii) and (ix) (for (OH)) as a function of (K) for different values of (He), and Figure 10, the resulting plot of $(k' - k_{diff})/(K)$ vs. (He), the slope of which yields the value of k_7 for the temperature of 530 K. There are various constraints restricting measurements of the present type to single temperatures including the physical limitations of the reactor and photon counting detection system, and the elimination of the role of, say, K_2, in the reactor with OH. For such reasons, the reaction of Li lies outside the range of the present experimental system.

Table 2 lists the values of k_7 for the single temperature measurements derived from this series of investigations.[22-25]

Table 2 (X + OH + He)

X	k_7/cm^6 molecule^{-2} s^{-1}	T/K
Na	$1.07 \pm 0.2 \times 10^{-30}$ (23)	653
K	$8.8 \pm 1.8 \times 10^{-31}$ (22)	530
Rb	$8.8 \pm 1.3 \times 10^{-31}$ (24)	490
Cs	$10.0 \pm 1.5 \times 10^{-31}$ (25)	481

The unimolecular reactions rate theory of Troe may be applied to such systems, including Li + OH + He, and incorporating the effect of hindered rotation, to calculate the temperature dependence of these processes[22-25] (Table 3). Extrapolations of this kind are seen to yield better accord with flame data[1,2] when particular account is taken of the high efficiency (β_c) for the collisional stabilisation of XOH^* initially formed, by flame gases such as H_2O.

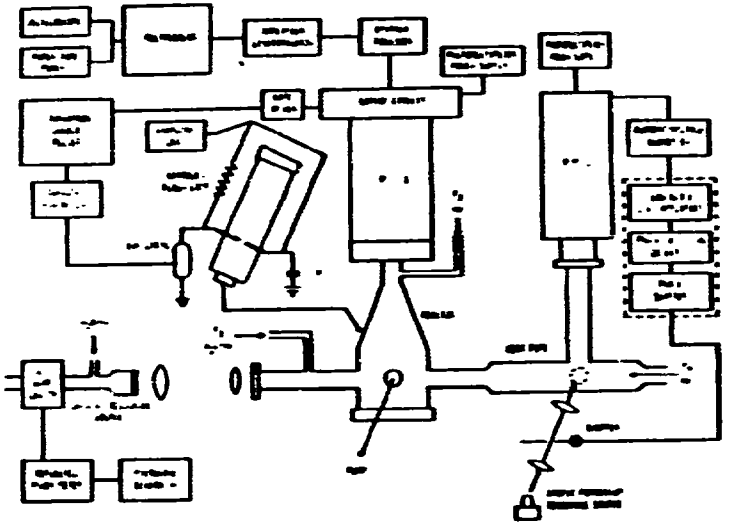

Figure 7

Block diagram of the apparatus for the kinetic study of the reaction K + HX + R ⟶ KX + R at elevated temperatures employing (a), time-resolved molecular resonance fluorescence measurements on KX($A^2\Pi$) at λ = 387 nm ((0,0), KX($A^2\Sigma^+ - X^2\Pi$)) following the pulsed irradiation of H_2O vapour and (b), steady resonance fluorescence coupled with phase sensitive detection on atomic potassium at λ = 404 nm (K(5^2P_J) - K($4^2S_{1/2}$)) derived from a heat pipe oven using a flow system kinetically equivalent to a static system.

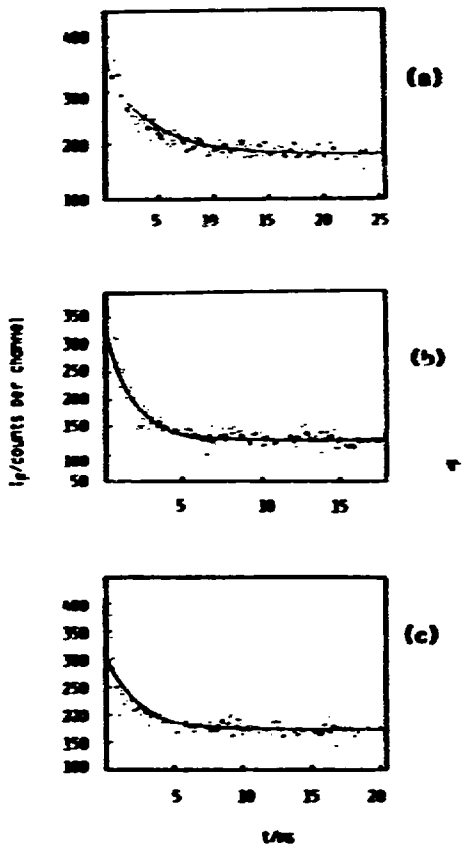

Figure 8

Digitised time-variation of the light intensity at λ = 387 nm indicating the decay of time-resolved molecular resonance fluorescence due to KX (I_F, counts per channel, (0,0), KX($A^2\Sigma^+ - X^2\Pi$)) following the pulsed irradiation of H_2O vapour in the presence of atomic potassium derived from a heat pipe oven and monitored in the steady state using atomic resonance fluorescence at λ = 404 nm (K(5^2P_J) - K($4^2S_{1/2}$)) coupled with phase sensitive detection

T = 530 K ; E = 50 J ; Repetition Rate = 1 Hz ; No. of individual experiments = 256 ;
Full curve ——, computerised fit to the form $I_F = a_1 + a_2\exp(-k't)$

	$[K]/10^{15}$ atoms cm^{-3}	$[H_2O]/10^{17}$ atoms cm^{-3}
(a)	6.6	8.7
(b)	53	8.7
(c)	50	3.8

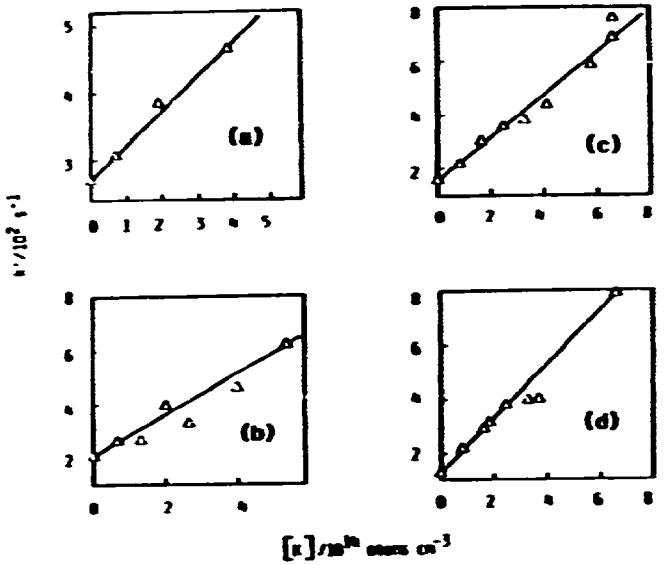

Figure 9

Variation of the pseudo first-order rate coefficient, k', for the decay of OH obtained by time-resolved molecular resonance fluorescence measurements on OH($X^2\Pi$) (λ = 307 nm, OH,0), OH($A^2\Sigma^+ - X^2\Pi$)) following the pulsed irradiation of H_2O vapour in the presence of different concentrations of atomic potassium, monitored in the steady mode using atomic fluorescence of the resonance transition at λ = 404 nm ($K(5^2P_J) - K(4^2S_{1/2})$) coupled with phase sensitive detection (T = 530 K).

$[M]/10^{17}$ atoms cm^{-3} : (a) 5.05 ; (b) 8.71 ; (c) 10.0 ; (d) 12.4

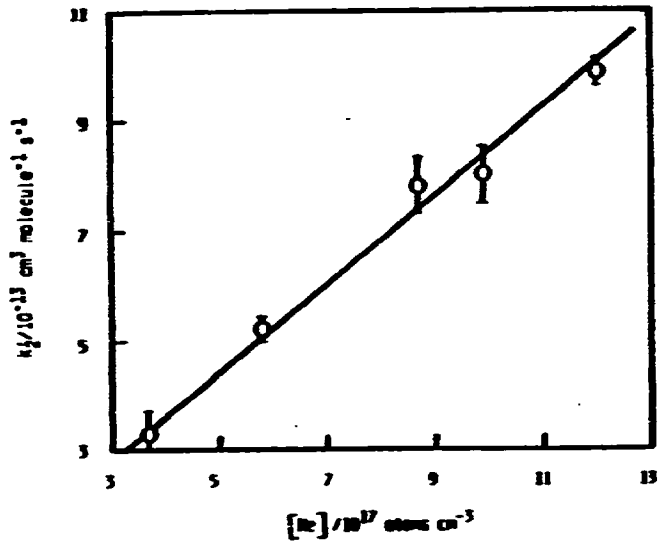

Figure 10

Variation of the pseudo second-order rate coefficient, k_2'' (= $k'/[K(4^2S_{1/2})]$), for the decay of OH as a function of the atomic helium concentration obtained by time-resolved molecular resonance fluorescence measurements on OH($X^2\Pi$) (λ = 307 nm, OH,0), OH($A^2\Sigma^+ - X^2\Pi$)) following the pulsed irradiation of H_2O vapour, with monitoring of atomic potassium by steady resonance fluorescence at λ = 404 nm ($K(5^2P_J) - K(4^2S_{1/2})$) coupled with phase sensitive detection (T = 530 K).

Table 3

	k_7/cm^6 molecule^{-2} s^{-1}
Li + OH + He	$(4.2 \pm 1.7) \times 10^{-27} T^{-1.40}$
Na + OH + He	$(4.7 \pm 1.0) \times 10^{-26} T^{-1.65}$
K + OH + He	$(1.5 \pm 0.4) \times 10^{-26} T^{-1.55}$
Rb + OH + He	$(1.5 \pm 0.4) \times 10^{-26} T^{-1.57}$
Cs + OH + He	$(2.8 \pm 0.7) \times 10^{-26} T^{-1.66}$

(III) X + I + M ⟶ XI + M

The technique for studying the group of reactions (II) above has been extended to the study of reaction (8) for X = K, Rb and Cs by time-resolved resonance fluorescence on ground state atomic iodine, $I(5^2P_{3/2})$, at λ = 178.3 nm ($I(5p^4 6s(^2P_{3/2})) - I(5p^5(^2P^o_{3/2}))$) in the vacuum ultra-violet.[26-28] The apparatus for the kinetic study of K + I + He is shown in Figure 11, the principal modification to the system given in Figure 7 for OH being the flushing of the optical path of the iodine atom resonance source with nitrogen, permitting flexibility with vac. u.v. focussing. With such measurements, it is necessary to produce KI in situ by the reaction

$$K + CH_3I \longrightarrow KI + CH_3 \qquad (9)$$

K is again derived from a heat pipe oven. Resonance fluorescence decay measurements on the I atom generated photochemically from the KI produced in reaction (9) must be carried out on a time scale short compared with that for nucleation as the density of KI is well above its equilibrium vapour pressure at the temperature of the reactor. The expressions for $I_F(t)(\lambda = 178.3$ nm) are analogous to those for $I_F(t)(OH(A - X))$ given in equations (viii) and (ix). Figure 12 gives examples of $I_F(t)(\lambda = 178.3$ nm) in the presence of K and He, and Figure 13, the variation of k' for $I(5^2P_{3/2})$ derived from the analogues of equations (viii) and (ix) as a function of (K) at different (He). Figure 14 shows $(k' - k_{diff})/(K)$ vs. (He), the slope of which yields k_8 for K + I + He. It may be shown that the intercept in Figure 14 can be attributed to the reaction between $I + K_2$. Similar considerations apply to measurements of k_8 for X = Rb and Cs.[26,28] The analogous measurements for X = Li and Na lie outside the temperature range accessible to the present system for reasons similar to those indicated above for X + OH + M.

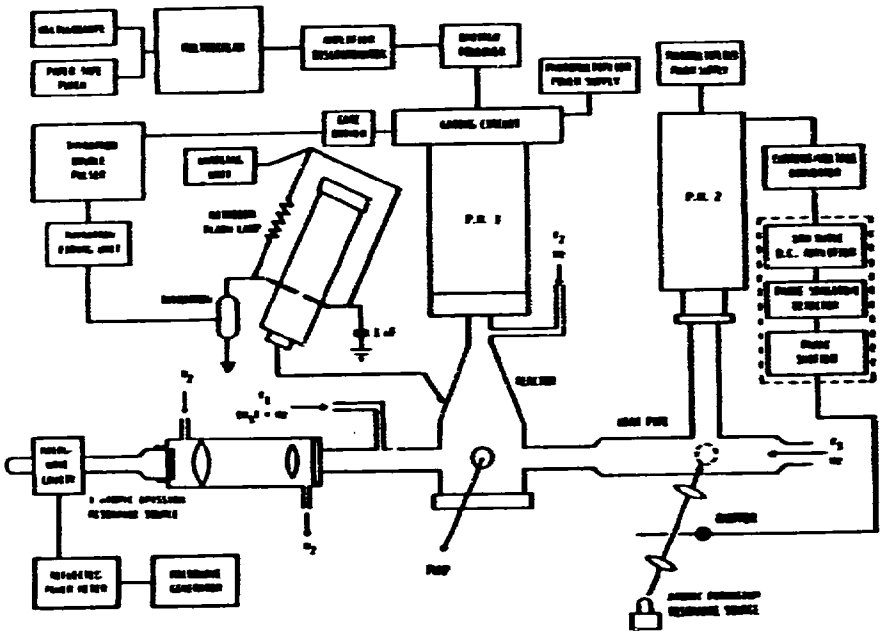

Figure 11

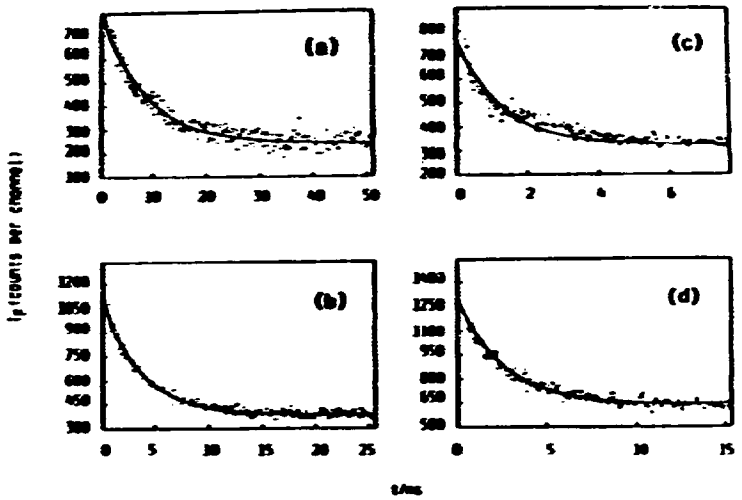

Figure 12

	$[X]/10^{16}$ atoms cm^{-3}	$[M]/10^{17}$ atoms cm^{-3}
(a)	0	7.7
(b)	2.8	7.6
(c)	9.2	7.6
(d)	2.6	19.8

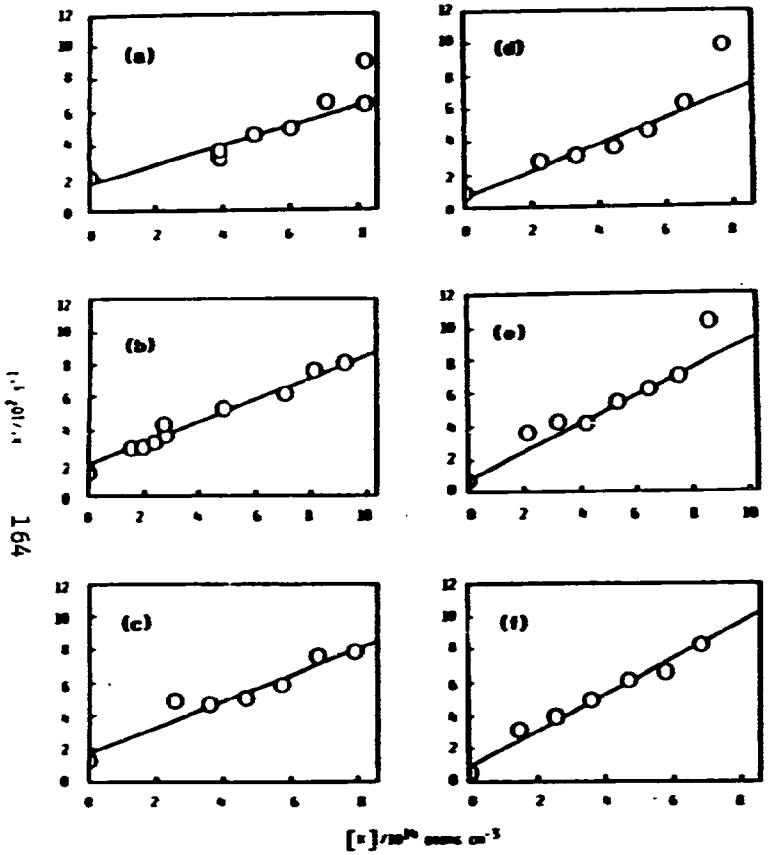

Figure 13

Variation of the pseudo first-order rate coefficient, k', for the decay of $I(5^2P_{3/2})$, obtained by time-resolved atomic resonance fluorescence at λ = 178.3 nm ($I(6s(^2P_{3/2})) - I(5p^5(^2P_{3/2})$) following the pulsed irradiation of KI vapour in the presence of different concentrations of atomic potassium, monitored in the steady state using atomic fluorescence of the resonance transition at λ = 404 nm ($K(5^2P_J) - K(4^2S_{1/2})$) coupled with phase sensitive detection (T = 567 K).

$[He]/10^{17}$ atoms cm^{-3} (a) 3.4, (b) 7.4, (c) 9.5, (d) 12.8, (e) 15.8, (f) 19.8

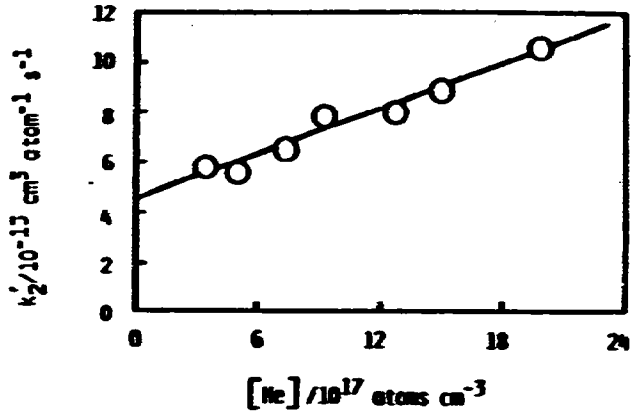

Figure 14

Variation of the pseudo second-order rate coefficient, k_2' (= $(k' - k_{diff})/[K(4^2S_{1/2})]$ for the decay of $I(5^2P_{3/2})$ as a function of the atomic helium concentration obtained by time-resolved atomic resonance fluorescence at λ = 178.3 nm ($I(6s(^2P_{3/2})) - I(5p^5(^2P_{3/2})$) following the pulsed irradiation of KI vapour, with monitoring of atomic potassium by st fluorescence at λ = 404 nm ($K(5^2P_J) - K(4^2S_{1/2})$) coupled with phase sensitive detectio (T = 567 K).

Table 4 list the results of the single temperature rate measurements of k_8 for X = K, Rb and Cs. Table 5 gives the results of molecular dynamic calculations for k_8 that have been carried out for the appropriate potential surfaces which are highly ionic in character,[26-28] accounting for the small negative temperature dependences.

Table 4 (X + I + He)

X	k_8/cm^6 molecule^{-2} s^{-1}	T/K
K	$(3.04 \pm 0.73) \times 10^{-31}$ (27)	567
Rb	$(3.34 \pm 0.67) \times 10^{-31}$ (28)	540
Cs	$(7.9 \pm 1.2) \times 10^{-31}$ (26)	491

Table 5 ((26) - (28))

	$k_8(500 \leq T/K \leq 2400)/cm^6$ molecule^{-2} s^{-1}
Li + I + He	$2.7 \times 10^{-32} T^{-0.09}$
Na + I + He	$8.4 \times 10^{-32} T^{-0.15}$
K + I + He	$6.9 \pm 1.7 \times 10^{-31} T^{-0.13}$
Rb + I + He	$1.0 \pm 0.2 \times 10^{-30} T^{-0.18}$
Cs + I + He	$4.1 \pm 0.8 \times 10^{-30} T^{-0.24}$

The results of the measurements are of fundamental interest in general terms from the viewpoint of recombination reactions of alkali atoms. In experimental terms, they point the way to future measurements with halogen atoms of closer relevance to flames as in the case of Cl. This would require the construction of an evacuated optical path suitable for atomic resonance fluorescence measurements deep into the vacuum ultrav-violet.

REFERENCES

(1) D.E. Jensen, G.A. Jones and A.C.H. Mace, J.Chem.Soc. Faraday Trans. I (1979) 75, 2377.

(2) D.E. Jensen and G.A. Jones, J.Chem.Soc. Faraday Trans. I (1982) 78, 2843.

(3) D.E. Jensen, J.Chem.Soc. Faraday Trans. I (1982) 78, 2835.

(4) A.J. Hynes, M. Steinberg and K. Schofield, J.Chem.Phys., (1984) 80, 2585.

(5) D.E. Jensen, Combustion and Flame, (1972) 18, 217.

(6) R. Friedman and J.B. Levy, Combustion and Flame (1963) 7, 195.

(7) A. Cohen and L. Decker, Proc. 18th. Int. Symposium on Combustion (The Combustion Institute, Pittsburgh, 1981) p. 225.

(8) D.E. Jensen and B.C. Webb, AIAA J., (1976) 7, 947.

(9) W.E. Kaskan, Proc. 10th. Int. Symposium on Combustion (The Combustion Institute, Pitsburgh, 1965) p. 41.

(10) M.J. McEwan and L.J. Phillips, Trans. Faraday Soc., (1966) 62, 1717.

(11) R. Carabetta and W.E. Kaskan, J.Phys.Chem., (1968) 72, 2483.

(12) D. Husain and J.M.C. Plane, J.Chem.Soc. Faraday Trans. II (1982) 78, 163.

(13) D. Husain and J.M.C. Plane, J.Chem.Soc. Faraday Trans II (1982) 78, 1175.

(14) F. Kaufman, Canad.J.Chem. (1969) 47, 1917.

(15) D. Husain, P. Marshall and J.M.C. Plane, J.Chem.Soc. Faraday Trans. II (1985) 81, 301.

(16) D. Husain, P. Marshall and J.M.C. Plane, J.Photochem., (1986) 32, 1.

(17) J.A. Silver, M.S. Zahniser, A.C. Stanton and C.E. Kolb, 20th. Int. Symposium on Combustion (The Combustion Institute, Pittsburgh, 1984).

(18) J. Troe, J.Phys.Chem., (1979) 83, 114.

(19) J. Troe, J.Chem.Phys., (1981) 75, 226.

(20) L.W. Crossman, G.S. Hurst, S.D. Kramer, M.G. Payne and J.P. Young, Chem.Phys.Letters (1977) 50, 207.

(21) S.D. Kramer, B.E. Lehmann, G.S. Hurst, M.G. Payne and J.P. Young, J.Chem. Phys. (1982) 76, 3614.

(22) D. Husain, J.M.C. Plane and Chen Cong Xiang, J.Chem.Soc. Faraday Trans. II (1984) 80, 1465.

(23) D. Husain, J.M.C. Plane and Chen Cong Xiang, J.Chem.Soc. Faraday Trans. II (1984) 80, 1619.

(24) D. Husain, J.M.C. Plane and Chen Cong Xiang, J.Chem.Soc. Faraday Trans. II (1985) 81, 561.

(25) D. Husain, J.M.C. Plane and Chen Cong Xiang, J.Chem.Soc. Faraday Trans. II (1985) 81, 769.

(26) D. Husain, J.M.C. Plane and Chen Cong Xiang, J.Chem.Soc. Faraday Trans. II (1985) 81, 1675.

(27) J.M.C. Plane and D. Husain, J.Phys.Chem., (1986) 90, 501.

(28) J.M.C. Plane and D. Husain, J.Chem.Soc. Faraday Trans. II (1986) in press, paper no. FAR 2, 5/1777.

INFLUENCE OF POTASSIUM ON OH DECAY RATES IN METHANE-AIR FLAMES

M. Slack, J. Cox, A. Grillo, R. Ryan and O. Smith*
Grumman Corporate Research Center
Bethpage, New York 11714

ABSTRACT

An investigation of the kinetic mechanism, and associated rate coefficients, by which potassium catalyzes recombination reactions in flames is in progress. Hydroxyl radical decay rates have been measured in atmospheric pressure flat CH_4/Air flames (stoichiometry ϕ = 0.9 to 1.2) with and without the addition of potassium, mole fraction 7×10^{-6} to 4×10^{-4}. Axial OH number density was determined from integrated absorption of the $Q_2(6)$ line of the $A^2\Sigma^+(v' = 0) \leftarrow X^2\Pi(v'' = 0)$ transition at 309.28 nm scanned with a Nd:YAG-pumped, frequency-doubled dye laser. Flame temperatures ranged from 1900 to 2000 K. Addition of potassium, in the form of an aerosol of $K_2CO_3 + H_2O$, accelerated the OH axial decay from the equilibrium overshoot at the flame front. Measured OH decay rates increased rapidly on addition of low potassium mole fractions ($<5 \times 10^{-5}$), then continued to increase slowly at higher additive levels. For a fixed concentration, the potassium was more effective with increasing stoichiometry. Potassium emission at 766.5 nm was monitored with a diode array spectrometer, was found to be in the square root region of the curve of growth, and was used to determine the potassium atom concentration which showed a small decay rate above the flame front, confirming a catalytic role. Preliminary measurements have been made of the influence of sodium. Our OH concentration measurements in unseeded CH_4/Air flames are in excellent agreement with earlier measurements by Cattolica (1982). An initial analysis of our data, using the SANDIA premixed flame code to compute flame properties, reveals that Jensen's (1982) mechanism ($K + OH + M \rightarrow KOH + M$, $KOH + H \rightarrow K + H_2O$) fails to predict the nonlinear influence of increasing K concentration. In agreement with the critiques by Heimerl (1983) and Schofield (1984), we conclude that Jensen's mechanism is a global approximation of a more complex mechanism. We are currently testing such mechanisms against our measured data.

---

* Department of Chemical Engineering, U.C.L.A., California 90024

1. INTRODUCTION

While it is observed that the addition of sodium or potassium to flames reduces the flame speed and increases the overall recombination rates in the post flame region, the details of the chemical mechanism and the associated rate coefficients are in dispute. Jensen et al.[1] measured the influence of potassium (mole fractions $< 10^{-3}$) on fuel-rich, atmospheric pressure hydrogen, oxygen, and nitrogen flames and concluded the following mechanism

$$K + OH + M = KOH + M \quad (1)$$

$$KOH + H = H_2O + K \quad (2)$$

was responsible for their observations of accelerated hydrogen atom decay. They obtained rate coefficients for reactions 1 and 2 by fitting predicted hydrogen decay rates to their measured data. Parallel measurements were made with sodium[2]. Heimerl[3], in a critique of Jensen's work, questioned the speculative nature of the proposed mechanism and the method of introducing potassium, i.e. as potassium dipivaloylmethane, $((CH_3)_3CCO)_2CHK$. The possibility of the organic radical, to which the potassium is bonded, playing a role in hydrogen abstraction was raised by Heimerl, together with alternative mechanisms.

Hynes, Steinberg and Schofield[4] have pointed out that Jensen's rate coefficient for the reaction

$$Na + OH + M = NaOH + M \quad (3)$$

was about 60 times larger than the corresponding recombination of H and OH at 2000 K, and that the backward rate has a pre-exponential term three orders of magnitude greater than expected from gas kinetic theory. Similar comments apply to Jensen's rate coefficient for reaction 1. Hynes et al. suggest that reactions 1 and 3 are global simplifications of a more complex set of reactions. Their investigation of sodium (mole fraction $< 3 \times 10^{-9}$) kinetics in oxygen-rich hydrogen flames supports the following mechanism

$$Na + H_2O = NaOH + H \quad (4)$$

$$Na + O_2 + M = NaO_2 + M \quad (5)$$

$$NaO_2 + H \rightarrow NaO + OH \quad (6)$$

$$NaOH + OH = NaO + H_2O \quad (7)$$

in which they observe that the algebraic addition of reactions 5, 6, and 7, together with the bimolecular steps of the H_2 - O_2 chain, reduces to reaction 3. An analogous argument applies to potassium. Hynes et al. recommend that the catalytic influence of large concentrations of both sodium and potassium on radical recombination in flames requires further study.

In contrast to the premixed flame results [1], Friedman and Levy [5] studied opposed jet diffusion flames (CH_4 and O_2) and observed that the addition of potassium vapor (mole fraction ≤ 0.06) to the fuel flow did not quench the flame. Similar quantities of CH_3Br successfully quenched the flame. The failure of large amounts of potassium, at least six times greater than used by Jensen et al.[1], to inhibit the flame is puzzling and cannot be readily explained. Since Jensen's experiments were the only ones in which accelerated recombination was measured with the addition of high concentrations of potassium, it is clearly important that the mechanism and rate coefficients be tested in an independent experiment.

The objective of our experimental investigation is to elucidate the mechanism and associated rate coefficients, by which potassium accelerates recombination in flames. We report here on our initial effort involving quantitative measurements of OH radical concentrations in CH_4-Air flames (ϕ = 0.9 to 1.2) seeded with large concentrations of potassium introduced as an aerosol of K_2CO_3 in water.

2. EXPERIMENTAL APPROACH

Flames were stabilized on a 2.54 cm diameter flat-flame burner constructed of bundled 1 mm I.D. tubing, operated at 1 atm pressure and shrouded by a nitrogen flow; this apparatus is shown in Fig. 1. The OH number density was determined from integrated absorption of the $Q_2(6)$ line of the $A^2\Sigma^+(v' = o) \leftarrow X^2\Pi(v'' = o)$ transition at 309.28 nm scanned with a Nd:YAG-pumped, frequency doubled dye laser (Quanta-Ray PDL-1). Axial OH number

density profiles were obtained by vertical translation of the burner relative to the laser beam. Our approach is similar to that used by Cattolica[6] to monitor OH radical nonequilibrium, and is based on well-documented methodology[7].

Potassium was fed to the burner in the form of an aqueous solution of K_2CO_3 from a calibrated aerosol generator. By controlling the concentration of K_2CO_3 in the solution we could introduce known mole percentages of potassium into the flame. The additional carbon and oxygen atoms entering the flame were a small perturbation to the existing levels of CO, CO_2 and oxygen, and were preferable to the addition of halogen atoms or large organic radicals as used in previous studies.[1-3] Complete evaporation of the aerosol 1 mm above the burner top was confirmed by monitoring the forward scattering of a HeNe laser. Potassium emission ($4p^2P°_{3/2} \rightarrow 4s^2S_{1/2}$) at 766.5 nm was monitored with a diode array spectrometer, was found to be in the square root region of the curve of growth, and was used to determine the potassium atom concentration.

Methane, oxygen, nitrogen and argon were fed to the burner via calibrated TYLAN mass flow meters. Total flow rates were maintained close to 8.0 liters/min. We commenced our investigation with methane-air flames, but in the majority of experiments argon replaced 50% of the N_2, thereby increasing the flame speed and maintaining a flat stable flame in the presence of potassium. A coaxial N_2 shroud was maintained to minimize O_2 diffusion into the flame.

Temperatures in the flame were measured with platinum-10% rhodium/platinum thermocouples (uncoated .125 mm diameter, butt welded). Recorded temperatures were used for data analysis without correction for the partially cancelling influence of catalytic effects, conduction along the wire, and radiative loss. Preliminary rotational temperature measurements compare adequately with the uncorrected thermocouple readings.

3. EXPERIMENTAL RESULTS

A typical measured OH number density profile (in the absence of K) is shown in Fig. 2. It reaches an equilibrium overshoot peak at the flame front 1 mm above the burner and then decays under the influence of recombination

reactions. Also shown in Fig. 2 are the earlier results of Cattolica[6] for almost identical conditions, and excellent agreement is observed between the two sets of experimental data.

Addition of potassium had a small influence on the equilibrium overshoot OH at the flame front. The subsequent OH axial decay rate was accelerated by the addition of potassium, in the range 0.0007 to 0.04 mole percent, as shown in Fig. 3. The efficiency of potassium in accelerating the OH decay rate decreased at higher potassium additive concentrations, as illustrated in Fig. 3, where 0.0007 mole percent is about half as effective as 0.015 mole percent. For a fixed seeding level the influence of potassium increased with increasing ϕ in the range 0.9 to 1.1, as shown in Fig. 4.

Post-flame temperature (typically 1900 to 2000K) increased monotonically with increasing additive mole percentage. For example, a rise of 62K was measured 8 mm above the burner on addition of 0.04 mole percent K to a $\phi = 1$ flame. These observations are consistent with increased overall radical recombination rates.

Typical measured potassium number density profiles above the flame front are shown in Fig. 5. The measured potassium concentrations were directly proportional to the seeding levels, while the axial profiles (relative dependence on distance above the burner) were independent of seeding level. The changes in K number density in Fig. 5 are probably due to conversion to KOH and are essentially insignificant since the incremental decrease in OH number density due to K addition is an order of magnitude greater than the total K number density. Clearly, the reaction mechanism by which potassium accelerates the OH decay rate is catalytic in nature.

Preliminary results of sodium carbonate addition to a $\phi = 1.1$ flame showed that sodium was as effective as potassium in accelerating OH recombination.

4. DATA ANALYSIS

Analysis of our data has proceeded in two stages. First, the simple reduction of the measured OH decays to an empirical rate constant (based on the observation that the decay is approximately second order in OH concentration). Second, flame properties were computed with the SANDIA flame

code and predicted OH and K concentrations compared with experimental data.

Following the approach of Kaskan[8], the measured OH concentrations were plotted as 1/(OH) versus time and an approximate linear relation was obtained, implying a second order dependence on OH concentration. (Note, for example, that the recombination of OH and H will mimic a second order OH reaction because of the fast bimolecular reactions coupling these two radicals). From the slope of the 1/OH plots we obtained effective decay rate constants α, and representative results from the $\phi = 1.1$ case are shown in Fig. 6, as a function of the initial K mole fraction. The nonlinear relationship between α and the additive mole fraction is highlighted in Fig. 6; α rises rapidly for initial potassium mole fractions up to 1×10^{-4}, beyond which the rate of increase falls off, suggesting an eventual asymptotic limit. Reproducing the trend in Fig. 6 will be an important test of a detailed kinetic mechanism. The rate constant α is not a global rate coefficient because the measured OH decay profiles include the influence of diffusion.

The second stage of data analysis is presently incomplete and only progress to date will be discussed. We are using the SANDIA flame code [9] to compute one dimensional flame properties based on initial oxidizer/fuel/additive mass flow rates and composition, measured temperature profiles and measured burner top temperatures. The computations account for diffusion and chemical kinetics, the latter using the Warnatz reaction mechanism[10] for a CH_4/Air flame and test reaction sets for the potassium chemistry. We have begun by testing Jensen's reaction mechanism (see discussion) and Jensen's inferred rate coefficients[1]. Jensen's model and rates fail to predict our measured nonlinear influence of potassium as shown in Fig. 6.

5. DISCUSSION

Our measurements to date show that addition of potassium to methane flames accelerates the axial decay of OH downstream of the flame front, that this acceleration is a nonlinear function of potassium concentration (see Fig. 3), and that potassium is least effective for $\phi < 1$. These quantitative results represent a stringent test of a kinetic mechanism, especially when used together with the observations of Jensen et al. and of Hynes et al.

The nonlinear influence of potassium in the present work contrasts with

the linear influence on H observed by Jensen over a small concentration range in fuel rich hydrogen flames. Furthermore, our preliminary finding that Na and K are about equally effective in accelerating OH decay rates in a fuel rich flame contrasts with Jensen's result that Na is a factor of 3 more efficient than K in catalyzing H atom decay.

Testing of reaction mechanisms against our data base has been initiated. The failure of Jensen's mechanisms to reproduce our observed nonlinear influence on K suggest his mechanism may be a global simplification of a more complex reaction set and that the simplification only applies over a limited experimental parameter space. It will be important to test Jensen's mechanism for $\phi = 0.9$, the case in which we observe K to be least effective as an OH scavenger.

Further work is recommended in the areas of (a) kinetic reaction model testing and (b) flame experiments, in order to drive out a viable reaction mechanism and a reasonable estimate of the associated rate coefficients. In addition to our measurements of OH and K, we believe it is essential to monitor intermediates (such as KO, KO_2, K_2, KOH and KH) in order to obtain more direct evidence for the chemical pathways by which potassium influences recombination reactions in flames. We plan to conduct a spectroscopic survey of flames heavily seeded with potassium (mole fraction $> 10^{-3}$) using a Fourier Transform IR spectrometer, a visible/UV grating spectrometer, and laser-induced fluorescence excitation. A complete parallel set of experiments with sodium should also be conducted. In the area of reaction mechanism testing, we plan to test both the Hynes, Steinberg and Schofield model[4] and the comprehensive reaction set of Heimerl, Keller and Klingenberg[11] against our experimental data base, making full use of recent rate coefficient measurements[12-14]. An acceptable mechanism will have to reproduce the observed dependence on additive concentration and on stoichiometry.

6. REFERENCES

1. D. E. Jensen, G. A. Jones, and A. C. H. Mace, J. Chem. Soc. Faraday Trans. 1 Vol., 75, p. 2377 (1979).
2. D. E. Jensen and G. A. Jones, J. Chem. Soc. Faraday Trans. 1 Vol. 78, p. 2843 (1982).

3. J. Heimerl, Ballistic Research Lab Tech. Report ARBRL-TR-02479 (1983).
4. A. Hynes, M. Steinberg and K. Schofield, J. Chem.,Phys. Vol. 80, p. 2585, (1984).
5. R. Friedman and J. Levy, Combust. Flame Vol. 7, p. 195 (1963).
6. R. Cattolica, Combust. Flame, Vol. 44, p. 43 (1982).
7. R. Lucht, Purdue University Rept PURDU-CL-78-06 (1978).
8. W. E. Kaskan, Combust. Flame, Vol. 2, p. 119 (1958)
9. R. J. Kee, J. F. Grear, M. D. Smooke & J. A. Miller, Report # SAND85-8240, Sandia National Laboratories, Livermore, CA (1985)
10. J. Warnatz, Combustion Chemistry, W. C. Gardiner, Jr., ed, Springer-Verlag, New York, p197 (1984).
11. J. M. Heimerl, G. E. Keller and G. Klingenberg, Ernst-Mach-Institut Report 1/85 (1985).
12. D. Husain, J. M. C. Plane, and C. C. Xiang, J. Chem. Soc., Faraday Trans II 80, 1465 (1984).
13. D. Husain, and J. M. C. Plane, J. Chem. Soc. Faraday Trans 2, 78, 1175, (1982).
14. J. A. Silver, M. S. Zahniser, A. C. Stanton, and C. E. Kolb, Proceedings of Twentieth Symposium (International) on Combustion, Aug (1984).

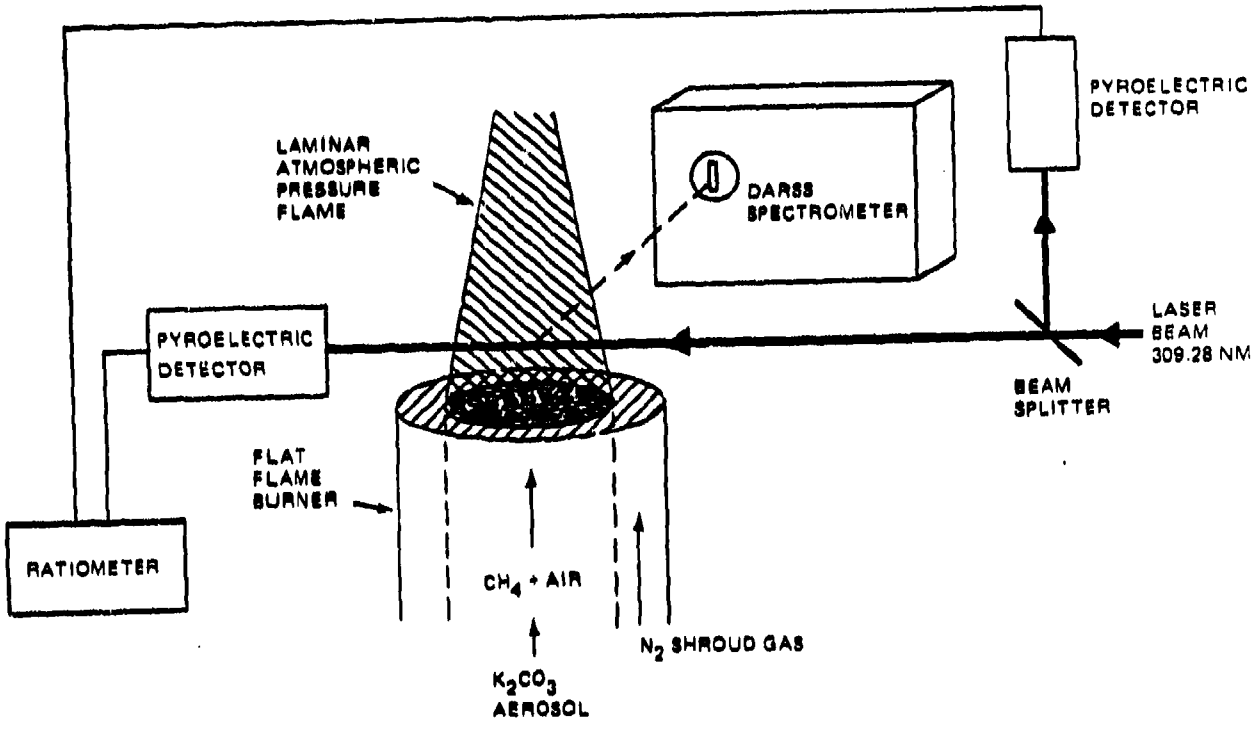

Fig. 1 Schematic of Apparatus

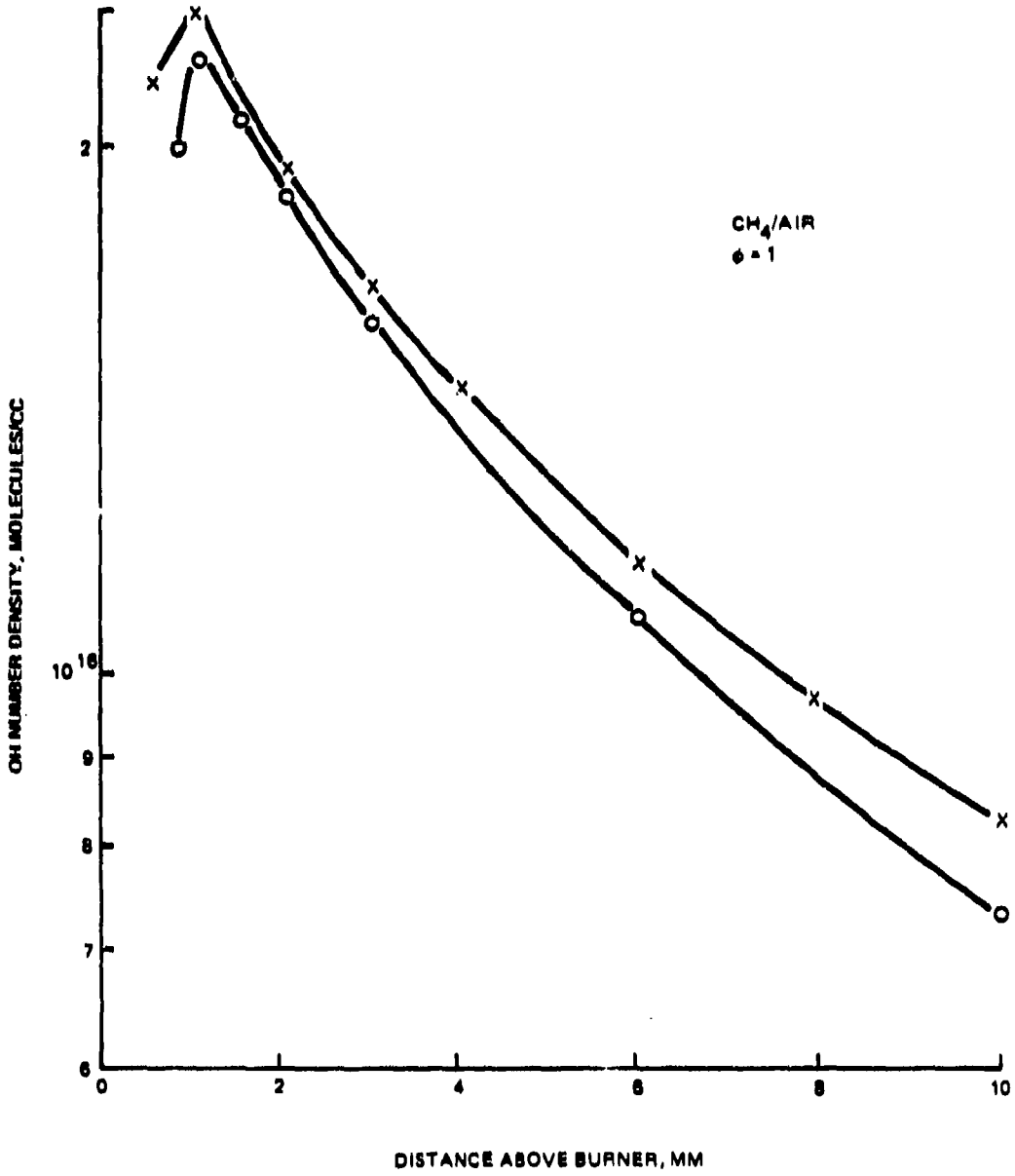

Fig. 2 Comparison of Measured Hydroxyl Number Densities above a Laminar Flat CH_4/Air Flame: Present Data, O; Cattolica, x

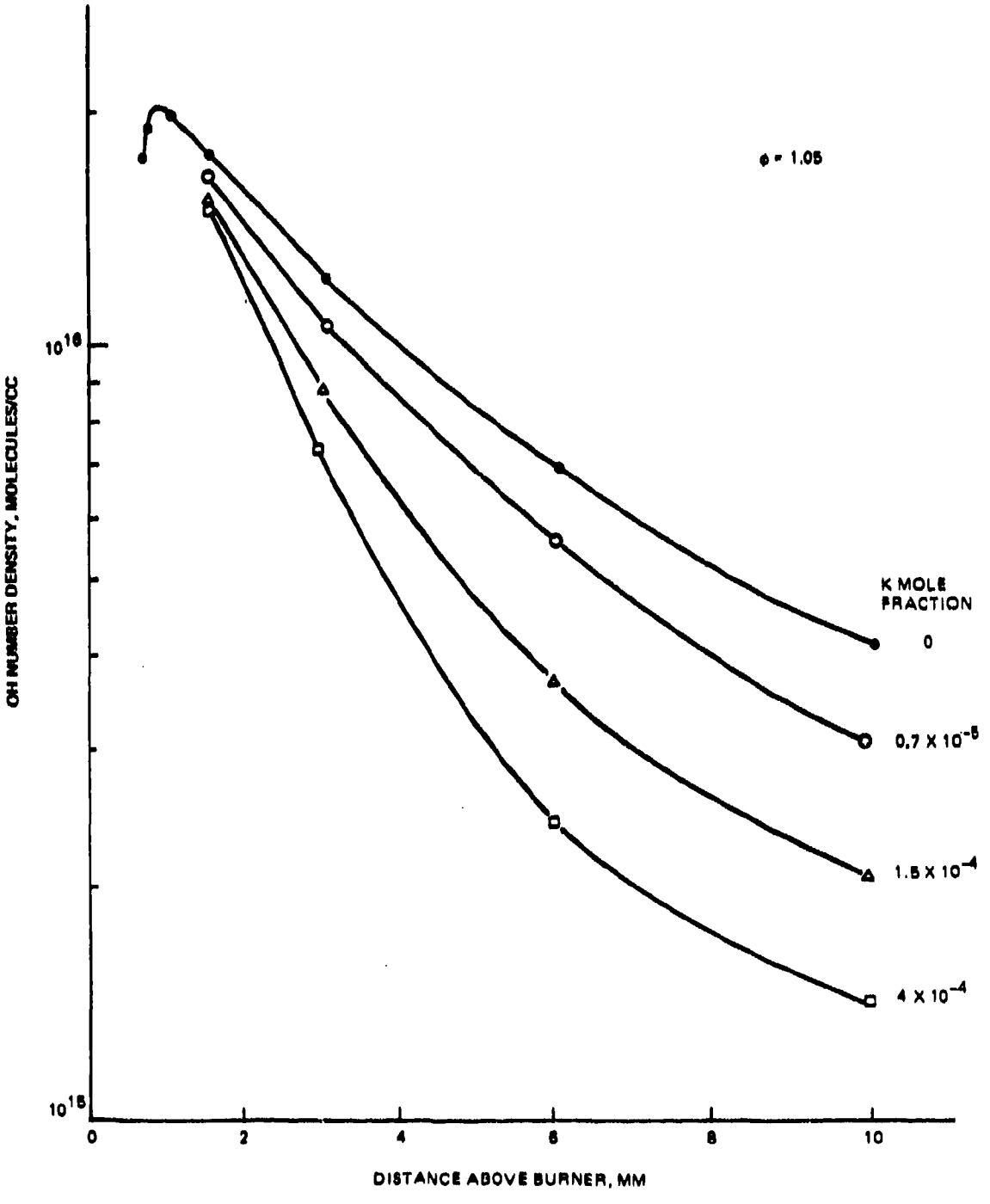

Fig. 3 Influence of Potassium on OH Decay Rates in a CH_4/O_2-N_2-Ar Flame

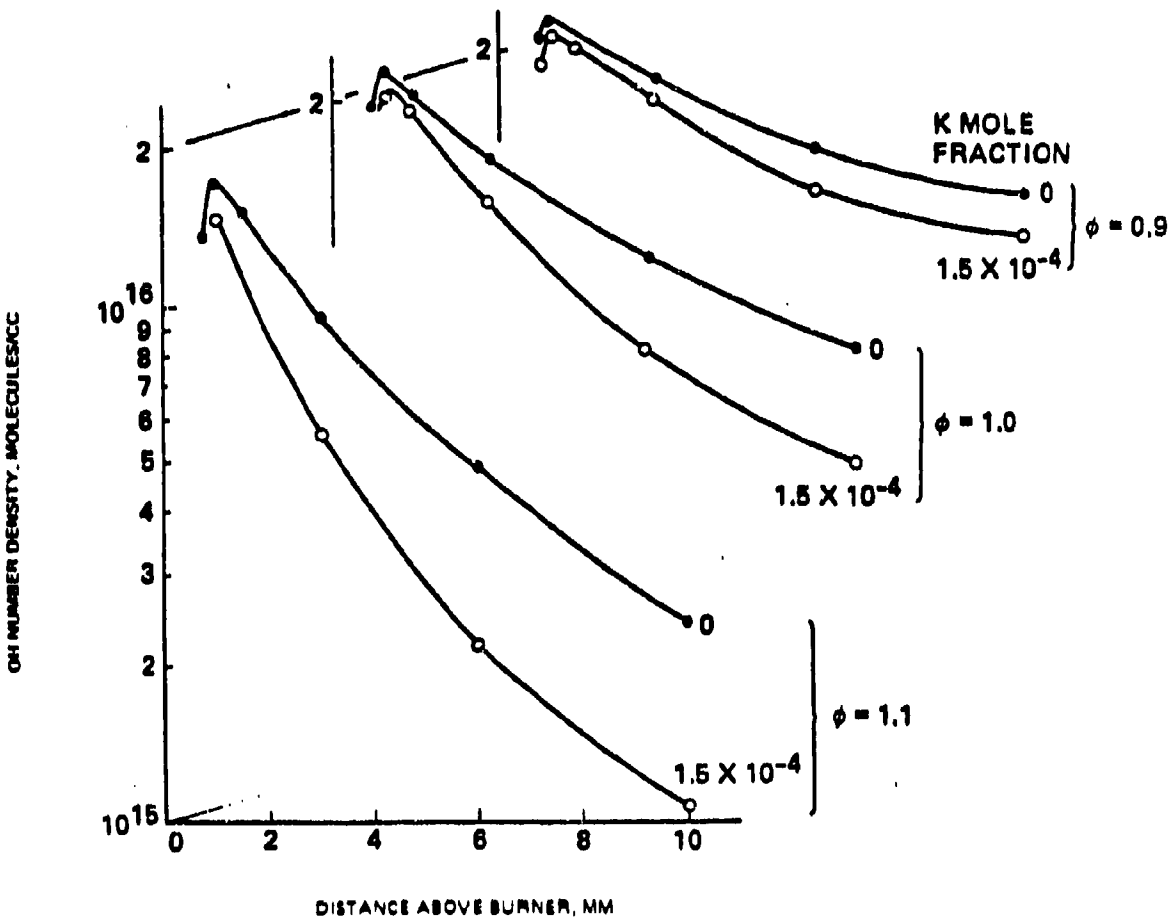

Fig. 4 Influence of Potassium on OH Decay Rates in a CH_4/O_2-N_2-Ar Flame

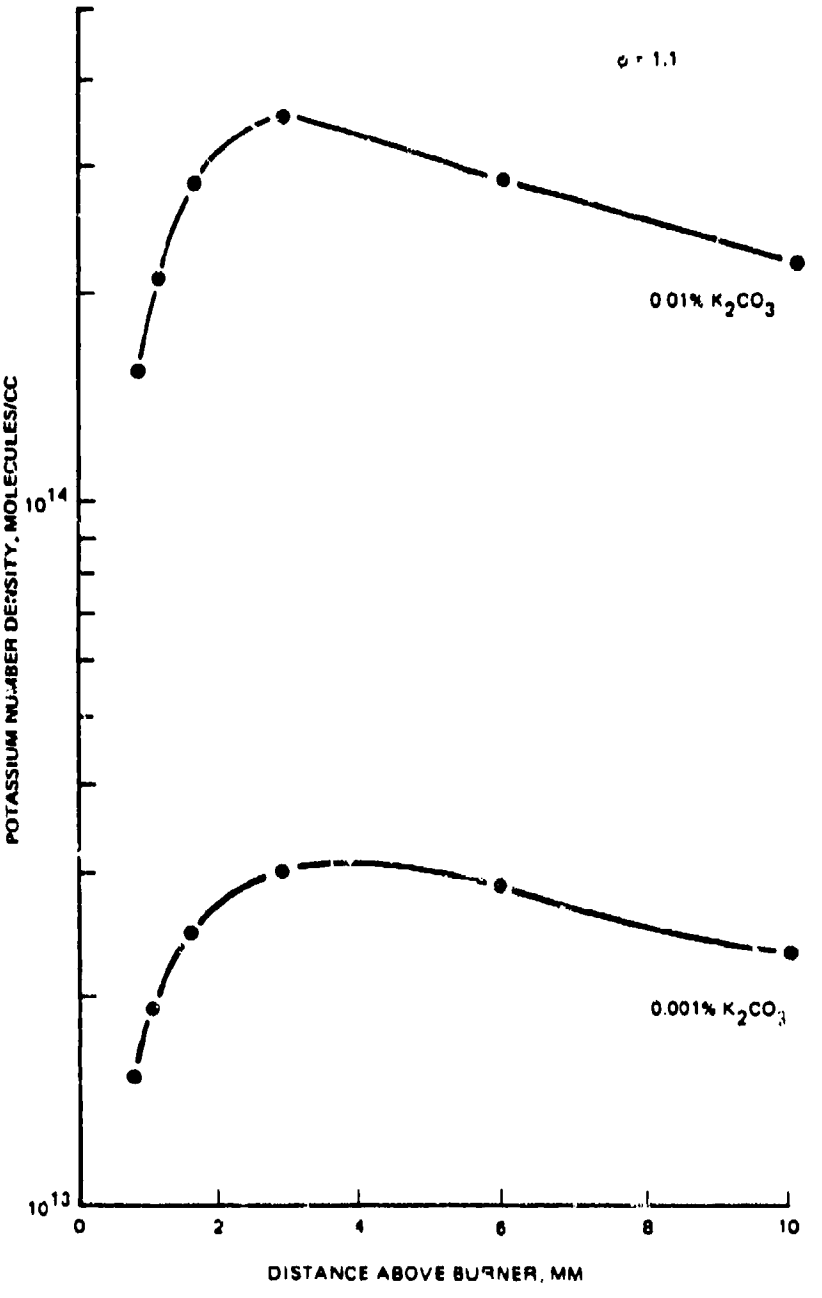

Fig. 5 Typical Potassium Number Density Profiles Measured in a CH_4/O_2-N_2-Ar Flame

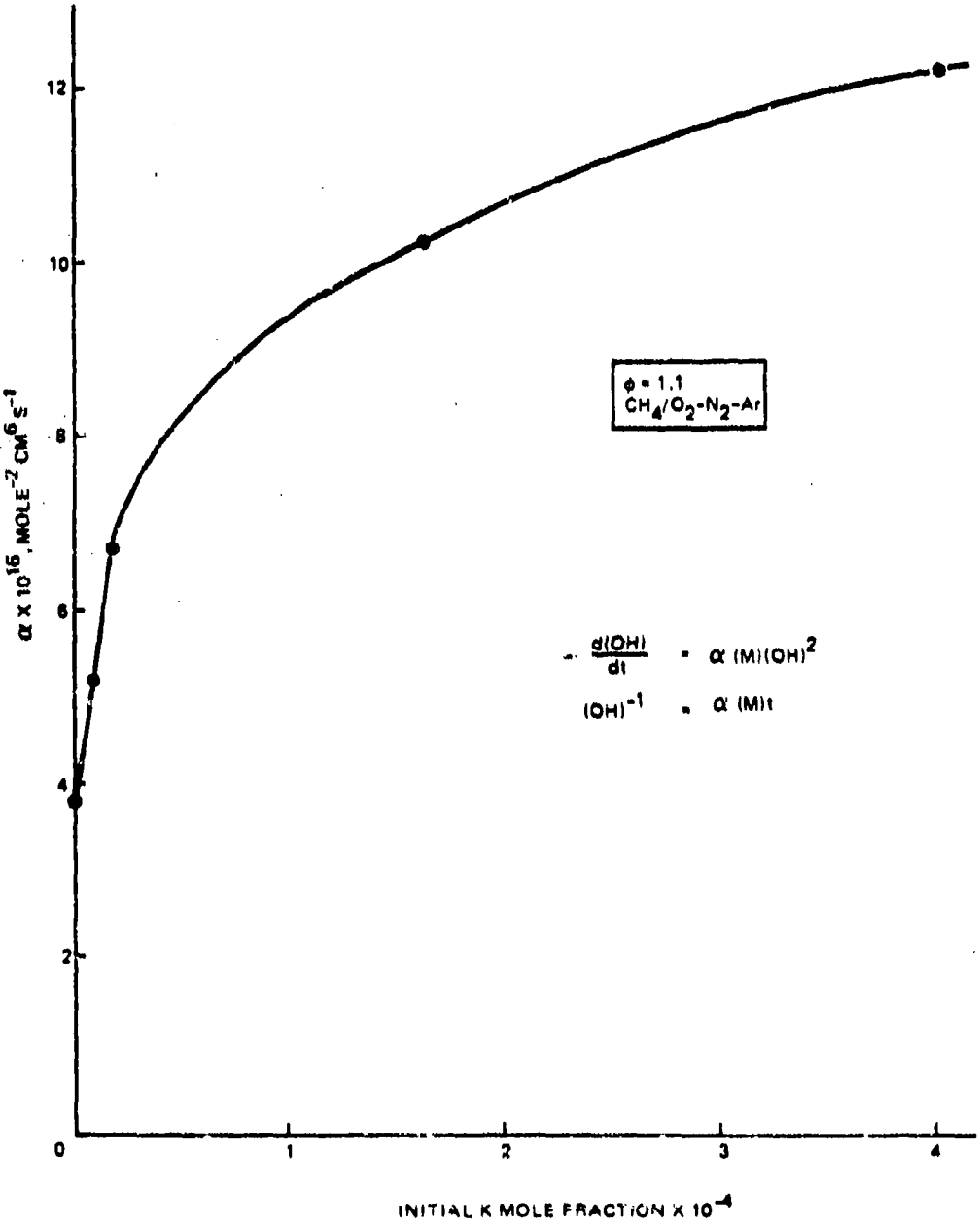

Fig. 6 Empirical OH Decay Rate Constant α as a Function of Additive Mole Fraction

THE FEASIBILITY OF A CARS TECHNIQUE FOR THE STUDY OF MUZZLE FLASH

J. A. Vanderhoff, R. B. Peterson and A. J. Kotlar
US Army Ballistic Research Laboratory

INTRODUCTION

Muzzle flash is observed during firing of large and small caliber guns. It typically appears as a bright flash of light outside the muzzle and is associated with the release of rich combustion products from the barrel of the gun. Controlling and suppressing this phenomenon is of major practical concern since the energy release is sufficient to produce blast waves and large visible/thermal signatures, both being of use in locating the position of the gun.

Past studies[1,2,3] have indicated the existance of three separate regions of the flash. They are, in order of increasing distance from the muzzle, primary, intermediate, and secondary. Luminosity from these three regions arises primarily from glowing particulates and sodium emission. Thus the spectrum associated with muzzle flash displays line emission as well as a broad background emission characteristic of blackbody radiation. Primary flash occurs at the barrel exit and is a result of the hot luminous combustion products leaving the muzzle after the bullet uncorks. Subsequent rapid expansion of the combustion gases quenches much of the remaining gas phase reactions thus producing a dark region following the primary flash. As the process continues, over expansion leads to a shock being generated in the form of a Mach disk downstream of the muzzle. This shock structure reheats the incompletely reacted combustion products and initiates new combustion. As a result, a second luminous

region develops downstream of the Mach disk and is called the intermediate flash. The propellant stoichiometry is such that major products include CO and H2, thus as oxygen from the atmosphere is entrained with the growing flow field, a third combustion region, the secondary flash develops. It is much larger than the previous two and accounts for the major portion of energy release occurring outside the gun barrel.[4]

The study of muzzle flash is motivated by the desire to control and suppress the secondary flash. It has been observed that small amounts (1-2%) of an alkali metal salt added to the propellant will suppress the flash, but the mechanisms associated with the suppression are well understood. For example, it is still unclear whether these metal salts act thermally or chemically, and if the latter, whether the process occurs heterogeneously (i.e. on the surface of a particle) or homogeneously in the gas phase. A recent study[5] has shed some light on this subject, but much work remains to be done.

When muzzle flash is considered in the context of studying the condition leading to its suppression, the relevant mechanisms involved must be guessed at. The reason for this is a lack of information on the conditions present within the developing muzzle flow field. High luminosity, extreme temperature and density gradients, high concentrations of particulates and the transient nature of the event are responsible for preventing many of the traditionally accepted diagnostic techniques from being applicable. Williams and Powell[6] and Lederman et al.[7] have used laser Raman spectroscopy to investigate the muzzle

blast region of a 20 mm gun. Both studies used downloaded rounds which achieved muzzle velocities in the neighborhood of 400 m/s. Williams and Powell looked at the region from 0.32 to 1.3 cm downstream of the barrel exit for times up to 3 ms after bullet exit. Laser induced particulate incandescence prevented any temperature measurements from being determined. Relative densities for N2 and CO were measured; however, these relative values depe nd on an assumed gas temperature. Lederman et al. made measurements at a position 5 cm downstream of the barrel exit for a time frame of 0.33 to 2 ms. Over this region they obtained an essentially constant temperature of about 1500K. The lack of a time dependent temperature caused the authors to doubt the measurements however they could not substantiate alternate explanations. Petrow and Harris[8] have looked at the muzzle flash region of a 7.62 mm rifle using coherent anti-Stokes Raman spectroscopy (CARS). They searched for a CARS signal of the H2 molecule in the muzzle flash region. Due to inadequate triggering only one noisy H2 spectrum was obtained in several hundred shots, which indicated CARS spectra could be observed. Emission spectra and sodium and potassium line reversal techniques have been used with success[2,4] to obtain temperature measurements of the various flash regions. These techniques are applicable where the probe region is luminous and also, for spatial resolution, depend on the validity of Abel-inversion data analysis (i.e. a symmetric temperature distribution and a uniform alkali metal concentration).

CARS appears to be well suited for obtaining temperature profiles in the muzzle flash region. It is non-intrusive in

the sense that there is no physical probe placed in the flow region. Since the CARS signal emerges as a collimated beam a high signal to noise ratio is possible. A high degree of spatial and temporal resolution can also be obtained. The CARS technique relies on the ability of high energy lasers to pass through the measurement field, hence its applicability is limited to systems of relatively high light transmission.

Typical solid propellants burn rich and the major gas products of combustion are approximately 40% CO, 17% H2, 16% H2O, 14% CO2 and 11% N2.[9] CO has been selected as the molecule to be probed in the muzzle flow field. There are several obvious reasons for this choice. Diatomic spectroscopy is simpler than triatomic thus eliminating H2O and CO2 as candidates. N2 is present in ambient air which can result in problems when using collinear geometry for generating CARS signals. CO and H2 still remain as candidates. CO is present in larger concentrations and there exists more efficient dyes for producing the Stokes beam appropriate for CO than for the H2 Stokes beam. One further point should be made with reference to the H2 molecule. H2 has a large rotational constant thus the individual rotational lines within the vibrational Q- branch are well resolved. This permits a simpler computation as well as permitting lower temperatures to be fitted more precisely. This well resolved structure has a drawback however; which arises when taking single shot data. The shot-to-shot fluctuation of the dye laser can introduce serious errors into the results unless it is monitored with each laser shot. This moritoring adds to the experimental complexity and consequently CO is deemed the choice molecule.

In this paper we report data on the feasibility of using CARS to study muzzle flash. CARS spectra (broadband) for the CO molecule have been obtained on a flat flame burner and in the intermediate flash region of an M-14 rifle. These spectra have been fitted to determine temperatures. Muzzle flash temperatures have also been derived from emission spectra to compare with the CARS results. Apertured light transmission data at various times and positions in the flow field are obtained in order to assess the effects of beam attenuation and steering. Major problems that seem to be present when using CARS as a probe of the muzzle flow field are discussed.

EXPERIMENTAL DESCRIPTION

The experimental apparatus consisted of a modified M-14 rifle, having a nominal muzzle diameter of 7.62 mm and a shortened barrel length of 451.5 mm. This previously used barrel length has been incorporated here so that a better comparison with past studies[2,10,11] can be made. The rifle is held in a fixture and attached to a large metal box of dimensions 0.6x1.0x1.4 m. Design features of this box included a retractible flat flame burner for generating hot CO, a vent for gas removal, and a nitrogen line for purging. In addition, plexiglass windows were incorporated into the design to provide optical access to the interior regions of the box. However, for CARS signal generation, simple access ports were provided through the plexiglass because of the high power of the laser pulses. For trapping bullets during each experiment, a bullet catcher was used on the opposite side of the box from the rifle. Standard ball ammunition with WC-846

deterred surface coated propellant has been used for all the data reported here. Table 1. lists the chemical composition of this propellant. The nominal mass of propellant in each round was 2.99 gm. When used in the barrel with the dimensions specified above, this gave a muzzle velocity of approximately 815 m/s.[11]

TABLE 1. WC-846 PROPELLANT SPECIFICATIONS

Ingredients	Percentage(%)
Nitrocellulose	87.01
Nitroglycerin	9.71
Diphenylamine	0.90
Dinitrotoluene	0.71
Moisture & Volatiles	0.85
Residual solvent	0.29
Calcium carbonate	0.46
Sodium sulfate	0.07

The experimental set up for collecting light emission and transmission data is shown in Fig. 1. One He-Ne laser beam is positioned just in front of the muzzle exit and when this beam is interrupted by the bullet and flow field a trigger pulse is produced by a photodiode. This trigger provides the source of timing for all the muzzle flash experiments. When taking light transmission data a second He-Ne laser is directed through the flow field at specified downstream locations from the barrel exit and a photodiode monitors the intensity of the beam. Laser path and barrel axis are perpendicular. This photodiode output is fed into a digital oscilloscope and the first mentioned photodiode provides the trigger sweep. An effort was made to insure that the detector behaved in a linear fashion to the amount of light received. The photodiodes have an active circular area of about 0.8 square cm thus for beam steering studies a small aperture is inserted in front of the photodiode and the nominal

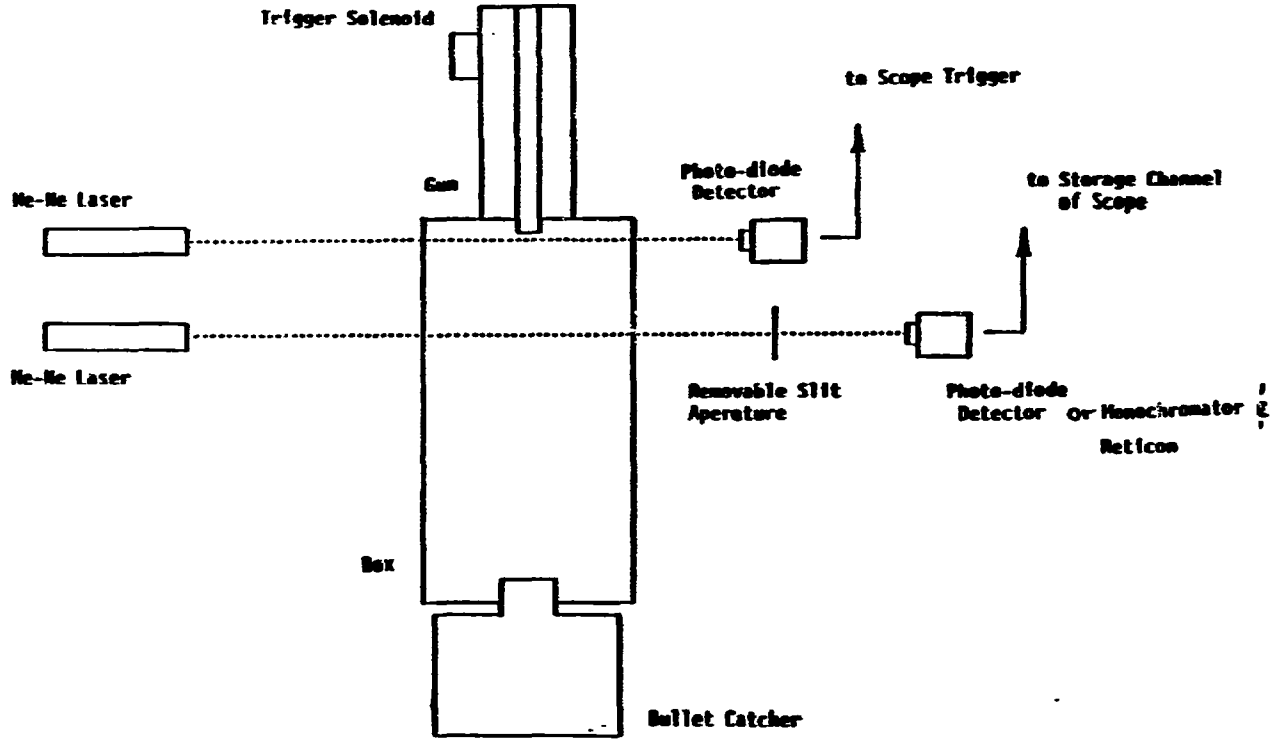

Figure 1. Experimental arrangement for light emission and transmission studies in the muzzle flow field of a 7.62 mm rifle.

1.0 mm diameter He-Ne laser beam is focussed to diameters less than or equal to the aperture size. For some of the light emission studies an unapertured photodiode was used; when spectral intensity as a function of wavelength was desired, the monochromator - reticon system used to detect CARS signals was employed. This monochromator had a 1/4 m focal length and a 100 micron entrance slit. A 1200 groove/mm grating in this system which included an intensified micro channel plate reticon detector had a FWHM resolution of about 12 cm-1. For CARS data a 2400 groove/mm grating gave a FWHM resolution of about 6 cm-1.

CARS spectra for CO were obtained during gun firing and on a porous plug flat flame burner using the experimental setup shown in Fig. 2. This arrangement, along with the triggering system described later, provided the opportunity of recording single shot CARS signals during the experiment. A co-linear phase matching scheme was employed with pump beam and Stokes beam wavelengths of 532 and 600 nm, respectively. The latter value was the center of the broadband dye laser emission which had a bandwidth of approximately 4 nm. This bandwidth permitted data to be obtained from the ground and the vibrationally excited levels of the CO molecule thus yielding vibrational temperature information on the molecules in the probe volume. A previous study on CO in a diffusion flame[12] used a binary dye mixture of Rhodamine 640(R-640) and Kiton Red (KR) for the dye laser. Our choice of dyes was similar with approximate percentages by weight of 70% R-640 and 30% KR. Exact dye mixture concentrations were adjusted during laser operation to "peak" the output while observing CARS signals of hot CO from a burner. A flat flame

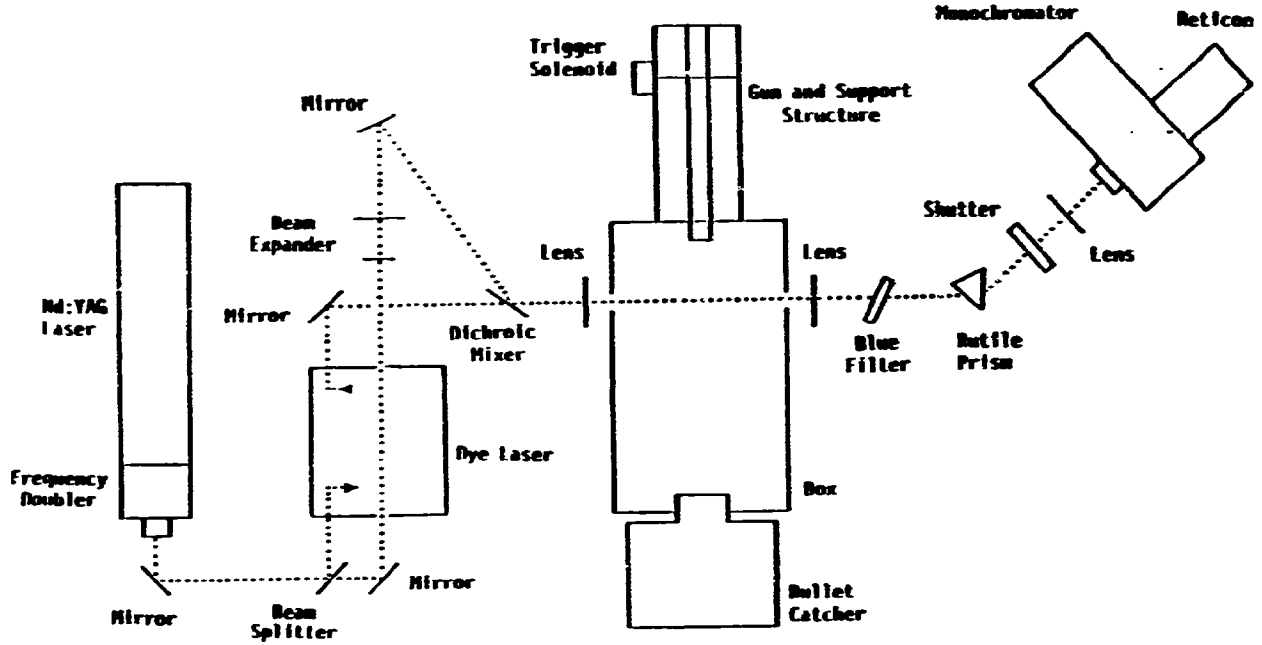

Figure 2. Experimental arrangement for obtaining CARS data in the muzzle flow field of a 7.62 mm rifle.

burner having a 6 cm diameter sintered bronze porous plug with water cooling coils imbedded in the sintered material was used. Rich mixtures of CO and O2 resulted in flames with ample hot CO molecules for probing with CARS. The top of the burner is centered 5 mm below the beam waist of the overlapped pump and Stokes beams. From this position final tuning and alignment is accomplished. CO CARS spectra from this burner are also analyzed to insure the proper operation of the experimental system and analysis procedure.

The optical train consisted of a Quantel model YG-481C Nd:YAG laser with frequency doubling, an in-house constructed longitudinally pumped broadband dye laser and various anti-reflection coated optics to direct and combine the horizontally polarized CARS signal generating beams as shown in Fig. 2. The 532 nm radiation was separated from the 1064 nm fundamental left over from doubling by dichroic mirrors. The 532 nm output was measured as about 350 millijoules per pulse. Of this, a beam-splitter directed 60% to pump the dye laser which produced a Stokes beam energy of 30 millijoules per pulse. The remaining 40% was used for the CARS pump beam. The path lengths of both the Stokes beam and pump beam were matched for temporal overlap and then the two beams were combined into one with a dichroic mixer. A pair of 30.5 cm focal length lenses were employed to direct the CARS generating beams into the probe volume and then to recollimate the emerging radiation which included the CARS signal. Also shown in Fig. 2 are the details of the CARS signal acquisition system. After the collecting lens recollimated the emerging laser beams and CARS signal, a blue glass filter atten-

uated most of the 532 and 600 nm radiation from the signal train leaving the CARS signal at 478 nm. Further rejection was achieved by spatial separation withe rutile prism. By the time the light reached the monochromator, oriented such that the long axis of the 100 micron entrance slit was horizontal, the CARS beam was sufficiently isolated that only it passed into the monochromator.

The CARS probe volume was experimentally determined by translating a 1 mm thick glass slide through the interaction region while monitoring the non-resonant CARS signal. A plot of the peak height of the CARS signal versus position is shown on Fig. 3. Spatial resolution is commonly defined as the position at which the signal drops to 1/e of its maximum value. Using this criterion the interaction length, determined from Fig. 3, is 0.55 cm. The diameters of the focussed beams are about 0.005 cm thus the probe volume approximates a cylinder 0.55 cm in length and 0.005 cm in diameter.

Although the details of the timing circuitry will be presented in the next section, the operation of the detection system requires some explanation here. The gun firing mechanism consisted of a solenoid actuated trigger. From the time the solenoid is energized to the time the bullet exits the barrel, approximately 20 ms elapsed. At the same time the trigger sequence is begun, the control unit of the OMA receives a signal initiating a time interval of 33 ms during which the detection elements of the reticon are active. Also during this time interval, a shutter is opened for approximately 100 ms. In this way, detection of CARS spectra originating from a single laser pulse

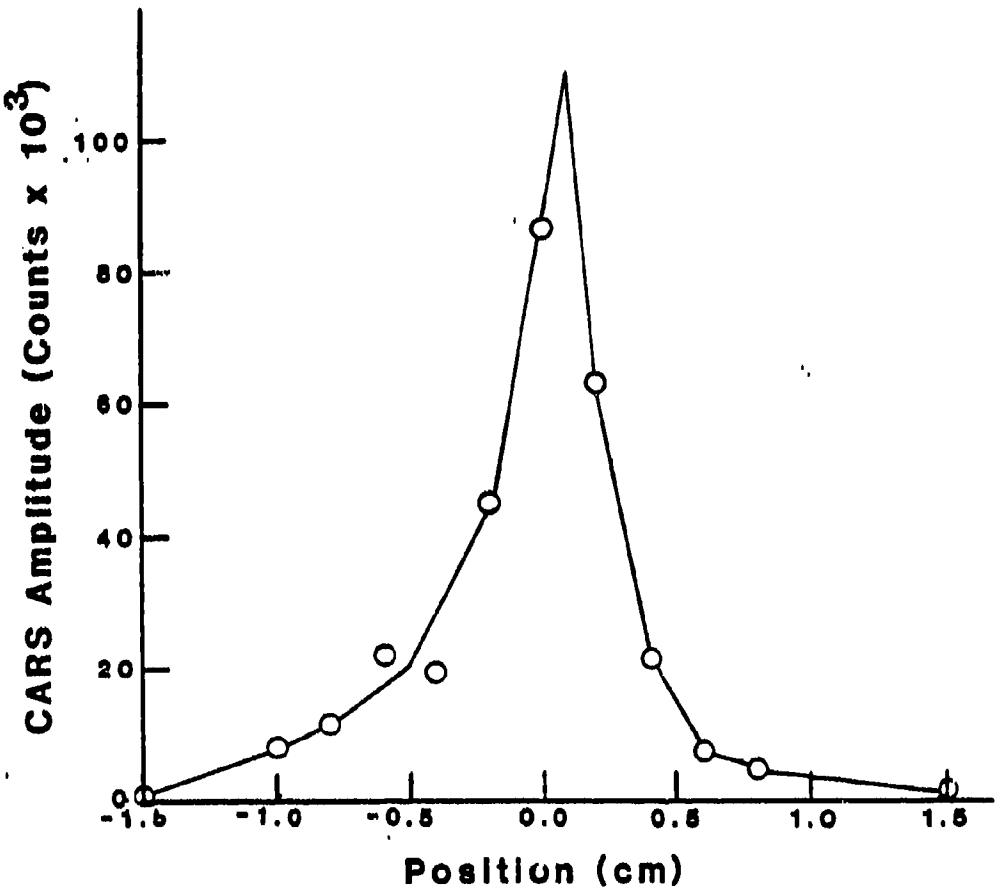

Figure 3. The spatial resolution of the focussed CARS signal as shown by the interaction length.

was achieved.

EXPERIMENTAL TIMING

There were two major design constraints in developing the laser control circuitry. The first was associated with the need to have the laser pulsing continously (at 8.9 Hz) while adjusting the system for maximum signal generation. The second constraint involved synchronizing a single laser pulse withthe firing of the gun for acquiring data. This latter constraint meant precisely triggering the laser (within a few microseconds) from a repeatable source. We chose the interuption of a He-Ne laser beam positioned in front of the gun barrel as the trigger source of the laser.

A schematic diagram of the timing system is shown in Fig. 4. The hardware used to fulfill the experimental requirements proved to be an integration of a specially built one-shot control circuit with the commercial laser control unit. During pre-firing optical adjustments, the laser ran at a set internal frequency of 8.9 Hz. However, when a single laser pulse was to be synchronized with the gun firing, the one-shot circuit assumed control of the experiment. The following sequence of events describes the operation of the system.

---

* Normally the laser operates at a repetition rate of 10 Hz; however, due to aging of the power supply system it now takes longer to charge the capacitor bank when operating at full power thus we had to lower the repetition rate.

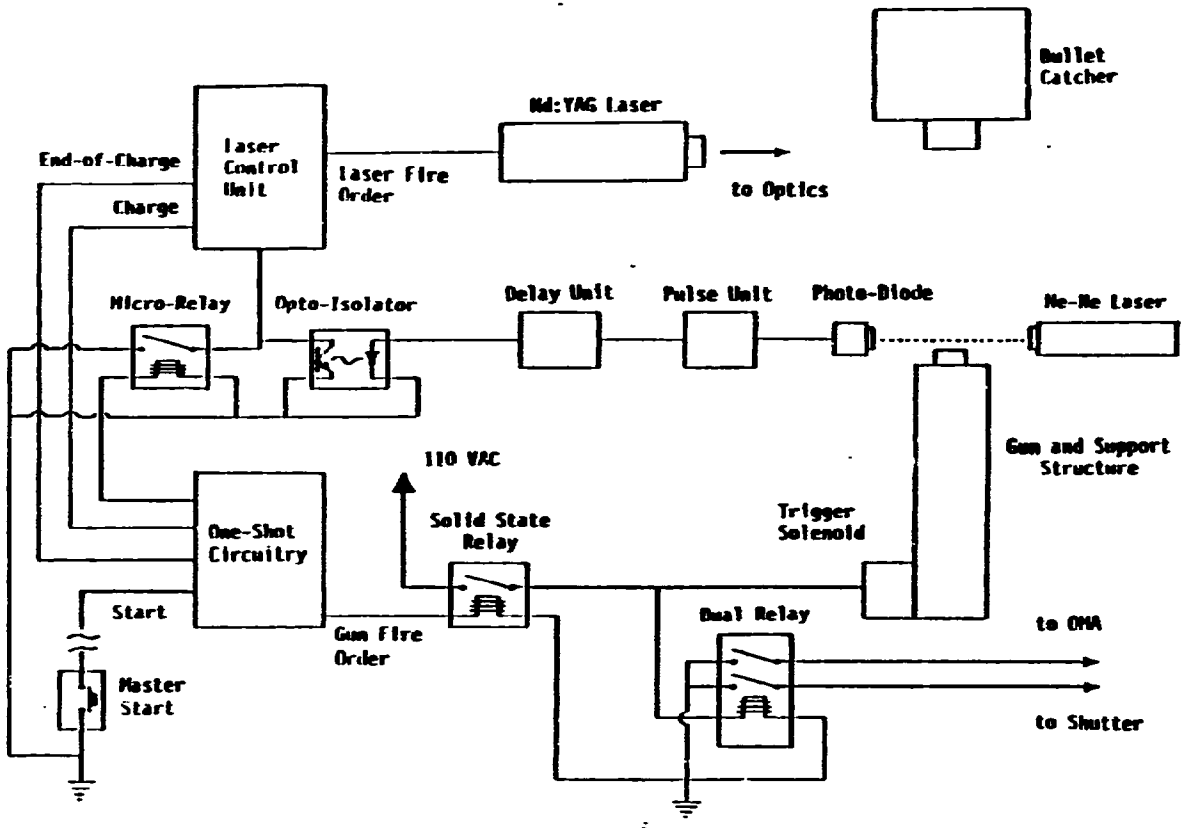

Figure 4. Timing diagram showing the method used to fire the laser at precise time delays after the bullet exit from the 7.62 mm rifle.

CARS signal generation was first optimized with the laser pulsing at 8.9 Hz. At the time the experiment was to be initiated the operator actuated a push button which signalled the one-shot circuit to assume control of the experiment on receipt of the next laser charge order. Upon receiving the order, the micro-relay (see Fig. 4) was de-energized thus inhibiting the laser from firing on its own. The reason for this is that when the micro-relay is closed, the rotary switch of the laser control unit was grounded thus allowing the end-of-charge order to trigger the laser. When the relay was open, the switch floated high preventing the end-of-charge from being acted upon. However, when this order was issued by the laser control unit, the one-shot circuit sensed its presence and issued a gun firing order by energizing the solid state relay, triggering the OMA, and opening the shutter. Approximately 20 ms later, the bullet emerged from the barrel interupting the He-Ne laser beam. The resulting output pulse from the photodetector through an appropriate delay triggered the laser by bringing the rotary switch on the laser control unit to near ground potential through the optical isolator. It should be noted that the logic for the one-shot circuit was built from CMOS chips operating on a 15 volt power supply. This choice was dictated by the requirements of extremely high noise immunity and compatibility with the logic of the laser control unit.

We should point out that the procedure described above triggers the flash lamps of the Nd:YAG laser. The actual lasing process occurs 200 microseconds later when the laser oscillator is Q-switched. Thus if data at times less than 200 microseconds

were required, then a modified triggering procedure would be needed. The data reported here, however, has been independently timed by monitoring a portion of the 532 nm radiation reflected from the blue glass filter. Thus the data recorded reflects the true time interval between the interuption of the He-Ne laser and the detected CARS signal. An upper limit of approximately 10 microseconds is the associated overall jitter that exists for the timing system used.

The characteristic times of the experiment include those associated with the data acquisition system and the muzzle flow field. The laser system operated at a free running time-between-pulses of 115 ms (8.9Hz). From when the trigger solenoid was energized to when a bullet emerged from the barrel was about 20 ms. The muzzle flow field developed on time scales of the order of 5 ms while the primary and intermediate flashes occurred in the first millisecond after the bullet leaves the barrel. Through the use of the variable delay unit that transmitted the laser fire order to the opto-isolator, the data acquisition time could be varied from near zero (time bullet uncorks) to beyond 10 ms. Thus the laser timing allowed virtually all times of interest in the developing muzzle flow field to be studied.

RESULTS AND DIS CUSSION

Our studies began by measuring the light emission primarily secondary flash, with a photodiode when firing into ambient air. Fig. 5 displays the temporal profiles of the light observed 18 cm downstream of the muzzle exit for four shots. These dual oscilloscope traces were trigger ed by the breaking of a He-Ne

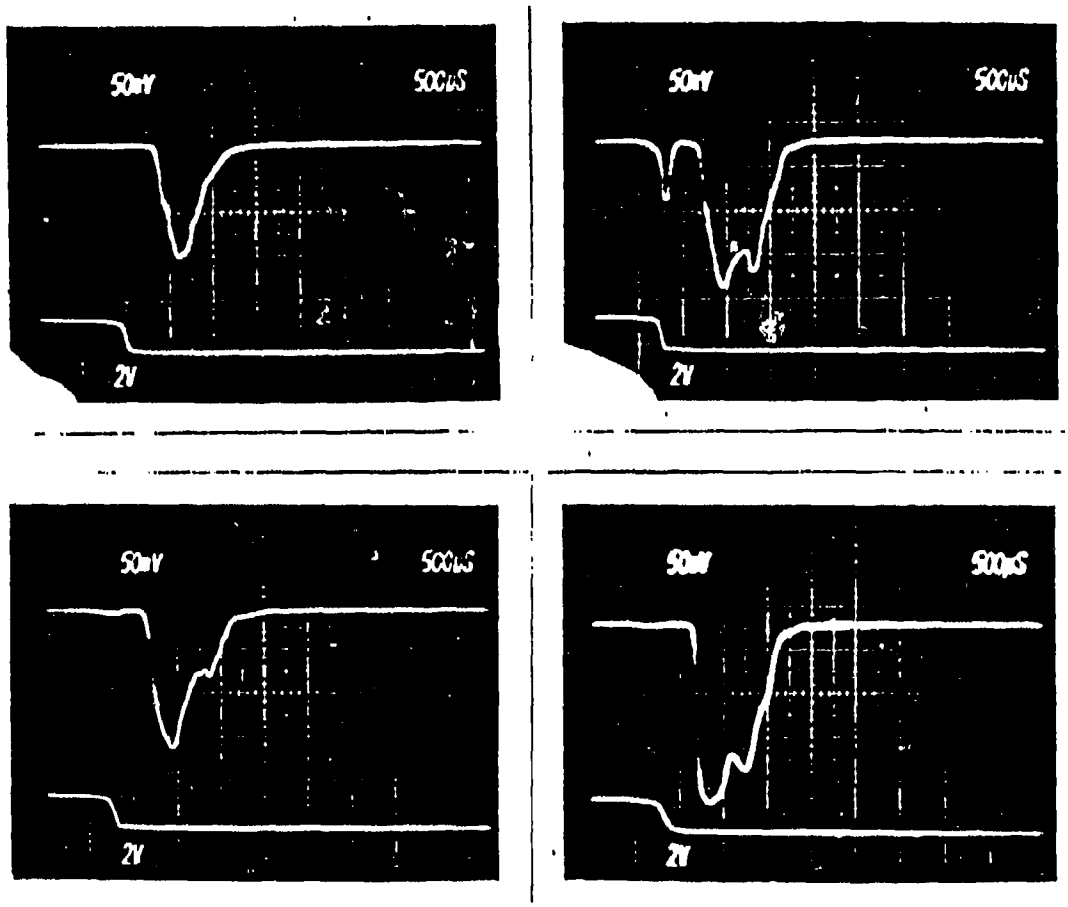

Figure 5. Light emission from the muzzle flash of a 7.62 mm rifle using standard ball ammunition. The measurement point is 18 cm downstream of the muzzle exit. The horizontal time scale is 500 microseconds per division and the vertical scale is intensity in arbitrary units. All four shots are taken under identical conditions.

laser beam positioned at the muzzle exit. The bottom traces represent the detected He-Ne laser light where the high value indicates total blockage of the beam and the low value full transmission. The top traces are the muzzle flash light emission. Light emission begins about 1.2 ms after bullet exit and lasts for about 1 ms however; as can readily be observed, there is substantial shot to shot variations. This variation is indicative of the irreproducible turbulent nature of secondary flash which becomes problematic in that we can only obtain a single CARS data point per rifle shot. To properly assess the data in this region it is necessary to construct a probability distribution function which would be extremely time consuming. Since the intermediate flash is less turbulent and current ideas[13] suggest it is the controlling region, in the context of muzzle flash suppression, we decided to begin the measurements here.

Purging the metal box shown on Fig. 1 with nitrogen suppressed the secondary flash as is demonstrated by Fig. 6. The photograph was taken under self light conditions as the rifle fired into a nitrogen atmosphere. Here, only the primary and intermediate flashes appear together with the gas dynamic processes associated with them

It was deemed desirable to verify the CARS experimental technique and CO temperature analysis prior to making any muzzle flash temperature measurements. From previous results a temperature around 1900K[2] and a CO concentration around 40%[9] was expected in the intermediate flash region of the M-14 rifle. To obtain steady state conditions similar to these parameters a rich CO/O2 mixture (ϕ = 2.93) was burned on a flat flame burner and

Figure 6. Self-light photograph of the primary and intermediate flash. The distance from the primary to intermediate flash is about 10 cm.

probed initially by a spontaneous Raman technique described elsewhere.[14] By fitting the Stokes Q-branch Raman spectrum for CO a temperature of 1785K with an estimated total error of ±4% was obtained. Using this temperature in the NASA-Lewis[15] thermochemical equilibrium calculation results in a value of 0.65 for the mole fraction of CO present in the burnt gas region of this flame. Next the CARS apparatus was used to obtain spectra for CO employing the same burner with identical flame conditions. The measurement point for both techniques was 5 mm above the burner surface on center. Q-branch CARS spectra for CO obtained from this flame are on Figs. 7 and 8. An accumulation of 50 laser shots produced the spectrum of Fig. 7 while Fig. 8 resulted from a single laser shot. The reason for comparing single and multiple shot spectra is to find out if there are any fluctuations in the CARS signal that wash out when multiple spectra are summed. Comparing Fig. 7 with Fig. 8 and also other single shot spectra (not shown) it was concluded that fluctuations would be a negligible effect. The squares represent the data points and the line is a least squares fit to the data. More information on the CARS equations and the least squares fitting procedure is given elsewhere.[16,17] The results of the fits show there is excellent agreement between single and multiple shot data; moreover, the temperatures obtained from the Raman technique agree, within experimental error, with those obtained by CARS.

Having satisfied ourselves that the CARS technique was behaving properly we next recorded CARS spectra of CO in the intermediate muzzle flash region. Figs. 9 and 10 display two

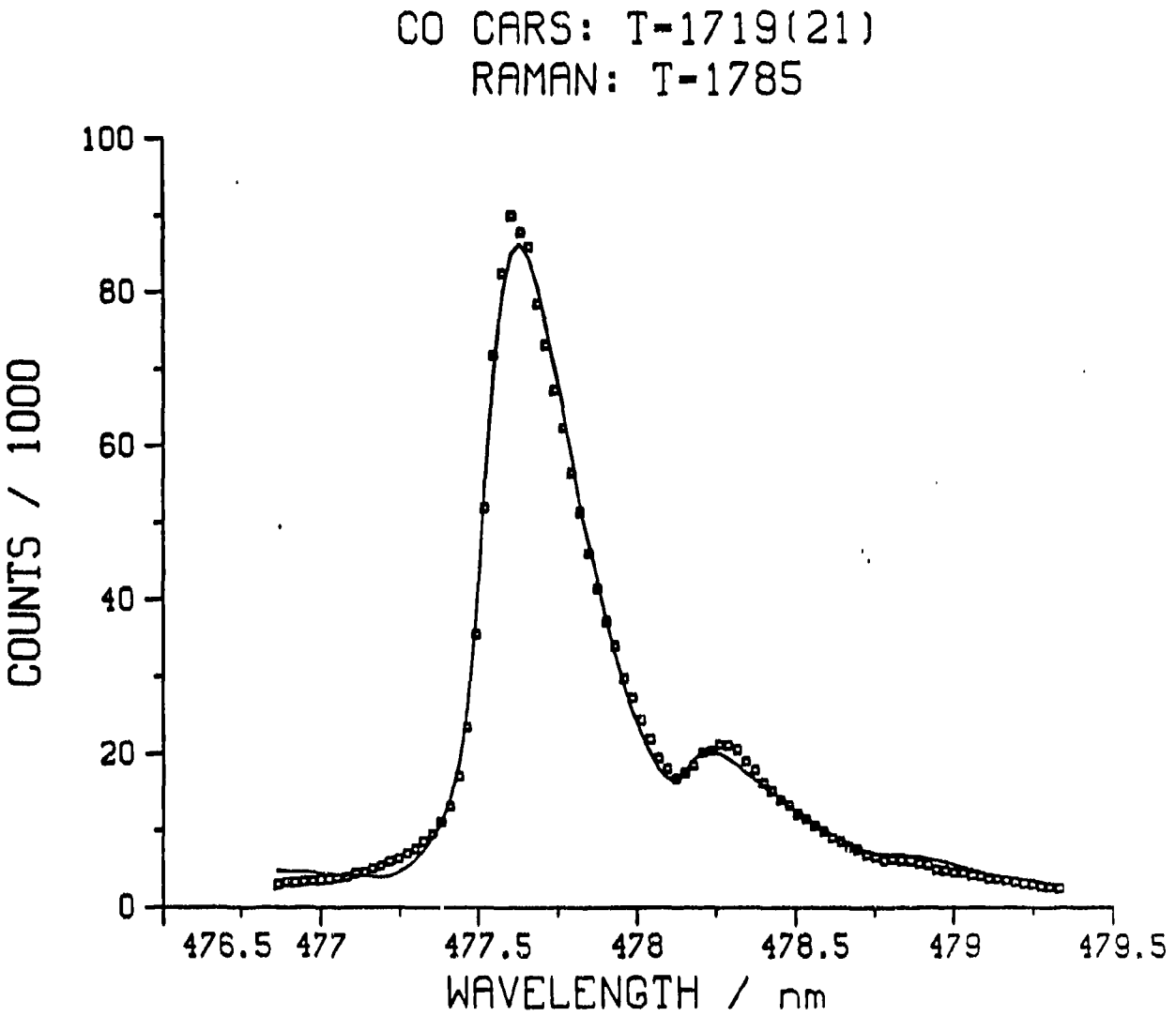

Figure 7. CO CARS spectrum in a rich premixed CO/O2 laminar flame. An accumulation of 50 laser shots.

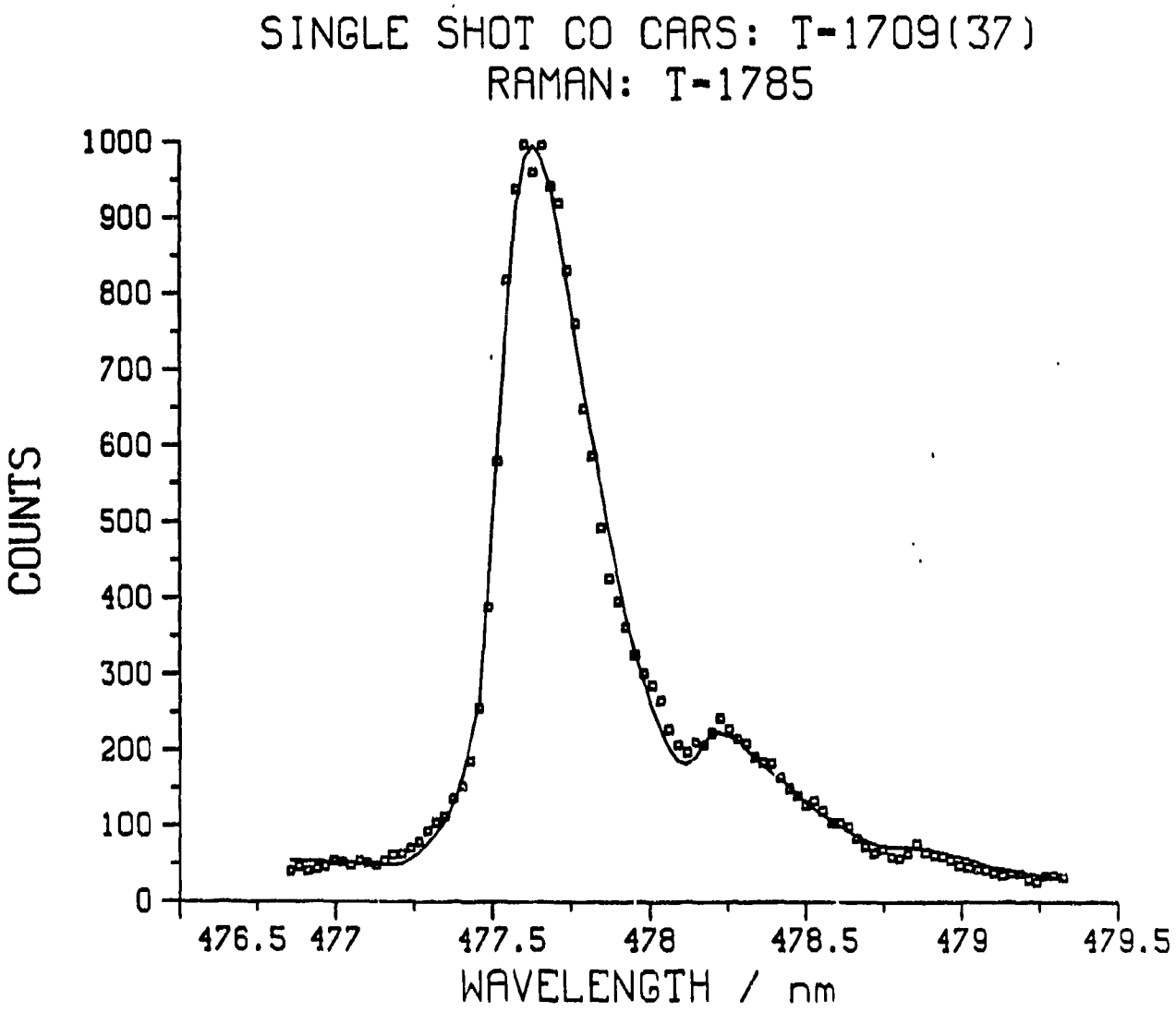

Figure 8. Same as Fig. 7 except here only a single laser shot is accumulated.

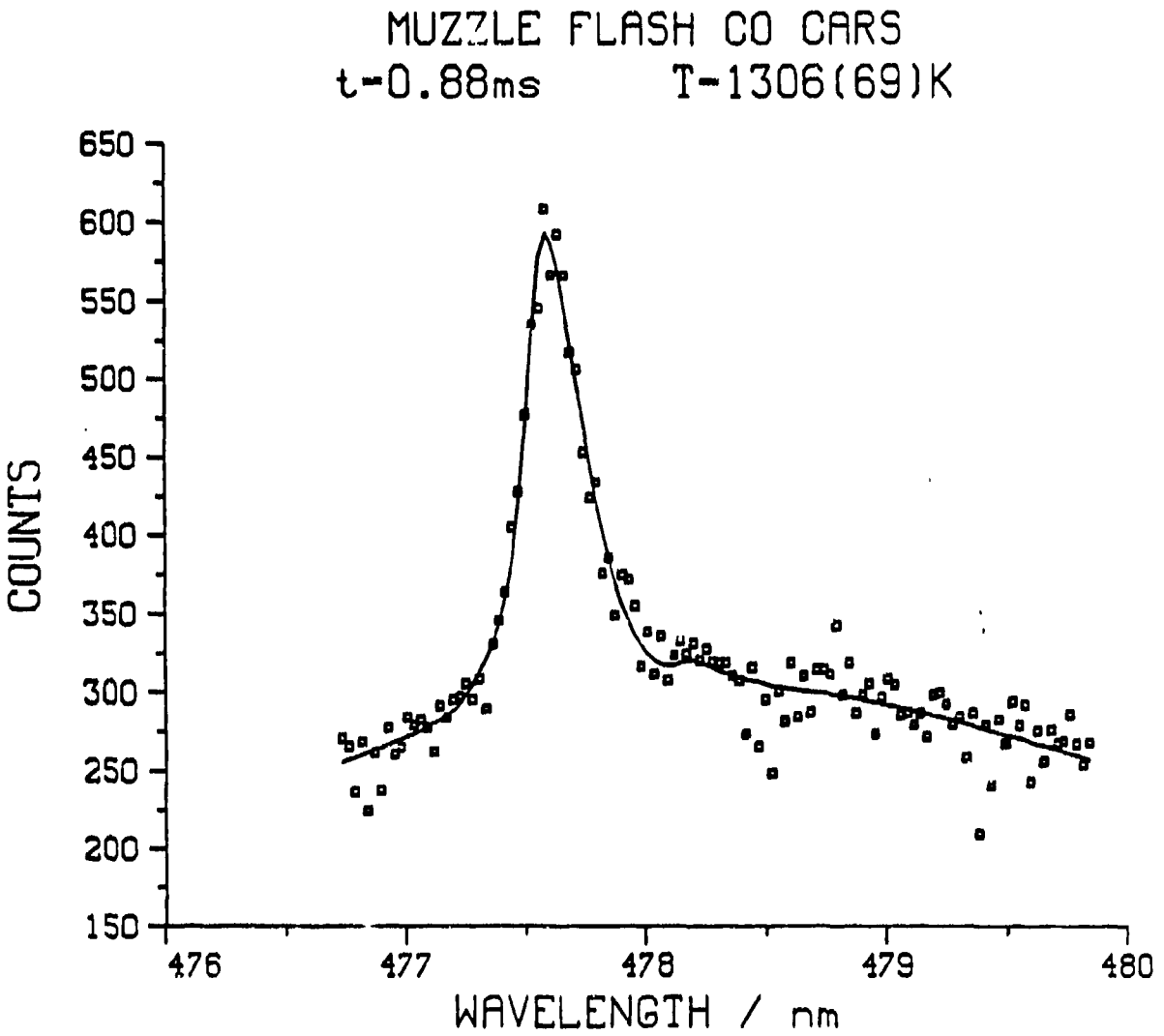

Figure 9. CO CARS spectrum in the intermediate flash region of a 7.62 mm rifle fired into a nitrogen atmosphere. The measurement position is 12.5 cm downstream of the barrel exit 0.88ms after the bullet exit.

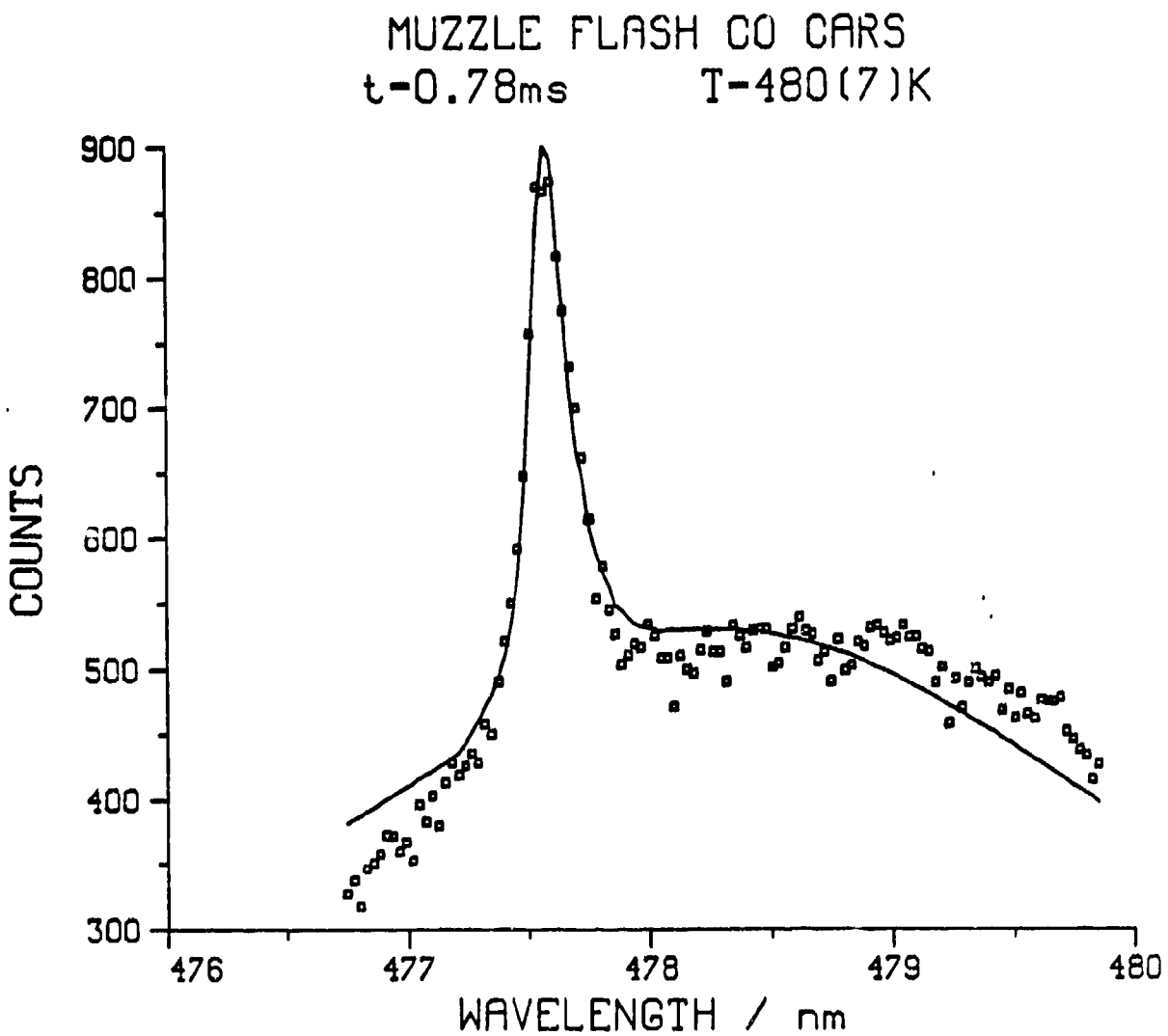

Figure 10. Same as Fig.9 except the time is 0.78 ms after bullet exit.

such spectra for a downstream position of 12.5 cm past the end of the barrel on centerline. Both spectra are taken at similar times after the bullet exit (0.88 and 0.78 ms) nonet heless the temperatures obtained from the fits are drastically different (1306 and 480K) and lower than what was expected. Other muzzle flash spectra (not shown) have also been obtained at various times between 0.6 and 3.0 ms after bullet exit and these too appear to be cold. That is , there is no indication of a hot band occurring as one can readily observe for the flame spectra of Figs. 7 and 8. In order to obtain a rough idea of what the temperature is in the intermediate flash region of our system some emission spectroscopy was performed. An intermediate flash emission spectrum is shown on Fig.11. This spectrum is pieced together from shots taken for different monochromator settings since the monochromator-reticon system could only capture a fraction of the spectral region on any one shot. The only emission comes from blackbody and sodium line emission. Using Wien's radiation law a temperature of 1700±200K is obtained as a rough estimate of the intermediate flash characteristic temperature. This temperature is in line with previous studies and indicates problems with the CARS measurements.

While the experiment was set up for emission studies an emission spectrum for the secondary flash was obtained and is shown on Fig. 12. Here the measurement position was 40 cm downstream of the barrel exit. The firings took place in ambient air. Again the spectrum is pieced together and a resulting rough estimate of temperature in this region is 2200±400K from Wien's radiation law. In addition to the blackbody emission there

are

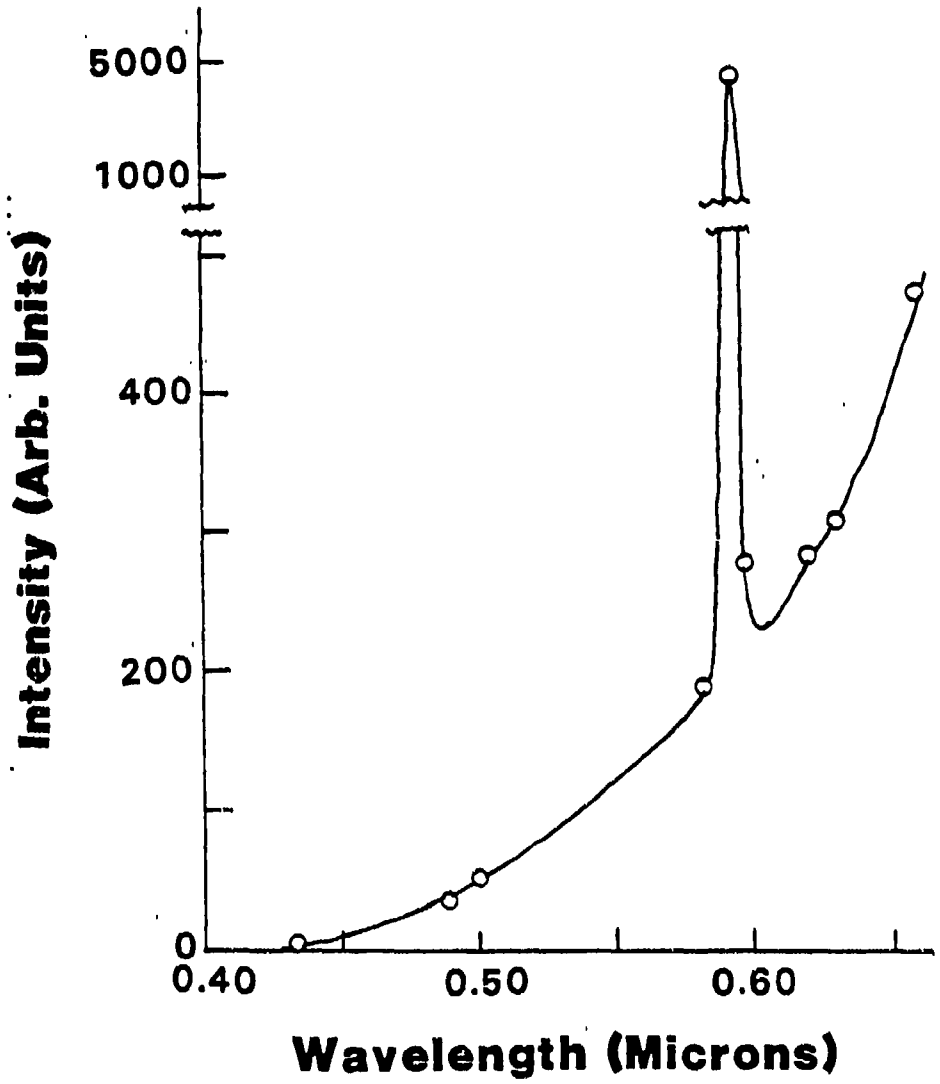

Figure 11. The time integrated emission spectrum of the intermediate flash region obtained by firing into a nitrogen atmosphere. The measurement position was 12.5 cm downstream of the barrel exit.

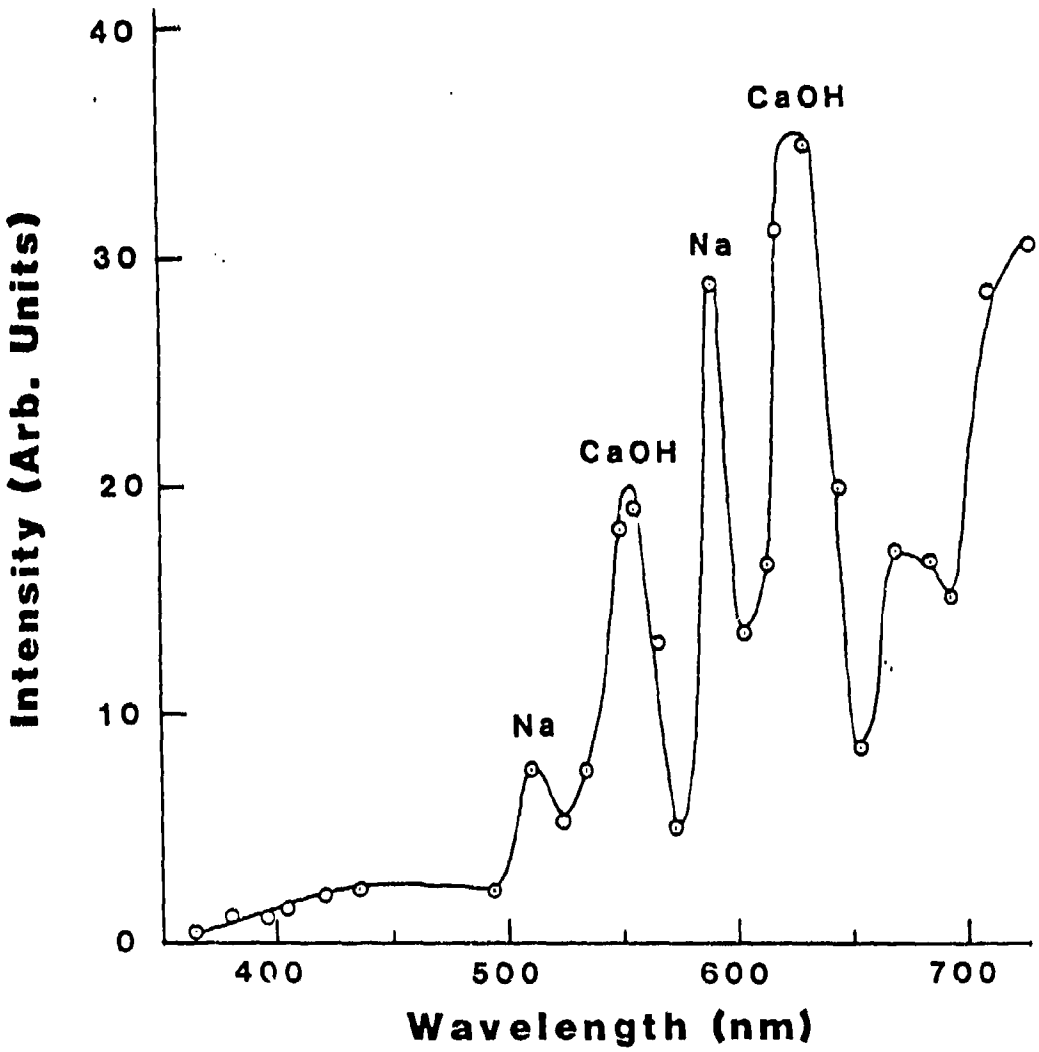

Figure 12. The time integrated emission spectrum of secondary flash obtained by firing into ambient air. The measurement position was 40 cm downstreamof the barrel exit.

line emission peaks from sodium and calcium hydroxide.

Now that we are fairly certain that the temperature in the intermediate flash region is substantially higher than the CARS data indicates an explanation for this difference must be addressed. The intensity of the CARS signal for muzzle flash is noticed to be much less than for the single shot flame data and is less than intuitively expected. From this observation it was thought that beam steering might be causing the CARS signal to appear outside the acceptance angle of the entrance slit of the monochromator. To test this hypothesis light transmission experiments were performed and the data is shown on Fig. 13. For these tests several monochromator entrance slits were used as apertures and mounted in both horizontal and vertical orientations. As for the CARS measurements, a downstream position of 12.5 cm was chosen for study and the He-Ne laser light transmission as a function of time and aperture size recorded. For all cases (a - d) there is maximum transmission at t = 0 and the light is essentially blocked or steered completely off the photodiode at 0.17 ms. A shadowgraph of the flow field taken at 0.25 ms after bullet exit, shown on Fig. 14, helps to understand what is happening in Fig. 13. From Fig. 14 it is evident that the blockage and steering of the He-Ne laser beam occurring from 0.17 to 0.35 ms is caused by the precursor blast wave and the passage of the bullet. When the 300 micron slit is used another loss of He-Ne light signal due to beam steering occurs around 0.43 ms. This time corresponds to the passage of the inner shock disk. When the 100 micron slit is used much more loss of He-Ne signal is

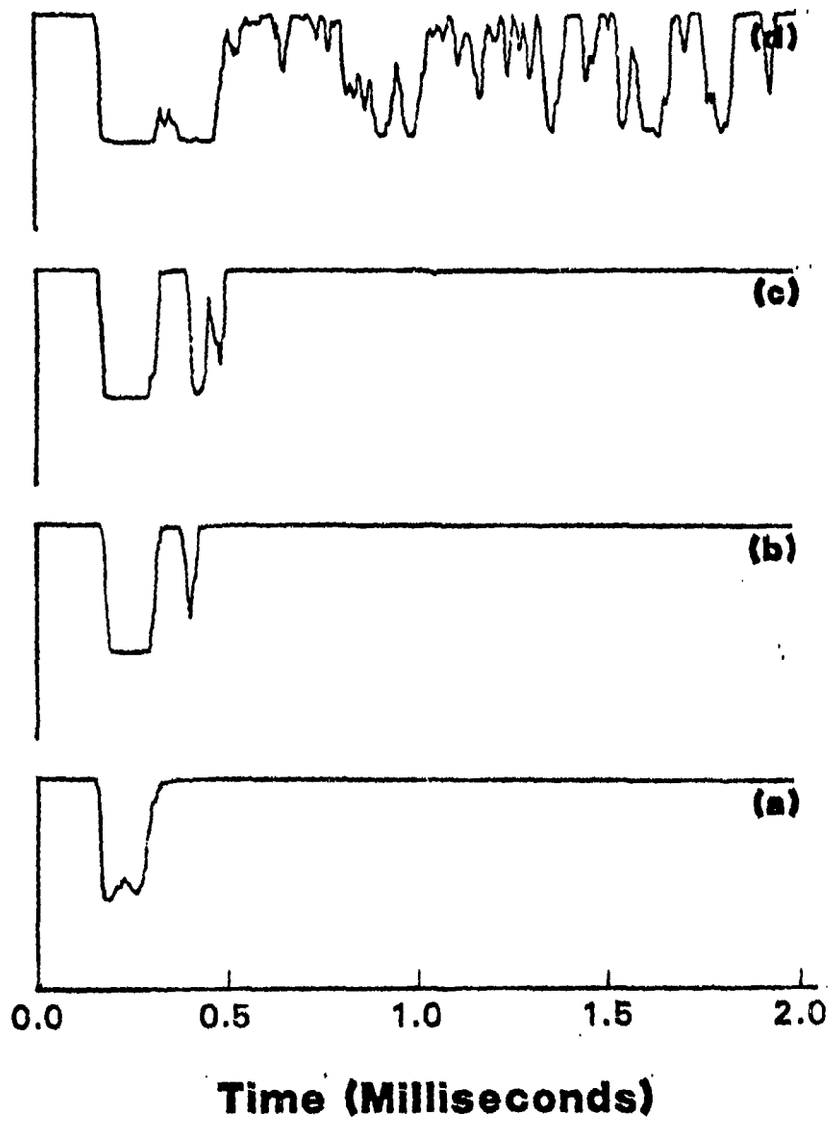

Figure 13. He-Ne laser light transmission as a function of time after bullet exit. The measurement position was 12.5 cm downstream of the barrel exit; a - no aperture b - 300 micron slit oriented horizontal, c - 300 micron slit oriented vertical and d - 100 micron slit oriented vertical.

Figure 14. Shadowgraph of the muzzle flow field 0.25 ms after bullet exit.

observed and is present for most times of interest. This test was repeated at a downstream location of 24.5 cm to see if the effect would be diminished due to expansion. The results are displayed on Fig. 15. Being further downstream the bullet alone causes the initial loss of signal at around 0.35 ms then the blast wave results in signal loss after about 0.55 ms. The situation appears worse here than at the 12.5 cm location. It should be pointed out that at the 24.5 cm position the firing took place in ambient air rather than a nitrogen atmosphere and this allowed secondary flash to occur. This secondary flash provides more temperature gradients and turbulence which can add to the steering effects.

These apertured light transmission studies explain why a weak CO CARS signal is observed when using 100 micron entrance slits and also suggest a reason why low aporadic temperatures are obtained. Beam steering occurs upon passage of a light beam through non-perpendicular index of refraction gradients which are present in the muzzle flow field. The amount of steering is dependent on wavelength and CARS is generated by light beams of substantially different wavelength. A wavelength dependent steering effect can result in the CARS beams not being overlapped at the position of interest and thus different CO temperatures are then possible.

CONCLUSION

The study of muzzle flash is a difficult task due to the presence of high luminosity, high particulate loadings and extreme density and temperature changes. These effects cause index of refraction gradients in the muzzle flow field which provides a mechanism for wavelength dependent beam steering. This mech-

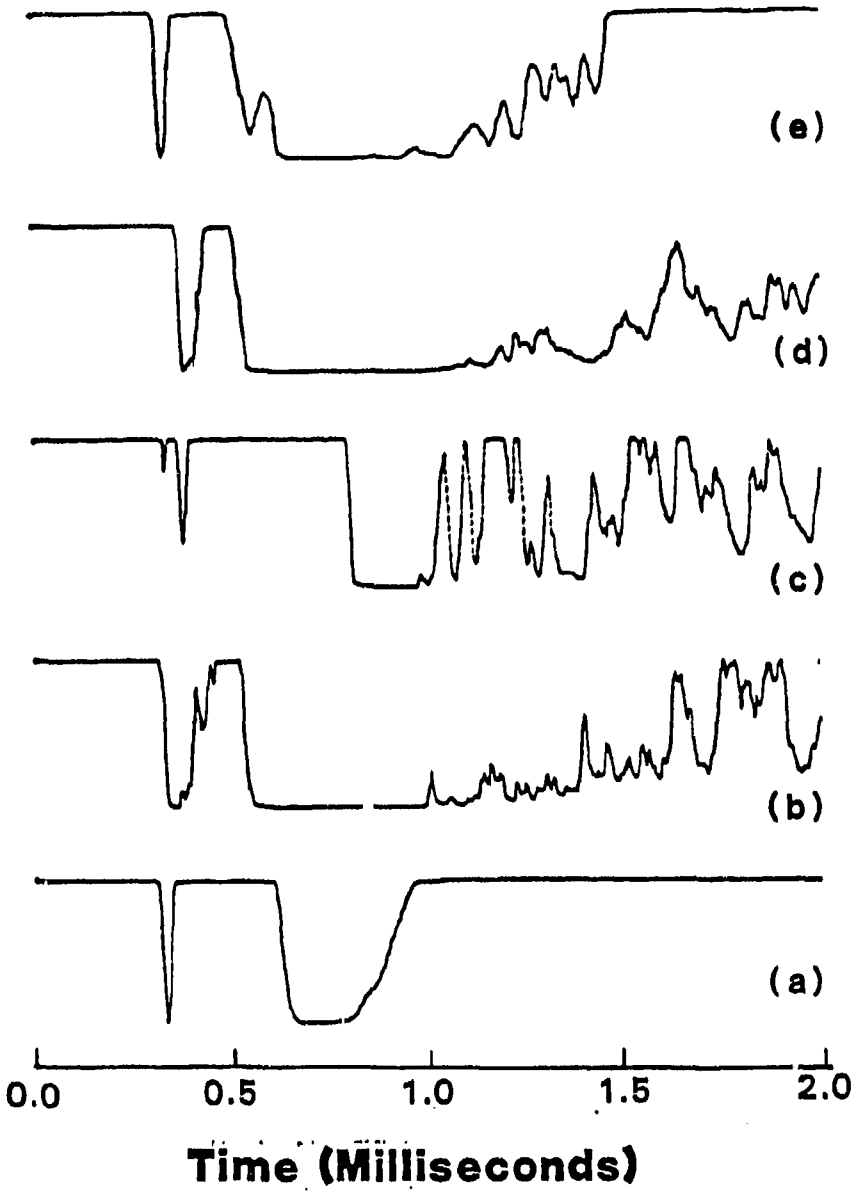

Figure 15. He-Ne laser light transmission as a function of time after bullet exit. The measurement position was 24.5 cm downstream of the barrel exit; a - no aperture, b - 50 micron x 50 micron square aperture, c - 100 micron x 100 micron square aperture, d - 200 micron x 200 micron square aperture and e - 300 micron slit oriented horizontal.

anism makes CARS unattractive as a simple , reliable technique for muzzle flash studies. Furthermore scaling up to larger guns will magnify the problem because of longer required distances between the interaction region and detector.

REFERENCES

1. R. Ladenburg, "Studies of the Muzzle Flash and Its Suppression", BRL Report No. 618, Aberdeen Proving Ground, MD, 1947.

2. G. Klingenberg and H. Mach, "Investigation of Combustion Phenomena Associated with the Flow of Hot Propellant Gases. I: Spectroscopic Temperature Measurements Inside the Muzzle Flash of a Rifle", Combustion and Flame, Vol. 27, p. 163, 1976.

3. E.M. Schmidt, "Secondary Combustion in Gun Exhaust Flows", BRL Report No. ARBRL-TR-02373, Aberdeen Proving Ground, MD, 1981.

4. Engineering Design Handbook, Spectral Characteristics of Muzzle Flash", AMCP 706-255, US Army Materiel Command, June 1967.

5. T. Mitani and T. Niiona, "Extinction Phenomenon of Premixed Flames with Alkali Metal Compounds", Combustion and Flame, Vol. 55, p. 13, 1984.

6. W.D. Williams and H.M. Powell, "Laser Raman Measurements in the Muzzle Blast Region of a 20 mm Cannon", Arnold Engineering Development Center Report, AEDC-TR-79-72, AD-A088729, August 1980.

7. S. Lederman, R. Cresci, and T. Posillico, "Diagnostics of Gun Barrel Propellants", Ballistic Research Laboratory Contract Report ARBRL-CR-00519, November 1983.

8. E.D. Petrow and L.E. Harris, "CARS Spectra from a 7.62 mm Gun", Large Caliber Weapons Systems Laboratory, Dover, NJ, Technical Report ARLCD-TR-84003, March 1984.

9. G. Klingenberg and J.M. Heimerl, "Investigation of Gun Muzzle Exhaust Flow and Muzzle Flash", Fraunhofer-Institut fur Kurzzeitdynamik, EMI-AFB Report 1/82, 1982.

10. G. Klingenberg, "Investigation of Combustion Phenomena Associated with the Flow of Hot Propellant Gases. II. Experimental Survey of the Formation and Decay of Muzzle Flow Fields and of Pressure Measurements", Combustion and Flame, Vol. 29, p. 289, 1977.

11. M.L. Bundy and E.M. Schmidt, "Muzzle Exhaust Flow Through a Circular Channel", BRL Report ARBRL-MR-03340, Aberdeen Proving Ground, MD, March 1984.

12. A.C. Eckbreth and R.J. Hall, "CARS Concentration Sensitivity With and Without Nonresonant Background Suppression", Combustion and Flame, Vol. 25, p. 175, 1981.

13. J.M. Heimerl, G.E. Keller, and G. Klingenberg, "Muzzle Flash Kinetics and Modeling", Fraunhofer-Institut fur Kurzzeitdynamik, EMI-AFB Report 1/85, 1985.

14. J.A. Vanderhoff, W.R. Anderson, A.J. Kotlar, and R.A. Beyer, "Raman and Fluorescence Spectroscopy in a Methane-Nitrous Oxide Laminar Flame", Proceedings, 20th International Symposium on Combustion, The Combustion Institute, p. 1299, 1984.

15. R.A. Svehla and B.J. McBride, "FORTRAN IV Computer Program for Calculation of Thermodynamic and Transport Properties of Complex Chemical Systems", NASA, TND-7056, 1973.

16. A.J. Kotlar and J.A. Vanderhoff, "A Model for the Interpretation of CARS Experimental Profiles", Applied Spectroscopy, Vol. 36, p. 421, 1982.

17. J.A. Vanderhoff and A.J. Kotlar, "Application of CARS to Obtain Temperature in Flame Environments", BRL Report No. ARBRL-TR-02417, Aberdeen Proving Ground, MD, August 1982.

ARDEC Laboratory Flash Studies

J.K. Salo and A.J. Bracuti
Army Research, Development and Engineering Center
Dover, New Jersey 07801-5001

Abstract

Flash intensity measurements had been made of several alkali and non-alkali salt additives to determine their efficacy as potential flash suppressants. The results of these experiments showed that ammonium bicarbonate and potassium bicarbonate were among the most effect flash reducers. Therefore, additional laboratory scale firings were made to test these salts vs K_2SO_4, the standard additive. The results of these tests showed NH_4HCO_3 to be better than $KHCO_3$ or K_2SO_4. A simplified computer simulation of each of these firings was used to determine the point in the combustion gas flow when the salt vaporized and reacted. These simulations suggested that flash suppressants reacted with the combustion gases outside the gun.

Experimental

Laboratory test firings were conducted in the ARDEC erosion tester which is a modified 200 cm^3 closed bomb vented with a 22.86 cm (9.0 in) barrel having a 0.95 cm (0.375 in) bore (Fig. 1). This shortened barrel modification was used to insure that secondary flash would occur every time unsuppressed propellant was fired [1]. A pressure transducer positioned inside the 200 cm^3 chamber was calibrated to display pressure versus time. To control pressure, a rupture disc was inserted between the barrel and the chamber.

Secondary muzzle flash was measured with a silicon diode detector which reproduced the spectral response of the human eye. These spectra traces revealed flash onset time; peak intensity; integrated intensity; and, termination time. Typical traces for flash suppressed and unsuppressed propelling charges are presented in Figure 2.

All propelling charges were fabricated by sealing the propellant in polyethylene bags. To best emulate an artillery propelling charge, 50g of M30 (Table 1) triple base propellant was used. (Radford Lot No. 69531). This loading density (0.25 g/cm) was selected to maintain an average peak pressure of 172 MPa (25,000 psi). In order to compare the various flash suppressants, 8% by weight (4g) of the additive was placed in front of each of the bagged propelling charges [1].

To simulate mortar-like propelling charges, M10 (Table 2) and ball powder (Table 3) propellants were sealed in polyethylene bags [2]. In the first case, 20g of M10 flake propellant (Radford No. 89233) was placed in polyethylene bags (0.10 g/cm^3 loading density) to achieve an average peak pressure of 58 MPa (8400 psi). In the second case, two sets of propelling charges were fabricated. In one set each charge contained 22g (loading density 0.11 g/cm^3) of ball powder (Olin Lot No. 3640.5) which yielded a peak pressure of 58 MPa, while in the other set each charge contained 28g of ball powder (loading density 0.14 g/cm^3) in order to achieve a peak pressure of 85 MPa. Flash suppressants were mixed with the propellant inside the polyethylene bag in concentration of 4% and 8% by weight. The candidate flash suppressants for these tests were potassium bicarbonate ($KHCO_3$) and ammonium bicarbonate (NH_4HCO_3). Relative intensity values were obtained by normalizing with flash intensity values obtained from unsuppressed propelling charges.

Results

The alkali and non-alkali candidate flash suppressants which were tested with M30 propellant gave the following results:

Suppressant	Flash	Smoke
None	100	Yes
KN_3	32	Yes
K_2SO_4	80	Yes
K_2CO_3	46	Yes
$KHCO_3$	1	Yes
KNO_3	46	Yes
KOX	3	Yes
OXA	25	No
Slurper	20	No
$(NH_4)_2CO_3$	17	No
NH_4HCO_3	11	No
NH_4NO_3	43	No
$(NH_4)_2SO_4$	34	No
TAG Cl	100	Yes
TAG NO_3	100	No
TAG PIC	100	No
GAC	100	No
Oxamide	87	No

The results of the firings with the M10 propellant and Ball Powder are given below:

20g M10 at 58 MPa

Additive Wt., g			Intensity	
NH_4HCO_3	$KHCO_3$	K_2SO_4	I	I_{rel}
---	---	---	196 ± 27	1.00
1.6	---	---	40 ± 13	0.20
---	1.6	---	113 ± 30	0.58
---	---	1.6	96 ± 18	0.50
0.8	---	---	74 ± 17	0.38

22g Ball Powder at 58 MPa

Additive Wt., g			Intensity	
NH_4HCO_3	$KHCO_3$	K_2SO_4	I	I_{rel}
----	----	----	146 ± 35	1.00
1.76	----	----	21 ± 12	0.14
----	1.76	----	89 ± 29	0.61
----	----	1.76	73 ± 23	0.50

28g Ball Powder at 85 MPa

Additive Wt., g			Intensity	
NH_4HCO_3	$KHCO_3$	K_2SO_4	I	I_{rel}
----	----	----	285 ± 33	1.00
2.24	----	----	97 ± 28	0.34
----	2.24	----	205 ± 30	0.72
----	----	2.24	296 ± 34	1.04
1.12	----	----	160 ± 24	0.56
----	1.12	----	240 ± 31	0.86

Simulation

The experimental firings of M30 propellant* and the additive NH_4HCO_3, $KHCO_3$ and K_2SO_4 were simulated with the use of interior ballistic [3] and thermochemical computer codes[4,5]. The temperatures of the theoretical combustion gases were traced from ignition in the chamber to their reactions with oxygen in the atmosphere. All simulations ignored shock heating effects. Each firing was simulated in two ways. The first simulation assumed the additive salt vaporized and reacted with the propellant in the chamber, while the second simulation assumed the salt vaporized and reacted with the expanded product gases in the atmosphere.

The firing was first simulated in the Baer-Frankle interior ballistic code, where the projectile weight was that of the rupture disc and the resistance

*M10 firings are currently being simulated

at shot start was the pressure at which the disc ruptures. The thermochemical properties of the M30 propellant and those with 8% salt added were calculated from the Blake code. From the resulting muzzle temperature and pressure it was possible to calculate the temperature and gas composition when expanded isentropically to 1/2 atmosphere. The combustion of these gases when reacted with O_2 then give the flash temperature at one atmosphere. The second type simulation used the muzzle conditions of the M30 propellant alone and determined the flash temperature by reacting the salt with the combustion gases and oxygen at 1/2 atmosphere.

The results of these simulations are given below:

M30 + additive	Mechanism 1	Mechanism 2	I_{rel}
-------	2119	2119	100
NH_4HCO_3	2020	1813	11
$KHCO_3$	2106	1847	1
K_2SO_4	2129	1847	80

The results suggest that suppressant efficiency is minimized if the salt reacts with the combustion gases in the chamber and that the greatest benefit from a salt additive would occur if it reacts in the atmosphere.

Conclusions

From the experimental relative flash intensities of 11, 1, and 80 for NH_4HCO_3, $KHCO_3$, and K_2SO_4 respectively, it would appear as if most of the salt did react outside of the gun. This would account for the significant reduction in flash caused by the bicarbonates, but it would not, however, explain the higher flash intensity observed with K_2SO_4. Potassium sulfate has a boiling point of 1962°K, which is considerably higher than the 373° and 313°K for the ammonium and potassium bicarbonate salts. It is possible that in the 10msec the propellant burns in the bomb, the potassium sulfate does not completely vaporize to react with the combustion gases, while the bicarbonate salts will vaporize due to their considerably lower boiling points.

Table 1

M30 Composition and Physics-Chemico Properties

Component	Composition %
Nitrocellulose (12.6%)	28.00
Nitroglycerin	22.50
Nitroguanidine	47.70
Ethyl-Centralite	1.50
Graphite	.10
Cryolite	0.30
Ethanol (residual)	0.30
Water (residual)	0.00
Properties*	
$T_f(K^o)$	2990.
C_p J/mol-K^o	43.9
I^PJ/mol-K^o	1072.0
CO (mol/kg)	11.9
H_2	5.8
H_2O	10.4
N_2	11.9
CO_2	3.0
Total (Mol/kg)	43.1
M (g/g-mol)	22.3

*Calculated by Blake Thermodynamic Gun Code.

Table 2

M10 Propellant Composition and Physico-Chemico Properties at 0.10 g/cm^3 Loading Density

Component	Composition %
Nitrocellulose (13.15%N)	98.00
K_2SO_4	1.00
DPA	1.00
Properties*	
T_f (K^o)	3181
I (J/g)	1048
M_w (g/g-mol)	23.25
CO (Mole fraction)	0.42
H_2	0.09
H_2O	0.24
N_2	0.13
NO_2	0.14
OH	0.01

*Calculated with NASA-Lewis Thermochemical Code.

Table 3

Ball Powder Composition and Physico-Chemico Properties at 0.11 Loading Density

Component	Composition %
Nitrocellulose (13.15%N)	97.941
Nitroglycerin	0.501
DPA	1.005
KNO_3	0.050
DNT	0.201
DBP	0.301
Properties*	
T_f (K^o)	3184
I^f (J/g)	1062
M_w (g/g-mol)	24.93
CO (Mole fraction)	0.42
H_2	0.10
H_2O	0.23
N_2	0.12
CO_2	0.12

*Calculated by NASA-Lewis Thermochemical Code.

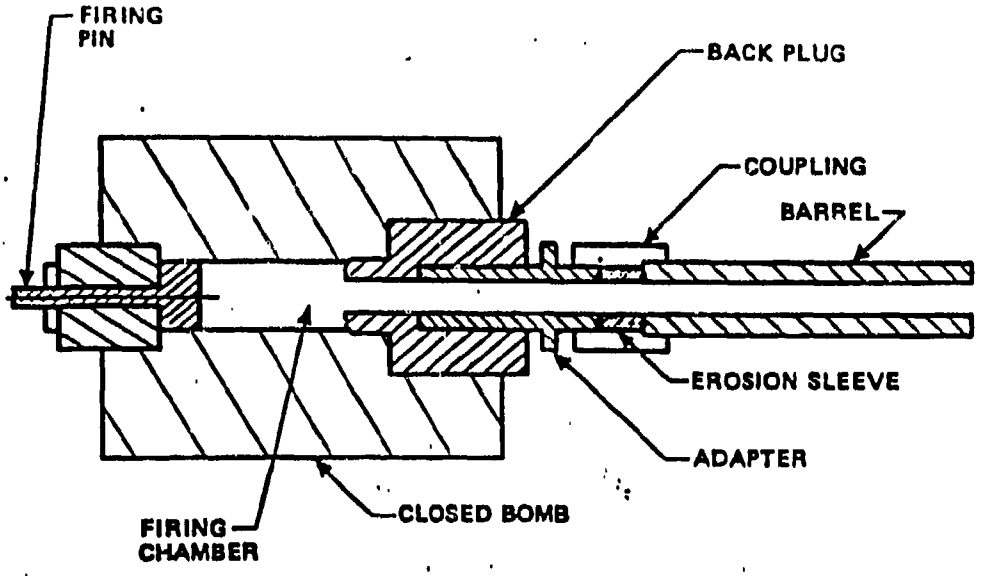

Figure 1: Sketch of Erosion/Flash Apparatus

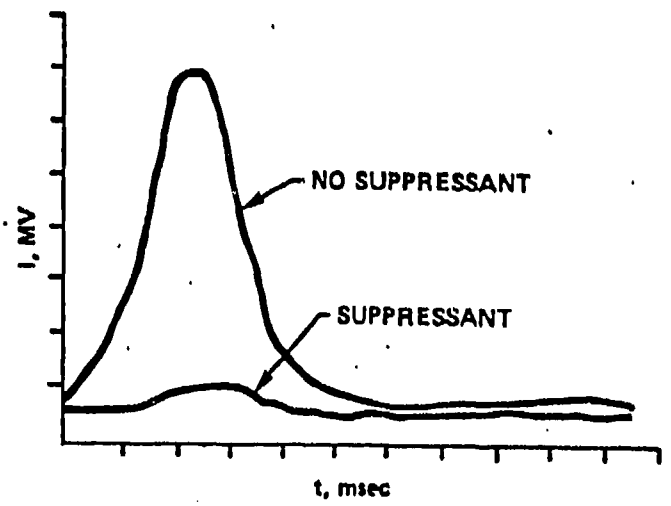

Figure 2: Light Intensity vs Time for Typical Unsuppressed and Flash Suppressed 50g M-30 Propelling Charges in ARDC Erosion Tester.

References

1. Bracuti, A.J., Bottei, L.A., and Davis, R., "Evaluation of Potential Multipurpose Propellant Additives: Flash-Erosion Suppressant", J. of Ballistics, Vol. 7, No. 1, pp 1609-1626, 1983.

2. Bracuti, A.J., and Bottei, L.A., "Multipurpose Additives - Wear and Erosion Reducers: Part II", Proceedings of 1985 JANNAF Propulsion Meeting, San Diego, Cal., in press.

3. Baer, P.G. and Frankle, J.M., Interior Ballistic High Velocity Guns (IBHVG) Computer Code.

4. Freedman, E., "A Brief User's Guide For the Blake Program", Interim Report No. 249, Ballistic Research Laboratories, Aberdeen Proving Ground, MD (1974).

5. Gordon, S. and McBride, B.J., "Computer Program for Calculation of Complex Equilibrium Compositions, Rocket Performance, Incident and Reflected Shockes, and Chapman Jouguet Detonations", NASA-Lewis Research Center, Interim Revision, March 1976.

AN OVERVIEW OF THE RARDE FACILITIES FOR GUN MUZZLE FLOW AND FLASH STUDIES

P S HENNING

ROYAL ARMAMENT RESEARCH AND DEVELOPMENT ESTABLISHMENT
FORT HALSTEAD
SEVENOAKS, KENT
ENGLAND

COPYRIGHT - CONTROLLER HMSO, LONDON 1986

INTRODUCTION

This paper reviews the equipment and instrumentation available at RARDE (Fort Halstead) for the study of gun in-bore and muzzle flows, blast and flash. So far the research programme of the Guns and Rockets Group at RARDE has been aimed at developing theoretical and experimental tools for the analysis of the unsteady flows of the propellant gases. The problems of secondary flash and its suppression by chemical means has not as yet been specifically addressed. However in the near future initial studies on the behaviour of chemical flash suppressants are proposed.

The main experimental facilities reviewed in this paper are:

a) High Enthalpy Blast Simulator (HEBSIM)

b) Ballistic Simulator with specialist instrumentation.

c) Laser Doppler Anemometor

HIGH ENTHALPY BLAST SIMULATOR

Figure 1 is a schematic representation of the RARDE High Enthalpy Blast Simulator (HEBSIM) which provides the opportunity for studying simulated muzzle flows under varying conditions with inert gases.

Figure 1

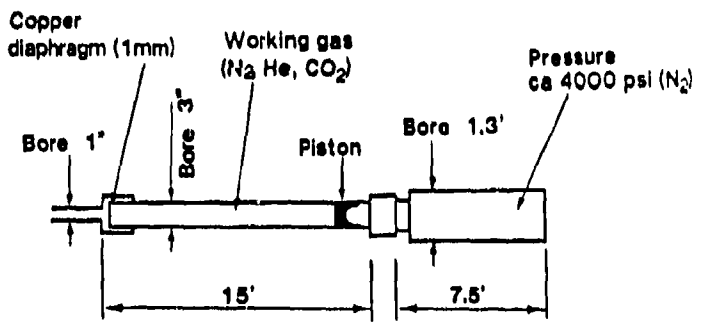

HIGH ENTHALPY BLAST SIMULATOR

The simulator breech chamber initially contains high pressure nitrogen gas separated from the

Figure 2

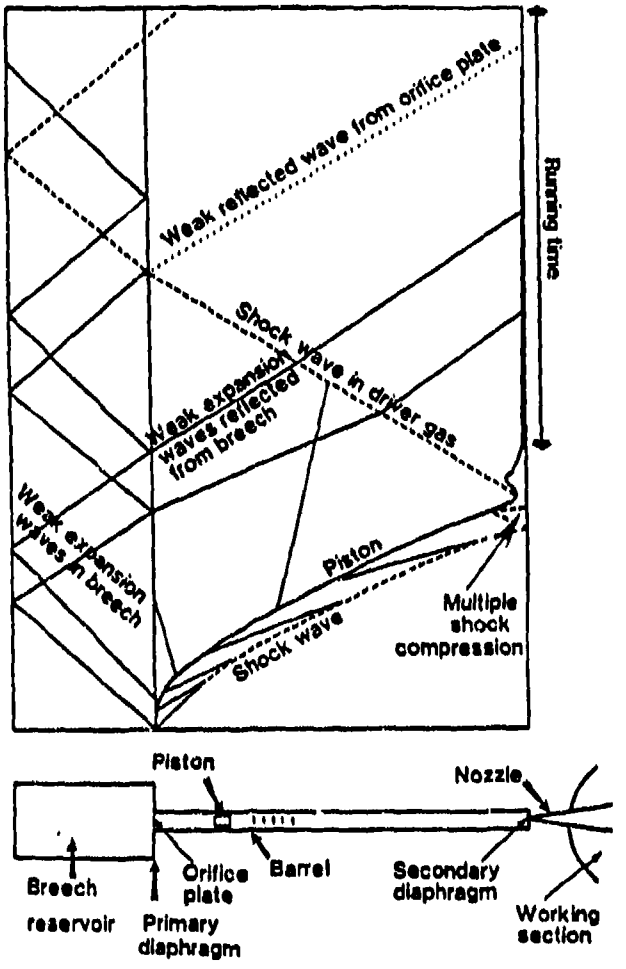

SCHEMATIC VIEW OF TUNNEL AND WAVE SYSTEM

drive piston by a double bursting diaphragm. During setting-up the pressure between the diaphragms is maintained at about 50% of the breech pressure to prevent diaphragm rupture. Upon dumping of the inter-diaphragm pressure, the two diaphragms rupture and the resulting gas flow drives the piston along the compressor chamber. Compression waves form ahead of the piston and coalesce to form a shock wave which compresses and heats the working gas. This shock wave is reflected from the closed end of the tube to produce a further increase in the temperature and pressure of the working gas. It is reflected again at the piston which is still moving forward. Several shock reflections take place as the piston rapidly decelerates. The piston mass is selected so that it does not overshoot and oscillate and thereby produce rarefaction and compression waves in the nozzle.

As the pressure in the compressor barrel builds up a point is reached at which the 1 mm copper diaphragm separating the working gas from the exit nozzle ruptures to develop a high enthalpy flow in the working section. A diagram of the wave trajectories is shown in figure 2.

The temperature generated in the working gas is a function of its initial pressure (see Table 1) At lower working gas pressures the temperature increases at the expense of the running time.

TABLE 1
HEBSIM OPERATING CONDITIONS
(Oxygen free nitrogen)

Breech Pressure	2,000 psi	4,000 psi
Barrel Pressure	100 psi	15 psi
Stagnation Pressure	1,700 psi	3,500 psi
Stagnation Temp.	500 K	1,500 K
Running time	ca 8 ms	> 1 ms

The current HEBSIM research programme can be divided into four main areas:

1) Blast Flows

The study of blast flows from guns and mortars and in particular the effect of reflection and confinement in enclosed spaces are being investigated. Here the detailed flow is being used in support of a computational model.

2) Muzzle Brakes

As an aid to muzzle brake development measurements of their efficiency, blade stresses and propagation of blast waves are being studied.

3) Suppression of Blast

Work on the suppression of blast is being undertaken by the Intermediate Ballistics Division of RARDE. Although the primary aim of this work is to reduce blast from 'LAW' type weapons, it is to be extended to include guns and mortars. The action of the suppressor reduces blast in two ways: First the reduction in the rate of release of energy in the form of high pressure gases directly reduces the level of blast. Secondly, the delay in releasing the high pressure gases causes a reduction in the temperature of the released gases (due to thermal losses in the suppressor).

Sabot Separation

The HEBSIM facility provides a visual support to the computational work on the reverse flow over and separation of sabots.

RARDE BALLISTIC SIMULATOR

Figure 3 is a schematic representation of the RARDE ballistic simulator or blow-out gun (Ref 1). The driver section is based on a 30 mm RARDEN gun charge which can generate up to 407 MPa in the high pressure drive chamber. The 21 mm diameter working tube section is stressed to a working pressure of 228 MPa. The working section consists of a series of connected 1 m lengths of tube. At each connection a smooth transition from one section to the next is provided by an adaptor which also contains

provision for instrumentation. The vessel has been designed to accept a range of charge loadings and the following charge configuration:

Figure 3

BALLISTIC SIMULATOR

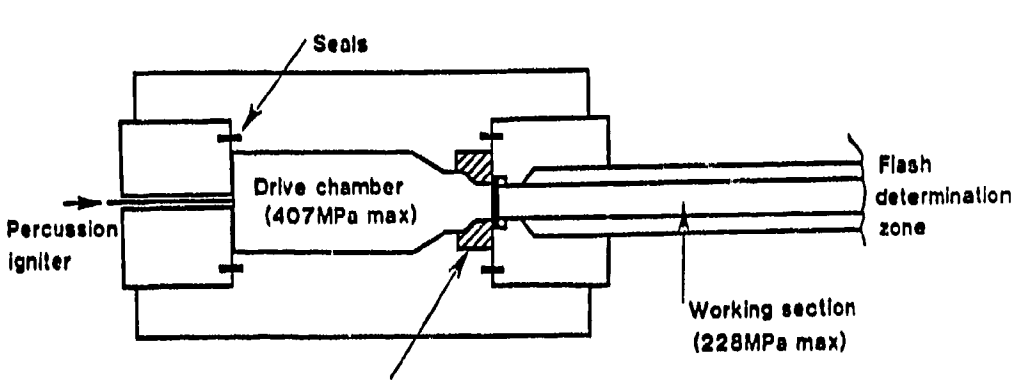

1) Brass Cased

The vessel can accept propellant contained in a conventional 30 mm brass RARDEN case. The projectile is not included and the case is capped with a consumable disc. The RARDEN case contains a percussion primer which is used for the initiation. In this mode the effect of wear/flash reducing additives to the charge can be studied.

2) Stub Case

In order to study the effect of wear/flash reducing additives when added to the combustible cartridge case material, a stub cased RARDEN ammunition with a combustible forward end can also be fired. Again the ammunition does not have a projectile and is percussion fired.

3) Bulk Loaded

In addition to case obturation as used in 1 and 2 above, the vessel has provision for obturation sealing rings and can therefore be fired using non-cased propellant. With this option the percussion firing mechanism is replaced with an electric vent tube initiation system.

The rupture pressure of the copper burst disc can be varied by varying its thickness from 2 to 10 mm

Flash suppression by additives to either the propellant or combustible cartridge case will be studied concurrently with wear assessment. The main problem with addition of the additives to the combustible cartridge case is that the majority of the materials to be assessed are water soluble and their addition is not commensurate with the current UK practice of forming these cases from aqueous slurries. However we are investigating the possibility of manufacture by reaction injection moulding which could overcome this problem. It is intended to commence this work using additives such as sodium and potassium salts, talc and titanium dioxide.

It is proposed that using this simulator vessel flash will be studied jointly along with erosion and two phase flow studies. Erosion will be assessed by the rate of removal of metal from the surface of the wear assessment zone. Flash will be assessed at the muzzle end using high speed temperature measuring techniques available within the Internal Ballistics Branch at RARDE. Laser Doppler anemometry, heat flux gauges and pressure measurement will also be used to characterise the flow of hot gas in the simulator. The development of high speed gas sampling techniques is also under consideration.

INSTRUMENTATION

In addition to the normal ballistic instrumentation techniques of pressure and high speed photographic methods RARDE have been developing the techniques of single beam Laser Doppler anemometry to study particle velocities both within and outside of the gun barrel. Modifications have been made to the equipment to additionally allow measurements of the transient temperatures in the region of muzzle flash.

Laser Doppler Anemometry

The problems associated with measurement of velocity fields behind the projectile in a gun barrel using laser Doppler anemometry techniques was initially investigated for the Internal Ballistic Division of RARDE in 1980. The original incentive was to obtain an increased understanding of the mechanisms of gun barrel erosion and in particular to understand the mechanism by which powder additives reduce the heat transfer in gun barrels.

The Laser Doppler Anemometer chosen for this application was the single beam system developed by the Institute, Saint Louis (Ref 2). In this system a Michelson interferometer is used to measure the Doppler shift in the light from a single focused laser beam scattered by moving particles in the flow. A schematic diagram of the electro-optics is given in figure 4. The laser light scattered from the particles in the flow is collected and fed to the interferometer by fibre optics. After passing through a Pockels cell two modes of linear polarisation are separated and passed through different path lengths in a Michelson interferometer. The two beams recombine and polarisation modes are mixed by a second polarising beam splitter. The two photomultipliers measure the complementary light power signals:

$P1 = P_o \cos^2(\pi L/\lambda)$

$P2 = P_o \sin^2(\pi L/\lambda)$

Figure 4

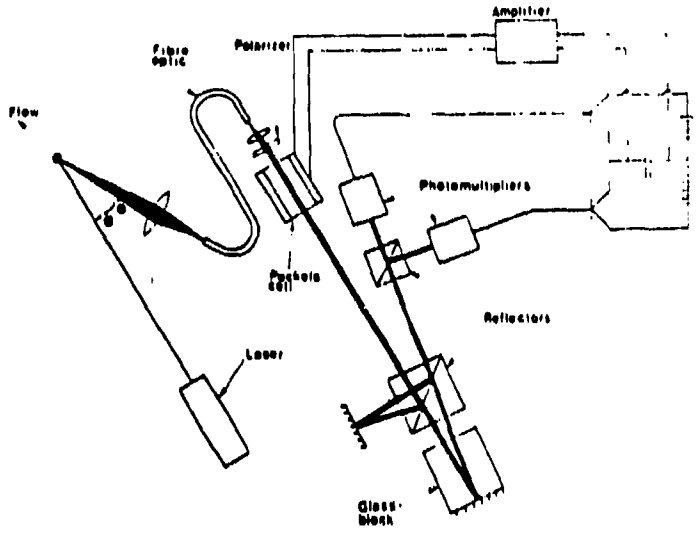

SCHEMATIC DIAGRAM OF THE LDA SYSTEM.

where λ is the wavelength, P_o is the incident light power to the interferometer and L the difference in optical path lengths.

If λ is gradually changed the photomultipliers see a series of light and dark fringes, the two signals always being in antiphase. In practice variations are produced by the Doppler shift of light scattered from particles in the flow. It is possible, though inconvenient to monitor P1 and P2 during a firing and convert these signals to a measurement of λ and thus particle velocity. Instead the interferometer incorporates a feedback system with the signals P1 and P2 being fed to a difference circuit.

The signal difference is amplified and fed to the Pockels cell in the input of the interferometer. The net effect is to keep P1 and P2 equal to each other by monitoring a constant value of the ratio L/λ. This arrangement generates a Pockels cell voltage directly proportional to the change in scattered light wavelength and hence to the particle velocity.

In practice the 4.5 watt argon ion laser and the laser Doppler anemometer are housed remotely from the gun and connected to it by fibre optic cables. Additional protection from ground shock is also provided.

The use of a 4.5 watt laser did permit some measurement of in-bore velocities using sapphire windows in the wall of a 30 mm smooth bore gun. However the high optical density and luminosity effects necessitated the gun being fired at reduced charge levels. Further improvements have been made with the effects of luminosity being reduced by the introduction of an Etalon narrow band filter.

More successful were the measurement made in the exhaust region of the gun and in the region of muzzle flash. In particular the particle velocity profile across a plane 53 mm downstream of a pressure vessel exit has been established (Fig 5).

Transient Temperature Measurements

By removing the phase shifting optics from the input to the Laser Doppler Anemometer interferometer the photomultipliers can be made to observe equal intensities of light (Ref 3). By inserting different optical filters in front of the photomultiplier windows, high speed, two colour measurements of temperature are possible. The temperature corresponds to the temperature at the focal point of the collection optics

Figure 5

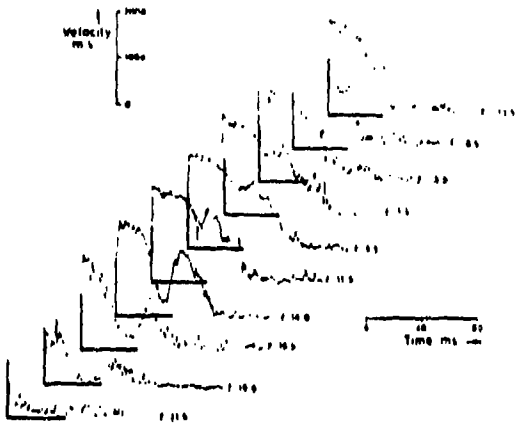

VELOCITY TIME HISTORIES AT DIFFERENT RADIAL POSITIONS (r) 50mm DOWNSTREAM OF VESSEL EXIT

The black body radiative power emitted in wavelength $d\lambda$ and centred on λ is:

$$E_\lambda = \frac{Cw^5}{\exp(hcw/kT)-1}$$

where E_λ is the radiated energy at the given frequency
w is the frequency
T is the absolute Temperature
C,c,k,h are constants

For finite wavelengths this reduces to:

$$E_\lambda d\lambda = \frac{Cw^5}{\exp(\beta hw)-1}.d\lambda$$

where β is the constant c/kT

Thus the ratio of powers due to 2 equal band wavelengths is:

$$R = \left(\frac{w_1}{w_2}\right)^5 \frac{\exp(\beta hw_2)-1}{\exp(\beta hw_1)-1}$$

or for $k<<hw$

$$R = \left(\frac{w_1}{w_2}\right)^5 \exp(\beta h(w_2 - w_1))$$

In practice the optical filters used were 488 nm and 514.5 nm. The ratio of black body emitted powers reduces to:

$$R = \beta \exp(-C'/T)$$

where constants $\beta = 1.30265$ and $C' = 1519$. The measurement of this ratio (R) for the two quoted wavelengths over the 500 to 5000 K temperature range will yield a temperature of:

$$T = \frac{1519}{\mathrm{Ln}(1.30265/R)}$$

It is observed that there is a good range in the ratios even though the wavelengths used are relatively close together. For the temperatures of interest the selection of wavelengths centred around 488 and 514.5 nm gives a usable range from 500 to 5000 K (Figure 6).

Figure 6

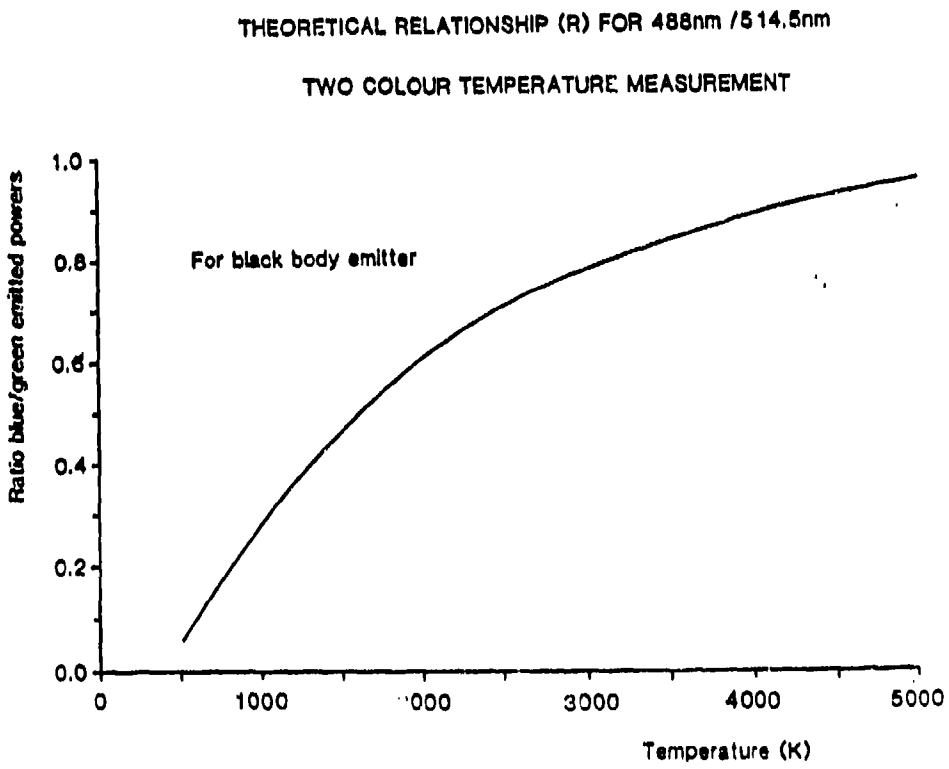

The photocurrents, typically a few microamps, are passed through a load resistor and the voltage across the resistor monitored.

The electronic circuit (Figure 7) is used with the standard photomultipliers. A variable load resistor for each photocurrent is placed across the inputs of an amplifier.

In practice the measured ratio varies from that predicted by a constant multiplying factor which is a function of the following experimental conditions:

1) The transmission characteristics of the optical filters used.

2) The values of the load resistors.

3) The quantum efficiency of each photomultiplier over the wavelength range defined by the filters.

Figure 7

CIRCUIT FOR HIGH SPEED TEMPERATURE MEASUREMENT

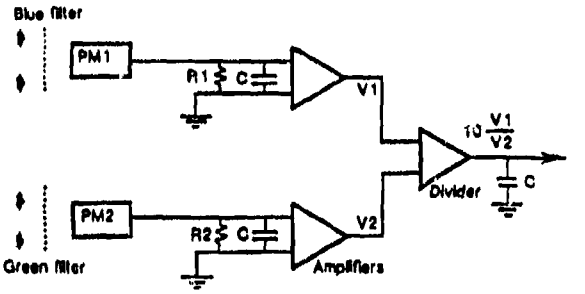

The system was therefore calibrated at a single point (1775 K). This temperature was obtained from a calibrated tungsten filament lamp.

The system has been used in practice. Figure 8 shows a recording obtained from a small charge firing in a 30 mm smooth bore, short barrel gun. In addition to the temperature measurement the light level at 514.5 nm is plotted. The recording is seen to slow-up in its response as the light level reduces.

Figure 8

TEMPERATURE MEASUREMENTS IN GUN MUZZLE FLASH-

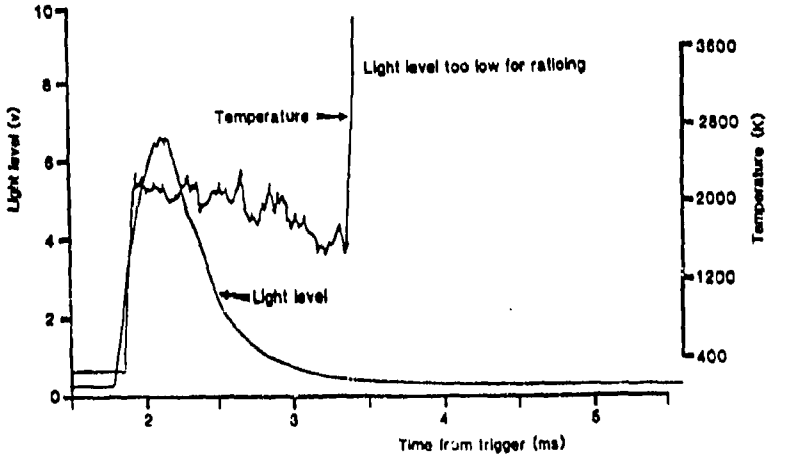

CONCLUSIONS

In the past, flash and flash suppression has not been studied as a specific research topic but has been examined on a project by project basis. In particular tank guns and mortars have attracted some work. It is now the intention of the Internal Ballistics Branch at RARDE to take a more active interest in this subject, although available resources will be low.

References

1) P S Henning Unpublished PE(MOD) Report. November 1983

2) A J Yule, P R Ereaut Measurements of High Velocity, Transient Gas Flow produced by a Vented Vessel. Progress report prepared for PE(MOD), RARDE Under contract MW31b/304. July 1983.

3) A J Yule, P R Ereaut The application of Laser Interferometry to Measurements within the Bore of a Cannon. Final Report Under PE(MOD), RARDE Contract MW31b/414.

Acknowledgements

The author wishes to express appreciation to Mr C J Hilderbrands and Dr K C Phan of the external Ballistics Division of RARDE for their assistance in the preparation of this report.

The author also acknowledges Dr A J Yule and Dr P R Ereaut for the LDA work carried out under contract to the RARDE.

SECONDARY COMBUSTION SUPPRESSION IN ROCKET EXHAUSTS

G.A. Jones and A.C.H. Mace

Royal Armament Research and Development Establishment
Westcott, Aylesbury, Buckinghamshire, England

1. INTRODUCTION

This paper presents a summary and review of the Plume Technology Group's work in flame suppression over the last five years or so. Much of the work has been published previously and is referenced accordingly.

One feature of chemically propelled rockets which has critical importance in the control of secondary combustion is that the gases expelled at high velocity from the nozzle of a rocket motor are usually fuel-rich. There are several reasons for this: high specific impulse is favoured by low molecular weight of combustion products, and H_2 has the lowest molecular weight of all; fuel-rich solid propellants offer advantages in manufacture and stability; and lower-oxidiser combustion products are less likely to cause nozzle erosion. The disadvantage in the exhaust context is that the unburned fuel, the sum of the mole fractions of hydrogen and carbon monoxide sometimes exceeding 0.5, may burn upon mixing turbulently with ambient air and produce a substantial elevation of temperature in the exhaust plume, giving rise to communications problems and greatly increased signature. (This external burning is called "secondary combustion" in the U.K. but "afterburning" in the U.S.A.) It may, on the other hand, fail to undergo rapid oxidation because ignition does not take place. Factors determining whether or not such secondary combustion occurs include not only the velocity and altitude of the missile, the motor thrust level, the pressure, temperature and fuel index at the nozzle exit, the presence of a base recirculation region, but also the presence or absence of certain combustion-inhibiting additives, of which potassium is an important example. Substantial experimental evidence exists that derivatives of potassium are capable of suppressing combustion in exhausts of rocket motors, [2,3].

The purpose of this paper is to describe the application of the latest version [4] of the rocket exhaust plume program REP3 to predicting whether or not secondary combustion occurs in the exhaust of a particular rocket motor with small proportions of potassium additive incorporated in its solid propellant. The REP3 model has been successful in accounting for a variety of experimental observations on exhausts whose secondary combustion is unsuppressed, [5,6]. The method used stems from coupling together a two-equation turbulence model, [7]. and a detailed treatment of non-equilibrium chemistry, [8]. The model is used here to demonstrate the signature reductions arising from the suppression of secondary combustion but its application in determining the precise amount of additive necessary for flame suppression in this especially challenging borderline region of marginal combustion has focussed attention on some of its inherent weaknesses. Fundamental deficiencies in its treatment of interactions between turbulence and chemical rate fluctuations have been recognised, [9]. A new procedure, [10], REX, has been formulated which is intended, when fully developed, to provide a more realistic description of such turbulence influences on chemical reactions in the near-nozzle regions where turbulence-chemistry processes may critically influence plume combustion.

2. CHEMISTRY OF FLAME SUPPRESSION

Secondary combustion of expelled fuel-rich products - principally CO and H_2 - is a major cause of high exhaust signature and communications problems. Secondary combustion takes place when the sequence of chain branching chemical reactions

$$H + O_2 \rightarrow OH + O$$
$$O + H_2 \rightarrow OH + H$$

and the chain propagation reaction

$$OH + H_2 \rightarrow H_2O + H$$

produces active free radicals like, H, OH and O faster than these radicals can be removed by the chain termination processes of mixing and such slow chemical recombination aided by energy-removing collision partners M, as

$$H + H + M \rightarrow H_2 + M$$

and

$$H + OH + M \rightarrow H_2O + M$$

The burning of carbon monoxide, which takes place concurrently with that of hydrogen, tends to propagate the combustion sequence rather than to result in net production or removal of radicals because the principal reaction controlling the oxidation of CO

$$CO + OH \rightarrow CO_2 + H$$

simply replaces one active radical by another.

The removal of flame radicals may be accelerated if an appropriate catalyst is present in the exhaust. If acceleration is sufficient secondary combustion may be prevented altogether; the excess fuel then simply mixes with the ambient air and is eventually oxidised very slowly at high dilution.

Potassium compounds have been demonstrated experimentally [3] to be effective suppressors of exhaust secondary combustion for double base propellant motors for a considerable range of thrust levels (200N - 12 kN). The mechanism of the effect has been interpreted [11,12] in terms of the kinetics of the radical-removing reactions.

$$K + OH + M \rightarrow KOH + M$$
$$KOH + H \rightarrow K + H_2O$$

This mechanism has been shown to be effective [11] in explaining the accelerated removal of hydrogen atoms observed when potassium was added to fuel-rich flames at concentrations [K]c of 3×10^{14} - 3×10^{15}

molecule cm^{-3} (mole fractions between 10^{-4} and 10^{-3}) as potassium dipivaloylmethane. Thermochemical data available [13-15] strongly suggests that potassium containing species such as KH, KO and KO_2 are present at concentrations too small (five or six orders of magnitude smaller than [K]) in these fuel rich flames to significantly influence the kinetics of the radical recombination processes. The mechanism adopted here consists of the two reactions above with the rate coefficients and uncertainty factors of Ref 11.

Other potential inhibitors of secondary combustion have been considered, but potassium appears to be as useful as any. Sodium gives rise to a mechanism analagous to reactions (7) and (8), [16], but weight for weight probably offers inferior prospects. The alkaline earths [1,17], iron [1,18], cobalt [19] and molybdenum and tungsten [1,20] have also received detailed attention. One important requirement of a suppressing additive is that it should produce active gas phase species in the exhaust rather than condensed products. This is a condition that several otherwise suitable additives may not meet. It is to the advantage of the potassium additives that the free metal and hydroxide produced in the exhaust have adequately high vapour pressures [13].

The set of reversible chemical reactions and rate coefficients used for the exhaust plume (and nozzle) calculations is shown in Table 1. Reactions (1) to (17) constitutes a basic combustion mechanism for hydrogen and carbon monoxide, HO_2 reaction being included because they may be expected to play some part in influencing onset of secondary combustion under borderline conditions. To this basic set are added the reactions of K, KOH and KO_2. Lead is treated as being present in the form of chemically inert particles that follow gas streamlines. Rate coefficients and uncertainty factors for reactions (1) to (17) are taken from Ref 8 and thermochemical data for the species involved from Ref (13). For Reactions (18) and (19), rate coefficients are taken from Ref (11) and thermochemical data again from Ref (13). For the species $K-O_2$ a bond energy of 170±25 kJ mol^{-1} has been assumed [14] giving $K_{eq20} = 7.0 \times 10^{-24} \exp(19500/T)$ ml $molecule^{-1}$. Rate coefficients of reaction (20) are taken from ref (21).

3. APPLICATION OF REP MODEL TO SECONDARY COMBUSTION SUPPRESSION

Previously a comprehensive study was made [9] of the predicted extent of secondary combustion in the initially fuel-rich exhaust of a particular double base propellant rocket motor with an axisymmetric (single nozzle) exhaust and a negligible base recirculation region. The present section is designed to provide an update of the current best estimates for these predictions using the latest version of REP3. The computational procedure employed in predicting rocket exhaust plume properties is summarised in Figure 1. Calculations were made for zero rocket velocity and ambient pressure and temperature of 100kN m^{-2} (approximately one atmosphere) and 288K respectively. The nozzle exit conditions of the double-base solid propellant rocket motor used in the present study are shown in Table 2. In the calculations of these conditions, chemical equilibrium was assumed to be established in the combustion chamber, but appropriate allowance was made for nonequilibrium effects in the nozzle.

The concentrations of the major species H_2, CO, CO_2, H_2O and N_2 do not vary significantly with the proportion of potassium-containing additive in the propellant. Those of the minor species do change with additive level; the higher this level, the greater the rate of recombination in the nozzle of the free radicals present. Slight variations of exit temperature and pressure with the additive level are also apparent.

Exhaust structures (distributions in space of temperatures, velocities, pressures, species concentrations and turbulence properties are calculated by the computer program REP3 (Rocket Exhaust Program) which allows for turbulent mixing of the nozzle-effluent and ambient-air streams, for the many chemical reactions occuring, and for gas dynamic features of shocks. The REP3 code incorporates a two-equation turbulence model and uses an implicit numerical technique to solve the fully coupled turbulent boundary-layer and chemical rate equations. The values used for the empirical turbulence modelling constants in Ref (9) used in the present work are given in Table 3. The two turbulence variables for which transport equations were solved were the turbulent kinetic energy k and the eddy energy dissipation rate ε. The eddy viscocity coefficient μ, governing the local mixing rate, is given by $\rho C_D k^2 \varepsilon^{-1}$ and the length scale l characteristic of the energy-containing eddies is obtained from $C_D k^{1.5} \varepsilon^{-1}$ (where ρ is the density and C_D is a turbulence model constant)

Full descriptions of the REP3 program have been given elsewhere [22,23] and will not be repeated here. Certain deficiencies in the incorporation of the chemical reactions into the REP3 computer program have also been identified and described elsewhere [24]. The latest version of REP3[4] has been demonstrated to overcome these deficiencies [25] and has now been applied to the prediction of the onset of secondary combustion. It is, however, worth noting some important assumptions implicit in the formulation of REP3.

(1) The flow is assumed to be quasi-steady: the average motion is steady and the governing equations are time-averaged.

(2) The flow is treated as locally incompressible.

(3) Turbulent density fluctuations are neglected.

(4) The Reynolds stresses are taken to be expressible in terms of mean velocity gradients via introduction of the eddy viscosity μ; the conservation equations for energy and species concentration are closed by appropriate gradient approximations.

(5) It is assumed that no detailed explicit account need be taken of molecular transport as a rate-determining process.

(6) The laminar viscocity is taken to be small by comparison with the turbulence eddy viscocity; the latter is expressed in terms of the two variables k and ε, for which conservation equations are solved.

(7) Coupling of fluid dynamic and chemical effects is assumed to be

accomplished legitimately by combining local time-mean values.

(8) The flow is treated as adiabatic.

(9) Turbulence is taken to be locally isotropic.

Some of these assumptions, such as (6), may readily be justified as acceptable for a wide variety of free turbulent flowfields. Others such as (5) may be argued to be reasonable in the present context, although not in many others. Still other assumptions - notably (3) and (7) are likely sources of significant error. Substantial attention to (7) will be given later.

3.1 $[K]_{min}$ required for flame suppression

From the exhaust structure calculated by REP3 the centre-line distribution of temperature is used as a criterion of secondary combustion. In Figure 2, line 1 the marked continuous rise in temperature with increasing axial distance x, which occurs before falloff at larger x is indicative that secondary combustion is present (The spatial fluctuations in temperature close to the nozzle exit, due to shock structure are readily distinguishable from this rise). In chemical terms, the rate of chain branching exceeds that of chain termination sufficiently for rapid heat-releasing oxidation of hydrogen and carbon monoxide to take place. Lines 2 and 3 of Fig 2 are axial temperature profiles calculated for different levels of potassium additive incorporated in the propellant but inputs otherwise identical to those used to produce line 1 ; line 2 corresponds to the presence of secondary combustion but line 3 (for the highest level of potassium) to its absence.

Because onset or suppression of secondary combustion under borderline conditions depends on the outcome of a delicately poised competition between chain-branching and chain-termination steps, the sensitivity of [K]min, the predicted minimum weight percent of potassium in the propellant required for secondary combustion to be suppressed, to a wide range of input quantities is hardly surprising. Uncertainties in these input quantities for the present model procedure lead to substantial uncertainties in predictions of [K]min. In particular a more precise characterisation of turbulence model constants remains a clear need in the context of secondary combustion suppression. However, the previously reported sensitivity of [K]min to KO_2 chemistry has disappeared with the present calculations. This stems from the changed value of the thermochemical stability of KO_2 described earlier. Similarly brief checks have indicated no sensitivity to KO chemistry. For the conditions described above the current best estimate for [K]min would be 1.7%, to which would be attached a factor of uncertainty as large as 5. For the rocket motor considered the measured minimum weight percent of potassium in the propellant required for suppression of secondary combustion is approximately 0.3. This discrepancy between best values from theory and experiment does not in itself immediately cast doubt on the model formulation because the uncertainties in the predictions imposed by these in the inputs are so large. However, with

the practical demands for more precise predictions of secondary combustion onset a critical examination of assumption (7) in the formulation, relating to the influence of turbulent fluctuation on the chemical reactions, is given below in section 4.

3.2 Signature Implications - Infrared Radiation

The effect of flame suppression on CO_2 infrared radiation emissions at spectral wavelengths 4.1-4.9μm is illustrated in Figure 3 For the first case (secondary combustion present), propellant was taken to contain typical trace levels of sodium and potassium at 50 ppm. For the second case (secondary combustion suppressed), the propellant differed only in that it contained 2% by weight potassium. Radiation levels correspond to small elements of the exhaust, along lines of sight passing through the flame, as a function of the axial distance from the nozzle exit. The radiation level in this waveband for the whole exhaust was about a factor of 40 lower when secondary combustion was suppressed. Most of the reduction was the result of lowered temperatures and reduced plume size, although local CO_2 concentrations dropped by factors between 2 and 3 when combustion was prevented.

3.3 Signature Implications - Sodium Resonance-Doublet Radiation

Figure 4 presents relative intensities of sodium resonance-doublet emissions as functions of spectral wavelengths for the unsuppressed and suppressed exhaust flames considered in the previous section. The peak intensities are reduced by factors of well over 1000 when secondary combustion is suppressed. The peaks of potassium resonance-line doublets also fell, by factors of about 1000, in spite of the fact that the suppressed flame contained much higher concentrations of potassium.

3.4 Signature Implications - Microwave Attenuation

Metallised propellant ingredients are considered to be the major source of free electrons in rocket exhausts. Nevertheless, raising propellant mass fractions of potassium to levels resulting in combustion suppression reduces electron concentrations. As a consequence, both attenuation and scattering of microwave radiations are significantly reduced. Figure 5 illustrates the predicted effects on the attenuntion of a microwave beam transmitted through the exhaust of the motor discussed in Section 3.1. Most of the reduction arises from lowered electron concentrations, although some is due to a change in plume shape.

4. KINETIC SCALES OF TURBULENCE AND CHEMISTRY

When the description of a flame turbulence field is formulated in terms of k and ε, the tractable set of equations of wide applicability that results enables much useful information to be generated [7]. A penalty paid for the convenience and tractability of this description, however, is that physical insight is lost into the nature of contributions from eddies of different scales . In order to regain some such insight for a rocket exhaust, one should consider the likely shape of the wave number

distribution of eddy energy in this flame This shape (cf. Refs. [26, 27] is shown in Fig. 6, the ordinate $E(\underline{k})$ being in arbitrary units. Also, the eddy energy dissipation function is proportional to $\underline{k}^2E(\underline{k})$.

Reference is conveniently made to various arbitrary length scales of turbulence in the following paragraphs. The length scale L_0 is that of the largest, energy-absorbing, eddies, which is of the same order as the exhaust half width. Next largest is the length scale 1 of the energy-containing eddies, identified with $C_D k^{1.5}/\epsilon$. The length-scale l_x is that of eddies toward the high wave number end of the inertial subrange but well to the low $\underline{k}$ side of the dissipating range, whereas l_s is associated with the very smallest eddies in the dissipating range and is given by $l_s \equiv (\nu^3/\epsilon)^{1/4}$[26,27]. The numerical values for wave numbers corresponding to these scales shown in Fig. 6, and values for the other quantities used below, are given for the position ($x = 0.5$ m, $r = 0$) in an exhaust with a structure calculated for $C_1 = 1.57$, $T_e = 1335°K$, 0.5% by weight of potassium in the propellant, and KO_2 omitted. Here $L_0 = 0.06$ m, $1 = 5 \times 10^{-3}$ m, $l_x = 3 \times 10^{-4}$ m, and $l_s = 1 \times 10^{-5}$ m. Other local properties take the values $k = 5.7 \times 10^4$ m^2 s^{-2}, $\epsilon = 2.6 \times 10^8$ m^2 s^{-3}, $\mu/\rho = 1.1$ m^2 s^{-1}, and $\nu = 1.3 \times 10^{-4}$ m^2 s^{-1}. No special significance attaches to the selection of the particular input quantities and position: Any other location in that part of an exhaust relevant to secondary combustion would have been equally suitable.

Intrinsic characteristic times may be associated with creation of eddies of different sizes. The time t_1 for formation of eddies of size L_0 will be $\approx L_0/u$ (cf., e.g. Ref[28]; with $u = 2 \times 10^3$ ms^{-1} and $L_0 = 0.06$ m, t_1 3×10^{-5}s. The time t_2 for the creation of eddies of size 1 is similarly $\approx 1/u'$, which, with $1 = 5 \times 10^{-3}$ m and $u' = 200$ m s^{-1}, gives $t_2 \approx 2 \times 10^{-5}$s. The velocity u_x associated with motion of eddies in the inertial subrange is $\approx [2/3\ k1.8^{*2/3}\underline{k}^{-5/3}]^{1/2}$ (see, e.g., Ref [27]), and the characteristic time t_3 for formation of eddies of length scale l_x, given by l_x/u_x, is greater than 1×10^{-5}s. The creation of eddies containing the bulk of the turbulence kinetic energy, and the creation of eddies in the inertial subrange thus have associated with them rather similar characteristic times. A significant loss of physical realism therefore accompanies the lack of separate allowance for these processes, which is implied by the formulation of the flowfield description in the REP3 model. In particular, the need for a more realistic treatment of the formation of energy-absorbing eddies is clear, especially for those near-field regions of the exhaust where eddy creation dominates over convective transport in determining local values of k.

It is instructive to compare t_1 - t_3 with the characteristic times t_4 associated with chemical reactions in the exhaust. The latter vary greatly with the reaction type. For a fast bimolecular exchange reaction, the relaxation time (i.e., the time for significant progress toward the position of equilibrium or balance of the reaction) may be $<10^{-7}$ s. For a slow three-body radical recombination like Reaction (3), this time may be in excess of 10^{-2} s. In any one rocket exhaust, values of t_4 anywhere between these rough limits are likely to be

encountered. For an exhaust with borderline secondary combustion, comparison between $t_1 - t_3$ and t_4 for the key chain-branching Reaction (8) in Table 1 is especially revealing. At (x = 0.5 m, r = 0) in the exhaust under consideration, $[O_2]$ is predicted to be 4.7×10^{17} molecule ml^{-1}, T = 1200°K, and $A_i \approx 2 \times 10^{-13}$ ml molecule$^{-1}s^{-1}$. Time t_4 for this reaction, given by $t_4 \sim (A_i [O_2])^{-1}$, is therefore about 10^{-5} s, of the same order as $t_1 - t_3$. Errors in prediction of secondary combustion onset must therefore inevitably arise both from inadequacies in the description of development of macroscopic eddies and from the lack of an appropriate treatment of scalar fluctuations and their interactions.

5. THE REX CODE

The REX code incorporates a new plume structure model [10] which attempts to remedy the deficiencies described in section 4 with regard to the need to describe adequately the processes of large eddy formation and the influence of turbulence induced fluctuation in concentrations and temperature on the chemical rate processes. To allow for fluctuations in a wholly Eulerian analysis for a complex multi-step chemical mechanism involves a formidable extension to previous studies [29-32]. The turbulence-chemistry plume model used in REX circumvents difficulties associated with a wholly Eulerian analysis by incorporating a time - evolution Lagrangian description of conditions within representative shear-layer eddies. The turbulence-chemistry analysis is based on a Lagrangian-Eulerian model developed at RARDE from the ESCIMO diffusion flame theory [33] proposed by Professor D.B. Spalding, Imperial College, London. Eddy-fold structured representations of plume turbulence are computed with detailed descriptions of chemical processes evolving within individual folds. The analysis is applied only to near-nozzle regions where turbulence-chemistry processes may critically influence plume combustion. Much of the code development work is now complete but it contains many assumptions and approximations which require further numerical investigation and mathematical analysis. As calculations are performed for more complex and progressively more realistic conditions, the merits of the method will become quantifiable. Ultimately, success will be determined by detailed comparison of REX/REP3 plume predictions with experimental measurements of flame suppression.

NOMENCLATURE

C_D, C_1	-	constants in turbulence model
$E(\underline{k})$	-	(energy in turbulence eddy energy spectrum at wave numbers between $\underline{k}$ and $\underline{k} + d\underline{k}/d\underline{k}$
k	-	turbulent kinetic energy
K_1	-	equilibrium constant of ith reaction
$\underline{k}$	-	wave number in turbulence eddy energy spectrum
L_0,l,lx,ls	-	length scales of turbulence
r	-	radial coordinate (=0 on exhaust axis)
u	-	mean axial flow velocity
u'	-	RMS fluctuating part of axial velocity component
x	-	axial coordinate (=0 at nozzle exit)
ϵ	-	eddy energy dissipation rate
k_i	-	rate coefficient of ith chemical reaction
μ	-	eddy viscosity coefficient
ν	-	laminar kinematic viscosity
ρ	-	density

REFERENCES

1 Jensen, D E
Webb, B C
Afterburning Predictions for Metal-Modified Propellant Motor Exhausts.
A.IAA, 14 1976, p 947

2 McHale, E T
Flame Inhibition by Potassium Compounds.
Combustion and Flame, 24 1975, p 277.

3 Smith, P K
Evans, G I
The Reduction of Exhaust Signature in Solid Propellant Rocket Motors. Paper 16, AGARD Meeting on Smokeless Propellants, Florence, 1985

4 Fuggle, D A B
Hills, D P
Mace, A C H
An Accurate and Efficient Procedure for Solving the Chemical Species Transport Equations in the Computer Program REP3.
PERME (W) TR 262, 1983

5 Cockle, S G
Donovan, J A
Ridout, J M
Infrared Emissions from the Exhaust Plumes of Solid Propellant Rocket Motors with Thrusts between 300N and 20kN, parts 1-3.
PERME (W) TRs 235,236,241, 1983

6 Cousins, J M
Jensen, D E
Microwave Attenuation and Modulation in Rocket Exhausts : Status of Prediction Capability.
PERME (W) TR 209, 1981

7 Launder, B E
Spalding, D B
Mathematical Models of Turbulence.
Academic Press, London, 1972

8 Jensen, D E
Jones, G A
Reaction Rate Coefficients for Flame Calculations.
Combustion and Flame, 32 1978, p 1

9 Jensen, D E
Jones, G A
Theoretical Aspects of Secondary Combustion in Rocket Exhausts.
Combustion and Flame, 41 1981, p 71

10 Mace, A C H
Turbulence-Chemistry Interactions in Rocket Exhaust Plumes.
RARDE Report 7/85, 1985

11 Jensen, D E
Jones, G A
Mace, A C H
Flame Inhibition by Potassium.
J. Chem. Soc. Faraday Trans I, 75 1979 p 2377

12 Jensen, D E
Jones, G A
Theoretical Aspects of Secondary Combustion in Rocket Exhausts.
Combustion and Flame 41, 1981 p 71

13
JANAF Thermochemical Tables, 2nd Edition, National Bureau of Standards, Washington, DC NBS-NSRDS No 37, 1971.

OW2AAC

REFERENCES cntd.

14 Jensen D E — Alkali-metal Compounds in Oxygen-rich Flames. J. Chem. Soc. Faraday Trans I, 78 1982, p 2835

15 Pedley, J B; Marshall, E M — Thermochemical Data for Gaseous Monoxides. J. Phys. Chem. Reference Data, 12 1983, p 967

16 Jensen, D E; Jones, G A — Kinetics of Flame Inhibition by Sodium. J Chem Soc Faraday Trans 1, 78 1982, p 2843

17 Jensen, D E; Jones, G A — Alkaline Earth Flame Chemistry. Proc. Roy Soc, A 364 1978, p 509

18 Jensen, D E; Jones, G A — Catalysis of Radical Recombination in Flames by Iron. J Chem Phys, 60 1974, p 3421

19 Jensen, D E — Aspects of the Flame Chemistry of Cobalt. J Chem Soc Faraday Trans 1, 72 1976, p 2618

20 Jensen, D E; Jones, G A — Mass-spectrometric tracer and Photometric Studies of Catalysed Radical Recombination in Flames. J Chem Soc Faraday Trans 1, 71 1975, p 149

21 Husain, D; Plane, J M C — Kinetic Investigation of the Third Order Rate Processes between K + O_2 + M by Time-Resolved Atomic Resonance Absorption Spectroscopy. J Chem Soc Faraday Trans 2, 78 1982, p 1175

22 Jensen, D E; Wilson, A S — Prediction of Rocket Exhaust Flame Properties. Combustion and Flame 25, 1975 p 43

23 Cousins, J M — Calculation of Conditions in an Axisymmetric Rocket Exhaust Plume: The REP3 Computer Program. PERME (W) TR 218, 1982

24 Cousins, J M — The REP3 Chemistry Problem and an Alternative Chemistry Treatment. PERME (W) TR 227, 1982

25 Jones, G A — Application of the Improved Rocket Exhaust Plume Program REP3-82 to Some Plume Chemistry Problems. RARDE Report 12/85, 1985

26 Hinze, J O — Turbulence : An Introduction to its Mechanism and Theory. McGraw-Hill, New York, 1959

REFERENCES cntd.

27	Reynolds, A J	Turbulent Flows in Engineering, Wiley New York, 1974
28	Lockwood, F C Syed, S A	Combustion Sci. Technol., 19 1979, p 129
29	Varma, A K Beddini, R A Fishburne, E S	Second Order Closure Analysis of Turbulent Reacting Flows, Proc 1976 Heat Transfer and Fluid Mech Inst, Stanford Univ. Press, 1976
30	Fishburne, E S Varma, A K	Investigations of Chemical Reactions in a Turbulent Media. Acta Astronautica, 6 1979, p 297
31	Borghi, R Dutoya, D	On the Scales of the Fluctuations in Turbulent Combustion. 17th Symposium on Combustion, 1978
32	Jones, W P Whitelaw, J H	Calculation Methods for Reacting Turbulent Flows. A Review, Combustion and Flame, 48 1982, p 1
33	Spalding, D B	The Influence of Laminar Transport and Chemical Kinetics on the Time-Mean Reaction Rate in a Turbulent Flame. 17th Symposium on Combustion Leeds, 1978.

TABLE 1

Chemical Reactions and Rate Coefficients

	Reaction	Forward Rate Coefficient[a]	Uncertainty Factor
1	$O + O + M \rightarrow O_2 + M$	$3 \times 10^{-34} \exp(900/T)$	10
2	$O + H + M \rightarrow OH + M$	$1 \times 10^{-29} T^{-1}$	30
3	$H + H + M \rightarrow H_2 + M$	$3 \times 10^{-30} T^{-1}$	30
4	$H + OH + M \rightarrow H_2O + M$	$1 \times 10^{-25} T^{-2}$	10
5	$CO + O + M \rightarrow CO_2 + M$	$7 \times 10^{-33} \exp(-2200/T)$	30
6	$OH + H_2 \rightarrow H_2O + H$	$1.9 \times 10^{-15} T^{1.3} \exp(-1825/T)$	2
7	$O + H_2 \rightarrow OH + H$	$3 \times 10^{-14} T \exp(-4480/T)$	1.5
8	$H + O_2 \rightarrow OH + O$	$2.4 \times 10^{-10} \exp(-8250/T)$	1.5
9	$CO + OH \rightarrow CO_2 + H$	$2.8 \times 10^{-17} T^{1.3} \exp(330/T)$	3
10	$OH + OH \rightarrow H_2O + O$	$1 \times 10^{-11} \exp(-550/T)$	3
11	$H + O_2 + M \rightarrow HO_2 + M$	$2 \times 10^{-32} \exp(500/T)$	10
12	$H + HO_2 \rightarrow OH + OH$	$4 \times 10^{-10} \exp(-950/T)$	5
13	$H + HO_2 \rightarrow H_2 + O_2$	$4 \times 10^{-11} \exp(-350/T)$	5
14	$H_2 + HO_2 \rightarrow H_2O + OH$	$1 \times 10^{-12} \exp(-9400/T)$	10
15	$CO + HO_2 \rightarrow CO_2 + OH$	$2.5 \times 10^{-10} \exp(-11900/T)$	10
16	$O + HO_2 \rightarrow OH + O_2$	$8 \times 10^{-11} \exp(-500/T)$	30
17	$OH + HO_2 \rightarrow O_2 + H_2O$	5×10^{-11}	30
18	$KOH + H \rightarrow K + H_2O$	$1.8 \times 10^{-11} \exp(-1000/T)$	10
19	$K + OH + M \rightarrow KOH + M$	$1.5 \times 10^{-27} T^{-1}$	10
20	$K + O_2 + M \rightarrow KO_2 + M$	$3 \times 10^{-27} T^{-1}$	10
21	$KO_2 + H_2 \rightarrow KOH + OH$	$5 \times 10^{-12} \exp(-10000/T)$	100
22	$KO_2 + OH \rightarrow KOH + O_2$	$2 \times 10^{-11} \exp(-2000/T$	30
23	$K + HO_2 \rightarrow KO_2 + H$	$1 \times 10^{-11} \exp(-1000/T)$	30

[a] In ml-molecule-second units. The sources of rate coefficients and uncertainty factors are given in the text.

TABLE 2

Nozzle Exit Plane Conditions

Quantity	With 0.1 wt. % Potassium	With 2.0 wt. % Potassium
Species concentrations (molecule ml^{-1}):		
H_2	9.6×10^{17}	9.6×10^{17}
CO	2.8×10^{18}	2.8×10^{18}
N_2	8.2×10^{17}	8.1×10^{17}
CO_2	9.2×10^{17}	8.9×10^{17}
OH	3.1×10^{13}	2.9×10^{11}
H	1.3×10^{15}	1.5×10^{13}
O	4.1×10^{10}	9.5×10^{6}
HO_2	7.6×10^{8}	2.7×10^{7}
O_2	1.1×10^{12}	7.9×10^{11}
H_2O	1.6×10^{18}	1.6×10^{18}
K	2.9×10^{15}	2.8×10^{16}
KOH	1.6×10^{15}	6.2×10^{16}
KO_2	7.0×10^{7}	7.7×10^{8}
PbO	1.7×10^{16}	1.7×10^{16}
Temperature (Kelvins)	1340	1300
Jet velocity ($km\ s^{-1}$)	2.0	2.0
Pressure ($kN\ m^{-2}$)	132	127
Nozzle exit radius (cm)	2.48	2.48
Ambient pressure ($kN\ m^{-2}$)	100	100

At the exit plane, the ratio of RMS fluctuating component of velocity to jet velocity was taken to be 0.1, and the turbulence length scale l to be 0.1 x the nozzle exit radius. All properties are assumed to be uniform across the nozzle exit.

TABLE 3 Constants for the k/ε Turbulence Model

C_D	= 0.09	σ_H	= 1.0
C_1	= 1.44	σ_M	= 1.0
C_2	= 1.92	σ_K	= 1.0
C_{g1}	= 2.8	σ_ε	= 1.3
C_{g2}	= 1.92		

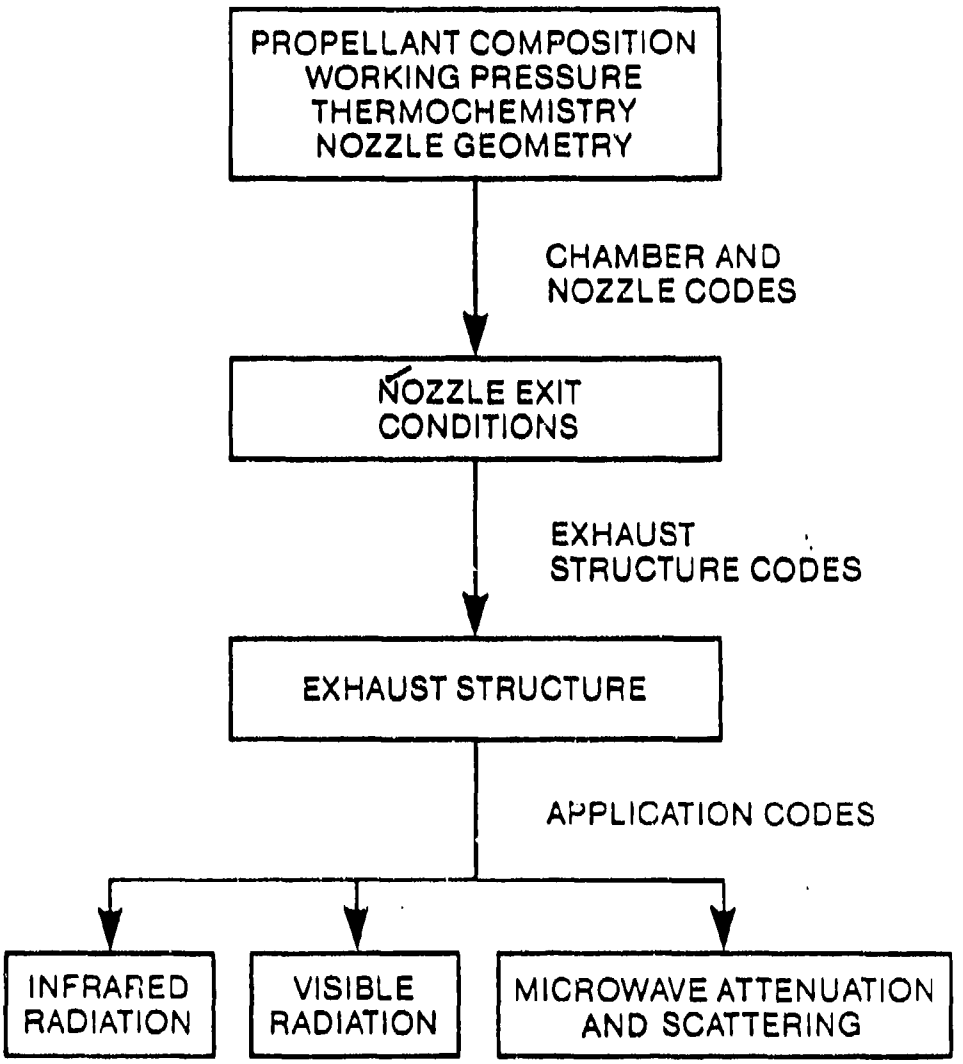

FIG. 1 COMPUTATIONAL PROCEDURE

UNCLASSIFIED

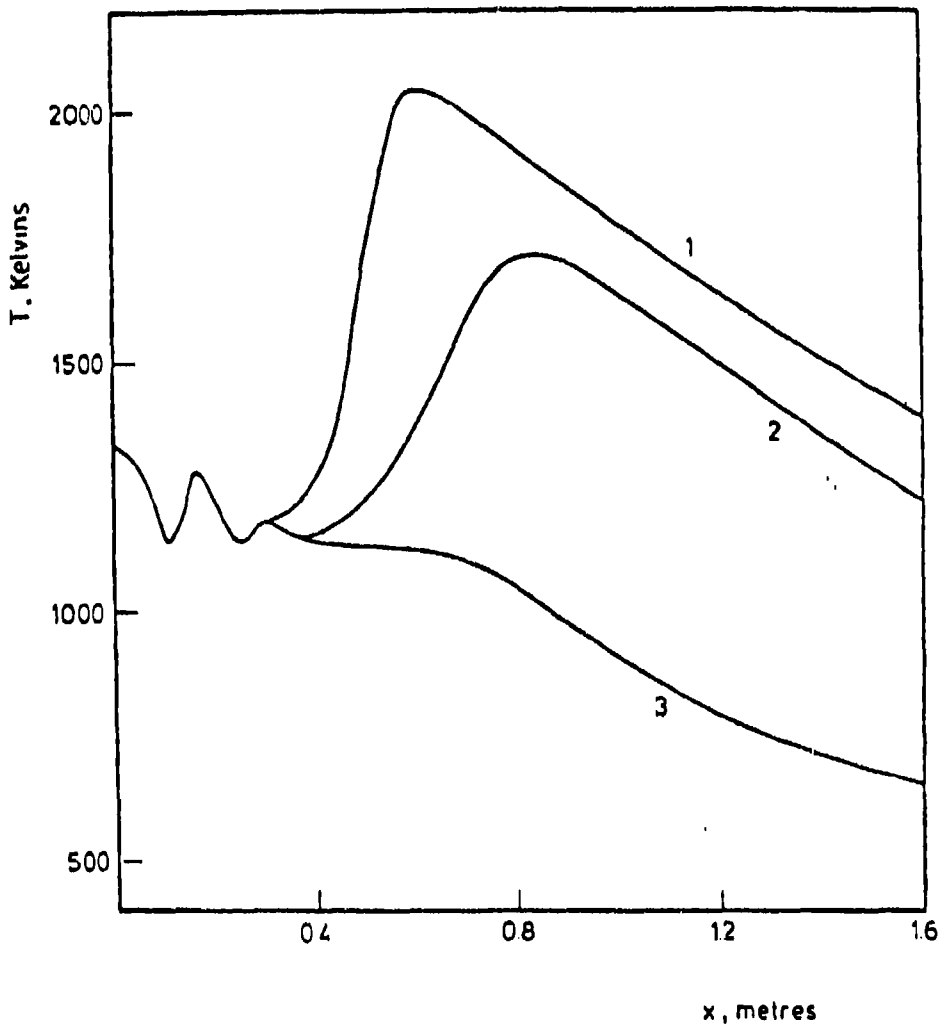

FIG. 2 AXIAL TEMPERATURE PROFILES FOR DIFFERENT LEVELS OF POTASSIUM IN THE PROPELLANT: C_1 = 1.44, KO_2 INCLUDED; EXIT TEMPERATURE APPROXIMATELY 1320 K. CURVE 1; 0.4 PER CENT BY WEIGHT OF POTASSIUM IN PROPELLANT: CURVE 2; 1.0 PER CENT: CURVE 3; 1.7 PER CENT.

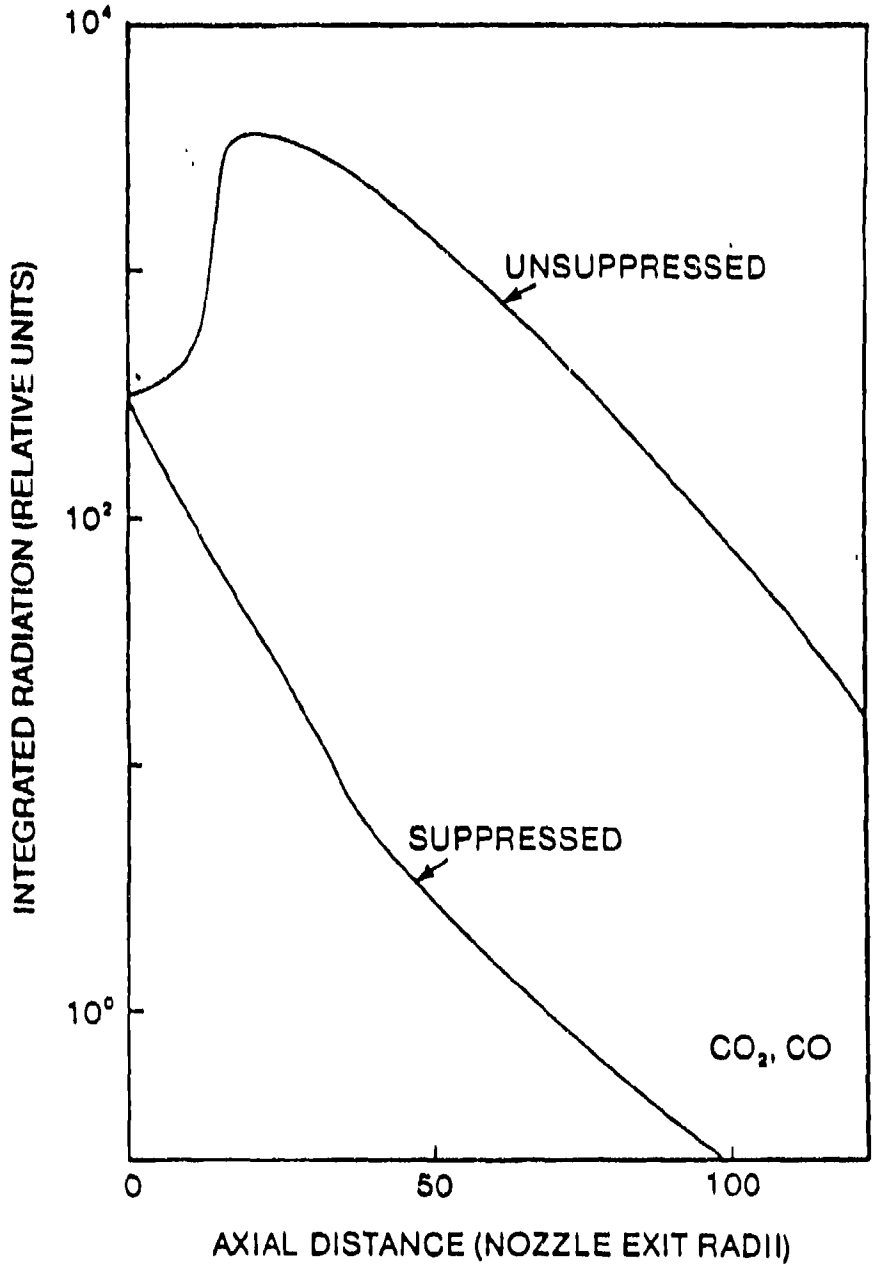

FIG.3 VARIATION OF RELATIVE RADIATION EMISSIONS FROM CO_2 IN THE INFRARED WAVEBAND 4.1 - 4.9 μm WITH AXIAL DISTANCE FOR UNSUPPRESSED AND SUPPRESSED SECONDARY COMBUSTION CONDITIONS.

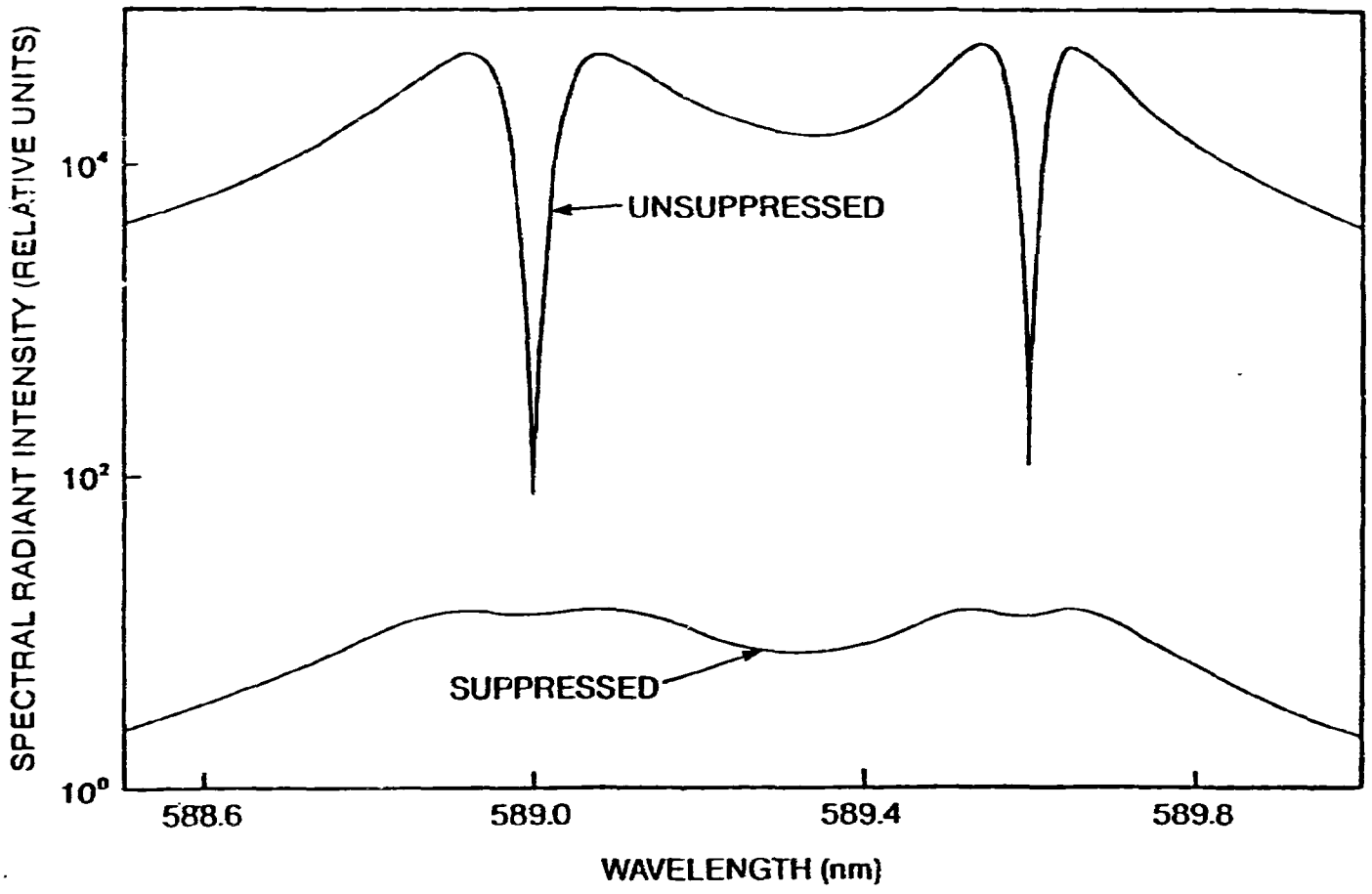

FIG.4 WAVELENGTH DISTRIBUTIONS OF SODIUM RESONANCE-LINE EMISSION INTENSITIES FOR UNSUPPRESSED AND SUPPRESSED SECONDARY COMBUSTION CONDITIONS

FIG.4

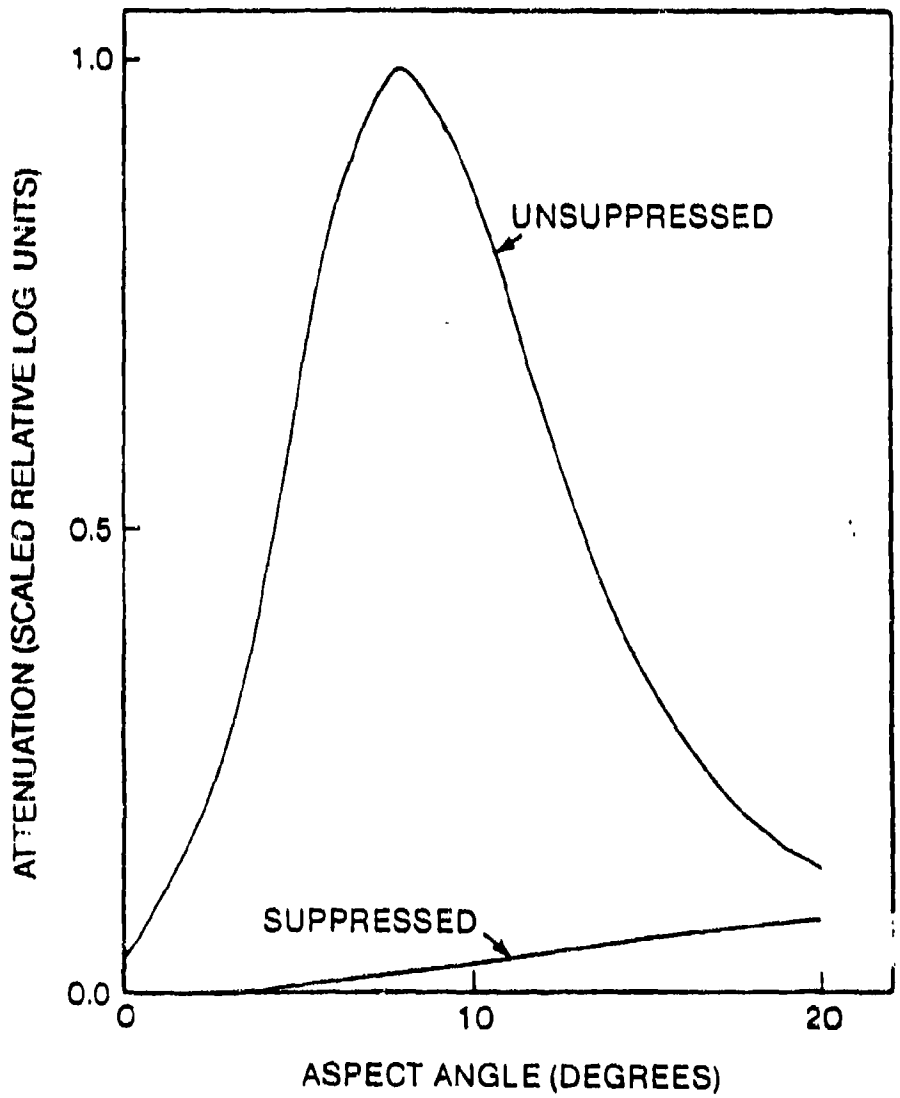

FIG.5 VARIATION OF MICROWAVE BEAM ATTENUATION WITH ASPECT ANGLE FOR UNSUPPRESSED AND SUPPRESSED SECONDARY COMBUSTION CONDITIONS. LOG UNITS REFER TO THE ORIGINAL ATTENUATION UNITS OF db

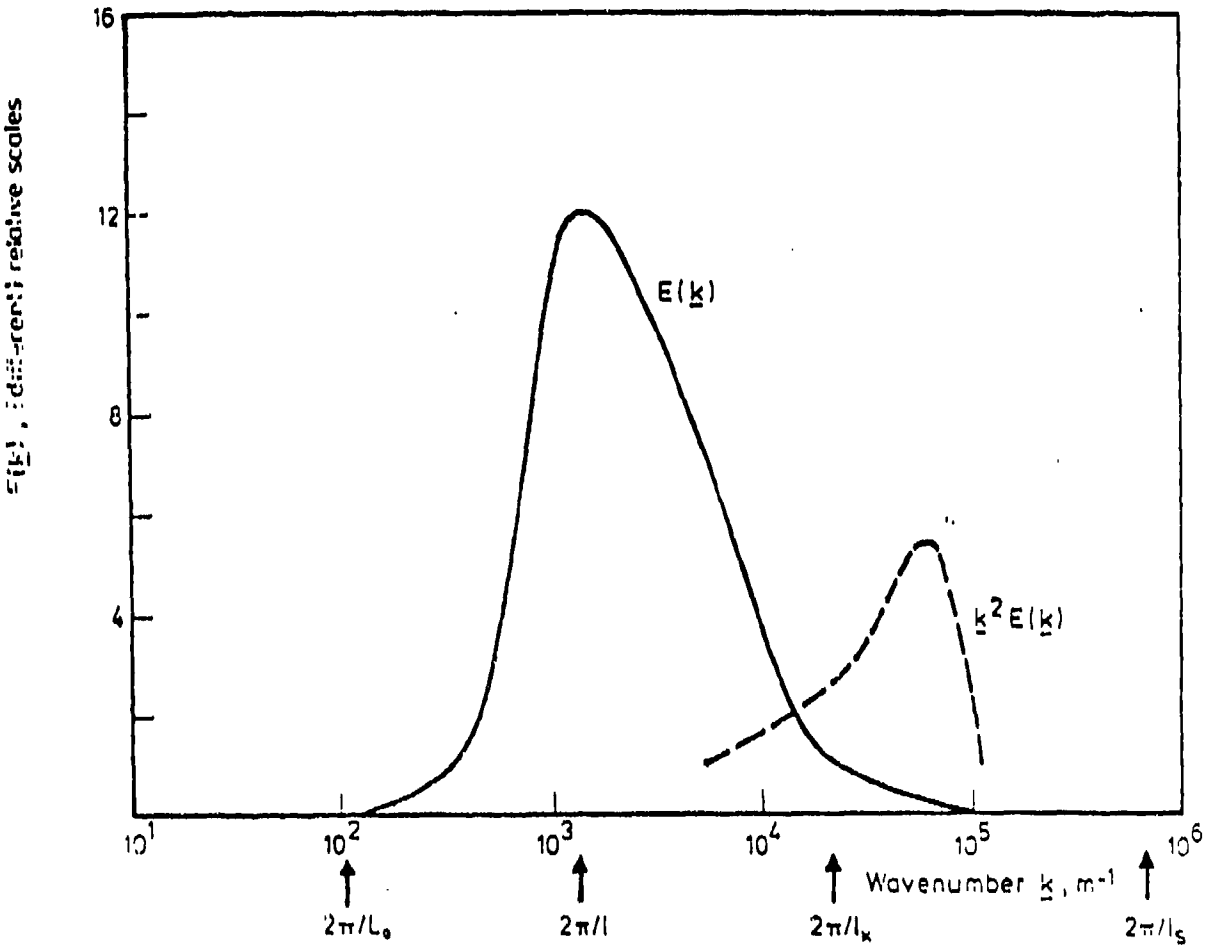

FIG. 6 TYPICAL SHAPES OF WAVENUMBER DEPENDENCE OF $E(\underline{k})$ AND $\underline{k}^2 E(\underline{k})$ IN A ROCKET EXHAUST FLAME. THE CURVES ARE DRAWN TO CORRESPOND TO THE POSITION (x = 0.5 m, r = 0) FOR THE EXHAUST STRUCTURE CALCULATED WITH $C_1 = 1.57$, EXIT TEMPERATURE 1320 K, 0.5 PER CENT BY WEIGHT OF POTASSIUM IN THE PROPELLANT AND KO_2 OMITTED.

Nagamasa Kubota
Rocket Propulsion Laboratory, TIT, Japan

Suppression Mechanism of Rocket Afterburning

Introduction

There have been numerous experimental and theoretical studies on the secondary flame of rocket exhaust gases.[1] The secondary flame is produced by the ignition of fuel rich exhaust gas accompanied with the diffusional mixing process of the oxygen in the air. The nature of the secondary is very dependent on the chemical composition of the propellant used and the physical geometry of the exhaust nozzle.

The secondary flame is eliminated by the addition of a small amount of potassium compounds. The suppression of the secondary flame is affected by the amount of the additives, chemical compositions of the propellants, and aerodynamic mixing process of the exhaust gases with the surrounding air. In this study, the physicochemical processes of the suppression of the secondary flame have been studied experimentally in order to elucidate the role of potassium compounds in the exhaust gases.

Experimental

The propellants tested in this study were double-base propellants consisting of nitrocellulose (NC) and nitroglycerin (NG). Two types of double-base propellants were formulated: low-energy and high-energy propellants. The energy contained in the unit mass of propellant was altered by changing the mixing ratio of NC/NG. The detailed chemical compositions of the propellants tested in this study are shown in Table 1. The chemical additives used were KNO_3 and K_2SO_4. Each additive was mixed within the low energy and high-energy propellants.

A micro-rocket motor was used to evaluate the nature of the combustion process of the gas exhaused from the nozzle. The size of the propellant grain was 120 mm in outer diameter and 140 mm in length. The geometry of the internal cross-section was five-pointed star geometry in order to

gain a nutral burning. In order to determine the effect of the concentration on the plume suppression two types of propellant grains were arranged along the motor axis: a low-energy or a high-energy propellant grain was positioned at the rear end of the motor and a KNO_3 added propellant grain or a K_2SO_4 added propellant grain was positioned at the fore end of the motor. Since all the additives genereted by the combustion of the KNO_3 or K_4SO_4 added propellant grain flowed out with the combustion gases of both propellant grains, the concentration of the additives in the combustion gas exhaused from the nozzle was adjusted with changing the length of the grains. The concentration was simpley determined as

$$\Phi = \rho_K r_K A_K \Phi_K / (\rho_0 r_0 A_0 + \rho_K r_K A_K) \qquad (1)$$

where Φ is the averaged concentration of the potassium compound in the combustion gas, Φ_K is the concentration of the potassium compound contained within the propellant grain, A is the burning area, ρ is the density, r is the burning rate, and the subscripts 0 and K are the propellants without and with potassium compound, respectively. The internal arrangement of the micro-rocket motor is shown in Fig. 1.

In order to examine the aerodynamic effect on the plume suppression the expansion ratio of the exhaused nozzle was altered. The temperature of the combustion gas at the exit of the nozzle was altered by changing the expansion ratio. The pressure in the rocket motor was also altered either by changing the length of the propellant grain or by changing the nozzle throat area.

Conclusions

The experimental investigation of the suppression of the after-burning flame for different types of propellant formulations permit the following conclusions:

(1) The increase of the expansion ratio results in the decrease of the size of the after-burning flame.

(2) In a similar way, the addition of alkali compounds to the propellants decreases the size of the after-burning flame which does not appear at expansion ratio = 1 for the propellant tested containing approximately 0.1% potassium.

(3) Since the potassium compounds are effective after the exiting combustion gases have formed a diffusion flame by their contact with the atmospheric oxygen, they delay the spontaneous ignition and thus prevent the formation of the after-burning flame.

SUPPRESSION IN PREMIXED $H_2/O_2/N_2$ FLAMES SEEDED WITH HBr

T. SINGH + DAVID P. WEAVER

ABSTRACT

The inhibition effects of HBr in H2-air flames have been studied theoretically. Experimental work is in progress. The effect of HBr addition on the laminar burning velocity, peak mole fractions for H and OH, the rate of fuel and oxidizer decay, the rate of production of product species and the rate of temperature rise has been studied.

1. Introduction

Various substances have been added to propellants in an effort to reduce or eliminate afterburning, and on an empirical basis alkali metal salts such as K_2SO_4 and KNO_3, have been found to be effective when used as suppressant additives. Tailoring of propellants has, therefore, been done largely by empirical variation of additives in extremely costly testing . This approach is critically limited by the lack of fundamental knowledge of the underlying chemical mechanisms controlling the suppression process. A program is currently in progress at the US Air Force Rocket Propulsion Laboratory to study the inhibtion mechanism of $H_2/O_2/N_2$ flames seeded with HBr,KCl, and KOH. This paper describes the work done so far (both theoretical and experimental) for $H_2/O_2/N_2$ flames seeded with HBr. The primary reason for the use of HBr is to caliberate both our theoretical model and the experimental data with those of other workers (ref. 1-4) reported in the literature.

A number of studies have been reported on the inhibition of hydrogen-air and hydrocarbon-air flames seeded with HBr and other halogen compounds (ref. 1-4). For an organic halide additive, the important primary reaction is probably the formation of halogen acid HX

$$RX + H = R + HX$$

For CH_3Br as an additive, this reaction would be:

$$CH_3Br + H = CH_3 + HBr$$

When HBr is the inhibiting species, the primary effect of the addition of the inhibitor is to remove flame radicals through the following reaction:

$$H(OH,O) + HBR = H_2\ (H_2O,OH) + Br$$

The reaction with hydrogen atoms predominate in fuel-rich flames. This reaction alone was found insufficient to explain the observed changes in flame velocity (1,2). Dixon-Lewis et al. (1,2) proposed the following series of reactions for the inhibiting effect of HBr.

$H + HBr = Br + H_2$	(R16)
$Br + HBr = H + Br_2$	(R17)
$Br + Br + M = Br_2 + M$	(R18)
$H + Br + M = HBr + M$	(R19)
$Br + HO_2 = HBr + O_2$	(R20)

The net result of the above inhibiting cycle is recombination of two H atoms into a relatively unreactive H_2 molecule. This recombination is catalyzed by the presence of HBr. Hydrogen atoms removed in this manner are unavailable for chain branching reactions with O_2 molecules through the reaction:

$$H + O_2 = O + OH$$

The validity of the the above inhibition reaction scheme is based on the observed changes in burning velocities and flammability limits No comparisons have been reported between the the experimental temperature and composition profiles and the corresponding computed profiles using the above reaction mechanism. One of the objectives of this study is to validate the inhibition reaction mechanism by comparing the computed temperature and composition profiles with those obtained experimentally. The experimental work is still in progress.

2. Experimental Facility

The experimental arrangement for this study is shown in Figure 1. The flat flame burner, constructed by McKenna Products, Inc., has a 6 cm diameter sintered porous disk through which the premixed samples of H_2-O_2-N_2-HBr flow. A 0.5 cm thick coaxial shroud ring can provide a N_2 flow or a $H_2/O_2/N_2$ shield flame. The burner is mounted on a motorized, x-y-z platform. Flow conditions and table position can be monitored by computer for each data series.

Several AFRPL laser sources are available for this study. Each source can be coupled into the focusing lens optical system via quartz prisms. The Lambda Physik eximer laser system (Model EMG 201 MSC) provides radiation at 308nm that can also be used to pump a dye laser (Model FL2002). The Quanta Ray Yag - pumped dye laser system (Model DCR-1A/PDL - 1) is equipped with a WEX (wavelength extender) system providing tunable radiation for probing OH radicals. A Coherent Radiation argon - ion laser (Innova -18) is also available. The source radiation is focussed through the centerline of the burner using a fused silica lens. Raman and Rayleigh scattering and laser - induced fluorescence techniques are used to obtain concentration and temperature measurements on the major species and OH radical.

The scattered radiation is collected by a lens system and imaged onto the entrance slit of a 0.75 meter spectrometer (Spex Industries Model number 1702). The signals were measured using a cooled photomultiplier tube (RCA Model C31034A). A reference signal was provided to monitor laser intensity by a photodiode. Output signals from the photomultiplier and photodiode were processed by either an EGG/Ortec photon counting system or an EGG/PAR boxcar averager (Model 4420). Some post processing of the signal was done with a EGG/PAR signal processor (Model 4402). All data was recorded on a PDP/11 - 73 computer system and subsequently transfered to a VAX 750/785 computer system for analysis.

The basic gas handling system provided for dilution of the oxygen, hydrogen, and HBr flows separately with any percentage of nitrogen. The mixed H_2/N_2, O_2/N_2, and HBr/N_2 gases were the delivered to the burner after mixing at a point well upstream.All gas flows were monitored continuously by measuring(approximately 2 percent accuracy) the differential pressure across a linear gas flow element.

3. Theoretical Work

Two computational models were used for calculating the temperature profile, composition profile and flame velocity (based on a given set of kinetic mechanisms) in the premixed flat flame.

The first model was developed by Coffee and Heimerl of the Ballistic Research Laboratory (ref. 1). This model is based on a general program for solving a set of N non-linear partial differential equations of at most second order on a finite interval . The spatial discretization is accomplished by finite element collocation methods based on B-splines (ref. 5). An initial solution is assumed (between the unburned composition and the equilibrium solution) and the differential equations are integrated in time until the species concentrations and temperature profiles converge. The details of the numerical procedures are discussed in ref. 6 and 7.

The ARBRL computer program gave satisfacory results for $H_2/O_2/N_2$ flames. The calculated composition and temperature profiles and flame velocity gave good agreement with those reported in the literature (ref. 8 and 9). However, as the kinetic mechanism was modified to include the suppression reactions due to the presence of HBr, KOH etc., the solution with ABRBL code did not converge for several conditions at different concentrations of suppressants.

The second computational model was developed by Kee, Grcar,Smooke and Miller of the Sandia National Laboratories (ref. 10). This program computes the composition and temperature profiles and burning velocity in steady laminar one-dimensional premixed flames. The program accounts for finite rate chemical kinetics and molecular transport. Finite difference approximations are made to discretize the governing conservation equations on a non-uniform grid from the cold boundry to the hot boundry. The Newton method is used for solving the boundry value problem . Global convergence of this algorithm is aided by invoking the time integration procedures when the Newton method has convergence difficulties(ref. 10).

4. Chemical Kinetic Mechanism

A fifteen step reaction mechanism (Table 1) is used for simulating the base $H_2/O_2/N_2$ flames. This mechanism has been shown to give agreement between the computed results and the corresponding experimental data (ref. 9). The associated thermodynamic data and transport data have been compiled (ref. 5) and a sensitivity analysis has been published for $H_2/O_2/N_2$ flames (ref. 11). A five step reaction mechanism as proposed by Dixon-Lewis et. al. (ref. 1 and 2) is added to the 15 step reaction mechanism for simulating the inhibtion effects. The rate constants for these reactions are taken from ref. 1 and the backward rate constants are calculated from the forward rate constants and the equilibrium constants (based on the associated thermodynamic data).

Table 1

Reaction Mechanism for $H_2/O_2/N_2/HBr$

Reaction	A- Pre exp	B- Temp Exp	E- Act Enrg*
1. $OH + H_2 = H_2O + H$	0.117E10	1.30	3626.0
2. $H + O_2 = OH + O$	0.142E15	0.0	16393.
3. $O + H_2 = OH + H$	0.180E11	1.0	8902.0

4. $H + O_2 + H_2 = HO_2 + H_2$	0.103E19	-0.7	0.0
5. $H + HO_2 = OH + OH$	0.140E15	0.0	1073.0
6. $H + HO_2 = O + H_2O$	0.103E14	0.0	1073.0
7. $H + HO_2 = H_2 + O_2$	0.125E14	0.0	0.0
8. $OH + HO_2 = H_2O + O_2$	0.750E13	0.0	0.0
9. $O + HO_2 = OH + O_2$	0.140E14	0.0	1073.0
10. $H + H + M = H_2 + M$	0.100E19	-1.0	0.0
11. $H + H + H_2 = H_2 + H_2$	0.920E17	-0.6	0.0
12. $H + H + H_2O = H_2 + H_2O$	0.600E20	-1.25	0.0
13. $H + OH + M = H_2O + M$	0.160E23	-2.0	0.0
14. $H + O + M = OH + M$	0.620E17	-0.60	0.0
15. $OH + OH = O + H_2O$	0.575E13	0.0	775.0
16. $H + HBr = Br + H_2$	0.530E14	0.0	2970.0
17. $Br + HBr = H + Br_2$	0.270E15	0.0	44110.0
18. $Br + Br + M = Br_2 + M$	0.130E18	-0.71	0.00
19. $H + Br + M = HBr + M$	0.977E18	-0.71	0.00
20. $Br + HO_2 = HBr + O_2$	0.340E13	0.0	0.0

*Rate coefficients are expressed as $k=AT^B \exp(-E/RT)$ in cm-mole-sec units

5. Comparison of Burning Velocity for Two Codes

Both Sandia Code and the ARBRL code were used for calculating the burning velocities, composition and temperature profiles for 6 different ratios of $H_2/O_2/N_2$ and for varying amounts of HBr as additive. The results for laminar burning velocity are summarized in Table 2.

Table 2

Laminar Burning velocity, cm/Sec

$H_2/O_2/N_2$ HBr Mole Ratio	ARBRL Code	Sandia Code
4/1/4/0.0	252.0	264.7
.44/.11/.444/.06	N.C.*	217.8
.44/.11/.44/.01	N.C.	194.1
.436/.105/.435/.02	N.C.	156.7
.427/.107/.426/.04	N.C.	109.1
4/ 1/ 5/ 0.0	199.5	190.0
.396/.099/.495/.01	N.C.	158.9
.392/.098/.490/.02	N.C.	120.7
.388/ .097/.485/.03	N.C.	83.2
.384/.096/.480/.04	N.C.	63.2
2.25/ 1/ 5/ 0.0	171.9	181.0
.27/.12/.60/.01	142.0	147.8
.267/.119/.594/.02	N.C.	119.3
.384/.096/.583/.04	N.C.	80.7

1/ 1/ 3/ 0.0	94.6	92.2
.198/.198/.594/.01	71.3	59.2
.196/.196/.588/.02	57.6	43.2
.192/.192/.576/.04	41.1	32.3
1.8/ 1/ 4/ 0.0	178.9	185.9
.262/.146/.582/.01	147.6	148.3
.259/.144/.577/.02	125.8	121.3
.254/.141/.565/.04	93.9	82.7
60% H2 - 40% Air		
.60/.084/.316/0.0	179.1	167.1
.594/.0832/.314/.01	N.C.	109.1
.588/.0823/.310/.02	N.C.	64.4
.576/.0806/.303/.04	11.5	21.9

* - No Convergence

Both codes used the same set of chemical kinetic mechanisms, rate constant data, thermodynamic data and the transport data for the above calculations. Both codes require the user to specify a set of numerical parameters such as tolerance for the termination of iteration, number of grid points, and other similar factors.

Some difficulties were encountered for obtaining convergence with the Sandia Code. Initially a solution was obtained for a given ratio of $H_2/O_2/N_2$ (with HBr mole fraction equal to .005) flame. These computations generally required between 20 minutes to 3 hours of CPU time on a FPS164 MAX processor attached to a VAX 750. The mole fraction of HBr was then changed in steps of .005. Each successive run used the solution of the previous run as its initial guess.These computations typically required 30 seconds to 50 minutes of CPU time on the FPS164 processor. If the changes in mole fraction of HBr exceeded 0.005 from one run to the next one , convergence was not obtained despite considerable computational time (up to 10 hours of CPU time on theFPS164 processor for some runs).

From Table 2, it is seen that the computed burning velocity from the two codes agree closely with each other. The experimental values of burning velocities have high uncertainy of the order of ± 20% . The computed burning velocity decreases as the percentage of HBr increases in a given fuel air mixture as expected.

Table 2 also shows that the burning velocity for fuel lean flames is less than the corresponding burning velocity for fuel rich flames. For example the fuel rich flame with H_2/O_2 ratio of 4/1 (100% fuel rich) has a burning velocity of 264.7 cm/s. The corresponding fuel lean flame with H_2/O_2 ratio of 1/1 (100% fuel lean) has a burning velocity of 92.2 cm/s. Thus fuel lean flames are somewhat inhibited as compared to fuel rich flames even without the presence of HBr.

Dixon-Lewis et. al. (1) have reported calculated burning velocity, temperature and composition profile for 60% H_2 - 40% air flames inhibited with 4% HBr. The results for the burning velocity and peak temperature are shown in Table 3.

Table 3

Ratio of $H_2/O_2/N_2$/HBr	Burning Velocity, cm/sec		Peak Temperature, °K	
	Dixon-Lewis(1)	This Work	Dixon-Lewis	This Work
0.6/.084/.316/0.0	163.0	167. 0	1644.0	1626.0
.576/.0806/.3034/.04	17.0	21.0	1585.0	1580.0

This shows good agreement between the results of Dixon-Lewis and this work. The change in temperature is small as the fraction of HBr changes from 0.0 to 0.04 in the unburned mixture. The reduction in burning velocity is,therefore, primarily controlled by chemical inhibition mechanisms, which become activated as the fraction of HBr increases in the unburned mixture.

6. Peak OH , Peak H Mole Fraction and Burning Velocity

Figures 2 and 3 show the variation of computed OH peak mole fraction vs the change in HBr mole fraction for two fuel rich and two fuel lean flames. Figures 4 and 5 show the corresponding peak H mole fraction. Figures 2- 5 show that the peak mole fraction for H and OH decrease as the % of HBr increases in the unburned mixture. This trend is similar to that of burning velocity which decreases as the mole fraction of HBr increases. This is consistent with the inhibition mechanism (ref. 1-4) used for these computations. The net result of the inhibtion cycle is the recombination of two H atoms into a relatively unreactive H_2 molecule. This recombination is catalyzed by the presence of HBr . Hydrogen atoms removed in this manner are unavailable for chain branching reactions with O_2 via the familiar reaction:

$$H + O_2 = O + OH$$

This leads to the reduction of H and OH mole fraction in the flame reaction zone .

7. Composition and Temperature Profiles

The computed mole fraction for H_2 and H_2O (two of the major species) are shown in Figure 6 for a 60% H_2-40% Air flames with and without 4% HBr.Figure 7 shows the corresponding computed temperature profiles for a 60% H_2 - 40% Air flame inhibited with 4% HBr and the corresponding uninhibited flame as a function of distance above the burner surface. Adiabatic flames are assumed for the solution of the energy equation. From Figures 6-7 it is seen that the rate of temperature rise, the rate of H_2 (fuel) decay and the rate of H_2O production are lower for the inhibited flames as compared to those for the uninhibited flames. Approximately 90% of the temperaure rise for the unseeded flame takes place over a distance of about .05 cm (from .125 cm to .175 cm above the burner surface). The same change of temperature for the flame seeded with 4% HBr requires a distance of about .15 cm or approximatey three times the the distance as compared to the uninhibited flame. Thus, the primary flame zone (reaction zone) is stretched for the inhibited flames.

This trend may be related to the the suppression of the afterburning in the rocket exhaust due to thepresence of similarly acting inhibitors. The exhaust gases from the nozzle of a rocket exhaust usually contain significant proportions of unburned fuel. This fuel mixes turbulently with the ambient air as the jet expands . Afterburning occurs where the local temperature and the local air-fuel ratio reach the auto-ignition limit. The exhast gases containing the suppressant would require a longer distance (time) to reach the same level of temperature rise for auto-ignition (afterburning) . A longer distance from the nozzle of a

rocket exhaust would also contain a larger amount of entrained air leading to the decrease of local temperature due to dilution effect. The auto-ignition temperatures are, therefore, not reached and the afterburning is suppressed.

8. Reaction $Br + HO_2 = HBr + O_2$

Westbrook (3,4) did not include the reaction $Br + HO_2 = HBr + O_2$ in the mechanism for hydrocarbon flames inhibited with HBr. Dixon-Lewis (1,2) found it necessary to include this reaction (R20) into their mechanism in order to observe the reduction in burning velocity (for a fuel rich H_2-O_2-N_2 flame seeded with .027% HBr) while at the same time maintaining reasonable values for the rate constants for the reactions (R18) and (R19). The calculated burning velocity changes by 5-6% if the reaction R20 is not included as may be seen from table 3.

Table 3

Ratio of $H_2O/O_2/N_2/HBr$	Burning Velocity cm/s R20 included	R20 excluded
1.8/1/4/0.0	185.5	185.5
0.262/.146/.582/.01	148.3	155.8
0.259/.144/.577/.02	121.3	128.0
0.2565/.1425/.571/.03	104.0	110.5

No significant difference in the calculated temperature and composition profiles when reaction R20 was included in the reaction set. This reaction was included for all the computations reported in this study.

9. Post Processor Analysis

A post analysis of some of the computed results has been done by using a post processor program (ref. 12).This program computes the sign and magnitude of three terms (net convective flux out of a differential element, net chemical formation rate and the net diffusion flux) in the one-dimensional , steady state species conservation equation at specified points in the grid. The mass flux due to chemical reactions and diffusion flux are computed from the flame code output (which also gives composition profiles) . The convective term is calculated by fitting 3 adjacent Y(k)'s (mass fraction of kth species) with a cubic spline , evaluating the derivative at the mid point.The chemical term is of special interest. The contributions of the individual reactions to the formation and destruction of the kth species within an element are calculated. The relative contributions of individual reactions are expressed in non-dimensional form. The non-dimensional numbers represent the ratio of the formation/destruction rate for the kth species due to each reaction (one direction at a time) to the "total rate". The "total rate" consists of the sum of the absolute values of the following:

- The chemical formation rate summed over all reactions that form the kth species
- The chemical destruction rate summed over all reactions that destroy the kth species
- The net convective rate
- The net diffusion rate

This normalizing factor has no physical significance. The non-dimensional ratio helps to illustrate the relative importance of various reactions in the formation/destruction of kth species in a given element (zone or grid point). The program also calculates the ratio of forward rates to the backward rates for each reaction in a given zone. Finally, the program points out any reactions that were never found to be important in the flame. These could likely be deleted from the mechanism.

A post processor analysis was done for 60% H_2-40% air flames seeded with 1%,2%,3% and 4% HBr . The following reactions were never found to be important:

Flame Composition	Reactions not important
60% H_2-40% Air - 1% HBr	-
- 2% HBr	8,14
- 3% HBr	8,9,10,11,13,14
- 4% HBr	8,9,10,11,13,14

These conclusions were verified by eliminating reactions 8-11 ,13 and 14 from the reaction mechanism given in table 1. The computations were repeated for 60% H_2-40% air flames seeded with 3% and 4% HBr using the modified 14 step reaction mechanism. There was no significant difference in the results computed with 20 step reaction mechanism and 14 step reaction mechanism:

Flame Composition	Laminar Burning Velocity, cm/s	
	20 step mechanism	14 step mechanism
60% H_2-40% air - 3% HBr	50.2	53.1
- 4% HBr	21.9	21.3

The composition and temperature profiles for the two cases (14 step and 20 step reaction mechanism) were similar.It is seen that a shorter mechanism consisting of 14 reactions is able to model the flame structure for 60% H_2-40% air flames seeded with 3-4% HBr satisfactorily. Reactions 8-11,13 and 14 involve primarily the reactions of species H,OH and O .For flames seeded with high concentrations of HBr , the mole fraction of H and OH is lower as compared to those for the uninhibited flames. The dominant inhibition reaction 16 (H + HBr = H_2 + Br) is close to equilibrium above 1000K. This reaction decreases the amount of H available for the main chain branching reaction

$$H + O_2 = OH + O$$

This leads to a reduction in the average concentration of H, OH and O in a given element of the flames. Thus the contributions of reaction 8-11, 13 and 14 become insignificant.

The processor analysis for 60% H_2-40% air flames showed that the reaction 16 was close to equilibrium above 1000K and reactions 1 and 3 were equilibrated above 1550 K for flames seeded with 1% to 4% HBr.

10. Summary and Conclusions:

•The inhibtion effect of HBr in hydrogen-air flames has been modelled. A fifteen step kinetic reaction mechanism was used for computing the structure of base hydrogen-air flames. Five additional reactions of HBr were used to simulate the inhubtion effects.

•The laminar burning velocity and peak mole fractions of H and OH decrease as the mole fraction of HBr increases in the unburnt fuel air mixture. This trend was exhibited by both fuel-rich and fuel-lean flames.

•The laminar burning velocity for fuel-rich flames is higher than the corresponding burning velocity for fuel-lean flames

•A simplified reaction mechanism consiting of fourteen reactions gives results similar to those obtained with twenty step reaction mechanism for 60% hydrogen 40% air flames seeded with 3 to 4% HBr in the unburnt mixture.

•The primary flame zone for hydrogen-air flames seeded with HBr is longer (stretched) as compared to that for hydrogen-air flames having no HBr. The rate of temperaure rise, the rates of fuel and oxidant decay and the rates of production for product species are lower for flames seeded with HBr.

•These results will be compared with the experimental data , which is expected within the next month. One set of experimental data for temperature is shown in Fig. 8.

11.References:

1. G. Dixon-Lewis, "Mechanisms of Inhibtion of Hydrogen-Air Flames by HBr and its relevance to the general problem of Flame inhibtion ", Combustion and Flame 36: 1-14 (1979).

2. G. Dixon-Lewis and R. Simpson, " Aspects of Flame Inhibtion by Halogen Compounds ", 16th Symposium (International) on Combustion/ The Combustion Institute, p. 1111, 1976.

3. Charles K. Westbrook, "Inhibtion of Hydrocarbon Oxidation in Laminar Flames and Detonations by Haloganated Compounds", 19th Symposium (International) on Combustion/The Combustion Institute, pp. 127-141, 1982.

4. Charles K. Westbrook, " Flame Inhibtion by CF3Br", Preprint UCRL-88180, Lawrence Livermore National Laboratory, Sept. 1982.

5. T.P. Coffee and J.M. Heimerl, Report ARBRL-TR-02457, U.S. Army Ballistic Research Laboratory, Aberdeen Proving Ground MD, Jan. 1983.

6. N.K. Madsen and R.F. Sincovec, "PDECOL: General Collocation Software for Partial Differential Equations", Preprint UCRL-78263 (rev. 1), Lawrence Livermore Laboratory, 1977.

7. C. DeBoor, SIAM. J. Num. Anal., 14, 441(1977).

8. G. Dixon-Lewis," Kinetic Mechanism, Structure, and Properties of Premixed Flames in Hydrogen-Oxygen-Nitrogen Mixtures", Proceedings, Royal Soc. of London, 292, 45-99 (1979).

9. J.D. Eversole and T. Singh, " Suppression in Premixed H2/O2/N2 Laminar Flames", Western States Section Combustion Institute Meeting, paper no WSS/Ci 84-52, April 1982.

10. R.J. Kee, J.F. Grcar, M.D. Smooke, and J.A. Miller, "A Fortran Program for Modelling Steady Laminar One-Dimensional Premixed Flames"' Sandia Report SAND85-8240, Dec. 1985.

11. T.P. Coffee and J.M. Heimerl, Report ARBRL-TR-02457, US Army Ballistic Research Laboratory, Aberdeen Proving Ground MD, Jan. 1983.

12. Owen I Smith, UCLA, Post processor program, Personal Communication, Jan. 1986.

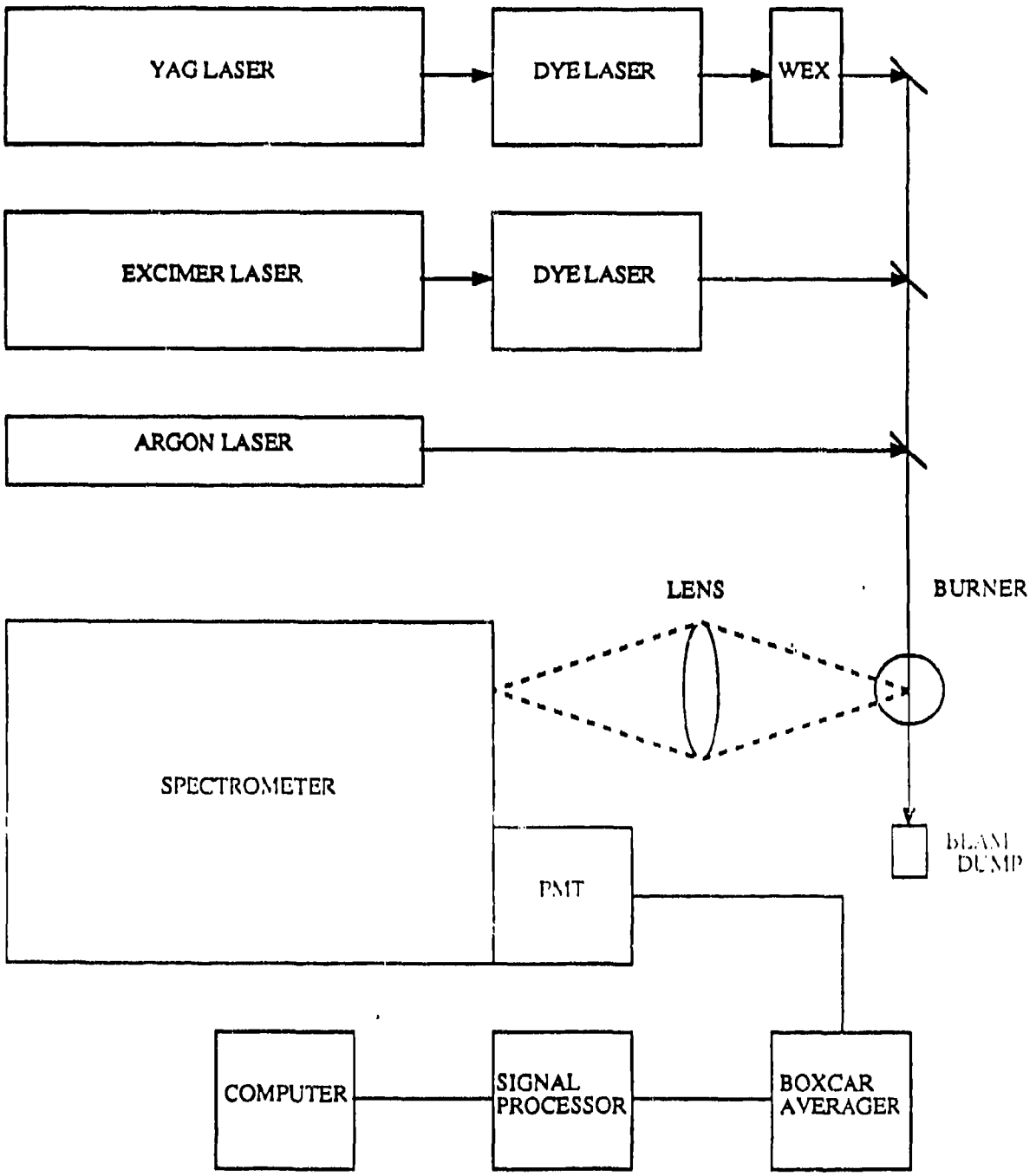

FIGURE 1. EXPERIMENTAL ARRANGEMENT

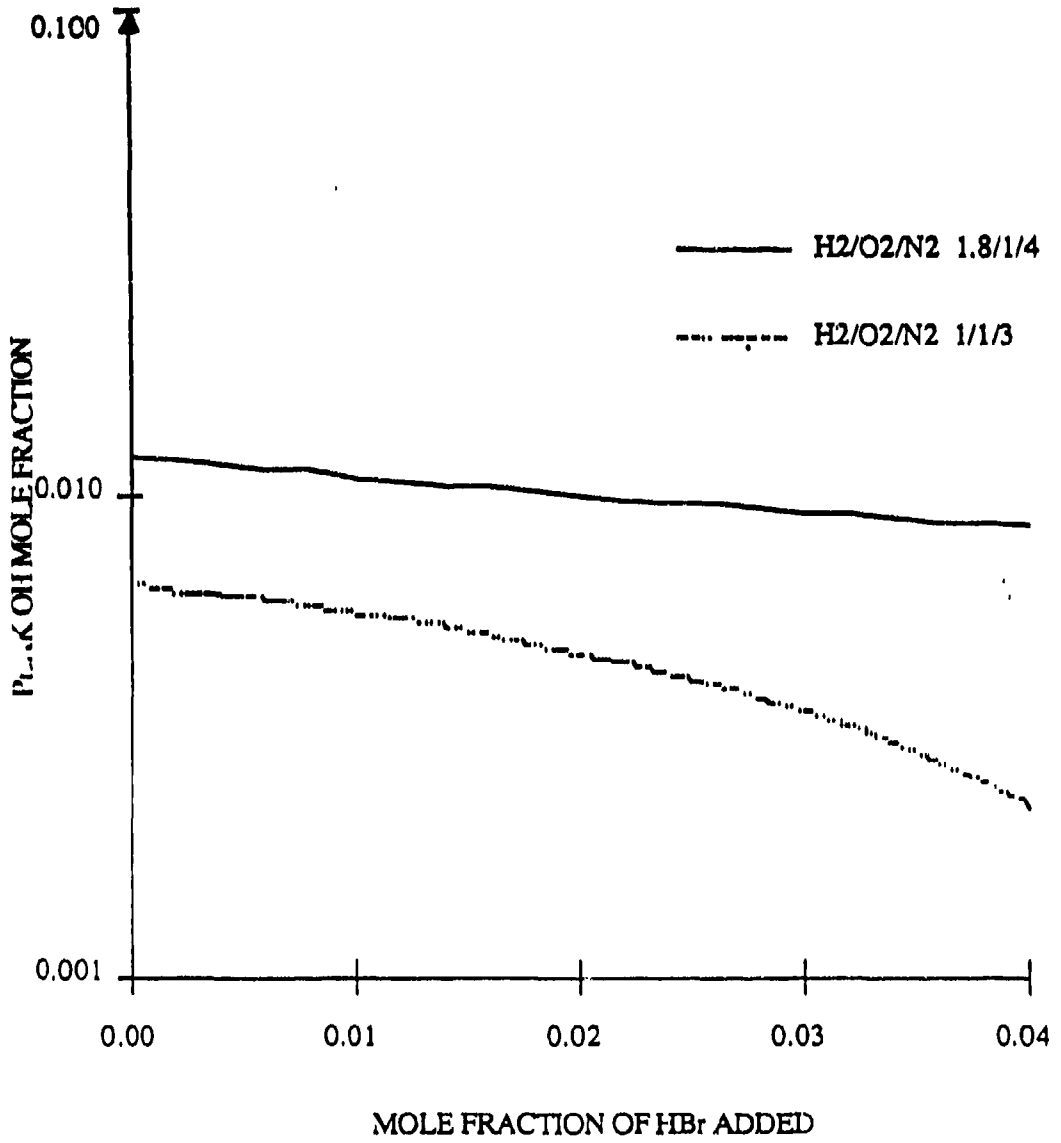

FIGURE 2. Computed peak mole fraction of OH as a function of HBr added. Values are given for a flame with a mole ratio for H2/O2/N2 of 1/1/3 compared to those with a mole ratio of 1.8/1/4

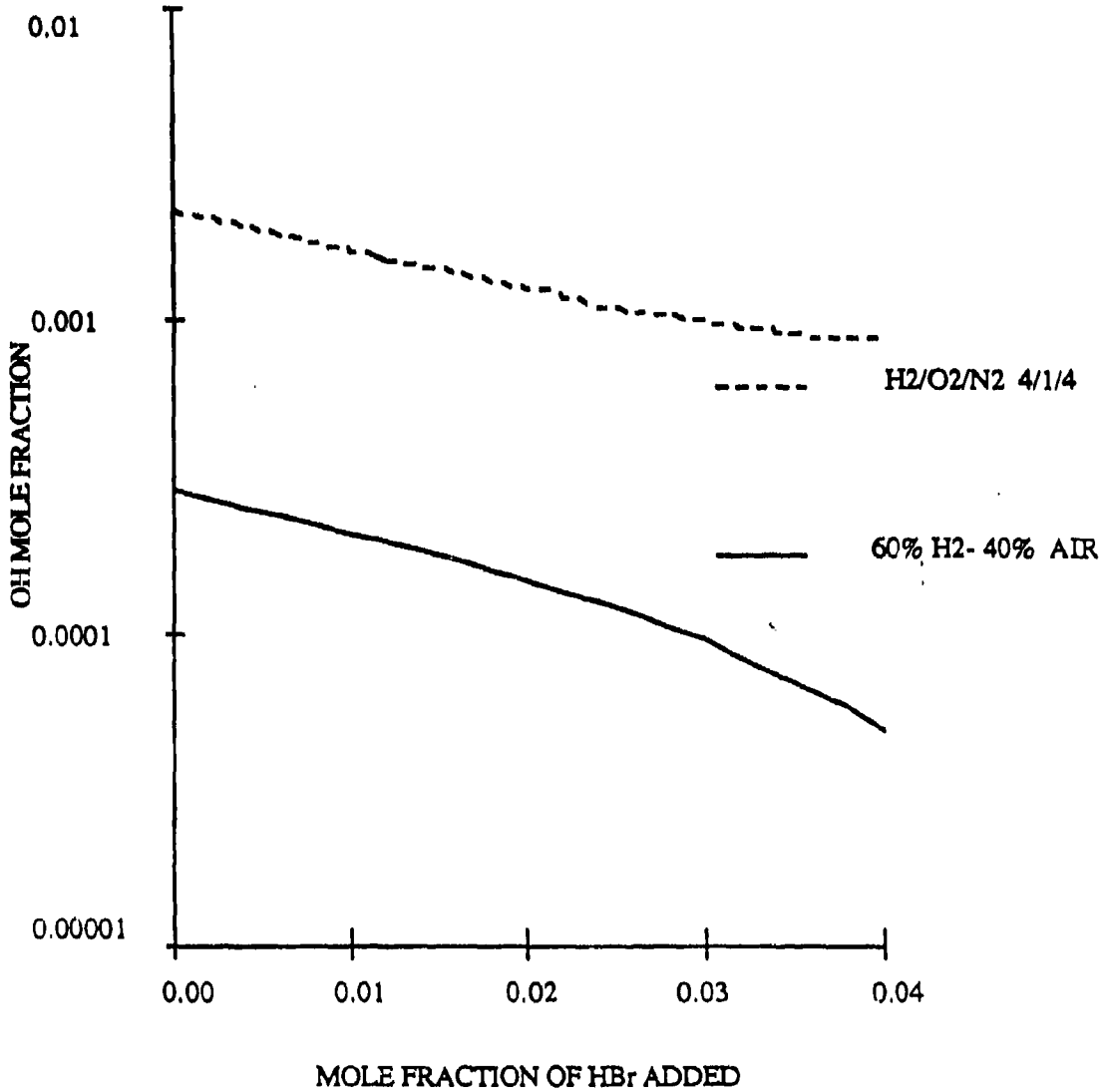

FIGURE 3. Com ıted peak mole fraction of OH as a function of HBr added. Values are given for a flame with a mole ratio for H2/O2/N2 of 4/1/4 compared to those with a mole ratio of 7.1/1/3.76.

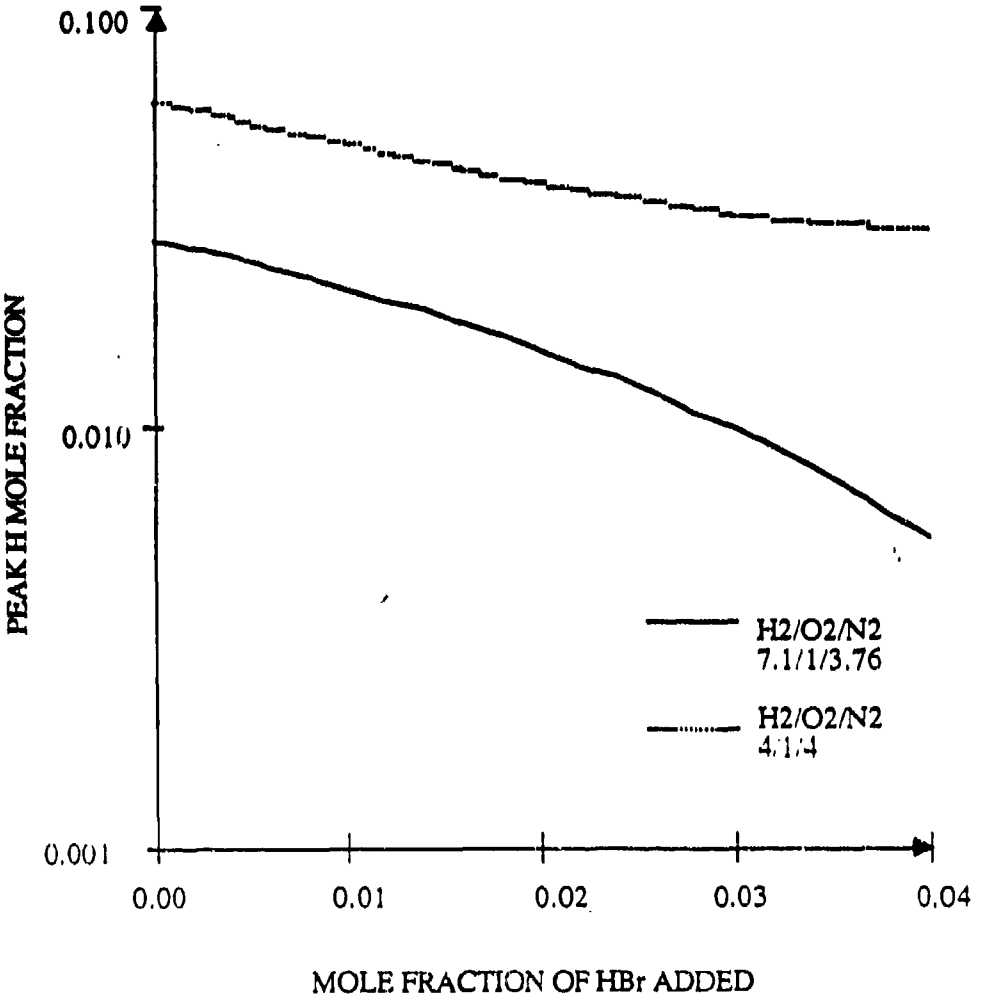

FIGURE 4. Peak mole fraction as a function of HBr added. Computed values for a flame with a H2/O2/N2 mole ratio of 7.1/1/3.76 compared to those with a H2/O2/N2 mole ratio of 4/1/4.

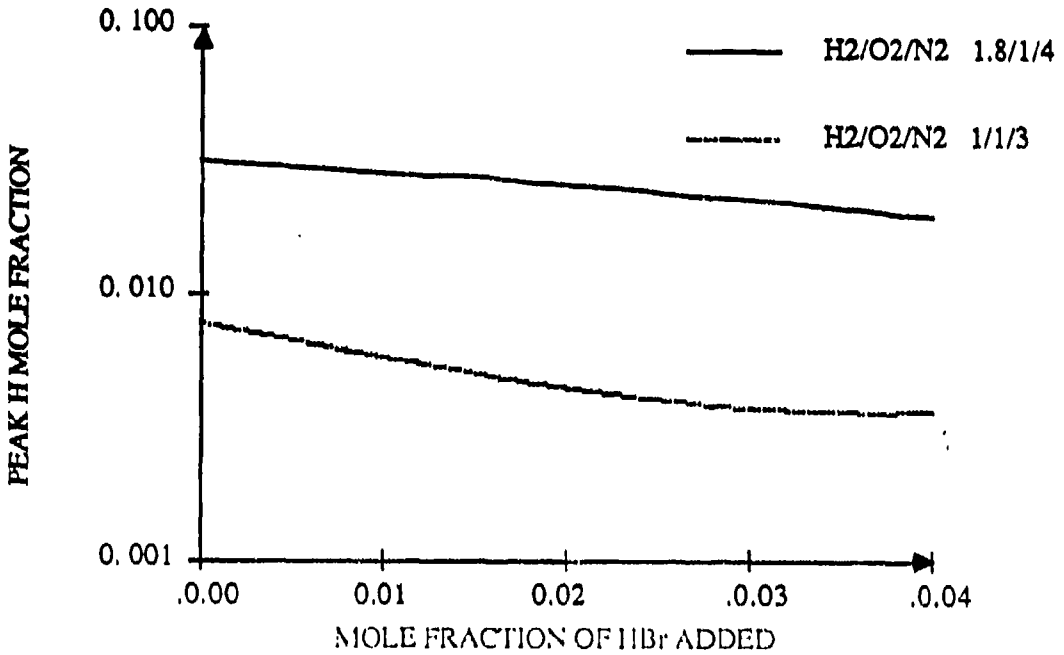

FIGURE 5. Peak mole fraction as a function of HBr added. Computed values for a flame with a H2/O2/N2 mole ratio of 1/1/3 compared with a H2/O2/N2 mole ratio of 1.8/1/4.

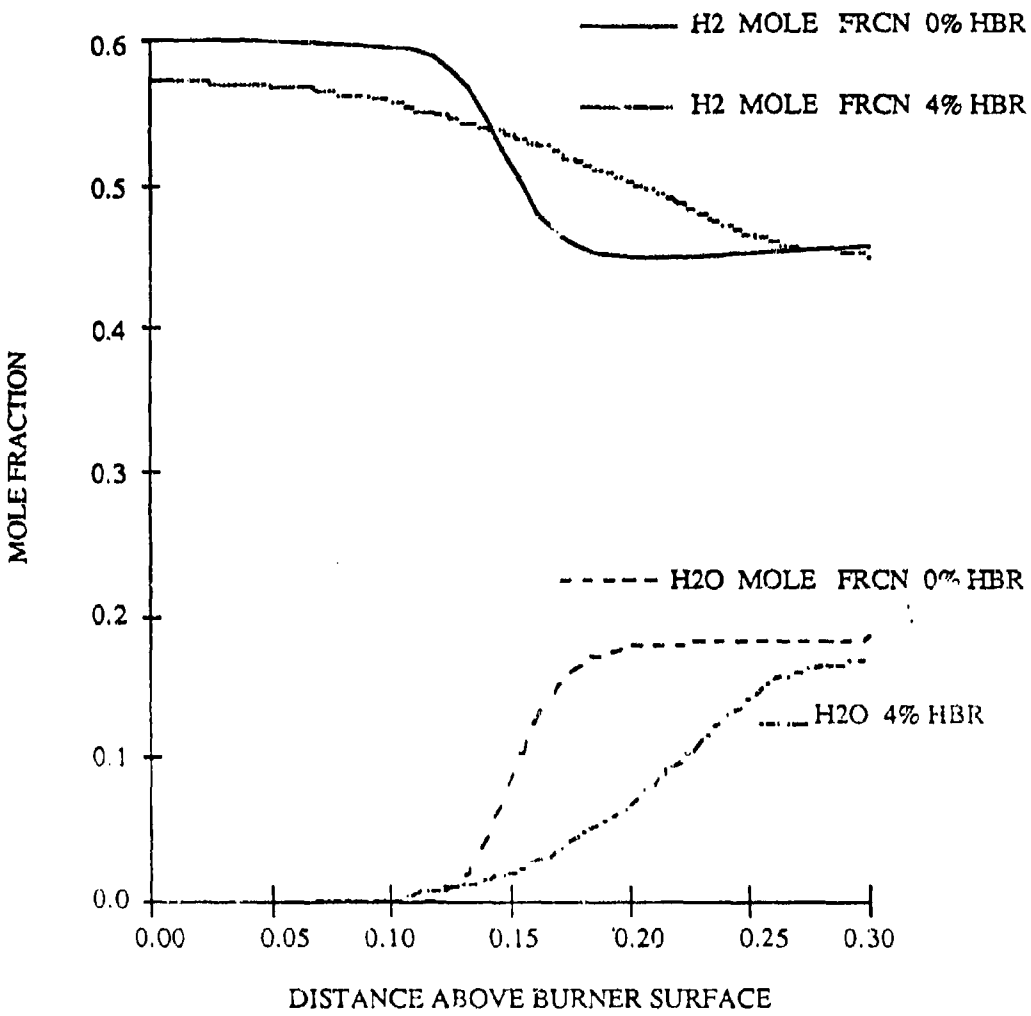

FIGURE 6. Computed H2 and H20 mole fraction as a function distance above the burner surface for 0.0 and 4.0% addition of HBr. The H2/O2/N2 mole ratio is 0.6/0.084/7.1.

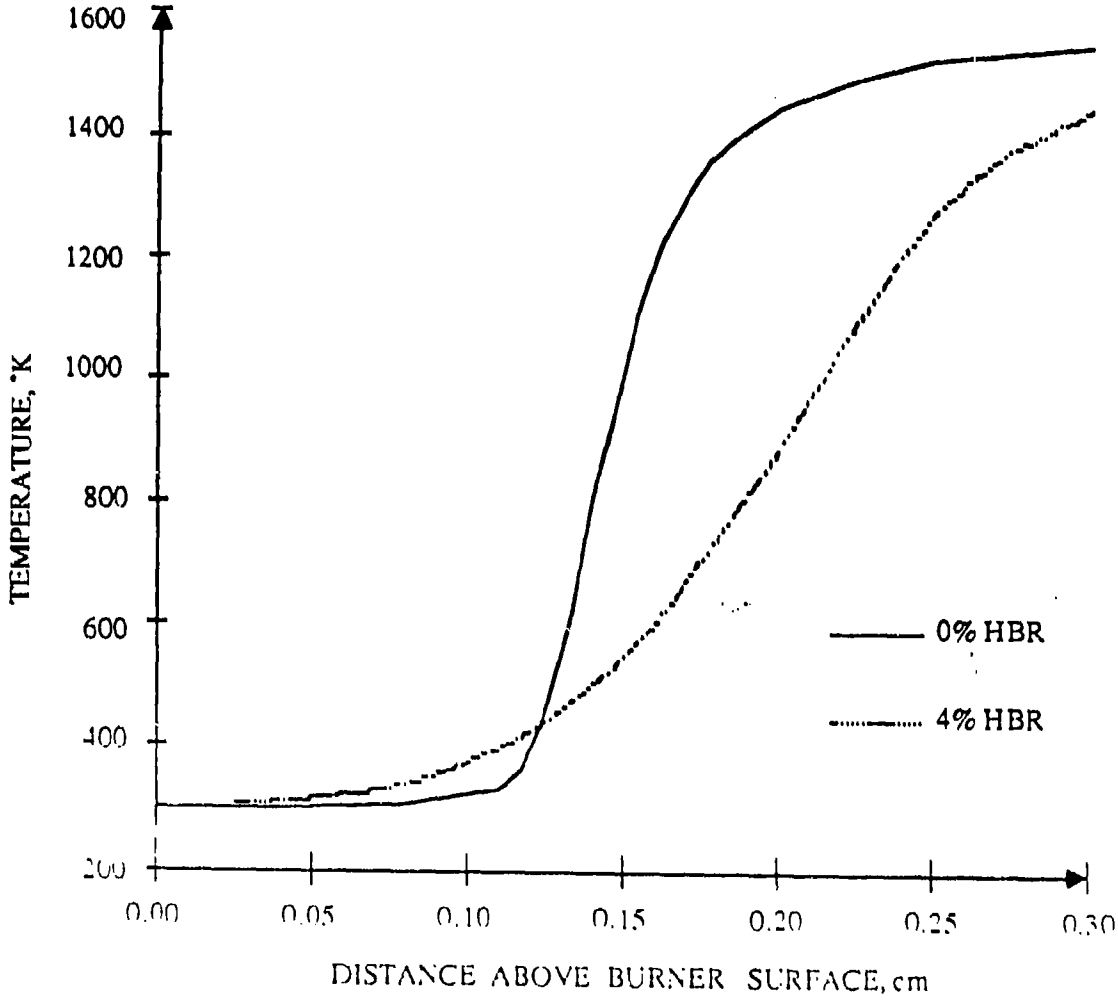

FIGURE 7. Computed temperature profile as a function of distance above the burner surface. The H2/O2/N2/HBr mole ratio is 0.6/0.084/0.316.

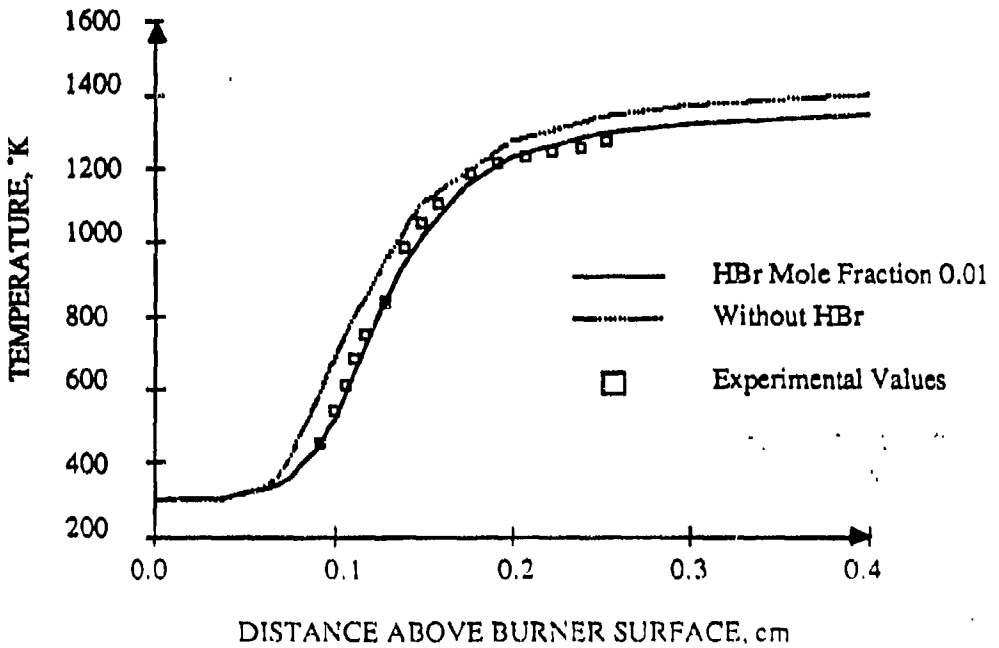

FIGURE 8. Computed temperature as a function of distance above the burner surface. The H2/O2/N2/HBr mole ratio is 0.19/0.07/0.73/0.01. An additional curve is shown without HBr for comparision. Experimental values are shown as squares.

DISTRIBUTION LIST

No. Of Copies	Organization
12	Administrator Defense Technical Info Center ATTN: DTIC-DDA Cameron Station Alexandria, VA 22304-6145
1	HQ DA DAMA-ART-M Washington, DC 20310
1	Commander US Army Materiel Command ATTN: AMCDRA-ST 5001 Eisenhower Avenue Alexandria, VA 22333-0001
10	Central Intelligence Agency Office of Central Reference Dissemination Branch Room GE-47 HQS Washington, DC 20505
1	Commander Armament R&D Center US Army AMCCOM ATTN: SMCAR-TSS Dover, NJ 07801
1	Commander Armament R&D Center US Army AMCCOM ATTN: SMCAR-TDC Dover, NJ 07801
1	Director Benet Weapons Laboratory Armament R&D Center US Army AMCCOM ATTN: SMCAR-LCB-TL Watervliet, NY 12189
1	Commander US Army Armament, Munitions and Chemical Command ATTN: SMCAR-ESP-L Rock Island, IL 61299
1	Commander US Army Aviation Research and Development Command ATTN: AMSAV-E 4300 Goodfellow Blvd. St. Louis, MO 63120
1	Director US Army Air Mobility Research and Development Laboratory Ames Research Center Moffett Field, CA 94035
1	Commander US Army Communications - Electronics Command ATTN: AMSEL-ED Fort Monmouth, NJ 07703
1	Commander ERADCOM Technical Library ATTN: DELSD-L, Reports Section Fort Monmouth, NJ 07703-5301
1	Commander US Army Missile Command Research, Development and Engineering Center ATTN: AMSMI-RD Redstone Arsenal, AL 35898
1	Commander US Army Missile and Space Intelligence Center ATTN: AMSMI-YDL Redstone Arsenal, AL 35898-5000
1	Commander US Army Tank Automotive Command ATTN: AMSTA-TSL Warren, MI 48397-5000
1	Director US Army TRADOC Systems Analysis Activity ATTN: ATAA-SL White Sands Missile Range, NM 88002

DISTRIBUTION LIST

No. Of Copies	Organization
1	Commandant US Army Infantry School ATTN: ATSH-CD-CSO-OR Fort Benning, GA 31905
1	Commander US Army Development and Employment Agency ATTN: MODE-TED-SAB Fort Lewis, WA 98433
1	Air Force Armament Laboratory ATTN: AFATL/DLODL Eglin AFB, FL 32542-5000
1	Air Force Weapons Laboratory AFWL/SUL ATTN: V. King Kirtland AFB, NM 87117

Aberdeen Proving Ground

Dir, USAMSAA
ATTN: AMXSY-D
AMXSY-MP, H. Cohen
Cdr, USATECOM
ATTN: AMSTE-TO-F
Cdr, CRDC, AMCCOM
ATTN: SMCCR-RSP-A
SMCCR-MU
SMCCR-SPS-IL

USER EVALUATION SHEET/CHANGE OF ADDRESS

This Laboratory undertakes a continuing effort to improve the quality of the reports it publishes. Your comments/answers to the items/questions below will aid us in our efforts.

1. BRL Report Number_____ Date of Report_____

2. Date Report Received_____

3. Does this report satisfy a need? (Comment on purpose, related project, or other area of interest for which the report will be used.)_____

4. How specifically, is the report being used? (Information source, design data, procedure, source of ideas, etc.)_____

5. Has the information in this report led to any quantitative savings as far as man-hours or dollars saved, operating costs avoided or efficiencies achieved, etc? If so, please elaborate._____

6. General Comments. What do you think should be changed to improve future reports? (Indicate changes to organization, technical content, format, etc.)

_____

_____

_____

CURRENT ADDRESS

_____
Name

_____
Organization

_____
Address

_____
City, State, Zip

7. If indicating a Change of Address or Address Correction, please provide the New or Correct Address in Block 6 above and the Old or Incorrect address below.

OLD ADDRESS

_____
Name

_____
Organization

_____
Address

_____
City, State, Zip

(Remove this sheet, fold as indicated, staple or tape closed, and mail.)

FOLD HERE

Director
US Army Ballistic Research Laboratory
ATTN: DRXBR-OD-ST
Aberdeen Proving Ground, MD 21005-5066

NO POSTAGE
NECESSARY
IF MAILED
IN THE
UNITED STATES

OFFICIAL BUSINESS
PENALTY FOR PRIVATE USE, $300

BUSINESS REPLY MAIL
FIRST CLASS PERMIT NO 12062 WASHINGTON, DC

POSTAGE WILL BE PAID BY DEPARTMENT OF THE ARMY

Director
US Army Ballistic Research Laboratory
ATTN: DRXBR-OD-ST
Aberdeen Proving Ground, MD 21005-9989

FOLD HERE